

**MODELLING AND EMPIRICAL CHARACTERISATION
OF ENVIRONMENTAL DEGRADATION OF FRP
LAMINATES IN SOUTHERN AFRICA**

N.K. Sookay

In fulfilment of the Doctoral Degree in Mechanical Engineering

Date of Submission: 30 March 2007

Supervisor: Dr. CJ von Klemperer

ACKNOWLEDGEMENTS

The author acknowledges the guidance and assistance of the supervisor through various stages of the development of the project.

Appreciation is expressed for the assistance, support and encouragement by parents and staff members throughout the period of this project. Gratitude is expressed to the various industrial partners who provided resources and shared practical knowledge obtained through their experience from working with fibre reinforced polymer composites.

ABSTRACT

As polymeric composite materials are being increasingly used in Southern Africa, there is a need to establish the modes and rate of degradation of these materials when exposed to the local natural environment, in order to predict long term performance.

A model has been proposed to describe the change in mechanical properties due to weathering. The basis of the model is that degradation is primarily a surface phenomenon, i.e. damage occurs predominantly at the surface of the material. The bulk mechanical properties of the laminate can thus be established and long term performance, less than 26 months, of the material may be computed. The empirical model requires as input, climatic and test data from exposed laminates. Based on these, exposure effects such as post-curing and plasticisation are accounted for.

The data gathered from mechanical tests was used to verify the assumptions and accuracy of the model. Laminates for exposure testing were manufactured using different resin systems with glass-fibre reinforcement. Six climatically differing regions have been identified for exposure testing. This study predominantly examines damage incurred on the epoxy laminates which have the longest exposure to the environment to date.

The inspection of specimens was performed visually, using an optical microscope and scanning electron microscope to determine the modes of degradation. Underlying fibres became increasingly visible and at present, cover most of the exposed surface of the laminate with virtually no resin being present on the surface. Using Scanning Electron Microscopy (SEM), the erosion of material from the surface and through the thickness of the laminate was observed and quantified. The depth of cracks observed during the early stages of exposure, was determined by SEM as well. Flexure tests were performed to determine the residual bulk material properties of the laminate after predetermined exposure durations. Strength tests of epoxy laminates at all six locations was completed and compared to determine the most detrimental environment and environmental factor.

Further, the use of protective measures in reducing the rate of degradation of FRP laminates to the natural environment is being assessed by exposure of these materials with the use of protective measures. Laminates with protective coatings subjected to accelerated exposure were compared to similar laminates in the environment. At present, the rate of material loss of resin from the surface of the epoxy laminates appears to have decreased on laminates that have been protected by shade cloth.

PREFACE

The use of polymer composite materials in an increasing number of applications and operational environments has generated increasing interest in determining the long term durability to establish the feasibility of these materials in the new environments. Durability and the related safe service life are becoming increasingly important when considering the maintenance schedules and life cycle of polymer composite structures or components. Much work has been performed on describing / modelling the effect of a specific environmental variable on the mechanical properties of the material. This work is complex due the degradation of both the fibre and matrix. Until recently, published works reveal that while success to different degrees has been achieved in modelling the effect of a specific environmental factor acting singularly on the material, an established degradation model incorporating the synergistic effects of degradation has not been achieved.

The scope of the project was to broadly investigate degradation processes in polymer matrix composites. Further, identify dominant degradation mechanisms that occur in laminates exposed to the local natural environment and construct a model to predict the degradation of the mechanical property with time during initial stages of exposure. In pursuance of the above, it is required that test methodologies be developed by which available equipment can be used for analysis and testing of specimens should the required specific test equipment not be available. If the available equipment cannot be used, it is expected that appropriate equipment will be designed, manufactured and commissioned before use in the testing and analysis.

As part of the development of the degradation models above, a comprehensive literature survey was studied in an attempt to understand possible degradation mechanisms and the extent to which they influence mechanical property degradation. Although degradation studies in specific operational environments other than the natural environment are included in the literature survey, and a variety of matrices and reinforcements tested, all these results contribute towards understanding the development of dominant degradation mechanisms and factors which accelerate or inhibit their growth.

From the literature it appears that the onset of degradation is visually manifested by the appearance of cracks at the surface. This observation and the effect of crack propagation in mechanical strength reduction has been the starting point for this project. During the early stages of the project, the mathematical model was developed based on the hypothesis that the degraded material behaved as a functionally graded material, having an upper cracked layer progressing into the laminate and a lower undamaged layer. However the hypothesis proved to

be inaccurate when compared to the result of examination of laminates exposed to the environment.

An alternative model was developed based on observation of damage formation and propagation into the laminate. From the examination of exposed laminates, damage mechanisms and intensity of degradation factors were measured. This model required as input, data obtained from the natural exposure tests. The output from the model favourably compares with the test data for exposure durations of 26 months. From the beginning of exposure until the most recent examination of specimens, there appear to be no new damage mechanisms manifesting, only the same damage mechanisms repeating themselves in varying degrees of dominance in influencing the mechanical strength of the laminate. The varying degrees of dominance were found to be dependent on the change of environmental factors measured. The model is therefore thought to accurately describe the change in mechanical strength based on a group of environmental factors measured. The model does not extend to an exposure duration of more than 26 months as at this stage of exposure an entire layer of woven reinforcement has been exposed to the environment and therefore does not contribute to the strength of the laminate. The laminate in this state does not comply with the original design specification.

As both degradation models relied heavily on experimental test data, more so with the alternative empirical model, the methodology of test preparation, specimen manufacture, exposure conditions, sampling and testing had to be developed to make use of existing available resources. As the initial aim of the project was to evaluate the degradation of polymer composites in Southern Africa, the most common polymer systems that are in use in the region were used as the matrix to manufacture the different laminate systems. Further as this was a Southern African study, multiple test sites were selected to represent the climate of the region. However due to five material systems being exposed at six locations in the country, logistical problems occurred in the manufacture and sampling of laminates from test sites as the project progressed. Therefore the limited resources available were used on activities from which the data obtained will aid in understanding the identification, development and propagation of the degradation mechanisms previously observed. Data presented is indicative of the general observations and not all possible data obtained has been provided herein.

Once specimens from the natural exposure racks were obtained, considerable effort was spent in developing a method for preparing specimens for examination and testing such that the results of a batch were consistent and accurately reflected the effect of damage without the process of specimen preparation influencing the results. This was necessary to ensure that the results presented and conclusions drawn were accurate and valid. Researchers who would have

previously obtained considerable experience in the type of tests performed and having developed the equipment necessary to perform the specimen preparation may consider the comprehensive description of the methodology and equipment design not significantly relevant to the results. These processes have nevertheless been documented for future students who would continue with research in polymer composites.

The design and manufacture of compression jaws was by far the most resource intensive and time consuming activity of all testing activities. Equipment design and manufacture was part of the scope of the project. Although the jaws were manufactured only after an intensive review process of the design, during commissioning it was realised that the specimens tested did not yield repeatable results when tested at an external test laboratory. The extensive troubleshooting was documented to illustrate that all possible sources of the error in the original design were considered as part of the design review process. Presently, from comparative tests, the error is thought to be due to the test frame and not the compression jaws designed.

Due to there being no conclusive agreement on the source of error, other mechanical tests were investigated. For the model purposes, flexural tests were decided upon as no complex equipment had to be manufactured and the results obtained from testing the specimens in a batch were repeatable with a range. Multiple configurations of measuring displacement were considered in order to obtain acceptable values of modulus.

This carefully documented work would therefore reassure users of its results in that care was taken to ensure that the results are accurate and valid although available non-standard equipment was used in order to obtain the results. It would also provide a reference for future work performed using similar equipment or development of new equipment for specimen preparation and testing.

CONTENTS

ACKNOWLEDGEMENTS.....	ii
ABSTRACT.....	iii
PREFACE.....	iv
LIST OF FIGURES.....	xi
LIST OF TABLES.....	xiv
1 INTRODUCTION.....	1
2 LITERATURE SURVEY	4
2.1 Operational environments.....	4
2.2 Weathering effects.....	7
2.2.1 Exposure tests	8
2.2.2 Degradation studies	9
2.3 Embrittlement	11
2.4 Ultraviolet (UV) radiation effects.....	13
2.5 Hygroscopic effects.....	15
2.5.1 Influence of moisture-induced stress on in-situ fibre strength degradation of unidirectional polymer composite	15
2.5.2 Hygroscopic aspects of Carbon/Epoxy fibre composite laminates in aircrafts	17
2.5.3 Moisture absorption effects on delamination fracture mechanisms of carbon fibre polymeric matrix composites	19
2.5.4 Degradation of fibreglass composites exposed to water.....	21
2.5.5 Effect of hygrothermal ageing on static fatigue of Glass/Epoxy composites	22
2.5.6 The effects of water on Glass-reinforced composites with different matrix materials	23
2.5.7 The effect of moisture on the interfacial strength of Graphite-Epoxy and E-glass/Epoxy composites	24
2.5.8 Effect of moisture on stiffness and strength of Carbon and Aramid laminates	25
2.5.9 Influence of environmental effects on structural stresses	26
2.5.10 Galvanic blistering in carbon fibre composites	26
2.5.11 Osmosis	28
2.6 Temperature effects.....	28
2.7 Combined hygrothermal effects	30

2.8	Mathematical modelling	32
2.8.1	Modelling of moisture absorption by epoxy resin	33
2.8.2	Modelling of the diffusion process	34
2.8.3	Assessing the environmental effect using cross-property correlation methods.....	34
2.8.4	Incorporating non-isothermal physical ageing effects for analysis of mechanical response of linear visco-elastic composite laminates	35
2.8.5	Modelling of environmentally induced damage in infinite composite plate	36
2.8.6	Moisture absorption.....	37
2.8.7	Mathematical model of stress corrosion cracking of GFRP in humid environments	39
2.8.8	Stress predictions	43
2.8.9	Predictions of glass transition temperature and modelling of DMTA relaxation spectra.....	43
2.8.10	Group Interaction Modelling (GIM) technique	44
2.8.11	Moisture induced dimensional changes in composites.....	46
2.8.12	Transverse diffusivity through a random fibre distribution.....	47
2.9	Accelerated environmental exposure testing	50
2.9.1	Ultraviolet (UV) radiation	52
2.9.2	Moisture.....	54
2.9.3	Temperature.....	55
2.9.4	Accelerated environmental testing vs. real environmental exposure.....	55
2.10	Experimental testing	56
2.10.1	Determination of in-plane stiffness properties of the ageing laminate	56
2.10.2	Modal analysis.....	57
2.10.3	Determination of content and distribution of moisture in a laminate	58
2.10.4	Assessing the water uptake by glass-fibre reinforced composites using thermal analysis and dielectric spectroscopy.....	59
2.10.5	Prediction of glass transition temperature and key engineering properties of a dry / wet epoxy based composite matrix	60
2.10.6	Thermo-gravimetric Analysis (TGA)	60
2.10.7	Non-destructive methods for evaluation of environmental damage	61
3	MATHEMATICAL DEGRADATION MODEL	62
3.1	Model of damage progression	63
3.2	Effective stiffness of a fibre reinforced composite containing cracks.....	65
3.3	Stiffness contribution tensor of a fibre	67

3.4	Stiffness contribution tensor of a crack, an approximate representation	68
3.5	Effective elastic properties of fibre reinforced composite containing cracks	70
3.6	Effective conductivity of a fibre reinforced composite containing cracks.	70
3.7	Explicit correlation between elastic and conductive properties.....	71
4	EXPERIMENTAL TEST PREPARATION	74
4.1	Material selection	74
4.2	Laminate manufacture	75
4.3	Exposure locations.....	78
4.4	Exposure frames	79
5	ENVIRONMENTAL CHARACTERISATION	82
5.1	Data.....	82
5.2	Discussion.....	87
6	SPECIMEN INSPECTION	89
6.1	Epoxy.....	89
6.1.1	Visual examination	89
6.1.2	Optical microscopy	91
6.2	Scanning Electron Microscopy – Epoxy	93
6.2.1	8552 epoxy laminates	93
6.2.2	5052 epoxy laminates	97
6.3	Epoxy matrix erosion rates	101
6.4	Vinylester	105
6.4.1	Optical microscopy	105
6.5	Protective measures – Shade Cloth	105
6.5.1	Visual examination	105
6.6	Discussion.....	106
7	COMPRESSION TESTS	112
7.1	Results	112
7.2	Discussion.....	115
8	FLEXURE TESTS	120
8.1	Results	121
8.2	Discussion.....	131
9	ACCELERATED ENVIRONMENTAL AGEING	136
9.1	Environmental chamber design	136
9.2	Test procedure	139
9.3	Results	139
9.3.1	Optical changes.....	139
9.3.2	Mass change.....	140

9.3.3	Strength change	142
9.4	Discussion.....	144
10	EMPIRICAL DEGRADATION MODEL	146
10.1	Empirical data.....	150
10.2	Prediction of resin loss / damage	150
10.3	Strength prediction of epoxy laminates	154
10.4	Discussion.....	158
11	CONCLUSION	161
12	REFERENCES	164
13	APPENDICES	
	Appendix A - Specimen preparation for examination.....	181
	Appendix B - Polishing procedure used for polishing polymer matrix composites.....	184
	Appendix C - Graphical technique for measurement of depth of resin loss.....	186
	Appendix D - Compression fixture design and commissioning.....	187
	Appendix E - Compressive strength data of epoxy laminates.....	198
	Appendix F - Fibre-volume calculation.....	200
	Appendix G - Test method refinement.....	203
	Appendix H - Derivation of dependence of stress on modulus.....	207
	Appendix I - Flexural strength data.....	208
	Appendix J - Environmental chamber maintenance.....	216
	Appendix K - Empirical model data.....	217
	Appendix L - Degradation modelling results.....	222

LIST OF FIGURES

Figure 1 – Sample environmental flight profile [8].....	7
Figure 2 – Lay-up configuration.....	19
Figure 3 a) Initial regular packed fibre array b) Randomly distributed hexagonal fibre array	48
Figure 4 – Principal diffusion axes.....	49
Figure 5 – Energy distribution of a fluorescent lamp compared to sunlight [1].....	52
Figure 6 – Illustration of damage	62
Figure 7 – Progression of damage	64
Figure 8 – Graphical illustration of 8552 cure cycle [226]	76
Figure 9 – Location of test sites in South Africa.....	78
Figure 10 – Variance of solar irradiation with angle of exposure [1]	80
Figure 11 – Exposure panels placed at Durban	81
Figure 12 – Radiation data at test sites.....	83
Figure 13 – Temperature and wind speed at test sites.....	84
Figure 14 – Moisture measurement in the natural environment.....	86
Figure 15 – Surface appearance of 8552 laminates at different exposure periods	89
Figure 16 – Surface appearance of 5052 laminates at different exposure periods	90
Figure 17 – Comparison of the masked area and exposed area of a laminate.....	91
Figure 18 – Cratering on the surface of 8552 epoxy laminates when viewed at 100× magnification after 2.5 months of exposure at Durban.....	91
Figure 19 – Boundary between masked and unmasked areas on 8552 epoxy laminates when viewed at 100× magnification after 2.5 months of exposure at Durban.....	92
Figure 20 – 8552 epoxy laminate transverse weave exposed when viewed at 100× magnification after approximately 9.5 months of exposure at Durban.....	92
Figure 21 – Surface of a 5052 epoxy laminate when viewed at 100× magnification after 2.5 months of exposure at Durban	93
Figure 22 – Unexposed 8552 epoxy laminate	94
Figure 23 – Cracked layer on surface of 8552 epoxy laminates after 5 months of exposure at Durban.....	94
Figure 24 – Uneven surface of 8552 epoxy laminates observed after approximately 9.5 months of exposure at Durban	95
Figure 25 – Loose fibres on the longitudinal tow of 8552 epoxy laminates after 14 months of exposure at Durban.....	96
Figure 26 – Resin attached to loose fibres at the surface	96

Figure 27 – Depth of surface resin on an unexposed 5052 epoxy laminate measured at approximately 40µm	97
Figure 28 – Cracks on the surface of 5052 epoxy laminates after 9.5 months of exposure at Durban.....	98
Figure 29 – Fibre visible through cracks on the surface of 5052 epoxy laminates after 9.5 months of exposure at Durban	98
Figure 30 – Cracks on the surface of a void present in a 5052 epoxy laminate when viewed after 9.5 months exposure at Durban.....	99
Figure 31 – Resin free fibres at the surface of 5052 epoxy laminates.....	99
Figure 32 – Comparison of depth of matrix erosion and / or damage of 8552 and 5052 epoxy laminates	104
Figure 33 – Surface of vinylester when viewed at 100× magnification after exposure at Durban	105
Figure 34 – Comparison of shade cloth protected specimens and unprotected specimens after approximately 9.5 months exposure at Durban	106
Figure 35 – Change in ultimate compressive strength of 8552 epoxy laminates	114
Figure 36 – Change in ultimate compressive strength of 5052 epoxy laminates	115
Figure 37 – Damaged region on a single layer of reinforcement at the surface due to buckling of fibres	117
Figure 38 – Delamination observed on failed laminates	122
Figure 39 – Fracture of exposed surface in compression	122
Figure 40 – Resin breaking free from the exposed surface	123
Figure 41 – Change in flexural strength of 8552 laminates with time	126
Figure 42 – Change in modulus of 5052 laminates with time	129
Figure 43 – Flexural properties of vinylester laminates.....	130
Figure 44 - Characteristics of strength change on 8552 epoxy laminates	132
Figure 45 – Accelerated environment test chamber	137
Figure 46 – Specimen mounting rack.....	138
Figure 47 – Cracks visible originating at voids in a 5052 epoxy laminate after ageing for 96 hours at 80°C	140
Figure 48 – Mass loss incurred on laminates after accelerated UV exposure and accelerated UV / moisture cycling	141
Figure 49 – Mass loss incurred on laminates after water immersion	142
Figure 50 – Relative strength of GRP when subjected to an accelerated UV and moisture environment [250].....	143
Figure 51 – Relative strength of GRP when measured after immersion in water [250].....	143
Figure 52 – Alternative model illustrating layers of resin and reinforcement.....	146

Figure 53 – Alternative degradation model.....	147
Figure 54 – Algorithm to illustrate calculation of laminate flexural strength	149
Figure 55 – Flow diagram used to illustrate calculation of depth of resin loss and / or damage	152
Figure 56 – Predicted material depth loss and / or damage of glass-fibre reinforced epoxy composites	153
Figure 57 – Prediction of laminate flexural strength based on Case 1 degradation behaviour	155
Figure 58 – Prediction of laminate flexural strength based on Case 2 degradation behaviour	156
Figure 59 – Predicted strength of 8552 laminates exposed in a wet climate.....	157
Figure 60 – Predicted strength of 5052 laminates exposed in a wet climate.....	158

LIST OF TABLES

Table 1 – Threshold UV wavelengths for breaking various bonds.	13
Table 2 – Activation spectra for various polymers.....	14
Table 3 – Wavelength regions of UV.....	14
Table 4 – Variety of damage observed on exposed laminates.....	100
Table 5 – Illustration of fibre exposure on the surface of 8552 epoxy laminates with increasing exposure duration.....	102
Table 6 – Illustration of extent of fibre exposure, at 300× magnification, on the surface of 5052 epoxy laminates exposed at Durban.....	103
Table 7 – Degradation rates of epoxy laminates	105
Table 8 – Ultimate compressive strength of unexposed epoxy laminates.....	112
Table 9 – Sensitivity of material properties to changes in depth of specimen for equal applied loads.....	124
Table 10 – Dependence of flexural strength on flexural modulus.....	125
Table 11 – Yellowness measurement of gel coated laminates	140
Table 12 – Percentage mass loss on GRP laminates with gelcoats	141
Table 13 – Test data of 5052 laminates subjected to accelerated UV and alternate exposure cycles	144
Table 14 – Wetness factor calculated for three test sites.....	149
Table 15 – Prediction of depth of damage of epoxy laminates tested.....	153

1 INTRODUCTION

Polymer composites are being used in increasingly new and varied environments as the material gains greater acceptance in industry. Apart from being used to a greater extent in high technology industries, these materials have provided effective solutions to existing problems in industrial and infrastructural applications. As with most materials, the mechanical and physical properties of the material change with time, and this may be considered as ageing due to changes in the structure of the material at a molecular level. The ageing process may be accelerated by environmental factors in the end-use environment causing chemical and physical damage to the material. Damage mechanisms observed are due to the complex interaction of environmental factors. Ideally, once the damage mechanisms are determined, resulting damage may be modelled and change in material properties determined. However, due to the complex interaction of degradation mechanisms, there is currently no complete model to determine the loss of mechanical properties of fibre-reinforced polymer composites with time, based on the environmental conditions to which the material is exposed. Primary environmental variables include radiation, heat and moisture. Secondary variables include factors such as atmospheric pollutants, physical stress and fatigue, biological attack, erosion, marine environments and component incompatibility. The effect of damage due to individual environmental factors has been studied but the results at best describe the response of the material tested using physical laws, to a controlled environment. No complete model has been published that describes the coupling effects of damage mechanism due to various degradation mechanisms acting simultaneously. Environmental degradation of polymer composite materials is thus the subject of continuing research.

Presently, the durability of polymer composites is determined by the results of outdoor exposure tests in the service environment of the material. Prediction of mechanical properties and hence safe service life is based on laminate exposure in the end use environment. Outdoor exposure tests may span several years and at best provide data on a specific material exposed in a specific environment. An alternative to traditional weathering tests is required due to increased consumer expectation of quality and durability. Market forces dictate that increasingly durable products be delivered in the shortest time possible. Due to material improvements, natural exposure tests may now even span decades. Archives of data have thus far been accumulated for a specific material response in a specific environment, generally chosen to be the service environment of the component.

Although both experimental and theoretical work has been performed internationally, this has focussed on North American and European climates, with smaller scale tests reported in Asia

and Australia. Due to the increasing acceptance of polymer composites globally, their use is no longer primarily in specific geographic locations in which the response to the material has already been established. As exposure test results are environment dependent, data on the modes and rate of degradation are gathered from local exposure tests. At present, there is insufficient information on the performance of polymer composites in the Southern African environment. There is therefore a lack of data for the design and maintenance of composite components and structures. South Africa has unique climatic and operating conditions, including temperature considerations, the “ozone hole” (high UV radiation), and industrial pollutants. It is not yet understood how this unique combination of environmental factors impact on the mechanical properties of polymeric materials. Composite structures may therefore be over-designed with respect to durability for use in Southern Africa, inhibiting product optimisation and attempts to minimise cost.

Further, degradation is of concern during the entire life cycle of a product beginning at the design conceptual stage through to the end of life at decommissioning. At the design stage, the degradation behaviour is important, to both determine the choice of material and in the selection of the correct design variables to ensure that the product meets its functional requirements throughout its life cycle. Knowing the change in mechanical properties that can be expected while the material is in service is therefore important in deciding on these parameters. Polymer composites, while offering improved resistance to corrosion in comparison to unprotected steel, are differently affected by environmental factors that result in a change in both physical and mechanical properties. Change in either the physical or mechanical properties may affect the functionality of the design, even if the change is just of an aesthetic nature. Knowing the type of changes, the extent of the changes and the environmental factors that are responsible for those changes are therefore important at the design and in-service stage of component development and use. The end user benefits from knowing the degradation behaviour of the material as such information will assist in optimising maintenance and inspection routines that are applicable to the specific environment in which the material is being used.

Failure to understand the degradation mechanisms, their rates and their effect on the component may result in catastrophic failure. Also failure of components due to material failure would result in costly down time and reduce the return on investment of the product.

As an alternative method to determine the response of polymer composites to the natural environment, accelerated exposure testing is conducted. Accelerated exposure tests entail exposing the material to environmental factors encountered in the natural environment, but at a higher intensity to accelerate the degradation. Specimens subjected to accelerated conditioning

in environmental chambers require much shorter conditioning time, as compared to outdoor exposure, to reach the same conditioning parameters. The conditioning parameters may be weight increase due to moisture or exposure to a specific quantity of ultraviolet radiation. The importance of an accelerated test programme and / or mathematical simulation has been outlined at a number of conferences and new committees have been formed within the American Society for Testing and Materials, to focus on the development of the methodology for prediction of service life through weathering [1]. Accelerated weathering techniques are generally used on a comparative basis to compare materials. It is at present difficult to correlate accelerated test results with real-time exposure [2]. This is due to the complex interaction of weathering mechanisms found in polymer composites being dependent on intensity of degradation factors during exposure. The results from accelerated exposure tests need to be used with caution, as accelerated conditioning may not accelerate all degradation processes equally [2].

A study has been initiated to determine the modes of degradation, rate of damage propagation and rate of change of mechanical properties of polymer composites exposed in the Southern African climate. The approach planned uses the combination of mathematical modelling, empirical techniques, natural exposure and accelerated exposure testing. This study includes examination and testing of glass-fibre reinforced laminates removed periodically from exposure racks in the natural environment. The exposure racks have been placed in climatically different locations representing the range of climates experienced in Southern Africa. Data from these tests will be used as input to a model that would enable the safe service life of the material to be estimated based on the rates of degradation measured and damage observed. Also, accelerated exposure testing performed would enable comparison of the effectiveness of selected gelcoats and provide data that may be used to establish a correlation between natural and accelerated exposure. Information gathered from testing will be used to provide design data for composite components in Southern Africa, optimise maintenance schedules for composite components and determine when strength has been compromised. By determining the predominant causes of degradation, investigation into possible approaches to protect composite components cheaply and simply for maximum service life may be undertaken. Such an investigation has been initiated by exposing laminates in the environment under the protection of woven netting referred to as shade cloth.

The science of environmental degradation continues to progress with the development of mathematical models and greater understanding of the degradation mechanisms involved. Current and future work by researchers in this field will add to the database containing the response of a range of polymer composites exposed in varied environments.

2 LITERATURE SURVEY

The voluminous body of research available on environmental degradation of polymer composites may be classified into three categories, namely, analysis of degradation based on principle physical laws, analysis of degradation based on characterisation of observed damage mechanisms and quantifying changes in properties with increasing damage. Due to the present incomplete understanding of degradation and variation in results among tests performed, test methodologies are being refined to measure as accurately as possible the causes and effect of damage induced on polymer composites and to facilitate understanding of the coupling of damage mechanisms. Thus the body of knowledge on polymer composite degradation is presently increasing.

The extensive literature review that follows provides the knowledge-base with which degradation mechanism development and propagation can be understood. Due to the complex coupling of degradation factors, the broad knowledge base assists in designing tests to improve upon and accelerate the understanding of the degradation of polymer composites. An extensive review of the literature of polymer composite degradation was previously performed as part of an environmental degradation study [3]. The review included degradation of polymer composites in applications ranging from marine to aerospace structures, degradation due to individual factors of acidic environments, temperature and moisture effects and concluded with a review of mathematical models to describe individual degradation mechanisms. Chapters from this study are included in the current chapter to provide a comprehensive review of the current state of knowledge.

2.1 Operational environments

Usually most fibre-reinforced materials are exposed only to the Earth's atmosphere. The average chemical composition, excluding water vapour, of the Earth's atmosphere is nitrogen 78%, oxygen 21%, argon <1%, and carbon dioxide 0,03% by volume. Prolonged exposure to the atmosphere gives rise to chemical and physical changes in polymers and composite materials. The polymers may absorb moisture from the natural environment, which subsequently cause dimensional changes and hence internal stress. Absorbed water may seek out and dissolve water-soluble inclusions, thereby creating pockets of concentrated solutions. This may lead to a loss of mechanical strength of the composite. The mechanisms of degradation range from static fatigue of fibres and creation of osmotic pressure filled interfacial cracks, to shattering due to crystallization of water. The consequent losses in mechanical properties can be, for carbon-fibre/epoxy resin composites, of the order of 50% for compressive strength and 10% for tensile strength.

Composite materials are progressively gaining acceptance for use in offshore applications, where their perceived virtues of low weight and good corrosion resistance are much sought after by designers and operators. Glass fibre reinforced plastics (GRP) in particular have won widespread acceptance in non-structural applications, including fire water piping, decking and cable trays. There is however considerable interest in the use of GRP of various types in more demanding applications offshore. Such new applications involve using the material in contact with aggressive process fluids at elevated temperatures. Examples of applications under consideration include separator vessels (where various hydrocarbons and water are present at 70-80°C, with possible excursions above 100°C), sub-sea flow lines and, perhaps the most demanding application, down hole tubing and drill stream parts. Although the temperatures involved in the most demanding down hole applications are too high to permit the use of organic matrix composites, there is a range of applications where the temperatures are somewhat lower and GRP offers significant potential advantages.

The prospect of large oil reserves at 2000m of ocean depth has created a significant interest in the possibility of using polymeric composite tubulars for both drilling risers and production risers. The higher specific strength of polymeric composite material systems can potentially allow conventional equipment designed for drilling and oil production using floating ships and platforms, for depths of less than 1000m, to be used at these greater depths by reducing the hanging weight of the tubulars. The potential use of polymeric matrix composites for offshore applications has been recently reviewed [4] and the economic feasibility of using polymeric composite tubulars for production risers has already been demonstrated [5].

As the world's land and shallow depth off-shore oil reserves are being depleted, there will be the need to drill for oil at even greater depths. Economic oil recovery at depths of 9000m or more will require new lightweight designs and new material systems with high specific stiffness and specific strength [6]. Many applications are being developed in this field, which utilize fibre reinforced polymers. Some of these applications include tubing tailored for bending, tension, and pressure, large-diameter tethers, risers, mooring rope, tubing having a low coefficient of thermal expansion and drill pipe for horizontal and extended reach wells.

Polymeric matrix composites are known to have excellent fatigue resistance, corrosion resistance and can be tailored to give optimal combinations of stiffness, strength, and thermal expansion by proper ply sequencing. The two technical obstacles to the use of polymeric composite materials for offshore risers are joining and long-term durability. While polymeric composite materials do not corrode like metals, they do absorb moisture, generally 1 - 3% of the weight of the matrix. This absorbed moisture can potentially soften the matrix, reduce the

strength of the glass fibres (carbon fibres appear to be much less affected by moisture), and / or degrade the strength of the fibre-matrix interface. Since production risers will be immersed continuously for 10 to 20 years, they will certainly reach saturation levels of moisture absorption eventually. Thermoplastic composites are required to perform over a wide temperature range. The mechanical performance of thermoplastics, including tensile strength and modulus, chemical resistance, and even electrical properties are temperature dependent. Thus, the design engineer must consider temperature as one of the important design parameters in addition to low cost manufacturing processes.

Aircraft systems such as High Speed Civil Transport (HSCT) experience severe cyclic environments during normal operations. Aircraft skins reach extreme temperatures due to high vehicle speeds. These temperatures accelerate the diffusion of moisture and oxygen into the material. This in turn can cause property changes and / or permanent material degradation. An example of exposure cycle with time-dependent temperature and moisture levels is shown in Figure 1 overleaf. Similar cycles may be repeated over 20,000 times in an aircraft's lifetime. Under such conditions, thermal, hygroscopic, and chemical degradation effects result in a complex and time-varying stress profile over the course of many use-cycles.

Another group of environmental agents that cause damage to composites are electromagnetic effects; fire [7]; lightning and electrical discharges; ozone (chemical degradation); ultra-violet radiation; out-gassing at high-vacuum; erosion by rain and sand, etc.; low-energy impacts (e.g. by hail or gravel) that induce Barely Visible Impact Damage (BVID); contact with organic liquids such as fuels, lubricants and de-icing fluids. During normal service, aircrafts are exposed to all these agents in a time-variable manner [8].

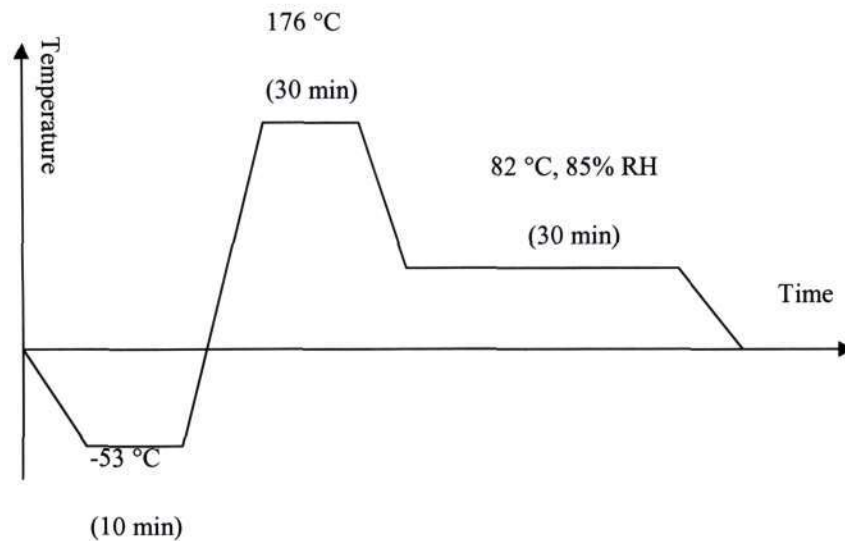


Figure 1 - Sample environmental flight profile [8].

Polymer composites are thus finding increasing use in marine, land, air and space applications. Besides the environments described above, composites are used in harsh industrial environments found in the manufacturing and processing industries. These environments can be particularly harsh (high stresses, high temperatures and acidic environments) due to the functional requirements of a process.

Together with meeting functional requirements, composites also need to display good resistance to weathering in the end-use environment. Poor weathering resistance increases the cost of maintaining the composite structures exposed to the environment, by either additional cost of providing shelter for the structure from the natural elements, or increasing the number of inspections performed on the exposed structure. Although composites are used in varied environments, this study specifically examines the degradation of polymer composites due to exposure in the natural climate, viz. to determine the effect of weathering on land based composites.

2.2 Weathering effects

Research, available in the literature, has been conducted to determine the change of bulk material properties with time due to exposure in natural and selected operational environments. The effect of environment on integrity of composite panels that have been repaired has also been reported. With most published tests, the test specimens were placed in the natural environment and sampled to determine the changes in the polymer composite. Thus the cumulative action of climate factors, also referred to as weathering, would result in the

degradation of the composite. Weathering studies were found to be of two types i.e. exposure tests and degradation studies. Exposure tests generally documented strength changes and descriptions of physical changes observed at selected time intervals. However degradation studies presented data on mechanical and physical changes as well as some type of analysis to determine the action of underlying degradation mechanisms. Both types of weathering studies are relevant to the general study of degradation polymer composites and have been reviewed.

2.2.1 Exposure tests

Environmental exposure tests conducted over a 10 year period in Brazil, North America, Germany and New Zealand, on both stressed and unstressed laminates, have been documented by Dexter [9]. The tests performed on ground-based and in-flight specimens, were conducted to determine service life of composite materials used in the manufacture of aircraft components. From examination of strength and modulus data after different exposure durations, Dexter concluded that damage / degradation is dependent on the type of material and specific climatic factors at the exposure location. Moisture absorption was most severe in humid climates and where intense ultraviolet radiation was predominant, causing the most degradation to resin and fibres. Unprotected specimens were observed to be most affected by exposure with no significant effect between stressed and unstressed, quasi-isotropic, graphite-epoxy, tensile specimens being measured. Over the ten year exposure period, an average of 25% strength loss was measured on most materials tested.

Chester and Baker [95] focused on the degradation of a specific aerospace material at tropical test sites in Australia and Malaysia. Changes in mass of specimens protected from direct solar radiation was thought to be due to absorption of water from the air, however it was noted that it is not possible to make accurate conclusions about the amount of water absorbed as the competing weight loss due to resin or paint degradation was difficult to quantify. Unpainted specimens appeared to lose weight almost immediately due to rapid degradation of surface layers of epoxy resin by UV radiation. Material was initially rapidly lost from the surface of the specimen and thereafter the rate of weight-loss slowed and eventually stabilised. The subsequent slow continuing weight loss was attributed to the bare surface fibres being removed from the surface by wind and rain exposing undamaged resin beneath. Conclusions of the study were that composite aircraft components rapidly degrade when unprotected by a primer or paint finish, and should be sheltered from UV exposure which was found to be the most damaging environmental factor.

Komorowski [10] reported test results on exposure panels mounted on-board carrier ships with the aim of determining the response of the material to a marine environment. Yoosefinejad and

Hogg [11] have reported test results on mechanical property degradation of composite components in the building industry after 20 years of service. The components of the bus shelter examined, showed a 40% decrease in strength when compared to new panels. The panels did not support any structural loads for a significant period while in service. Deterioration in strength has been attributed primarily to weathering. Cracks were found in the gel coat during examination of the components.

Fukuda [12] has reported results on an outdoor exposure test, over a period of five years, that was conducted in Japan. No significant change in flexural strength and modulus of exposed specimens was measured after three years of exposure, but the surface coating had sustained damage during this period.

Environmental exposure tests of polymer composite materials have been reported in North America, Europe, Asia, and Australia. The archives of data collected do not in themselves explain the degradation of the material. It is simply mechanical properties of a specific material measured after various exposure durations in a specific location or climate.

2.2.2 Degradation studies

Exposure tests in the warm, humid conditions at the Black Sea have been reported by Startsev and Krotov [13] in which both increases in micro and macro-heterogeneity were reported. Increases in heterogeneity resulted in a gradient of strength, deformational and thermal properties across the thickness. Moisture diffusion was found to be the most sensitive parameter to changes on the surface due to exposure. The efficiency of the diffusion model used was highlighted. Due to a gradient in strength across the thickness, the inaccuracy of standard tests in determining the strength of the material was highlighted and the change in interlayer shear strength with depth of aged specimens was graphically illustrated. The dependence of interlayer shear strength on depth has been ascribed to the outer layers being primarily affected by the climate with the properties of the inner layers being closest to the initial properties. Further research reported by Startsev *et al* [14] quantified the gradient of mechanical properties on polymer composites exposed at Batumi on the Black Sea coast. It was found that the surface layer exposed to solar radiation was destroyed and disrupted to a greater extent than subsurface layers and the gradient of mechanical properties across the thickness was found to be significant. Analysis of laminates showed that post-curing and destruction of the matrix occur simultaneously. Mechanical properties were found to be dependent on both changes in the fibre-matrix interface and changes in the structure of the matrix due to natural exposure. The combined effect of gamma radiation and climatic exposure was performed as a separate study

by Startsev *et al* [15]. Gamma radiation was found to cause damage to the fibre-matrix interface while further cross-linking after manufacture was found to be negligible.

Dubois *et al* [16] have studied degradation due to artificial and natural ageing using a method allowing for the morphological evolution analysis of the surface. Accurate measurements of loss of the material from the surface was performed using 3-D surface scanning. Material loss from the surface was described as the materials observable response to photo-oxidation. The study confirmed the presence of a photo-oxidative layer close to the surface with the rate of material loss from the surface layer found to be strongly influenced by hydrolysis due to leaching. Chemical processes have been proposed based on the results of physico-chemical analysis of the surface. The rate of progression of the photo-oxidised layer, without leaching, was found to be constant and equal to the speed of material loss from the surface initiated by the loss of volatile photo-oxidised products. It was suggested that in the natural environment, rain provokes hydrolysis and loss of molecular fragments from the photo-oxidised layer resulting in larger quantities of material being lost from the surface. Material loss measured was found to affect 1% of the thickness and it has been suggested that degradation of the surface is considerable when compared to the interior of the laminate. Measurements of interlayer shear strength and moisture diffusion appear to confirm the assumption that degradation is primarily a matrix phenomena.

McManus *et al* [17] have considered modelling degradation by assembling models describing fundamental material mechanisms of thermal, oxygen and moisture diffusion, chemical reactions, composite micromechanics, modified laminated plate theory and fracture mechanics. The models are coupled resulting in dependencies between material mechanisms. A diffusion model was developed to predict the growth of a degraded layer of material at the surface. Coupling this model to the moisture analysis model and applying typical flight cycles as input, the results obtained from this composite model revealed that degradation occurred at the surface and proceeded slowly into the interior. Applying a stress field due to mechanical, thermal, hygro and degradation-shrinkage-induced stress, the severe stresses that build-up in the degraded layer were illustrated. Due to these stresses and low material toughness at the surface, microcracking was predicted using a previously developed computer code. No cracking was predicted at the interior of specimens which are relatively unaffected by moisture and degradation, and not sufficiently stressed by thermal cycling to crack. Microcracking, as predicted by the model, was qualitatively confirmed by observation of extensive cracking not more than a millimetre in depth from a surface of a polyimide composite. In the cases examined, the combination of models has assisted in explaining observed phenomena but a complete model for describing the degradation of polymer composites was not established.

Choi *et al* [18] examined the problem of fracture initiation in polymers. The model proposed was based on the observation that degradation of polymers was manifested by, amongst other factors, reduction of molecular weight and reduction in toughness. Fracture initiation was thought to be due to shrinkage of the degraded layer being constrained by adjacent undamaged material resulting in tensile stresses within the degraded layer. These stresses would be in addition to pre-existing manufacturing stresses and service stresses. At a certain level of degradation, the combination of toughness reduction and increased tensile stresses is thought to result in fracture initiation. From observation of specimens, microcracks that have formed an irregular cell pattern were orientated along maximum shear stress directions. Upon examination of polymer tubing, the depth of cracks was found to be approximately two orders of magnitude smaller than the wall thickness of the tube, and independence of stresses with respect to depth of the surface layer was illustrated.

Characterisation of the damaged surface layer by molecular weight [18] and its relationship to toughness was described in terms of the structure of polymers as follows. Polymers consist of single units (monomers) combined (by polymerisation) to form long, chain molecules. The properties of the polymer are largely influenced by the chemical makeup and structure of the molecular chains. As polymerisation proceeds, the chain lengths increase with a resulting increase in molecular weight. Mechanical properties such as tensile and impact strength, toughness and yield strength increase with increasing molecular weight. Degradation resulting in breaking up of the molecular chain (chain scission) results in decreasing molecular weight and consequently lower mechanical properties.

On the basis of the literature survey [3 - 29], it would appear that environmental degradation, and particularly the damage resulting from exposure to outdoor conditions is primarily a matrix process, with damage beginning at a degraded layer on the exposed surface. On unprotected laminates, the loss of matrix material from the surface was observed in all cases.

2.3 Embrittlement

In tests reviewed some type of embrittlement occurred, whether on the surface or subsurface, which may have resulted in the decrease in mechanical properties of the laminates. Embrittlement may be defined as the reduction in the elasticity of a material due to chemical or physical factors. Brittle material that may be easily fractured or cracked, and its development is thought to be due to chain scission within the polymer. The deterioration of properties may be due to a preferential attack of load bearing components or irregularities in the material. Cracks observed on the surface layer of weathered laminates, may result in the embrittlement of

material at the surface constituting the degraded layer. Work performed on polymer embrittlement [10 - 20] has been presented by White and Turnbull [2] in a review study of polymer degradation.

So and Broutman [19][20] have studied the effects of a brittle surface layer and found that cracks at the surface can facilitate the failure of less degraded material below the embrittled layer. The critical flaw size given by linear elastic fracture mechanics correlated well with thickness of a layer containing cracks. Similar work by Wolkowicz and Gagger [21], in which the impact resistance of thermally aged ABS recovered significantly after the degraded layer was scraped away, supports the theory that an embrittled layer may facilitate failure of less degraded material.

Schoolenberg [22][23] observed that the depth of embrittlement of weathered polymers does not necessarily equal the depth of the surface cracks as, though there may be a distinct layer of embrittled material, degradation may occur at a greater depth. Also embrittlement due to UV exposure was observed [24]. Karpukhin [25], upon investigation of crack depth, has reported that the crack depth calculated is equal to the depth of the oxidised layer. The formation and propagation of cracks in the case examined is thought to be due to shrinkage stresses.

A decrease followed by an increase in fracture energy after prolonged exposures was observed by Schoolenberg and Meijer [26] on specimens that were exposed to radiation. The fluctuation in fracture energy recorded at different stages of exposure is thought to be due to the degraded layer becoming too weak to transmit stresses to the interior when strained. Work performed by Magnus [27] in which degradation was observed to occur in cycles supports the conclusion by Schoolenberg and Meijer. Magnus explained the results in terms of a formation of a brittle layer followed by a loss of material, of the order of a few micrometers, from the brittle layer. Material loss is accompanied by partial recovery of colouration and mechanical properties. Magnus refers to the cycling as multilayer weathering which can be noticed under severe weathering conditions. In temperate climates, the cycles may occur over long time periods.

Damage at an existing flaw within the material may lead to it becoming the critical flaw rather than surface cracks [28]. Qayyum and White found that when the surface facing the sun becomes sufficiently degraded that fracture cannot nucleate, failure may then nucleate in the less degraded material at a greater depth [29].

Thus weathering produces aesthetic, physical and mechanical changes in laminates. It is expected that the specific climatic factors of ultraviolet radiation, moisture and temperature are

responsible for the changes in the chemical structure of the constituents of laminates. Various studies have been conducted (the review of which follows) to establish the mechanism of degradation of the individual effects in an attempt to understand its contribution to the final degraded state of the composite material.

2.4 Ultraviolet (UV) radiation effects.

UV-light is known to be the form of radiation responsible for weathering. Electromagnetic radiation is commonly divided into the following groups according to increasing wavelength; gamma rays, X-rays, UV, visible light, infra-red, microwaves and radio waves. The Earth's atmosphere filters out the gamma rays, X-rays and the lower wavelength UV. The shortest sunlight wavelength found on Earth is about 295nm. UV (295nm to 400nm) constitutes only 5% of the sunlight falling on Earth, however these short wavelengths are responsible for virtually all the damage to polymers.

Quantum theory states that light comes in discrete particles, photons. The photon size is inversely proportional to the wavelength. That is, the shorter the wavelength, the bigger the photon. Photochemical reactions are caused by a single photon colliding with a single electron. If the photon is "big" enough (that is, if it contains more energy than the organic bond strength), the electron is knocked out of its orbit and a reaction occurs. For each type of chemical bond, there is a critical threshold size photon (and hence a threshold wavelength) with enough energy to cause a reaction. Light of any wavelength shorter than the threshold wavelength can break the bond, however wavelengths longer than the threshold cannot break the bond - regardless of the intensity (brightness). For example, if a certain plastic is only sensitive to wavelengths below 295 nm (the solar cut-off point), it will never deteriorate outdoors. Table 1 shows various dissociation energies for common bonds and the respective threshold wavelengths.

Table 1 - Threshold UV wavelengths for breaking various bonds.

Bond	Dissociation Energy [kCal/g·mol]	Threshold Wavelength [nm]
C-N	72.8	392.7
C-Cl	81.0	353.0
C-C	82.6	346.1
S-H	83.0	344.5
N-H	85.0	336.4
C-O	85.5	334.4
C-H	98.7	289.7

*All wavelengths shorter than the threshold have sufficient energy to break the bond.

Table 2 shows the threshold wavelengths which lie in the UV-range. On Earth, the UV in sunlight is the only part of the spectrum responsible for photochemical damage.

Table 2 - Activation spectra for various polymers.

Polymer	Wavelength of maximum damage
Polyvinyl acetate film	<280
Polycarbonate film	285, 305, 330, 360
SAN film	290, 325
CAB film	295, 298
Polyethylene	370
Polypropylene	300, 310
PVC	320
Polyester	325
PVC/vinyl acetate copolymer	327, 364

UV is divided into three regions, as appears in Table 3, UV-A, UV-B and UV-C. In summary, the shorter the wavelength - the more readily it is absorbed and therefore the more harmful it is. This explains why the Sun's lower wavelengths are absorbed by the atmosphere, and why UV-B is absorbed by window glass. This also suggests that shorter wavelengths are more susceptible to absorption by transparent media such as air and glass as mentioned above.

Table 3 - Wavelength regions of UV

UV-A 315-400 nm	Causes some polymer degradation. Causes suntan but not sunburn. Transmitted by window glass.
UV-B 280-315 nm	Shortest wavelength in sunlight at the surface of the Earth. Responsible for most polymer damage. Causes sunburn. Absorbed by window glass.
UV-C below 280 nm	Found in sunlight only in outer space. Filtered out by ozone in atmosphere. Can cause abnormal reactions. Germicidal: kills micro organisms.

Exposure to sunlight causes physical degradation of surface layers of polymers about 10nm in depth. This depth is sufficient to reduce the intensity of ultraviolet light to half its initial value. Degradation proceeds by composites absorbing radiation in this range resulting in the breaking of chemical bonds. UV radiation is frequently responsible for the initiation of weathering degradation [1]. The mechanism of degradation by photo-oxidation is due to the formation of radicals caused by the breakdown of long chain polymer molecules, which when unstable undergo scission reactions [2] resulting in shrinkage and embrittlement. The process is initiated by collision of a photon with sufficient energy with a polymer molecule. Osawa *et al* [30] have found that these type of reactions may proceed slowly in the absence of sunlight.

2.5 Hygroscopic effects

The study of hygroscopic effects relate to the effect of moisture on composite laminates. This would include determining the method of water uptake and its effect on physical dimensions and resulting associated stresses. The study also includes the effect of moisture on the chemistry of the constituents in an attempt to understand changes in mechanical properties as a result of the moisture absorption.

Naturally, materials will be exposed to moisture in the form of rain, humidity and condensation. The effect of moisture has been investigated in depth by Springer *et al* and published in three volumes [31]. Moisture generally produces a plasticization of the matrix in epoxies which result in a decrease in mechanical properties. This plasticization may appear to improve the mechanical properties of the laminate under ambient conditions [32], but the elevated temperature performance of the laminate decreases. Hydrocarbon-like, low polarity polymers have excellent resistance to moisture absorption but fibre bonding is relatively poor [32], hence the effect of moisture should not be considered in isolation. Further, absorption of water may cause swelling which would result in stresses being developed within the laminate. These stresses may develop even if the laminate is allowed to expand freely. The stress would in such a case be due to the constraints imposed by adjacent plies of a single lamina in a laminate. Some polymers undergo hydrolysis that may lead to chain scission and hence a reduction in mechanical properties. Cold water falling on a warm surface may produce thermal shock resulting in surface cracking [33]. Further, a wet period followed by a dry period may result in volume expansion and contraction resulting in stress reversals. Such cycling of stresses result in chemical and mechanical damage. The extent to which diffusion takes place within the laminate depends upon the constituent materials and not only the physical parameters of the external environment. Tests performed to investigate the rapid diffusion of moisture into jute composites have found that the low activation energy of diffusion in the jute composite was factor that resulted in a high moisture diffusion coefficient [31]. Internal properties that affect the diffusion of moisture into the laminate include fibre orientation to the diffusion direction. This effect is significant on impermeable fibres and increases as the fibre angle to the direction of diffusion increases [31]. The dependency of moisture diffusion on fibre angle was not as pronounced when permeable fibres were used.

2.5.1 Influence of moisture-induced stress on in-situ fibre strength degradation of unidirectional polymer composite

Assessing retention/degradation of properties during environmental ageing of composites, especially for glass fibre composites, requires analysis of:

- Hygrothermal stresses;
- Change in physico-chemical nature of the constituents;
- Damage mechanisms and damage modes resulting from different stress states and environmental loads.

Liao and Tan [34] have shown that zero-stress ageing of unidirectional composite under hygrothermal loads does not imply that fibre and matrix are stress free. Rather there are internal stresses, induced by hygrothermal loads. These stresses accelerate the rate of strength degradation. This conclusion was drawn from a widely accepted strength degradation model for slow crack growth for glasses and glass fibres, Equation (1) [35, 36]:

$$V = V_0 \exp \left[\left(-E^* + \frac{bK_I}{RT} \right) \right] \quad (1)$$

where V is crack velocity; and V_0 , E^* and b are constants. E^* is known as the apparent activation energy at zero load and it does not vary strongly with environments [36]. The crack velocity is related to the magnitude of applied stress, σ , through the expression of mode I stress intensity factor, K_I

$$K_I = Y\sigma\sqrt{a}, \quad (2)$$

where Y is a geometric parameter and a the crack size. Equations (1) and (2) show that the rate of fibre strength degradation depends on applied tensile stress and temperature. Therefore contribution from moisture-induced stresses should be taken into consideration when interpreting results from environmental ageing experiments.

Changes in physico-chemical nature of the constituents during environmental ageing include dissolution of matrix and the sizing, as well as corrosion of the fibre surface [37]. Damage mechanisms may be different under different ageing conditions. For instance, fibre/matrix debonding is promoted by radial stress at high moisture content and elevated temperatures. Once fibre/matrix debonding has occurred, the internal stress-state is altered and more moisture will diffuse into the debonded regions, which further accelerates the degradation process. Despite these more complicated scenarios involving coupled processes, a first step for correlating accelerated ageing results is to obtain a reasonable estimation of the stress-state in the material.

It has also been established by Liao and Tan that strength of glass and ceramic materials is related to the fracture mirror size [34] through the following empirical relation:

$$\sqrt{r}\sigma_u = A, \quad (3)$$

where r is the radius of the fracture mirror, σ_u the breaking stress, and A the material constant. Since σ_u is inversely proportional to \sqrt{r} , therefore by measuring fracture mirror size, r , the strength of a fibre can be estimated.

Results of zero stress ageing of glass fibres in water from previous studies suggest that strength degradation is negligible at room temperature for the time of about 10^7 s. Haslov *et al* showed that no strength degradation has occurred in acrylate coated optical fibres before 300 days of stress-free ageing in water at 65°C. However, the strength degradation process is accelerated under applied tensile stress, a phenomenon known as stress corrosion. It has been shown in a previous study that the strength of glass fibres does degrade in a pultruded composite during stress free ageing in water at room and elevated temperatures [38].

2.5.2 Hygroscopic aspects of Carbon/Epoxy fibre composite laminates in aircrafts

Primary and secondary composite structures used in state of the art aircraft usually experience repeated absorption/de-absorption of water in a wide range of humidity and temperature. This type of non-mechanical fatigue is considered to be closely associated with the long-term durability of composite materials especially when the water absorption is accompanied with high environmental variations of temperature and pressure as well as mechanical load variations during the service usage of aircraft. Accordingly, for the applications of high performance composite materials in aircraft environments, the composite materials have been strongly required to satisfy the hot-wet mechanical properties designated in the material specifications, where the specimens are tested after being exposed to water at high temperatures for a specified time [39].

A change in temperature and moisture content usually induces hygrothermal forces and moment resultants as well as dimensional changes in the composite body. In addition, the thermal stresses produced during the cooling process of composite laminate after cure at elevated temperature could be combined with hygrothermal stresses [40,41]. The resulting hygrothermal and mechanical stresses combined with each other may be sufficiently large enough to influence the failure of the laminate and thus should not be neglected in modern design analysis and lifetime estimation. Furthermore, the recursive changes of internal stresses due to water absorption–de-absorption processes may induce fatigue damage in the inter- and intra-laminar regions of composite laminates influencing long-term durability and performance of composites [42]. In addition, in the field of composite applications utilizing electric and electromagnetic characteristics of carbon fibre reinforced composite, the water absorption is one of the key

issues that should be addressed. The composite laminates exposed to water for a time usually swell and thus the interfacial characteristics and local stress concentration of matrix and fibres tend to change and then consequently influence the electric conductivity. Accordingly, the electric resistivity and the closely related conductivity is known to be proportional to the square of the moisture weight gain in the longitudinal direction of epoxy/carbon fibre composite laminate [43].

Hygroscopic effects on carbon/epoxy composites were studied by Choi *et al* [44] and it was found that the diffusion coefficient in the 95% RH chamber is smaller than the one immersed in the liquid water bath at the same temperature (70°C). However, the equilibrium water uptake obtained in the humidity chamber shows a larger amount of saturated water uptake than in the water bath. In contrast, the isothermal experimental results found the equilibrium water uptake at lower temperatures (35°C) higher than the one at higher temperatures (95°C) under hygrothermal conditioning. When temperature changes suddenly from 95°C to 35°C, the additional gain of the composite specimen is about 0.25%. This unexpected behaviour of water uptake has been viewed and analysed by assuming two hypothetical states of water, as bound water and free water [45,46,47,48]. The bound water may be viewed as a reversible thermodynamic quantity. Complying with Henry's law, it is known that the amount of bound water decreases as temperature increases. The free water was assumed to be immobilized by irreversible micro-cavitation damage or crazing in hygrothermal environmental conditions. Accordingly, the amount of free water increases with hygrothermal temperature in an irreversible way.

It was also observed [44] that the glass transition temperature decreases linearly with the increment of moisture absorption. It was found that the moisture absorption behaviour is affected by the hygro-thermal temperature history. The diffusion coefficient increases with the increment of matrix volume ratio and void volume ratio, which seemed to deviate from the Fickian water absorption mode. For the water absorption in the through-thickness direction, the laminate thickness or lay-up sequence does not affect the diffusion rate or equilibrium water uptake. However, the water absorption rate of 90°-z composite laminates (Figure 2) is greater than 90°-y because of the interlaminar resin-rich area usually present in thick composite laminates. As a result the curvature of [0/90] specimens decreases with the increment of water absorption due to the release of internal stresses resulting from the plasticisation of water molecules.

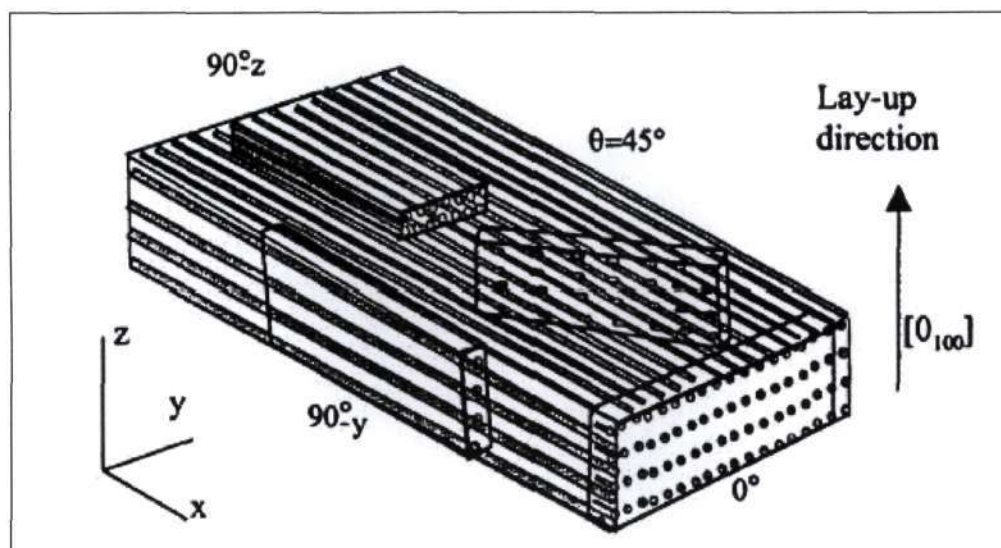


Figure 2 - Lay-up configuration.

2.5.3 Moisture absorption effects on delamination fracture mechanisms of carbon fibre polymeric matrix composites

Depending on matrix phase chemistry, water or other fluids that are absorbed by the bulk matrix and by the interface can induce degradation. For most thermoset (epoxy) composites, the absorption of moisture modifies the strength, stiffness, and delamination fracture behaviour [49, 50, 51, 52, 53, 54]. In contrast, for thermoplastic (PEEK, poly-ether-etherketone) composites, experimental results show essentially no effect of moisture on longitudinal or transverse mechanical properties. Moisture-induced property degradation manifests a strong correlation with the degree of moisture absorbed by the matrix. The rate of moisture absorption and the solubility limits are governed by the matrix phase chemistry and by the fibre/matrix interface composition. Moisture absorption can be up to 10 times greater in thermoset composites than in thermoplastic composites. Moisture-related degradation is associated with chemi-absorption and reactivity characteristics of the permeating environment and matrix materials. Moreover, defects such as voids, cracks, and other micro-structural inhomogeneities associated with the fibre/matrix interface contribute to the severity of moisture effects in resin matrix composites [55]. Environmental effects such as moisture, on static (strength and stiffness) properties of PMC's have been relatively well studied compared to the effects of moisture on fracture mechanisms and crack propagation behaviour.

Studies [53,56] have shown that the fracture toughness of Graphite/PEEK thermoplastics is unaffected by moisture absorption. The striking difference in moisture-induced delamination fracture toughness (DFT) between thermoset and thermoplastic composites is attributed

partially to the fact that thermoset resin matrix composites absorb considerably more moisture than do thermoplastic resin matrix composites. As a consequence, plasticisation of the matrix and interfacial regions is substantially more severe for thermoset matrix composites. Moisture saturation levels (M_{∞}) for Graphite/PEEK and Graphite/Epoxy laminates are $\sim 0.2\%$ and $\sim 2\%$, respectively. Absorption of moisture in Graphite/Epoxy laminates is about 10 times greater than in Graphite/thermoplastic laminates. The maximum moisture content is dependant on other factors such as fibre volume fraction, void content, residual stress resin composition, etc. Nonetheless, M_{∞} for thermoplastics laminates is considerably less. It has been suggested that plasticisation of the matrix can lead to an increase in delamination fracture toughness [57, 58]. The fact that DFT should increase was attributed to the enhancement in the moisture-induced crack tip plastic zone size. The suggestion was made, that the increase in plastic zone size due to plasticisation enhances plastic energy dissipation at the crack tip, thus, effectively increasing the fracture toughness of the laminate. The decrease in the laminate fracture toughness was observed in the study of Lucas *et al* [59] with matrix plasticisation (softening) in contrast to the previously published results [57, 58]. This dichotomy can be rationalized by realizing that there is a competing effect of plasticisation to dissipate crack tip strain energy, and thus enhance fracture toughness. This competing effect is the weakening of the bulk matrix and the fibre/matrix interface in the laminate due to matrix plasticisation by absorbed moisture.

Morgan [60, 61] and others [53, 62, 63] have reported several degrading effects of moisture on physical and mechanical properties of thermoset resins. Among these effects is that moisture lowers the tensile strength, elongation and modulus of epoxy. Also, absorbed moisture tended to enhance the susceptibility of the matrix to cavitation and plastic flow processes. Examination of the crack tip region shows major cracking in the interfacial region and micro-crack link up of the inter-matrix region with interfacial cracking. In addition to the primary fracture along the interfacial region, significant secondary cracking was also observed. The secondary cracking is caused presumably, by residual stresses in the matrix resin as a result of plasticisation by moisture.

Irrespective of the testing method, absorbed moisture was found to have no significant effect on the delamination fracture of the PEEK/IM6 laminate [59]. However, moisture induced degradation was quite evident for the 934/T300 composite laminate. The delamination fracture toughness of the 934/T300 composite laminate was lowered by approximately 60% after sustained exposure to moisture. Plasticisation of the bulk matrix and the interface by absorbed moisture influenced the reduction in fracture toughness. Moisture induced plasticisation caused the resin softening and strength loss. Moreover, moisture tended to weaken resin in vicinity of the fibre/matrix interface. It was concluded [59] that preferential cracking along the weakened

fibre/matrix interface manifested the degrading effect of moisture in epoxy composites. Persistent fracture mechanisms appear to be interfacial cracking, micro-crack growth and coalescence in the plasticised matrix material.

2.5.4 Degradation of fibreglass composites exposed to water

Although glass fibres offer corrosion resistance at a competitive price, glass is not totally inert in chemically corrosive environments [64]. As all polymeric matrices will absorb some water after an extended period of time, these environments can be simulated to determine the extent of degradation caused by water on the fibres and fibre/matrix interface.

As the strength of fibre-reinforced polymers depends on the strength of the fibres as well as the ability of the matrix to transfer the applied load to them, if the strength of the fibre/matrix interface is reduced, the composite will fail at a lower level of stress. When water comes into contact with glass fibres, the molecules penetrate into microcracks, which are present on the surface of the glass. This causes the cracks to propagate, which makes the fibres much more brittle and prone to failure. Loss of adhesion or debonding at the fibre/matrix interface will accelerate the degradation process of fibres due to water contact [6, 64, 65, 66]. Stress concentrations may also develop which will cause a loss in fibre strength. Reduction in glass fibre strength and modulus can be accelerated by static fatigue. As a result, loading conditions can act simultaneously causing the composite to deteriorate at an increased rate. The combination of thermal and water absorption stresses can cause microcracks in the matrix, which accelerate the absorption and degradation process.

Although there are numerous research reports [6, 64, 65, 66] on the tensile failure of fibreglass reinforced composites after exposure to water, there is little information regarding the bending stresses and related failures of these materials. Bending stresses are quite common in many structural members such as beams, frames, etc. The study of Grami *et al* [67] indicates that there is a tendency for the material to fail at lower strength values (possibly due to stress corrosion cracking) under conditions of static bending when FRP composites are exposed to aqueous solutions. The bending stress creates compressive, tensile and shear stresses on the cross-section.

Water penetration into the composite occurs by diffusion through the resin as well as through cracks and voids in the matrix [64,65]. This indicates that the failure of glass reinforced polymers is caused by the eventual seepage of the water to the fibres. The increased number of cracks observed in the matrix on the tensile side of the specimens caused by the bending loading provided a path of least resistance for the water to penetrate and degrade the glass fibres, when

compared to the compression side which has more resistance toward water penetration. As more fibres failed due to the water exposure in the tension region, additional glass fibres were exposed to moisture resulting in propagation of the tensile failure.

The effect of seawater exposure on the fatigue damage development of a carbon/epoxy composite was investigated by Chiou and Bradley [68] using the edge delamination test. It was observed that seawater exposure has a significant influence on the edge failure mode. As the amount of seawater in the sample increases, the dominant crack path changes from interply to intraply cracking, but the overall growth of cracking remains approximately the same. Microscopic examination was used to monitor failure mechanisms that manifested.

The trend for the transverse cracks in the -45° plies was found to be decreasing as the moisture content of the sample increases. This was attributed to the fact that the matrix properties are more prevalent in the angle plies. The moisture softens the resin matrix, leading to a higher toughness. A clear trend of transverse cracks in the 90° plies was not established. A reduction in the number of transverse cracks in the 90° ply, observed by Kriz and Stinchcomb [69], was attributed to the reduction in the in-plane normal stress as a result of relief of residual thermal stresses caused by the moisture absorption. It was suggested that the degrading effect is offset by the stress relieving effect.

Edge cracking was observed to form at the $-45^\circ/90^\circ$ interface, in the 90° ply, at the mid-plane of the $90^\circ/90^\circ$ interface, and at the $0^\circ/-45^\circ$ interface with characteristics of the edge damage pattern different between dry and moisture-conditioned samples. For fatigue tests with dry samples, the delamination at the $-45^\circ/90^\circ$ ply interface was found to be the dominant mode of damage.

2.5.5 Effect of hygrothermal ageing on static fatigue of Glass/Epoxy composites

During water exposure, three major kinds of ageing processes are prone to act:

- Reversible plasticisation of the epoxy network resulting from water diffusion.
- Macroscopic damage such as matrix cracking and/or fibre/matrix debonding.
- Loss of bearing properties of the glass reinforcement due to chemical attack.

The effects of these processes on the fatigue behaviour have been investigated by two different approaches, that is, by a physico-chemical approach involving the analysis of the material viscoelastic behaviour in relation with water diffusion and a mechanical approach focused on the identification of the damage initiation and propagation processes during static fatigue (i.e. relaxation).

Static fatigue behaviour of glass-fibre/epoxy composites has been investigated by Chateauminois *et al* [70] during water ageing between 30°C and 90°C. Hygrothermally induced defects resulted in a temperature dependent decrease in fatigue properties. This decrease in fatigue strength was associated with a transition from progressive damage to non-progressive damage after exposure at 90°C. The analysis of ageing effects has been undertaken using damage maps. Different damage areas were considered which are characterized by either progressive or non-progressive propagation. Each of these damage areas was delimited by a set of parameters, which are representative of the individual fatigue behaviour of each of the composite constituents. It has been concluded that the damage map evolution upon ageing involved predominately the loss of static properties of the glass fibres and enhanced interfacial degradation at 90°C.

2.5.6 The effects of water on Glass-reinforced composites with different matrix materials

Most tests carried out to date to determine the response of composite materials to environmental degradation have been carried out at ambient temperature. However, it is known that elevated temperature softens most resins, particularly above the glass transition temperature (T_g) [71]. This reduces the interlaminar shear strength and the strength of the composite when it is loaded, such that the fibres are not in pure tension. The glass fibres are not susceptible to corrosion unless the absorbed water is acidic, in which case the effect can be dramatic [72]. The flexural strength of glass/polyester laminates and glass/epoxy pipes aged in seawater at ambient temperature was observed to reduce by up to 20% within a year [73]. Absorbed water is known to act as a plasticiser [74] thereby reducing T_g , and has been shown to reduce the strength and modulus of amine cured epoxies [71]. The presence of oil is believed to have little effect on fibre composites. Polyester/glass laminates exposed to dehydrated oil at temperatures up to 90°C for 90 days have been shown to behave in the same way as unexposed laminates [75].

A programme of tests has been conducted by Hale *et al* [76] to characterise the strength reduction of three GRP composites as a function of temperature and testing environment. The materials were two E-glass reinforced epoxies and an E-glass reinforced phenolic. These resins represent the materials which are of greatest interest to the offshore community:

- Aromatic amine (MDA) cured epoxy,
- Cycloaliphatic amine (IPD) cured epoxy,
- Acid-cured phenolic.

These resins are all capable of being processed into GRP components by liquid fabrication methods such as contact moulding and filament winding. The epoxy resins were of the type

widely employed in the fabrication of GRP pipe-work. The testing environments were sea water and crude oil condensate at temperatures from ambient to 150°C.

During experiments [76] it was found that:

- a. The expected high initial rates of water absorption varied between materials (epoxies show 1-2% increase in mass and phenolic 2.2%), but that in all cases the rate of absorption fell quickly. In the case of the IPD epoxy and phenolic systems there was little further uptake after two days immersion. With the MDA cured epoxy the time to effective saturation was five days.
- b. A very little absorption of oil into the epoxy materials was found. In the case of the phenolic, which is known to contain voids in the matrix, it is believed that the increased mass is due to these voids being filled rather than any interaction with the fibre or matrix materials.
- c. In matrix dominated failure mode, the strength of both epoxy-based materials falls off rapidly at elevated temperatures. This effect occurs at lower temperature in IPD cured epoxy than MDA cured epoxy.
- d. In matrix dominated failure mode, the strength of phenolic based GRP is less affected by high temperature. However, its strength is lower than epoxy materials at ambient temperature. It was found to be stronger than IPD/epoxy GRP above 60°C (40% strength reduction) and stronger than MDA/epoxy GRP above 100°C (30% strength reduction).
- e. At all temperatures the phenolic-based GRP composites are less sensitive to temperature change than either of the epoxy based systems. This is due to the softening of the resin, particularly close to and above the glass transition temperature (T_g). As an alternative to an absolute residual strength, rate of strength loss might be a useful criterion for upper temperature limit of integrity since this reflects the sensitivity to small temperature excursions.

Seawater was found to be the most aggressive of the environments tested, reducing the strength of all the materials at all temperatures. The strength reduction due to seawater absorption was approximately independent of temperature in MDA/epoxy GRP, but increased with temperature in IPD/epoxy and phenolic GRP's.

2.5.7 The effect of moisture on the interfacial strength of Graphite-Epoxy and E-glass/Epoxy composites

The effect of absorbed moisture on the fibre/matrix interfacial strength and 90° ply strength has been studied by Bradley *et al* [77] for E-glass and carbon-fibre reinforced epoxy. Single fibre fragmentation tests have indicated a 19% reduction in the interfacial strength in carbon/epoxy

composites, and absorption of moisture to the value of 1.4% of matrix weight in seawater. Micro-indentation measurement on E-glass/epoxy composites indicated a 25% reduction in the interfacial shear strength when the absorbed seawater increased from 1.2% to 2.2% of the matrix weight. In-situ observations of fracture in an environmental scanning electron microscope with associated calculations indicated reductions in interfacial strength ranging from 0 to 30%, with two-thirds attributed to reduction in interfacial strength and the balance due to changes in the residual thermal stresses.

On the basis of the obtained results it was concluded that the failure scenario begins with interfacial failure by debonding leading to transverse cracking, and subsequently, delamination. Absorbed moisture can perturb this failure scenario by reducing the chemical adhesion at the fibre/matrix interface, relaxing the residual compressive stresses at the fibre/matrix interface, reducing the ply level residual tensile stresses in the 90° plies, and toughening the polymeric matrix. Since these various effects of absorbed moisture can potentially postpone interfacial failure or cause it to occur prematurely, a more careful study has been undertaken by Bradley *et al* [77] to determine the effect of absorbed moisture on the interfacial strength and on the ply level mechanical stress at which interfacial failure leading to transverse cracking occurs.

In order to experimentally determine the effect of absorbed moisture on the initiation of ply level damage in a multi-axial laminate, micro-indentation tests [78] and tensile tests in-situ in an environmental scanning electron microscope can be performed on specimens as received, and specimens aged in seawater until a saturation level of moisture absorption has occurred. Single fibre fragmentation tests [79] can also be used to investigate the effect of absorbed moisture on the interfacial shear strength.

2.5.8 Effect of moisture on stiffness and strength of Carbon and Aramid laminates

Even in the absence of holes and impact damage, moisture absorption modifies the static and fatigue behaviour of composites in relation to the hygroscopicity of fibres and matrix, and the stacking sequence [80]. The hygroscopicity extremes are represented by carbon (non-hygroscopic) [81, 82, 83] and aramid (hygroscopic) [84, 85, 86] fibres. Aramid composites absorbed about 70% more water at saturation than carbon-fibre-reinforced composites, due to the hygroscopicity of the aramid fibres. The stacking sequence extremes are represented by $[0^\circ/90^\circ]_s$ (fibre dominated behaviour) and $[+45^\circ/-45^\circ]_s$ (matrix dominated behaviour).

For the $[0^\circ/90^\circ]_s$ carbon/epoxy laminate, water uptake decreased stiffness negligibly (by 2.4%) [87] both in tension and compression, but seriously reduced compressive strength (by 26.5%). For the $[-45^\circ/+45^\circ]_s$ carbon/epoxy laminate stiffness is reduced much more (48.8% in tension,

22.6% in compression), while the decrease in compressive strength is moderate (4.1%). No changes in tensile stiffness or strength occurs in either unconditioned or wet-conditioned $[0^\circ/90^\circ]_s$ aramid/epoxy laminates, however, stiffness in compression is considerably reduced (by 10%). Water uptake induced matrix plasticisation in $[-45^\circ/+45^\circ]_s$ aramid/epoxy laminates resulted in large reductions in stiffness in both tension (60%) and compression (12%). Fluid uptake always induces resin plasticisation, and hence reduces the performance of laminates. This performance reduction is greater in matrix-dominated than fibre-dominated laminates and is increases with impact damage.

2.5.9 Influence of environmental effects on structural stresses

Calculations performed by Foch and McManus [88] suggest that the environmentally induced stress state is determined primarily by thermal stresses. If degradation takes place, it results in significantly enhanced stresses near the surface. This explains the surface microcracking observed in numerous studies [89, 90, 91, 92, 93, 94, 95]. The moisture stresses, though smaller in magnitude, are non-trivial and can induce stress gradients through the thickness. The worst-case moisture-induced stresses are of the same order of magnitude as the thermal stresses. In particular, moisture stresses can be severe in unidirectional laminates undergoing dry-out from a saturated condition. The computed stresses do not fully explain the increased cracking observed under exposure to moisture [96, 97, 98, 99, 94, 100] suggesting that there are mechanisms for moisture-induced cracking beyond moisture-induced stresses. The presence of moisture in the laminate could cause temporary or permanent changes in material properties, in particular the transverse fracture toughness, or it could enhance the cracking mechanisms in ways not yet understood.

A set of models and computer codes has been developed by Foch and McManus [88] to aid in the calculation of severe environmental effects. Using as inputs ambient temperature, relative humidity (RH), oxidative environment, material properties and laminate geometry, the developed codes predict the material state, degraded properties, and resulting stress state as functions of position and time.

2.5.10 Galvanic blistering in carbon fibre composites

Carbon/polymer composites form blisters when galvanically coupled to steel or aluminium in seawater or sodium chloride solution. Chemical analyses of blister fluids were conducted by Miriyala *et al* [101] and a mechanism of galvanic blistering was proposed.

Carbon is an electrically conductive material and also a noble cathode material. Therefore, engineering metals like steel and aluminium undergo rapid corrosion when galvanically coupled

to carbon in aqueous electrolyte environment like seawater or salt water [102]. When carbon fibres of a carbon/polymer composite are subjected to such galvanic conditions, the composite forms blisters containing liquids of pH 14. Samples of carbon composite with vinylester matrix exposed to both seawater and NaCl solution under non-galvanic conditions did not show blisters (which implies that the vinylester used is highly resistant to hydrolysis) whereas galvanically coupled samples form blisters within two weeks. The blistering of carbon fibre composites under galvanic conditions is termed “galvanic” or electrochemical blistering [102]. Galvanic blistering of carbon fibre reinforced vinylester was first reported by Tucker [103]. Other carbon reinforced composites which also blister under galvanic conditions are carbon reinforced polyester [104], epoxy [105], and polyamide [106] composites. Galvanic blisters in these composites were also filled with liquids of pH 14. Therefore, galvanic blistering appears to be a general phenomenon in carbon fibre composites with various polymeric matrices.

Microscopy studies [101] revealed blister opening in carbon/vinylester composites to be along the carbon-fibre and matrix interface [104]. However, the effects of galvanic coupling on the mechanical properties of the carbon composites are not well established although evidence for 30% reduction in shear strength in carbon-epoxy composites, subjected to galvanic conditions, has been presented by Sloan [106].

The cathodic reaction on carbon surfaces in neutral or basic solutions is the electrochemical reduction of oxygen,



with equilibrium potentials around 0.2V against the standard calomel electrode. The potential versus current density profiles (Tafel plots) for the carbon/vinylester composite [103] and the high pH of the blister fluids indicate that the cathodic reaction at the carbon/polymer interface is the oxygen reduction reaction described by Equation 4.

Sloan *et al* [107] observed dissolution of epoxy matrix of carbon/epoxy composites subjected to galvanic coupling with magnesium anodes in seawater. These researchers hypothesized that an intermediate step in the reaction described by Equation 4 is the production of perhydroxyl ions, HO_2^- OH^- which may have attacked the epoxy polymer as the perhydroxyls are several times more reactive than hydroxyl ions. However no experimental evidence exists in support of the above mechanism. Donnellan *et al* observed the dissolution of polyamides in galvanically coupled carbon-polyamide composites [106]. No visual attack of vinylester was observed when a piece of cast vinylester was exposed to pH 14 sodium hydroxide solution for two weeks.

A critical step in the investigation of galvanic blistering mechanisms is the chemical analysis of the blister fluids. Blister fluid analysis was conducted using several analytical techniques which produced different complementary information. Morphological studies of dried products of blister fluid were also conducted [101] using optical and electron microscopy.

The galvanic blistering mechanism proposed by Miriyala *et al* [101] is based on analytical results. Carbon fibres develop a surface charge when galvanically coupled. As a result, the electron dense parts of the adhering polymer chains repel away from the carbon surface, which will result in debonding. Water droplets nucleate in these debonded zones. This brings sodium ions and oxygen into the region and oxygen reduction to hydroxyls takes place on the carbon surface. As a result a sodium hydroxide solution is formed which is highly hygroscopic and draws more water into this region. The relatively greater diffusion rates of water through the polymer compared to sodium hydroxide solution builds an osmotic pressure in the debonded region and the blister grows under this osmotic pressure. The growth is sustained by continuous production of hydroxyl ions, which maintains high concentration of sodium hydroxide in the blister liquid. Blister growth results in increased interface debonding with time.

2.5.11 Osmosis

The uptake of water, as an independent process, causes osmotic pressure. This can lead to delamination of the gel-coat under circular blisters and delamination of the laminate plies under ellipsoidal shaped defects [108, 109]. The problem may affect 20-30% of reinforced polyester hulls after twenty years of immersion in seawater and also composite swimming pools [110].

This phenomenon represents a flow of aqueous solutions through semi-permeable membranes, and particularly through cellular membranes of living organisms and is described as "osmosis". The process takes place when a solvent and an aqueous solution are separated by a semi-permeable membrane, which is permeable only to the solvent. A flow of solutes through a membrane wall occurs due to the difference in concentrations. The flow generates a hydrostatic (osmotic) pressure. It is now well known that unsaturated polyester resins, epoxy resins and also laminate plies behave like osmotic membranes [111, 112]. The osmotic delamination may only be cosmetic (gel-coat blistering). In the worse cases it can cause a serious loss of properties.

2.6 Temperature effects

Since thermosetting resins are never "fully cured" after the standard cure cycles, when they are aged at temperatures approaching their glass transition temperature (T_g), additional cure reactions are likely to occur along with other chemical effects such as oxidative degradation.

What can be usually expected starting from the earliest stages of processing and continuing during the ageing duration, is a simultaneous involvement of resin cure, physical ageing and chemical ageing. The relative importance of each of these is different during cure, post-cure and ageing. Moreover, when considering isothermal ageing below the glass transition temperature of the resin, it is not the absolute temperature but the distance between the ageing temperature and T_g that regulates the three effects mentioned above [113].

In the case of a high temperature (well above T_g) environment combined with an oxidative atmosphere, physical ageing does not occur but cure reactions and chemical ageing (oxidation) are both active. Polymers subjected to these isothermal treatments are usually characterized by weight loss processes caused by chain scission with the production of low molecular weight volatile molecules. Both further cross-linking and oxidation may generate weight loss, but generally the effect of the former on weight loss is negligible compared with that of the latter. When the composites are carbon-fibre reinforced, the presence of the fibre can affect the degradation process controlled by oxygen diffusion in the bulk as the fibres also degrade. Accelerated degradation experiments [114] at high temperatures represent the best option when long-term data is required and the test duration becomes the main experimental problem. However, data extrapolation at lower temperatures and longer times is only possible assuming a simplified degradation process and under particular restrictions [115].

Extensive experimental and analytical work conducted by Marino and Chartoff [113] focused on long term Thermal Oxidative Stability (TOS) of a relatively new bismaleimide resin based composite currently used as potential material for primary and secondary structures in the Air Force's F-22 program, the most demanding composite program in the aeronautical industry. Mathematical models that combine heat transfer and chemical reaction terms for oxidative, thermal, degradation have been used for modelling the response of the material to high temperature environments and a Time-Temperature Superposition (TTS) principle was applied to estimate the onset of the degradation process at longer times and lower temperatures.

Investigations on unidirectional composite samples of different sizes and shapes have also showed that different degradation mechanisms are operative in the three principal directions. Effective diffusion coefficients and time exponents for the weight loss fluxes per unit area generated from the three typical sample surfaces (cut perpendicular to the fibre direction, cut parallel to the fibre direction and the rich resin surface) were determined to predict the real composite degradation rates.

The results show that on the 0° surface, the process is reaction controlled while on the 90° surface it is diffusion controlled. A superposition of the two mechanisms and eventually also a switchover from one to the other might explain the low values of the time exponents found on the rich resin surface. The total weight loss of a generic anisotropic sample can then be expressed as the sum of each contribution as follows:

$$Q = \sum_{i=1}^3 A_i q_i \quad (5)$$

where the index i refers to the three different composite surfaces, A_i is the generic surface area (cm^2) and q_i is the weight loss flux per unit surface area (g/cm^2) in one direction. A and q can be obtained from experimental Thermo-Gravimetric Analysis (TGA) [113]. Equations similar to Equation (5) can be written for unknown weight loss fluxes per unit surface area in each of three directions. The solution of this system of three algebraic equations will yield the weight loss fluxes as a function of time.

Since the degradation process starts from the outside of the sample and then moves into the core, it can be modelled by the unreacted shrinking core model [116]. Two kinds of possible reaction mechanisms can be considered, i.e. the diffusion controlled and the chemical reaction controlled mechanism. In both cases the final generic expression for the total weight loss per unit surface is:

$$q = \frac{Q}{A} = D_e t^n \quad (6)$$

where D_e is a constant corresponding either to effective diffusion or kinetic constant. When the exponent n is equal 0.5, the reaction mechanism is likely to be diffusion controlled, while if $n = 1$, the kinetic controlled process is dominant.

The two parameters D_e and n , can be evaluated from experimental data by plotting $\ln q_i$ versus $\ln(\text{time})$. The slope of the linear interpolation yields n and the intercept yields D_e . The value, thus determined, of the parameter n can be used to distinguish between a diffusion and a reaction controlled mechanism. This information can be very useful for modelling and predicting the degradation process in a simpler way without considering the superposition of the two effects.

2.7 Combined hygrothermal effects

To understand the degradation mechanism due to moisture and temperature, researchers subjected the specimens to either a moist environment or dry warm environment, i.e.

degradation due to a single factor was investigated successively. However due to the complex coupling between the degradation mechanism due to moisture and temperature, the combined effect may not be a simple superposition of the two different degradation effects. As a result, hygrothermal testing, testing in which specimens were subjected to both moist environments and elevated temperatures was undertaken to improve understanding of degradation when these factors are simultaneously present. This situation more accurately resembles practical applications in moist hot environments commonly found in the tropical climates and particular end-use environments.

Hot and humid environments can degrade some aspects of the material performance, particularly, the compressive strength [117, 118]. Water absorption by the epoxy resin leads to a reduction in the glass transition temperature and to a softening of the resin with a loss of stiffness and strength which causes fibre micro-buckling and premature laminate failure [119]. The degradation increases as the conditions become more severe. The quantity of water absorbed by a laminate is therefore of considerable importance.

Soutis and Turkmen [95] evaluated the water absorption of the T800/924C carbon-fibre epoxy system and determined its effect on the compressive strength of unidirectional and multidirectional laminates with an open hole. A computer program [201] was used for the calculation of the quantity of water absorbed by the composite laminates and to determine the profile of the moisture distribution through the laminate thickness during exposure to boiled water (accelerated ageing).

A study conducted by Obst *et al* [120] focused on the effects of temperature, moisture and ageing conditions on the microcracking behaviour experienced by a woven graphite/epoxy composite during fatigue. The authors found that hygrothermally cycled material and material tested at elevated temperature had higher crack densities close to failure than un-aged material tested at room temperature. Since both hygrothermal cycling and temperature were found to have an effect on the fatigue damage accumulation, it was concluded that fatigue life is also affected. Smith and Weitsman [121] conducted a study on the effect of moisture on the fatigue behaviour of a graphite/epoxy system and found that previously saturated specimens fatigued in water had lower fatigue lives than previously saturated specimens fatigued in air and unsaturated specimens fatigued in air. Case [122] studied the effects of elevated temperature on the strength and stiffness degradation of IM7/K3B notched and un-notched composite specimens. A change in matrix properties as a result of elevated temperature (177°C) was evident from the decrease in transverse strength and stiffness properties from room-temperature

properties. Moreover, in the un-notched specimens, a greater reduction in residual strength was observed as a function of fatigue cycles.

Patel and Case [123] conducted an extended study to evaluate the durability and damage tolerance of composite material in fatigue loading under individual and combined service environmental conditions. The authors concluded that fatigue life and residual strength of the woven graphite/epoxy composite material is minimally affected by the elevated temperature, moisture or combined hygrothermal conditions imposed and stress levels considered, despite differences in damage accumulation processes.

The major damage mechanism resulting from quasi-static loading was cracking in transverse tows. The cracks extend across a single transverse fibre bundle at maximum length. The majority of the cracks appear relatively close to failure but do not reduce the axial elastic modulus. Damage progression during fatigue occurred in the following general order; transverse microcracking and delamination around the fibre bundle undulation regions, longitudinal microcracking around fibre bundle undulation regions, growth of transverse cracks across the entire height of the transverse fibre bundle, and cross-ply-like growth of edge and interply delamination. The rate at which damage progression occurred generally depended on the maximum fatigue stress amplitude and environment:

Also, in this study, the damage accumulation was found to be greater with decreasing fatigue stress levels. Fibre/matrix debonding and delamination were found to be greater for the elevated-temperature and moisture-saturated specimens than for room-temperature specimens, and hygrothermal cycling during fatigue was found to result in greater crack density during fatigue than did any of other conditions.

2.8 Mathematical modelling

Attempts to model environmental effects on composite structures have received a great deal of attention in the literature. Investigators have attempted to decouple temperature, moisture and chemical effects [124, 125, 126, 89, 90] as well as analyse the interactions during combined exposure [96, 127, 97, 128, 98, 91].

A good development of the behaviour of a substance diffusing into another is given by Crank [129], expanded by Springer [125] and, Tsai and Hahn [126]. For a limited range of environmental conditions, moisture absorption follows Fickian behaviour. Moisture absorption into a laminate has a much slower diffusion rate than does temperature ($\sim 10^6$ times slower). For

this reason the laminate response to temperature change is often considered instantaneous and constant across a laminate's thickness. Theories have been developed to account for the coupled distributions of moisture and temperature [92]. Several mathematical formulations have been developed in order to simplify the calculations required for predicting moisture absorption. Springer's "W8GAIN" model was developed in 1981 in order to predict the distribution of moisture and temperature in a laminate exposed to wet conditions [130], and Weitsman developed a code (also in 1981) that searched for the most efficient calculation for moisture absorption in a laminate over time periods with fluctuating ambient conditions [127].

Chemical changes in composite materials attributed to environmental exposure are less well understood than moisture effects. Several distinguishing characteristics mark chemical degradation, i.e. discoloration and embrittlement of the surface, weight loss, decrease of material strength, and microcracking. Recently, much work has been done to characterize the reactions occurring in the polymer in an attempt to understand these changes [89, 90, 93].

Calculations of stresses resulting from temperature, moisture, and degradation states in the material are common in the literature via micromechanics and Composite Laminated Plate Theory (CLPT). Tensile residual stresses that are inherent in general composite laminates after cool-down from cure temperature (due to ply coefficient of thermal expansion mismatches) may be at least partially relieved by moisture-induced stresses (resulting from swelling of the laminate) [131]. Chemical degradation adds complexity, altering the material properties at the exposed surface. The potential for microcracking damage is high during cyclic environmental exposure [128, 99, 94, 95]. Microcracking has been seen to increase the diffusion rate of moisture [96, 100, 132] resulting in non-Fickian absorption behaviour.

2.8.1 Modelling of moisture absorption by epoxy resin

Epoxy resins readily absorb atmospheric moisture which results in reduced mechanical performance of the composite. In order to characterise the effects of moisture and moisture gradient within an epoxy matrix composite, the parameters of material diffusivity and maximum moisture content must be known. These parameters will vary with environmental conditions, fibre volume fraction (V_f) and sample dimensions. Experimental and theoretical investigations into the effect of sample fibre volume fraction and the distribution of fibres within that fraction, on the transverse diffusivity of epoxy matrix composites were conducted by Bond *et al.* [67]. The difference was found to be negligible between fully random and regular packed distributions. However, if high and low fibre volume fractions are distributed in layered structures, the transverse diffusivity is significantly reduced.

2.8.2 Modelling of the diffusion process

Diffusion is one of several physical phenomena well described by a form of elliptic (in the steady state condition) or parabolic (in the non-steady-state condition) partial-differential equation. The diffusion equation, as proposed by Fick [133], with c representing moisture concentration at a specific Cartesian point (x, y, z) at time (t) and D the material's diffusivity, is:

$$\frac{\partial C(x, y, z, t)}{\partial t} = D \nabla^2 c(x, y, z, t) \quad (7)$$

Several authors [134, 135, 136] have reported on the general compliance of epoxy resins to this equation, which suggests that Equation (7) may be assumed to be an adequate approximation of the absorption characteristics for most epoxy resin systems. Based on this assumption, analogies between Fick's equation and such phenomena as heat and electrical conduction or potential and groundwater flow can be made to find theoretical approximations for diffusivity along principal axes.

Among the variety of models used analogously to predict composite diffusivity perpendicular to the fibres, the most commonly utilised ones include those based on combinations of thermal resistance [124], material shear properties [137], or electrical conductivity [135]. Additionally, numerical methods such as alternating direction implicit integration [138] or Finite Element Analysis (FEA) [139] have been utilised to solve Equation (7) directly.

2.8.3 Assessing the environmental effect using cross-property correlation methods

In many cases the environmental effect on the composites cannot be easily assessed in a straightforward manner and requires conducting a number of sophisticated tests [75, 193, 80]. Some of the properties of the composite laminate that change during the environmental exposure are easier to measure practically than others. One of the ways of forecasting the rest of the properties of the composite by measuring just a few can be implemented using the “cross-property correlation technique”.

It may present a complicated task to establish such a correlation, using the similarity between the governing mathematical laws described by different differential equations, which are characterized by tensors of different ranks. The importance of cross-property correlations for composites has been pointed out by Berryman and Milton [111] and was particularly emphasized by Gibiansky and Torquato [140]. Cross-property correlations between various effective properties of heterogeneous materials have been examined in several works. Levin [141] interrelated the effective bulk modulus and the effective thermal expansion coefficient of two phase isotropic composites. Milton [142] established cross-property bounds for the transport and optical constants of isotropic composites. Similar bounds for the electrical and the

magnetic properties were given by Cherkaev and Gibiansky [143]. The general approach to establishing various cross-property correlations was outlined by Milton [59] and Markov [144].

Results on the cross-property bounds were substantially advanced by Gibiansky and Torquato [140, 145, 146] who narrowed them under additional restrictions on the composite micro-geometry and on the properties of constituents. Gibiansky and Torquato [145] also considered the transversely isotropic material (fibre reinforced composite) and established bounds for two of the effective elastic constants in terms of the effective conductivities. Cross-property correlations were established by Kachanov *et al* [220] in the closed form that explicitly reflects inclusion shapes and properties of the constituents. Such correlations may also be used to optimise the microstructure for the best combined performance of both measured and correlated properties.

The correlations derived using this technique are approximate. The accuracy of the cross-property correlation method was examined by Sevostianov and Verijenko [223] on the basis of “accuracy maps” to identify various combination of parameters corresponding to errors.

2.8.4 Incorporating non-isothermal physical ageing effects for analysis of mechanical response of linear visco-elastic composite laminates

Over the past three decades, a number of researchers have modelled the time-dependent response of PMC's by using several approaches including linear viscoelasticity, non-linear viscoelasticity and non-linear viscoplasticity [147, 148, 149] to name a few. While these works demonstrate that several complete and general treatments of viscoelastic composite laminate response, few solutions have been extended to predict the effects of ongoing physical ageing. Physical ageing is a phenomenon that occurs in polymeric materials cooled to temperatures $T < T_g$, which causes the material to achieve thermodynamic equilibrium only after a finite (often extremely long) period of time. One effect of physical ageing is that material properties (such as specific volume, compliance, modulus) change continuously.

Physical ageing differs from degradation phenomena (such as chemical ageing and damage) because it is thermo-reversible when heated above T_g for a nominal rejuvenation period. Ageing materials “forget” past ageing histories and behave as they did previously upon a subsequent quench.

For the composite solution methods mentioned earlier, which are linear viscoelastic and thermo-rheologically simple, these effects can be included by modifying the effective (or reduced) time

function in the analysis. Since the effects of physical ageing in composite laminates have been experimentally observed to vary in the shear and transverse lamina directions, [150, 151, 152, 153, 154] the effective time function needs to be directionally dependent for the most general solution (a feature generally not included in the derivations above). For the composite, solution methods using non-linear material models, inclusion of physical ageing effects is more problematic as two of the issues that must be addressed are the degree to which ageing has already been incorporated into determining the non-linear response of the material (which can itself be viewed as a non-linear response) and the effect large load levels (the typical impetus of non-linear material behaviour) have upon the state of physical ageing of the polymer matrix.

Several studies have already considered mechanical response of such systems. Brinson and Gates [155] used experimentally determined ageing compliance behaviour and several simplifying assumptions to predict laminate response under constant load. This approach was extended by Monaghan *et al* [156] for the case of a multiple step load history. Pasricha *et al* [157, 158] added the effects of physical ageing to the non-linear viscoelasticity (Schapery model) solution program, BONVICA via a change in the effective time. This approach adequately predicted long-term compliance results although concerns about the behaviour of physical ageing in nonlinear systems remain. BONVICA is limited to predicting either creep or stress-relaxation under either constant or cyclic loading conditions. In all of the above approaches, the ageing behaviour was assumed identical in both the shear and transverse lamina directions and non-isothermal ageing effects were not considered.

The model developed by Bradshaw and Brinson [123] decouples the ageing and mechanical response, since the ageing shift factors (the basis for the effective time) can be determined from the temperature history alone, without regard to the loading applied. This greatly simplifies development of both the non-isothermal physical ageing model and the mechanical response model by allowing them to be considered separately. Classical thin-laminate theory is then used to assemble the individual ply response equations and determine the overall laminate response to general in-plane force and moment loading. The method automatically recovers the ply-level stresses and strains, which are often critical to strength and durability predictions. The model can use either lamina compliance or modulus properties as its basis.

2.8.5 Modelling of environmentally induced damage in infinite composite plate

A computationally efficient model has been developed by Foch and McManus [88] for computing the response of composite laminates to hygro-thermal cycling. This model predicts two significant effects of cyclic moisture absorption, i.e. large fluctuations in absorbed moisture level at the material surface due to changing ambient conditions, and a slow increase of

moisture in the interior of the laminate to an equilibrium level. This equilibrium level can be calculated easily using a simple temperature-weighted average of the environmental conditions. User defined inputs include an environmental profile, in which temperature and moisture vary with time, relevant material properties, laminate geometry and number of cycles.

This mathematical model simulates an infinite plate exposed to uniform environmental conditioning on its top and bottom surfaces ($z = 0$ and $z = h$). Diffusion is assumed to be one-dimensional through the thickness (z direction). Temperature is assumed to be constant through the thickness, and instantaneously equal to the time-varying ambient temperature.

2.8.6 Moisture absorption

A one dimensional Fickian law model for moisture and oxygen diffusion into composite material is as follows [3];

$$\frac{\partial C}{\partial t} = D \frac{\partial^2 C}{\partial z^2} \quad (8)$$

where C is the concentration of moisture in the laminate, z is the through-thickness direction, and D is the diffusion rate calculated using Equation (9). The diffusion rate is dependent on the diffusion constant D_0 , activation energy E_A , gas constant R , and absolute temperature T [129]:

$$D = D_0 \exp\left[\frac{-E_A}{RT}\right] \quad (9)$$

Initial and boundary conditions are required to solve Equation (8) are listed below;

$$\text{for } t < 0 \quad C(z) = C_0(z); \quad (10)$$

$$\text{for } t > 0 \quad C(0) = C_\infty(t), \quad C(h) = C_\infty(t). \quad (11)$$

The value $C_0(z)$ is the initial state of moisture through the laminate. The quantity $C_\infty(t)$ represents the concentration at the surface. At every instant of exposure, the surface of the laminate is assumed to be saturated at the level corresponding to the current atmospheric relative humidity. Saturation level is a function of relative humidity Φ , and material constants a and B , which are determined empirically [125].

$$C_\infty = \alpha(\Phi)^B. \quad (12)$$

An efficient solution to the above problem is needed to compute moisture and oxygen levels in structures undergoing large numbers of complex thermal and environmental profiles. A number of profiles including relative humidity that remains constant over specified lengths of time and temperatures, or change at a constant rate can be considered. Such profiles can be repeated an arbitrary number of times.

A modal solution of Equation (8) in the time interval starting at t_{i-1} is:

$$C(z, t) = C_{\infty i} - \sum_{n=0}^{\infty} A_{ni} \sin\left(\frac{n\pi z}{h}\right) \exp\left[\frac{-n^2 \pi^2 D \Delta t}{h^2}\right], \quad (13)$$

where the change in time $\Delta t_i = t - t_{i-1}$ and $C_{\infty i}$ is calculated from Φ_i using Equation (12). In Equation (13), A_{ni} represents the amplitude of each mode calculated from the concentration at time t_{i-1} , and n is the index of each mode. In order to find the first set of modal amplitudes from the initial conditions, a Fourier series expansion [159] is used:

$$A_{n1} = \frac{2}{h} \int_0^h (C_{\infty 1} - C_0(z)) \sin\left(\frac{n\pi z}{h}\right) dz \quad (14)$$

where the subscript 1 represents values at the first time step ($i=1$). In order to find the concentration level $C(z, t)$, the first set of calculations for A_{ni} is performed. In order to calculate subsequent modal amplitudes $A_{n(i+1)}$, and thus new concentrations, $C_0(z)$ is substituted with $C(z, t_i)$ forming Equation (13), and $C_{\infty 1}$ is substituted with $C_{\infty(i+1)}$ in Equation (14). After the integration it can be shown that;

$$A_{n(i+1)} = (C_{\infty(i+1)} - C_{\infty i}) + A_{ni} \exp\left(\frac{-n^2 \pi^2 D \Delta t}{h^2}\right), \quad (15)$$

where $\Delta t_i = t - t_{i-1}$.

This equation is appropriate for periods of constant temperature since the moisture diffusivity D , is constant and can be calculated from Equation (9). For the segments with changing temperatures however, the calculations become complicated since the temperature is time dependant. This problem is solved by substituting Equation (9) into Equation (13) and defining a modified time step Δt^* . This yields an equation for the current moisture concentration during a temperature ramp;

$$C(z, t) = C_{\infty i} - \sum_{n=0}^{\infty} A_{ni} \sin\left(\frac{n\pi z}{h}\right) \exp\left[\frac{-n^2 \pi^2 D \Delta t^*}{h^2}\right], \quad (16)$$

where

$$\Delta t^* = \int_{t_{i-1}}^t \exp\left[\frac{E_A}{RT(t)}\right] dt \quad (17)$$

If the moisture and temperature profiles are repeated (cycled), the values of Δt^* for each segment must be calculated prior to the cyclical calculations:

$$\Delta t^* = \int_{t_{i-1}}^{t_i} \exp\left[\frac{E_A}{RT(t)}\right] dt \quad (18)$$

Consequently Equation (15) becomes;

$$A_{n(i+1)} = \frac{A}{n\pi} (C_{\infty(i+1)} - C_{\infty i}) + A_{ni} \exp\left(\frac{-n^2 \pi^2 D \Delta t^*}{h^2}\right) \quad (19)$$

This allows easy calculation of moisture concentrations for each segment. The coefficients A_{ni} , are found by progressive application of Equation (19), and then the concentration at any time can be found from Equation (16). The calculations are repeated for as many cycles as necessary.

The same scheme outlined above can be used to calculate the diffusion of oxygen into a laminate. Once the local oxygen concentration is calculated, both thermal and oxidative reactions altering the polymer structure in the laminate are calculated via the method outlined by Cunningham and McManus [93]. The resulting output is obtained in the form of a dimensionless level of completeness of the reaction, b , which is related to material mass loss, and reaching the value of one when all of the available material has been chemically degraded.

2.8.7 Mathematical model of stress corrosion cracking of GFRP in humid environments

Stress corrosion cracking (SCC) is controlled by the sub-critical growth of fibre surface defects under the combined action of stress and moisture [160, 161, 162]. In an earlier micro-mechanical investigation Pauchard *et al* [163, 164] demonstrated that fibre failure kinetics within an elementary composite volume subjected to a constant applied strain and a uniform ageing state can be modelled from a combination of the Weibull statistics of fibre strength and classical SCC laws. This approach resulted in a Weibull-based description of the dependency between the fibres' survival probability and the loading time. On the basis of an empirical correlation between the stiffness loss of a flexural beam and the associated number of broken fibres within a restricted elementary volume located on its tensile side, it was subsequently demonstrated that the macroscopic stiffness loss of the composite under static or cyclic fatigue conditions could be deduced from the SCC behaviour of the fibres [165].

The accuracy of the prediction was, however, found to be critically dependent upon the estimate of the Weibull modulus m , and static fatigue parameter n , which describe respectively the distribution of the flaw sizes on the fibres and the dependency between the crack velocity and the stress intensity factor. An improved methodology was proposed by Pauchard *et al* [163] to accurately determine these two parameters from stiffness loss measurements, which were carried out under monotonic and static fatigue conditions. The validity of theoretical model was investigated under different cyclic fatigue conditions based on frequency, the strain ratio and the

maximum applied strain. The limitation of the proposed approach is that it is restricted to the initial stages of the fatigue life, i.e. before the appearance of a significant macroscopic damage in terms of matrix cracking and delamination. Under such conditions, the stiffness loss behaviour can be assumed to be primarily driven by the delayed failure of the unidirectional reinforcement.

Consider the delayed failure of a glass filament within water aged composite. It involves sub-critical propagation of pre-existing surface flaws. The crack growth rate v , can be related to the stress intensity factor K_I , using a power law expression:

$$v = \frac{da}{dt} = AK_I^n, \quad (20)$$

where $K = Y\sigma\sqrt{a}$ is the mode 1 stress intensity factor, a is the crack length, σ is the applied stress and Y is a shape factor close to $\sqrt{\pi}$. A and n are two parameters assumed to be constant for a given reinforcement material within a given physico-chemical environment.

From the integration of Equation (20), the time to failure t_f , of a glass-fibre under a given stress loading $\sigma(t)$, can be expressed as follows:

$$\int_0^{t_f} \sigma(t)^n dt = \frac{2K_{IC}^{2-n}}{AY^2(n-2)} \sigma_i^{n-2}, \quad (21)$$

where σ_i is the strength of the fibre in an inert environment. For sufficiently high values of t_f , (i. e. $t_f \gg 1/v$) the integral term is approximately proportional to t_f . Equation (21) thus becomes:

$$\lambda t_f = \frac{2K_{IC}^{2-n}}{AY^2(n-2)} \sigma_i^{n-2} \sigma_{\max}^{-n}, \quad (22)$$

where σ_{\max} is the maximum applied stress and $\lambda \leq 1$ is a numerical constant depending upon σ_i/σ_{\max} and n .

In the case of a statistical population of fibre surface defects, the distribution of the fibre strength ε_i , in an inert environment can adequately be described by means of a Weibull [166] expression;

$$P_s(\varepsilon_i) = \exp\left[-\left(\frac{\varepsilon_i}{\varepsilon_0}\right)^m\right], \quad (23)$$

where m and ε_0 are respectively the Weibull modulus and scaling factor taking into account the gauge length of the fibres.

By substituting Equation (22) into this Weibull expression one obtains the lifetime distribution of a statistical population of fibres under monotonic or cyclic loading:

$$P_s(t) = \exp \left[- \lambda^{\frac{m}{n-2}} t^{\frac{m}{n-2}} \varepsilon_{\max}^{\frac{nm}{n-2}} C \right], \quad (24)$$

where C is a constant scaling factor and ε_{\max} is the maximum applied strain. In the study of Pauchard *et al* [165] it was demonstrated that during the early stage of damage development, the macroscopic stiffness loss of the flexural beam is linearly related to the measured density of broken fibres within an elementary composite volume located on the tensile side of the specimen. It was also found that, under a static fatigue loading (i.e. $R = 1$), the fibres' fracture processes within this elementary volume and the relative stiffness loss, $S(t)/S_0$, can be described by means of an expression derived from Equation (24):

$$\frac{S(t)}{S_0} \approx \exp \left[- t^{\frac{m}{n-2}} \varepsilon^{\frac{m}{n-2}} \lambda^{\frac{m}{n-2}} K \right], \quad (25)$$

where S_0 and $S(t)$ are respectively the initial stiffness and the stiffness at time t . K is constant scaling factor.

The SCC nature of the dependency of the stiffness loss upon time, maximum applied strain and loading ratio can be verified by plotting the experimental stiffness loss curves in a Weibull representation i.e. $\log(\ln(S/S_0)) = f(\log(t))$.

As it can be seen from the equations (20) – (25), the application of the stress corrosion model relies upon an accurate determination of the values of the microscopic parameters, m and n , which characterise respectively the statistical population of fibre defects and their sub-critical crack growth rates. These parameters can be determined from in-situ microscope observation of the fibre failures [164]. An alternative method based upon macroscopic load measurements on the basis of the stiffness loss measurements which were carried out under monotonic and static fatigue conditions was proposed by Pauchard *et al* [163]. The stiffness loss can be adequately described using the following Weibull expression:

$$\frac{S}{S_0} \approx \exp \left[- \left(\frac{\varepsilon}{\varepsilon^*} \right)^m \right], \quad (26)$$

where ε^* is a scaling factor.

The Weibull modulus was identified from a linear fit of the experimental data. This calculation yields a value of $m = 4.3$, which is close to the value ($m = 3.9$) determined from in-situ observation using similar glass fibres [164].

The stress corrosion parameter can be determined using the expression for the time to failure as a function of the crack velocity :

$$t_f = \int dt = \int \frac{da}{v}, \quad (27)$$

By taking into account that $K_{I0} = Y\sigma_{app}\sqrt{a_0}$ and $K_{Ic} = Y\sigma_i\sqrt{a_0}$, Equation (27) can be rewritten as follows:

$$t_f = \int_0^{t_f} dt = \frac{2}{\sigma_{app}^2 Y^2} \int_{K_{I0}}^{K_{Ic}} \frac{K_I dK_I}{v(K_I)}. \quad (28)$$

Taking a derivative with respect to K_{I0} produces;

$$\frac{dt_f}{dK_{I0}} = \frac{-2K_{I0}}{\sigma_{app}^2 Y^2 v(K_{I0})}. \quad (29)$$

It is noted that $K_{I0} = Y\sigma_{app}\sqrt{a_0}$ and $K_{Ic} = Y\sigma_i\sqrt{a_0}$, Equation (29) can be rewritten in the following form:

$$v(K_{I0}) = \frac{2K_{Ic}^2}{\varepsilon_i^2 E Y^2} \frac{d\varepsilon_i}{dt_f} \quad (30)$$

Strength data ε_i , corresponding to a given experimental lifetime t_f , can be generated using an expression derived from Equation (26);

$$\varepsilon_i = \varepsilon^* \left[\ln \left(1 - \frac{S_0}{S(t)} \right) \right]^{\frac{1}{m}} \quad (31)$$

where $\frac{S_0}{S(t)}$ is the relative stiffness loss measured at the time t under a static fatigue condition.

Knowing the Weibull modulus and the static fatigue parameters, it is possible to predict the stiffness loss under cyclic fatigue conditions at various frequencies and strain ratios. For each set of experimental conditions, the value of the shift factor λ , in Equation (22) can be calculated from the numerical integration of the following expression;

$$\lambda = \frac{1}{t} \int_0^t \left(\frac{\varepsilon(t)}{\varepsilon_{max}} \right)^n dt \quad (32)$$

This mathematical SCC model may provide an acceptable prediction of the stiffness loss under more complex loading involving the stacking block sequence. The model also confirms the SCC nature of the fatigue behaviour of the aged composites, in the sense that the stiffness loss is mostly governed by the time spent at a given strain level, independent of the strain rate. It must be noted that application of this model is restricted to the initial stages of the fatigue life, i.e. when the damage mostly consists in the accumulation, at the microscopic level, of delayed fibre failures under the combined action of stress and moisture.

2.8.8 Stress predictions

Varying thermal conditions, absorbed moisture, and chemical degradation of the material all affect the stress state in the structure. The resulting stress state in the laminate can be computed by including the environmental effects in a constitutive equation [167]:

$$\sigma_{ij} = E_{ijkl}(T, C, b)[\varepsilon_{kl} - \alpha_{kl}\Delta T - \beta_{kl}\Delta C - \chi_{kl}b] \quad (33)$$

In Equation (33), Young's modulus E , is dependent on the current temperature T , the moisture concentration C , and the chemical state b . The coefficients of thermal and moisture expansion (α and β respectively) determine the material expansion due to changes in temperature ΔT , from the stress free temperature, T_0 , and changes in moisture level from the dry condition. The degradation effects are treated in much the same way, with χ representing the coefficients of degradation induced expansion or shrinkage. This equation can be used in conjunction with composite laminate plate theory (CLPT) to determine the stresses in each ply.

2.8.9 Predictions of glass transition temperature and modelling of DMTA relaxation spectra.

$$T_g = 0.224\theta + 0.0513 \frac{E_{coh}}{N}; \quad (34)$$

The glass transition temperature given by Equation (34) can be extended for analysing complex thermoset polymers [168] as appears in Equation (35);

$$T_g = 0.224\theta + 0.0513 \frac{E_{coh\ mon} + x_{st\ H1}E_{coh\ H1} + x_{st\ H2}E_{coh\ H2} - \Delta E_{et} - \omega}{(N_{mon} - fN_L) + x_{st\ H1}N_{H1} + x_{st\ H2}N_{H2}}, \quad (35)$$

where f is an average functionality of the polymer unit, N_L is number of degrees of freedom lost by each reacted group, ω is the cohesive energy conversion coefficient, and θ is the GIM reference temperature.

The stoichiometric coefficient of hardener in Equation (35) can be found from the hardener weight fraction. It represents the amount of hardener per single polymer unit and is calculated from the component molecular weights and hardener weight fraction;

$$x_{stH1} = \frac{M_{ep}}{M_H} w_H, \quad (36)$$

where M_{ep} and M_H are relative molecular masses of the epoxy monomer and hardener respectively, and w_H is the weight fraction of hardener.

2.8.10 Group Interaction Modelling (GIM) technique

GIM is based on the energy balance, which considers inter-chain interactions. The GIM concept is based on the solution of the main model potential function, Equation (37), which allows derivation of a new set of simplified formulas, giving the practical estimates of major properties from the polymer molecular structure.

$$\phi = -\phi_0 + H_C + H_T + H_m = \phi_0 \left[\left(\frac{r_0}{r} \right)^{12} - 2 \left(\frac{r_0}{r} \right)^6 \right], \quad (37)$$

where H_C , H_T and H_m are configurational, thermal, and mechanical energies respectively, ϕ_0 and r_0 are the potential and separation distance at the state of lowest interaction energy respectively.

The key model input parameters (calculated from the group contribution tables) are the cohesive energy E_{coh} , number of degrees of freedom N , and van der Waals volume V_w . The cohesive energy sums all interaction forces and is proportional to the potential of the system at the lowest energy. A number of degrees of freedom introduce the ability of a structural segment to rotate and change its conformation, and van der Waals volume defines the impenetrable volume of the chain groups. A simplified predictive equation is derived from the main balance Equation (37). The GIM equation is then written in terms of these model input parameters [169].

Since the energy of interaction in GIM (introduced as the potential, ϕ) is calculated from the van der Waals forces between a single polymer unit and six surrounding repeat units, the yield in the model is described as an energy at which the distance r between these adjacent interactive sites begins to increase [169]. Important engineering parameters such as yield stress can be estimated from Equation (38), obtained by expanding the GIM potential Equation (37).

$$\sigma_y = 1.35B \left(1 - \sqrt{\tan \delta_B} \right) \frac{N}{E_{coh}} (T_g - T), \quad (38)$$

where B is the bulk modulus (MPa), and $\tan \delta_B$ is the loss of tangent through secondary relaxations.

Since for many cross-linked thermoset resins, failure by tensile fracture occurs before yielding [170] it was suggested by Attwood *et al* [168] that yield stress be determined in compression. Thus the predictive equation for compressive stress σ_{cy} in GIM is expressed from tensile stress (σ_y) by scaling it with Poisson's ratio.

$$\sigma_{cy} = \frac{\sigma_y}{2\nu}. \quad (39)$$

The bulk modulus in Equation (38) is expressed as the strength of interaction energy per volumetric expansion of the polymer. The bulk modulus may be calculated as follows;

$$B = 1.5 \frac{\phi}{V - V_0} \quad (40)$$

where V and V_0 are GIM specific volumes of a chain at the defined set of energy conditions and at minimum energy state of a conformation respectively. It is also given in GIM as a function of the chain separation distance.

$$B = 1.7 \cdot 10^6 \frac{E_{coh}}{V_w} \frac{\left[2 \left(\frac{r_0}{r} \right)^6 - \left(\frac{r_0}{r} \right)^{12} \right]}{\left(\frac{r_0}{r} \right)^2 - 1} \quad (41)$$

By using an empirical correlation for the separation distance, Equation (41) is further simplified and written for ambient temperature as:

$$B_{am} = 6.4 \frac{E_{coh}}{V_w} \quad (42)$$

By combining the Equations (38), (39) and (42), the yield stress in compression can be written as:

$$\sigma_{cy} = \frac{4.32}{\nu} \left(1 - \sqrt{\tan \delta_B} \right) \frac{N}{V_w} (T_g - T), \quad (43)$$

where the number of degrees of freedom N , in Equations (38) and (43) is taken as that of an average polymer repeat unit;

$$N = N_{mon} - fN_L + x_{stH1}N_{H1} + x_{stH2}N_{H2}. \quad (44)$$

The Poisson's ratio in Equation (43) is estimated by Seitz formula Equation (45), which is described in detail by Bicerano [171];

$$\nu = 0.513 - 0.03054 \sqrt{\frac{\sum V_w}{\sum L_m}}, \quad (45)$$

where L_m is the length in a fully extended conformation of the resin component. The original Equation (45) assumes the van der Waals volume and chain length of a polymer repeat unit. For complex resins it is impossible to parameterise the chain length of an average polymer unit on a stoichiometric basis, thus the component contribution principle for the length of the segments and van der Waals volumes was found to be accurate. The length in fully extended conformation for monomer and hardener can be determined by the specialized modelling software package HyperChem [172].

The loss tangent is a function of the Poisson's ratio and is calculated from Equation (46) given by Equation (47):

$$\nu = 0.5 \left[1 - 0.33 \left(1 - \sqrt{\tan \delta} \right)^2 \right]; \quad (46)$$

$$\tan \delta = \left(\sqrt{\frac{\nu - 0.5}{-0.65}} - 1 \right)^2 \quad (47)$$

The van der Waals volume in Equation (43) is that of an average polymer unit and is calculated from the stoichiometric coefficient:

$$V_w = V_{wmon} + x_{stH1} V_{wH} \quad (48)$$

where V_{wmon} is the van der Waals volume of the monomer, and V_{wH} is the van der Waals volume of hardener.

Group Interaction Modelling technique was verified by experimental data and showed to be in good agreement [172]. Modelling of relaxation envelope on the basis of this method can also explain secondary relaxation of a wet resin bond. Attwood *et al* [168] applied group interaction modelling techniques to predict broadening of the glass-rubber transition for dry state and after moisture absorption. The engineering properties such as yield stress and tensile modulus of the matrix were also successfully modelled using GIM principles.

2.8.11 Moisture induced dimensional changes in composites

Mass absorption is accompanied by dimensional changes in all polymeric materials, and for design purposes these frequently exceed thermally induced expansions or contractions. The coefficient of moisture expansion (CME or β_i) is considered to be equivalent in most composite laminate design codes. However, there are major problems with these assumptions. The major

causes of discrepancies are time effects. Complete understanding of moisture effects requires accurate measurements of saturation moisture contents, three dimensional diffusivities and mass and strain change curves versus time under a variety of environmental parameters such as temperature, pressure, humidity and stress state.

A major direction for investigation is the question of strain-moisture content proportionality at longer times. It was indicated by Wolff [173] that the moisture absorption of some systems does not stabilize at longer times but may either steadily increase with time (at least for a year) or exhibit secondary plateaus. These effects are often attributed to relaxation processes in the polymer and hence one might detect changes in the coefficient of moisture expansion (CME). Additionally, thermal and/or moisture cycling may cause changes in sample porosity, microcracking and debonding at the fibre/matrix interface. At first glance these effects should exhibit increased moisture absorption or desorption with a lesser effect on dimensional changes, hence a lower CME. Sudden environmental changes may involve, for example, rapid drying of the surface causing surface layer shrinkage, or increased surface density and hence an effective surface barrier against further drying (diffusion).

There is a need to measure various cross-coupling coefficients between mass and heat flow, stress, and their gradients and rates of change. For example, the Soret effect is a mass flux caused by a temperature gradient; the Dufour effect is heat flow caused by a concentration gradient. Sih [174] has measured these cross-coupling coefficients for T300/5208. Szekeres *et al* [175] have also extended these considerations to mechanical effects. Toman [176] has suggested that cross coupling coefficients may be detectable by observing deviations from Duhamel-Newman uncoupled constitutive relation [173]. However, few cross coupling coefficients have been measured, mainly because of lack of suitable experimental facilities and a need to define the boundary conditions.

A new approach was proposed by Wolff [173], which can solve current measurement problems. The technique allows simultaneous determination of mass, strain and temperature changes in controlled environments over both short and long periods of time. This requires non-contacting strain and temperature measurement techniques while continuously recording the sample weight change.

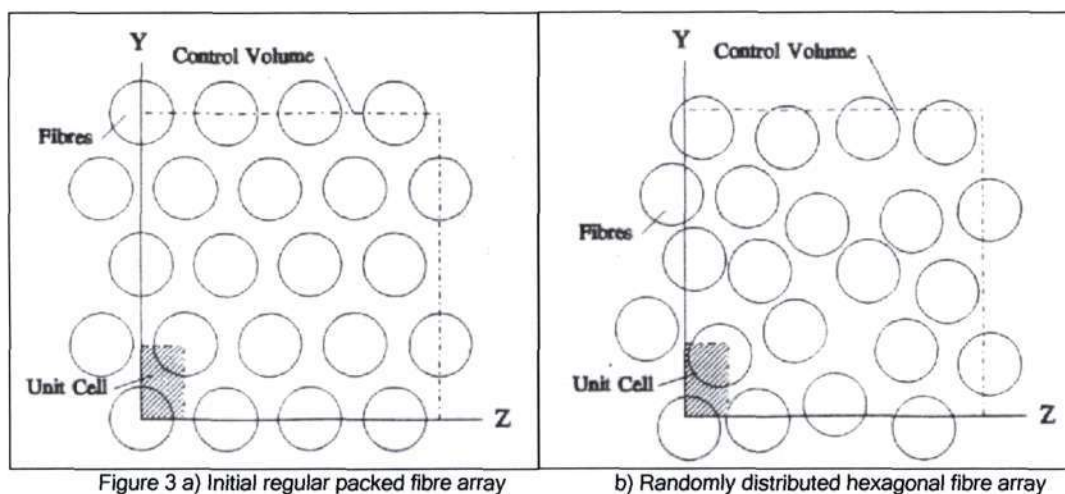
2.8.12 Transverse diffusivity through a random fibre distribution

Several physical parameters affect the transverse diffusivity of fibre reinforced composites. The effect of macroscopic fibre volume fraction has been shown in the previous section while other

factors such as stress [177], void content [135], interphase [135], fibre shape [178] and resin rich regions [179] have been studied quite extensively.

Examination of cross-sections of unidirectional fibre reinforced composites typically show microscopic variations in the fibre volume fraction. This leads to regions of higher-than-average and lower-than-average localised fibre volume fraction. Kondo and Taki [179] attempted to account for such irregularity by including a region of zero volume fraction within a region of higher-than-average volume fraction. This technique, however, remains valid only for resin rich regions within regular packed fibre arrays and fails to take into account irregular packed fibre arrays. Experimental test cases, where concentration at an upper surface was less than both the matrix and homogenised composite maximum moisture content suggests that Kondo and Taki's [179] model is incorrect and that the finite element model is a better approximation for the theoretical composite diffusivity.

In order to determine the effect of irregular fibre packing it is necessary to fully define the physical parameters that affect the absorption characteristics of unidirectional composites. Firstly an assessment of the irregularity is required. Theoretical unit cell volume fraction distribution can be determined from a hard-core Gibb's process simulated in a manner similar to Ripley [180]. A control volume of known bulk volume fraction can be constructed using a hexagonal regular packed fibre array (Figure 3a). From this array random fibres are removed and replaced randomly within the confines of the control volume (edges permitted to overlap: Figure 3b)



The simple one-dimensional solution of Fick's law is performed using FEA. It is important to note that the choice of unit cell affects predicted transverse diffusivity only at high (greater than

0.55) fibre volume fractions. The model proved to provide an excellent first approximation of the transverse diffusivity of fibre reinforced composites.

The transverse diffusivity may be modelled by considering the schematic in Figure 4.

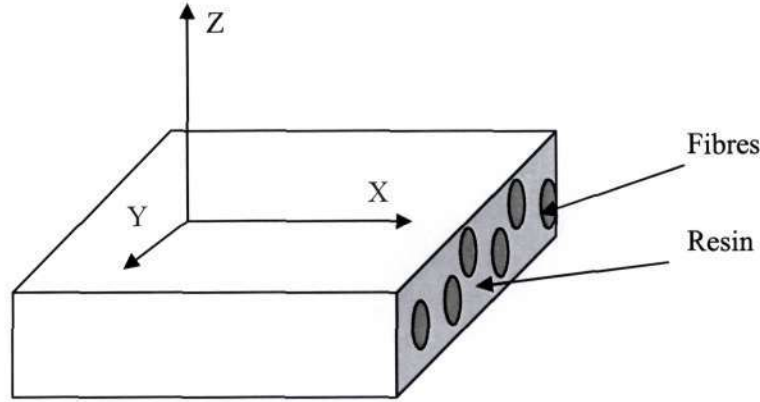


Figure 4 - Principal diffusion axes.

The moisture flux (F) in a particular direction n may be written as:

$$F_n = -D_n \frac{\partial C}{\partial t} \quad (49)$$

A unidirectional fibre-reinforced composite material has three principal diffusion axes as shown in Figure 4. The fibres and matrix are considered to be homogeneous and isotropic thus making the composite diffusivities perpendicular to the fibres equivalent. Fick's law for the steady state condition with no X-axis concentration gradient then reduces to a two dimensional elliptic equation:

$$D_t \left(\frac{\partial^2 C}{\partial y^2} + \frac{\partial^2 C}{\partial z^2} \right) \quad (50)$$

where D_t , represents the transverse diffusivity of the composite. The distribution of fibres within a composite is commonly assumed to be either a tetragonal or hexagonal packed array [124]. Combining Equation (50) and the law of conservation of mass within a control volume, the volume average flux, $([F]_v)$, within each of the cells may then be written as:

$$[F_y]_{\text{hexagonal}} = -D_t \frac{C}{\sqrt{3}(r+e)} \quad [F_y]_{\text{tetragonal}} = -D_t \frac{C}{(r+e)} \quad (51)$$

To homogenise the fibre and matrix contributions into a composite relation, the flux within the cells is integrated to produce an alternative expression for the volume average flux;

$$[F_y] = \frac{1}{V} \int_V (F_{ym} + F_{yt}) dt = \frac{1}{V} \left(\int_{V_m} D_m \left(\frac{\partial C}{\partial y} \right)_m dV_m + \int_{V_t} D_t \left(\frac{\partial C}{\partial y} \right)_t dV_t \right), \quad (52)$$

where the subscripts f and m represent the fibre and matrix properties respectively.

For composites comprised of glass or graphite fibres the contribution of the fibre to the diffusivity of the unit cell may be neglected as they do not absorb moisture. This allows Equation (51) and (52) to be combined to yield;

$$\frac{D_t}{D_m} = \frac{\int_{V_m} D_m \left(\frac{\partial C}{\partial y} \right)_m dV_m}{C(r+e)} \quad (53)$$

for both unit cells. The solution to the volume integral is obtained through use of FEA, utilising eight node iso-parametric quadrilateral elements to model the composite matrix, and applying the corresponding boundary conditions.

In the simulation conducted by Bond *et al.* [67] the diffusivity ratio was found to be unaffected by use of a random fibre distribution suggesting that the regular array model is adequate provided the fibres may be considered to be in a truly random distribution. If however, a resin layer is formed between two layers of randomly distributed fibres, a reduction in bulk composite diffusivity is predicted for a given bulk composite fibre-volume fraction. This effect may be used to account, in part, for the variation between the experimental and regular array model results.

2.9 Accelerated environmental exposure testing

Weathering overall is difficult to determine as polymers, hardeners and accelerators when used in different combinations, may have specific effects that apply to a particular combination. Accelerated testing may be used but with caution as acceleration of one degradation mode may change the overall degradation of all degradation modes acting together. Acting singularly, the degradation is different from the combination of effects. Lee and Neville [181] have described the degradation on epoxy castings as minor but detrimental on thin films which may be found on laminates. Restriction of the extent of degradation to surface films provides increasing evidence that degradation is a surface phenomenon.

In order to successfully accelerate the degradation of materials, the environmental variables and their effect on polymer composites in the natural atmosphere need to be understood and measured. These variables may then be intensified to accelerate the degradation of the materials

tested. The variability of environmental factors in the natural environment needs to be considered as this may result in varying degradation rates of specific degradation modes.

Attempts have been made to accelerate the degradation of polymer composite materials by accelerating single environmental factors responsible for the degradation, to determine the long term performance of FRP composites. Jacques [1] has discussed the relationship between environmental variables and current techniques employed to accelerate the degradation process. Test methodology and design have been outlined with the process beginning at site measurement through to establishment of a model to predict the behaviour of the degradation mechanism/s. Practical solutions to problems encountered in both natural and accelerated tests have been suggested.

Bank *et al* [182] have reviewed technical literature relating to the determination of accelerated test methods for the prediction of long term performance of FRP composites for highway structural applications. Further, a collaboration by gathering data from mechanical testing, Scanning Electron Microscopy (SEM) and chemical analysis has been suggested with a review of chemical techniques provided for the determination of chemical changes that occur due to degradation. Accelerated tests performed by accelerating one factor, may lead to failure in both fibres and matrix that would otherwise not manifest. Such a case has been described by Vauthier *et al*, [183] in which hygrothermal ageing caused changes in the matrix which facilitated degradation of the fibres. The repeatability of results due to accelerated exposure has been addressed by Martin *et al* [184] in which the lack of repeatability was attributed to systematic errors of accelerated exposure tests.

The degree of cure after manufacture needs to be considered in accelerated exposure studies. A fully cured system is one in which the degree of cross-linking provides optimal physical and mechanical properties. Curing proceeds when there is a conversion of reactive groups and coupling of molecules into three dimensional networks, known as cross-linking, from the long non-cross-linked structure. Both, the conversion of reactive groups and cross-linking are required, with temperature affecting the state of cure of the polymer. Methods to determine the extent of curing has been discussed by Lee and Neville [181]. In low temperature cure epoxies, e.g. laminating resin, curing at low temperature is thought to promote polymerisation with postcuring providing the necessary cross-linking.

In contrast to the natural environment, the environment in an accelerated conditioning chamber is carefully controlled. An understanding of these variables and their effects is important at the design stages of the environmental chamber as the ranges and intensity of each will provide

functional requirements that must be satisfied by the final design. Environmental chamber designs were reviewed and an alternative design proposed [184], with the conclusion being that an environmental chamber and correct test methodology are required in order to derive the maximum benefit from accelerated exposure tests. Test methodologies have been outlined by Gates and Grayson [185] for the screening of polymeric composites.

2.9.1 Ultraviolet (UV) radiation

To determine the effect of exposure to sunlight, it is required that the specimens be subjected to the same light distribution as natural light but at a higher intensity. Thus the light source used for the accelerated exposure is required to have the same energy distribution as natural light, which may not always be possible due to available lamps producing only a segment of the sunlight energy distribution as illustrated in Figure 5.

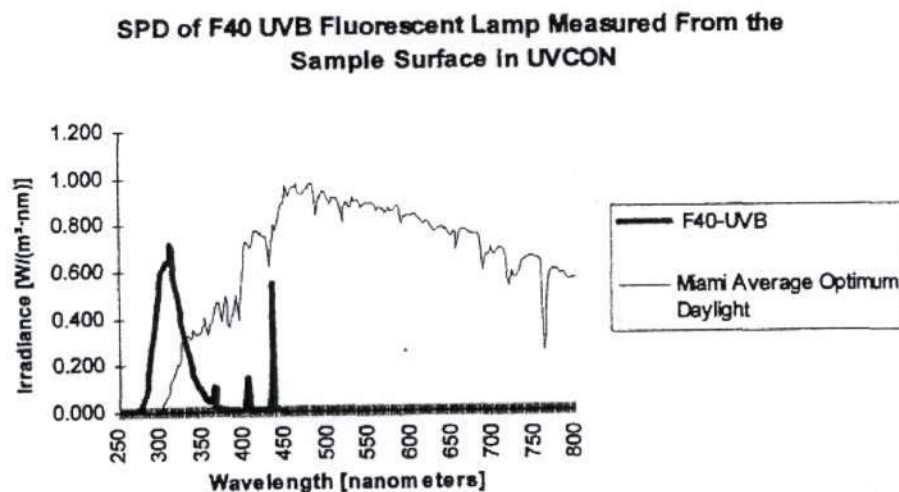


Figure 5 - Energy distribution of a fluorescent lamp compared to sunlight [1]

It is therefore important that the correct type of lamp be selected to provide the energy distribution in the segment of the radiation spectrum of concern. However these lamps may be suited to the application at the beginning of use but the output soon decays with time and the output energy distribution soon becomes unreliable. To average any change in output of a single bulb, a common practice is to rotate the lamps on a set of multiple lamps. This practice at best averages the output of a bank of lamps but does not prevent a decrease in the total energy output of the lamp bank.

Different types of sunlight simulation lamps, namely xenon arc, carbon arc and fluorescent, are commercially available but their effect on materials using similar settings differ [186]. For example, carbon arc and xenon lamps may have different effects on similar specimens under examination. Metal halide and mercury lamps are available but not commonly used. Xenon arc

lamps are commonly used and specified in ASTM G26 and ASTM G155. These lamps produce an irradiance over a larger range of the radiation spectrum when compared to fluorescent lamps. As this light source compares to sunlight over a larger range, it is possible to calculate radiant energy dosage and intensity comparable to natural radiation as reported by Jacques [1] on examining a building code [187] that specifies the xenon arc exposure for roofing materials.

On glass-fibre reinforced composites, the matrix is affected by exposure to UV radiation. The effect of radiation on the matrix cannot be studied by examining damage of neat cast specimens of the resin alone. Degradation behaviour would change when examining fibre-reinforced polymer composites as the surface of laminates is inevitably composed of a thin film of resin. The effect of radiation on this thin film is significant as physical deterioration may occur which would result in a change in mechanical properties. In contrast, the degradation of the surface of a neat cast specimen may be undetectable.

Wavelength cut-off and irradiance intensity need to be considered when conducting accelerated UV exposure. Using a light source with different wavelength cut-offs when compared to sunlight may result in damage occurring that would not otherwise manifest. This is particularly important at lower wavelengths, where damage induced due to higher photon energies may result in inaccurate test results. The extent of damage may be such that it leads to performance reversals of materials when compared to outdoor exposure test results [188]. Incorrect results may also be due to intensities increased to such an extent, to accelerate the tests, that different degradation mechanisms manifest that would otherwise not occur during natural exposure of the specimens. Crewdson [189] has found that unnatural degradation did occur when the irradiance level was too high. A further problem that may arise, is when at increased irradiation levels, some materials may rapidly degrade but not others as noted by Jacques [1] upon comparing the higher irradiance level used by the Japanese automobile industry to that used by the Society of Automotive Engineers. Increasing the level of irradiance threefold does not increase the degradation rate by a factor of three [189]. Discussion between Jacques and Searle [1] confirms reports of similar observations. It is thought that excess radicals that are formed during exposure at higher intensity cannot all be used as part of the normal degradation process. The free radicals may then recombine reducing the effect of higher radiation intensity on exposure.

Thus successful acceleration of UV exposure requires irradiation at the wavelengths of interest and at an intensity that would ensure free radicals for the degradation to proceed uninhibited, while ensuring that a minimum of free radicals remain in excess thus reducing the possibility of the radicals recombining. The intensity at which this would occur is difficult to establish. The wavelength of interest at which the test is performed will depend on the objective of the test.

2.9.2 Moisture

A conditioning process that simulates real ageing requires months or even years, which is experimentally unacceptable. Therefore accelerated ageing techniques have been developed that take several days or a few weeks [190]. The effect of moisture on glass-fibre reinforced laminates is predominantly related to matrix dominated strength properties [32]. From the data reviewed, [32] both moisture and temperature appear to result in a decrease in elevated temperature strength of the material while having no effect on low temperature strength. The extent to which the properties are affected is related to the change in glass transition temperature of the material.

Accelerated moisture conditioning involves the acceleration of the diffusion of water into a laminate until the level of moisture at the interior reaches a predetermined level. This would generally be the equilibrium level reached at the interior of the laminate in the service environment. After accelerated conditioning, the laminate would be removed and subjected to mechanical tests to determine the reduction in mechanical properties, if any. However not all service environments are steady and the problem of determining the moisture content of the interior of the laminate is complicated by cycling moisture and temperature profiles of the end-use environments. Accelerated moisture conditioning maybe performed by wetting specimens by condensation. This can be accomplished by mounting the specimens above a trough of heated water. Cooling of laminates above the trough by ambient air would result in condensation forming on the laminates [191]. Spray cycles may be employed to simulate rainfall. When degradation due to humidity is being examined, humidity within the environmental chamber needs to be measured and controlled. An elaborate system of moisture cycling involves the introduction of a fine water spray into a moving air stream that would be driven by a blower. The control of the flow of water into the water atomiser would control the humidity in the chamber. At 100% relative humidity, the weight gain on polymer composites may be between 1.0% to 2.5% [32]. Accelerated moisture conditioning does not simply entail exposing specimens to maximum humidity in a test chamber. A defined procedure and the proper selection of test parameters can result in moisture being diffused into the laminate at a faster rate than exposure to a maximum humidity environment [31].

The kinetics of the diffusion process depends on the temperature and relative humidity, i.e. the higher the relative humidity the greater the absorption rate, but this leads to non-uniform moisture distribution in the material. By contrast, if the relative humidity is held constant and the temperature is increased, the diffusion coefficient also increases and the kinetics of diffusion speeds up. These considerations also hold when the conditioning is obtained by immersion. The temperature must remain well below the resin glass transition temperature so as to avoid onset

of irreversible damage (swelling and cracks), which permanently changes the absorption characteristics of the material. In addition, if the temperature and relative humidity are too high, anomalous diffusion occurs [192, 193].

2.9.3 Temperature

The effect of temperature on laminates is similar to the effect of absorbed moisture in that it results in a decrease in stiffness and strength. Elevated temperature exposure results in a decrease in the glass transition temperature of the polymer matrix. The conduction of heat into the laminate is analogous to the diffusion of moisture into the laminate. The thermal conductivity may be determined from tests or calculated knowing the fibre-volume fractions, with the relations given by Springer [31]. Damage due to exposure at elevated temperature primarily affect matrix dominated properties in glass-fibre reinforced composites.

2.9.4 Accelerated environmental testing vs. real environmental exposure

Accelerated environmental testing of materials is commonly used to enable tests within a short time frame [194, 195]. However, it is often found that accelerated testing does not reveal the true long-term behaviour, or even provide the correct ranking of candidate materials. Also, many compromises are inherent in accelerated test procedures, meaning that fully realistic test conditions are often not used. For example, it is not realistic to examine the combined influence of UV radiation, varying humidity levels, wind speed (changing convective heat transfer conditions) and alternating load conditions on the mechanical properties of composite materials. During real environmental exposure of aircraft structures, it is likely that these influences will combine to provide actual conditions very different from those commonly used in test laboratories.

The reliability of aircraft materials during use in subtropical climates implies examining the influence of environmental conditions on the durability of aircraft components under field conditions, which include:

- Equilibrium moisture absorption level of the composite material,
- The environmental durability of the materials used (including paint finishes and sealants) with representative damage or repairs,
- The influence of exposure location and type on the environmental durability.

This information is necessary to:

- assess the need to dry out aircraft components prior to repair, and assess any residual strength degradation due to moisture absorption and its interaction with pre-existing damage,

- indicate the need for any preventative maintenance actions should the material systems be found to be significantly degraded by the exposure conditions and,
- permit assessment of the best options for the storage of aircraft and aircraft components at bases, for example, and hence to decide if aircraft shelters are necessary to avoid significant degradation of components.

An environmental durability trial is being conducted on F/A-18 (which has approximately 34% of its external surface constructed from graphite/epoxy) [95] at five tropical test sites in Australia and Malaysia. In this trial, laminates unprotected by paint rapidly degrade on exposure to UV radiation and shading of aircraft by shelters or hangers is desirable to extend the life of paint schemes. There was generally no consistent degradation of interlaminar shear strength values of laminates due to UV exposure. Sandwich beams representative of aircraft structure with damage and simple repairs, have demonstrated excellent durability under the combined effects of outdoor tropical exposure and cyclic loading to approximately the design limit load. These observations are inconsistent with specimens subjected to accelerated conditioning.

Kumar *et al* [196] have reported the presence of microcracks on specimens subjected to accelerated testing. Of the four exposure conditions, i.e. exposure to UV only, exposure to condensation only, sequential exposure to UV and condensation and cyclic exposure to UV and condensation, the microcracks were observed on specimens subjected to the cyclic exposure condition. The cyclic exposure consisted of six hours of UV exposure (295nm - 365nm) followed by six hours of condensation in a QUV/Se environmental chamber. From the literature reviewed, the specimens exposed to the above cyclic exposure condition incurred damage that correlated closely to damage incurred on naturally exposed specimens.

2.10 Experimental testing

Tests to measure the change in characteristics of degraded specimens are used in order to assess the state of degradation. This is accomplished by measuring changes in moisture content, glass transition temperature, weight loss and electrical properties amongst other characteristics. As these characteristics are found to change with increasing degradation state, attempts were made to correlate these characteristics to either assess the extent of degradation or provide input data into degradation models for the determination of the extent of degradation.

2.10.1 Determination of in-plane stiffness properties of the ageing laminate

Determination of mechanical properties of a laminate in the transverse direction is of a great importance, because it can be used for further estimation of matrix degradation. Degradation of

the bond between the matrix and fibres can be estimated by analysis of shear properties of a laminate.

A conventional way of determining these properties are destructive mechanical tests based on 3-point bending (standard EN 63) and interlaminar shear tests (standard NFT 57107 or ISO 4585). A disadvantage of these tests is that they require a large quantity of beam or dog-bone shaped samples when the ageing time is long. Also, it is difficult to quantify the influence of water absorption through the lateral faces of beams. Thus E_1 , E_2 , σ_{r1} , σ_{r2} , τ_{r1} and τ_{r2} are measured only at initial state, after 2000 hours of immersion when the gel-coat blistering has appeared, and then after 5000 hours of immersion when the delamination of the first ply has occurred. A faster way of determination of the in-plane moduli E_1 , E_2 , and G_{12} , (after every 200 hours of immersion) is carried out by modal analysis experiments on plates. The two methods are complementary.

2.10.2 Modal analysis

The method has been developed [197, 198] to evaluate the mechanical properties of rectangular, anisotropic and homogeneous plates with four free edges. The methods consists of measuring the natural frequencies of the plate and using these values to determine the rigidities. For the first step, the natural frequencies of the plate are measured using accelerometers and their associated mode shapes are identified. This is achieved by exciting the plate with a small hammer to stress the laminate with a bending load. Then the approximate rigidities of the plate are introduced into a theoretical model so that the calculated natural frequencies match as closely as possible the corresponding experimental values.

The theoretical model of the vibration behaviour of an anisotropic plate is based on the classical theory of plates [199, 200] in plane stress. The plate rigidities are calculated with an iterative method [197]. Measurement errors or rigidity uncertainties are dealt with using min-max approximation optimisation methods. The frequencies of orthotropic rectangular free edges plates are calculated in the following way:

$$f_{i,j}^2 = \frac{\pi^2}{4\rho h} \left[\frac{G_1^4 D_{11}}{a^4} + \frac{G_2^4 D_{22}}{b^4} + \frac{2H_1 H_2 D_k}{a^2 b^2} + \frac{D_{66}(J_1 J_2 - H_1 H_2)}{a^2 b^2} \right], \quad (54)$$

where $f_{i,j}$ is the natural frequency in Hz; i, j are the number of nodes in x and y directions respectively, ρ is the density, h the thickness, a the length (in x direction), b the width (in y direction) of the plate respectively and G_n , H_n , J_n are constant functions of the indices i, j [197, 198, 199, 200]. The rigidities are defined as follows:

$$D_{11} = \frac{E_1 h^3}{12(1 - \nu_{12}\nu_{21})}; \quad D_{12} = \frac{E_2 h^3}{12(1 - \nu_{12}\nu_{21})}; \quad D_k = D_{12} + 2D_{66}; \quad D_{66} = \frac{1}{12} D_{12} h^3. \quad (55)$$

E_1 is the elastic modulus parallel to the fibres or longitudinal modulus;

E_2 is the modulus in the direction perpendicular to the reinforcement (transverse modulus);

G_{12} is the in-plane shear modulus;

ν_{12} is the longitudinal Poisson's ratio.

The ultimate stresses are;

σ_{r1} is the ultimate flexural stress in the longitudinal direction;

σ_{r2} is the ultimate flexural stress in the transverse direction;

τ_{r1} is the ultimate interlaminar shear stress in the longitudinal direction;

The rigidities are deduced from the frequencies $f_{i,j}$. Knowing the first five natural frequencies and their associated mode-shapes allows one to determinate the elastic constants E_1 , E_2 , G_{12} and ν_{12} . This method also allows the study of the damping of the materials and thus the visco-elastic behaviour, and its evolution with time of ageing.

2.10.3 Determination of content and distribution of moisture in a laminate

In order to predict mathematically the content and distribution of moisture in a laminate it is necessary to know the equilibrium level, i.e. the maximum amount of moisture that can be absorbed by a laminate at a given humidity, and the diffusion coefficient D . To measure these data normally requires exposure times of over six months, even for relatively thin laminates being one millimetre thick [201].

The procedure described by Copley [201] can be found useful for experimental determination of content and distribution of moisture in a laminate. Specimens are immersed in boiling water so the equilibrium level can be reached in a period of few weeks. During the conditioning the specimens are periodically removed from the environment and weighed using an electronic balance. The weight gain, expressed as a percentage of their dry weight, is plotted against square root time. The slope of the linear segment is used subsequently in the calculation of the diffusion coefficient:

$$D_\infty = D \left(1 + \frac{h}{W} + \frac{h}{l} \right)^{-2} \quad (56)$$

After the maximum moisture content is reached, the specimens are removed and weighed once more before being machined in readiness for through thickness slitting. Each specimen is then

sliced carefully all the way through to give six slices. By weighing, drying and reweighing each slice its percentage uptake of water is found and plotted against through thickness position to give the moisture distribution. The diffusivity of the multidirectional laminate [201] was found to be about 30% higher than that of the unidirectional laminate. It was attributed to existence of more entrances available for the water to diffuse through the plate and due to larger interfacial absorption of the 45° plies [202].

2.10.4 Assessing the water uptake by glass-fibre reinforced composites using thermal analysis and dielectric spectroscopy

Degradation of the fibre-matrix interface and blistering significantly lower the reinforcement of the matrix by the fibre. An anti-plasticisation effect was observed by Boinard *et al* [203] for the vinylester laminate with subsequent reduction in toughness of the laminate. An in-situ monitor for water ingress into GRP has been demonstrated for the composites of the thickness of the order of 20 to 30mm.

Water uptake was assessed by McCrum [204] and Hasted [205], assuming that the variation in the dielectric permittivity of a material during exposure is caused by the increase water dipoles. The dielectric method of monitoring moisture has advantages over gravimetric measurements because it is not sensitive to the leaching of non-polar compounds and therefore will respond to water content independently of any loss of non-polar styrene monomer. Comparison of low and high frequency dielectric data allows differentiation between water molecules free to rotate and those undergoing hydrogen bonding interactions with the resin. The former rotates at a frequency of approximately 10 GHz whereas the latter relaxes at frequencies in the 10 kHz region [77].

The Kirkwood-Frohlich equation, which describes the dielectric response of dipoles in condensed material, has the form [206, 207];

$$\frac{(\epsilon_s - \epsilon_\infty)(2\epsilon_s + \epsilon_\infty)}{\epsilon_s(\epsilon_\infty + 2)^2} = \frac{4\pi N}{9kT} g\mu_0^2 \quad (57)$$

where ϵ_∞ is the dielectric permittivity at a frequency so high that the dipole orientation contributions have vanished, k is the Boltzman constant, T is the temperature, N is the number of molecules per unit volume, μ_0 is the dipole moment of the molecule and g is the orientation correlation function, a measure of the local ordering in the material.

2.10.5 Prediction of glass transition temperature and key engineering properties of a dry / wet epoxy based composite matrix

Much attention has been given to the study of the effects of moisture on key properties of matrix resins. It was found that absorbed water is located in nano-voids [208], which form the free volume of the material [209] and the total amount of absorbed moisture is not the same as the free volume.

The use of such experimental methods as positron annihilation spectroscopy [210, 211] allows one to measure the size and quantity of such sites. The polarity of the network has a strong influence over the moisture uptake resulting in greater moisture content at equilibrium for more polar systems [212]. The moisture transport phenomenon has also been studied in detail where two types of hydrogen links between water and a polymer were found. Type 1 mostly affects the inter-chain interactions resulting in plasticisation and lowering of the properties whereas the type 2 links bridge the segments by secondary cross-linking through hydroxyl groups [213]. The last mechanism is significantly affected by hydrothermal ageing [213]. Plasticisation of the network is generally believed to be a reversible process [213] and the equilibrium concentration of water mainly depends on the type of resin and conditioning [208]. Data on irreversible degradation of matrix and hydrolysis were also reported for some resin systems [214]. Some researchers believe that because a water molecule is linked to resin structural groups it may participate in the relaxation process. Assumptions were made from the study of secondary relaxations of polymers [215].

Since the glass transition temperature is moisture content dependent, several studies were conducted to examine the effect of moisture absorption on the glass transition temperature as a function of moisture content. Among experimental methods for measuring the glass transition temperature and the effect of moisture absorption, Dynamic Mechanical Thermal Analysis (DMTA) is the most common. It is efficient for the study of single component resins and multifunctional blends. Another method such as Thermally Stimulated Depolarisation Current technique can be applied for studying the influence of water on segment relaxation in polymers [216]. A theoretical background can be analysed by Group Interaction Modelling (GIM), a method derived on the basis of lattice model and rotational isomeric state theory.

2.10.6 Thermo-gravimetric Analysis (TGA)

Thermo-gravimetric Analysis (TGA) is a technique that can be used and is capable of measuring the weight loss of the material as a function of time and / or temperature. In this way the degradation kinetics can be studied by correlating the weight loss with the generic degree of reaction. Although TGA data may not give detailed information about the mechanism

complexity of the degradation process, for engineering purposes it can be a useful tool for analysing the overall behaviour of the polymer under extreme conditions. However, attention must be paid to the selection of the experimental temperature range, because the further it is from the real working temperature, the more risky will be the extrapolation [217]. On the other hand, when material is aged at temperatures very close to those of application, the weight loss is not easily detectable within a reasonable time [113].

2.10.7 Non-destructive methods for evaluation of environmental damage

Raman spectroscopy was proven to be a powerful technique for the investigation of micro-mechanical aspects of composites [218], deformation behaviour of fibres of different types [219] and the interfacial fibre-matrix behaviour. As a rule, investigations are normally undertaken by imposing carefully controlled levels of the mechanical load on mini-specimens of different configurations and monitoring the resulting strain in the axial direction of a fibre. Raman spectroscopy can be useful in measuring the physical mechanism responsible for water ingress, diffusion coefficient, saturation value of water in the matrix, relative magnitude of the diffusion coefficients of the constituents, i.e. the matrix and fibre, and interfacial behaviour during hygrothermal ageing with respect to the fibre surface treatment. Using a particular aramid fibre/epoxy resin, Raman spectroscopy has been demonstrated by Cervenka *et al* [87] to be an excellent technique for determining the effect of moisture absorption upon the behaviour of aramid epoxy composites, including the interfacial region.

3 MATHEMATICAL DEGRADATION MODEL

Due to the complexities of degradation as a result of multiple physical processes acting simultaneously, no complete model has yet been published to describe the degradation of mechanical properties of polymer composites with time. Models that have been developed explain degradation of specific materials due to exposure to specific environments. This therefore limits their usefulness to the general problem of degradation of fibre-reinforced polymer composites.

From the literature reviewed it appears that degradation is generally a matrix process. The load carrying capacity of polymer composites exposed to the natural environment was reduced due to the diminution in mechanical properties of the matrix thereby decreasing the ability of the matrix to distribute the applied load to the reinforcing fibres. From the natural exposure tests conducted, it also appears that the damage to the matrix begins at the exposed surface and progresses towards the interior of the laminate. The problem is therefore one of a damaged layer in the matrix of the composite, beginning at the surface and progressing toward the interior.

This situation may be theoretically considered as a single laminate composed of two layers of different materials. The first layer, surface layer, has properties of a degraded material, and the second layer, the undamaged interior, has properties of a polymer composite unaffected by exposure and degradation as appears in Figure 6. As the degraded surface layer consists of cracking, the properties of the degraded layer maybe be calculated by determining the stiffness contribution tensor of a crack. The properties of the undamaged matrix may be computed, and bulk material properties of the laminate can then be calculated as a combination of the material properties of the two layers.

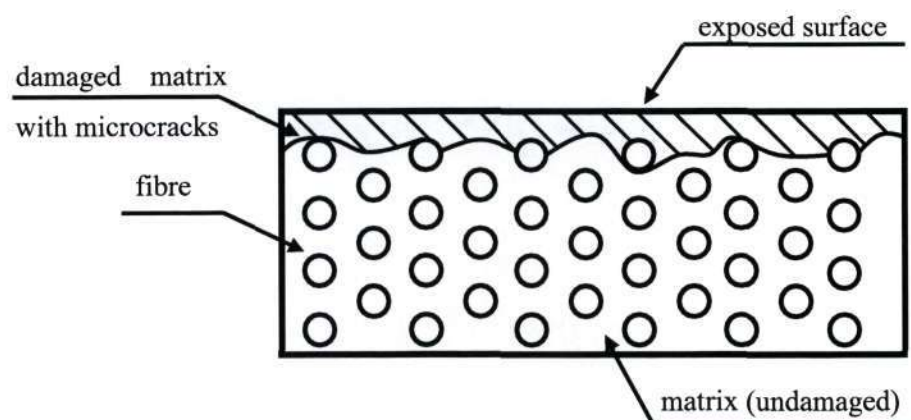


Figure 6 – Illustration of damage

As a further step, the conductivity of the laminate can be determined and a cross-property correlation be established such that by measuring the conductivity, the elasticity can be calculated.

The use of mathematics to construct a model relating the various variables responsible for degradation and their interaction with one another is preferred as such complex relationships may be easily managed using mathematical tools. Testing of the many types of fibre-reinforced polymer composites available in multiple climates is not practical or feasible. A mathematical model describing the simultaneous effect of the underlying damage mechanisms is therefore required to determine the response of the material to varied environments without the expense and time consuming nature of exposure tests. Progress in the development of materials resistant to degradation may be accelerated as the effect of changes may be rapidly determined using a model. Advantages of having a model available include the facility to calculate the degradation in mechanical properties and hence determine the safe service life of structures. Advantage to the end-user includes maintenance optimisation based on the output of the model that utilises inputs characterising the operational environment.

Development of a model, ideally should be based on underlying physical processes responsible for degradation. However material response to the environment can also be modelled by considering the damage induced due to exposure in the natural environment. Thus by knowing the result of exposure, the effect on material properties may be determined. The mathematical model developed and presented below, was based on the quantification of damage induced on a laminate and its contribution to bulk material properties.

3.1 Model of damage progression

The approach used during development of the model assumes that the matrix damage is characterised by a change in Young's Modulus, often an embrittlement of the material, and the development of microcracks. Embrittlement and microcracking are often linked and occur in conjunction. On the basis of this assumption, the approach developed focuses on "top down" damage propagation.

The underlying principle of operation of the model may be explained by considering the initiation and propagation of microcracks as illustrated in the first schematic in Figure 7. The material is assumed defect free after manufacture. A laminate would contain reinforcement uniformly distributed within the laminate. The matrix would be protected by a gelcoat that would act as a barrier between the interior of the laminate and the working environment of the

component. During service, microcracks would develop at the surface of the matrix and progress toward the interior of the laminate. The protective coating at this stage does not have to be completely damaged for microcracking to occur as damage may develop below the protective coating. The damaged layer would have properties different from the underlying undamaged layer which can be calculated knowing the thickness of the damaged layer. Knowing the properties of the remaining undamaged material, the material properties of the two layers may be combined to yield bulk material properties for the laminate. The laminate is thus treated as being functionally graded as bulk material properties change with depth.

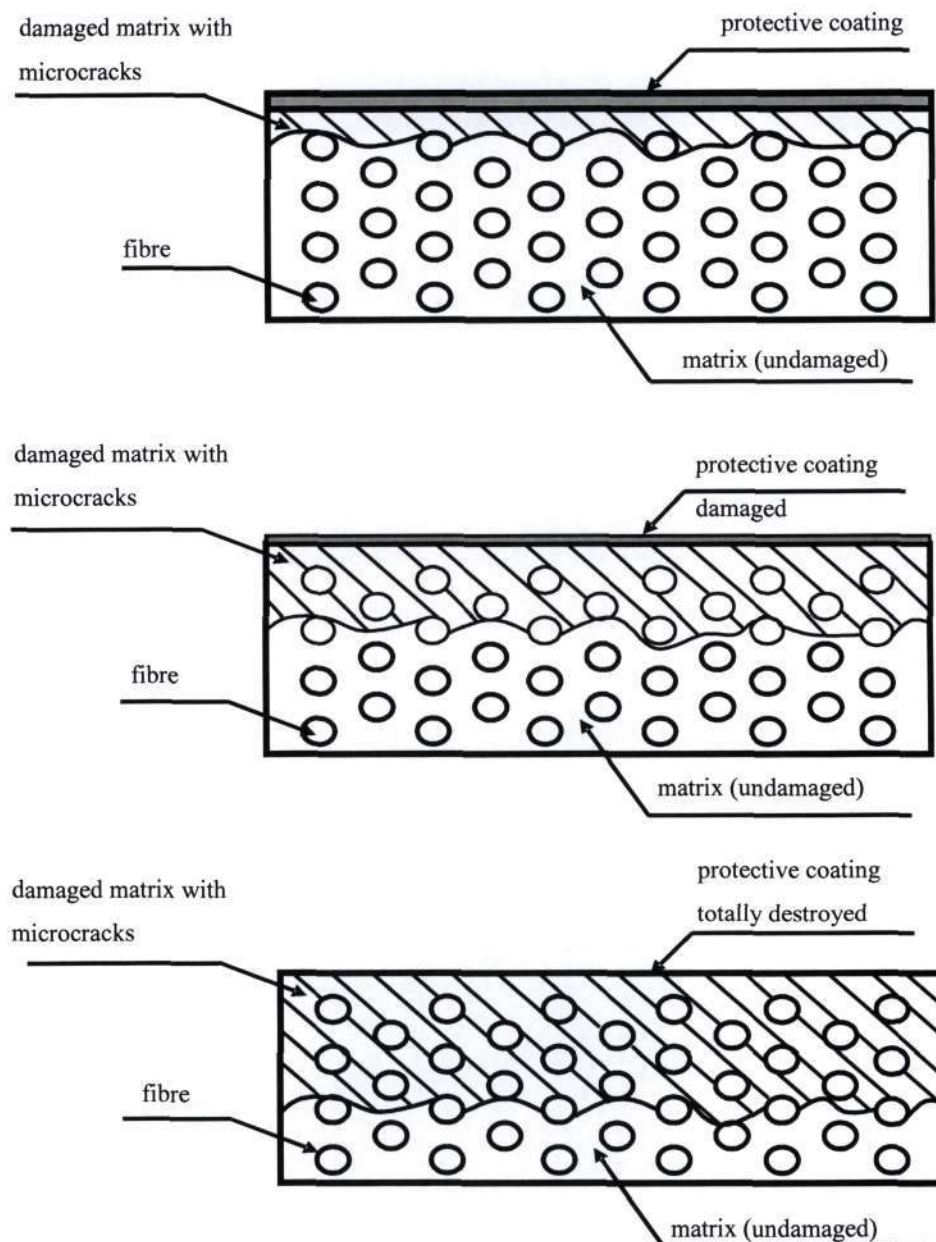


Figure 7 - Progression of damage

With reference to Figure 7, at each time step, knowing the depth of the degraded layer progressing through the material, a calculation is performed which combines the properties of

damaged and undamaged layers to produce overall bulk material properties. At a subsequent time step, the depth of damage increases, material properties for the larger volume of damaged material is calculated, and the bulk material properties recalculated. Damage to the gel coat is not considered as it is assumed that the gel coat does not contribute to the strength of the material. The final time step illustrated is when the gel coat is completely destroyed and the damaged material is predominant on a cross-section.

Simplifications and assumptions made in the development of the model are as follows:

- The microcracking and matrix embrittlement are moving linearly through the thickness.
- The damaged laminate behaves as a Functionally Graded Material (FGM).
- The protective coating does not affect the strength properties.
- Fibre strength is not reduced due to matrix degradation.
- The influence of edge effects on the overall strength of the component is ignored.
- Unidirectional reinforcement is assumed.
- Damage consists of microcracks and matrix embrittlement only.
- Water absorption / loss not considered at this stage.

Microcracks have been modelled as inclusions within the material and the effect on strength calculated in order to determine the overall properties due to both damaged and undamaged material. The damage in the form of inclusions is assumed to have different elastic and conductive properties in comparison to the matrix. Ellipsoid and spheroid inclusion shapes were initially considered.

Experimental data is required to verify the model and determine the rate of progression of the moving boundary. The model thus developed utilizes experimental data obtained from physical testing.

3.2 Effective stiffness of a fibre reinforced composite containing cracks

Following from work performed by Kachanov *et al* [220], the effective stiffness of a fibre reinforced composite containing cracks may be expressed by considering a reference volume V of an infinite three-dimensional medium with an inclusion of volume V^* , a region possessing elastic / conductive properties different from the ones of the surrounding material. Properties of the inclusion and of the matrix can be denoted by an asterisk and by “0”, respectively. The stiffness contribution tensor N of an inclusion is defined by the following relation for the overall stress per volume V :

$$\sigma_{ij} = C_{ijkl}^0 \varepsilon_{kl} + N_{ijkl} \varepsilon_{kl} \quad (58)$$

where the second term represents the stress change $\Delta\sigma_{ij}$ due to the presence of the inclusion.

The N-tensor depends on the inclusion shape and its elastic properties. The term C^0 is the matrix stiffness tensor and ε the “remotely applied” strain field, assumed to be homogeneous in the absence of the inclusion.

To derive an expression for tensor N in explicit form, the solution of Eshelby's problem in the form given by Kunin and Sosnina (1971) has been utilised. If a uniform field ε_{ij}^0 at infinity is prescribed, then the resulting uniform strains inside the ellipsoidal inclusion are obtained [3],

$$\varepsilon_{ij}^{(int)} = \Gamma_{ijkl} \varepsilon_{kl}^0 \quad (59)$$

where $\Gamma_{ijkl} = [J_{ijkl} + P_{ijmn} (C_{mnkl}^* - C_{mnkl}^0)]^{-1}$ and $J_{ijkl} = (\delta_{ik}\delta_{lj} + \delta_{il}\delta_{kj})/2$ is the fourth rank unit tensor. An inverse of symmetric fourth rank tensor X_{ijkl}^{-1} is defined by the relation $X_{ijmn}^{-1} X_{mnkl} = (X_{ijmn} X_{mnkl}^{-1}) = J_{ijkl}$. Tensor P obtained, can be expressed in terms of Eshelby's tensor S ,

$$P_{ijkl} = s_{ijmn} S_{mnkl}^0 \quad (60)$$

Utilizing these results, the tensor of stiffness contribution of the inclusion can be derived [3] and is given by the formula;

$$N = \frac{V_*}{V} \left[(C^* - C^0)^{-1} + P \right]^{-1} \quad (61)$$

For a general ellipsoid, components N_{ijkl} are expressed in terms of elliptic integrals. They reduce to elementary functions for the ellipsoid of revolution, that is, spheroid. In the general case of spheroid tensors, P and N were derived by Sevostianov and Kachanov [221,222].

Considering the limiting cases of cylindrical inclusion and penny-shaped (circular) crack, the analysis requires explicit analytic inversions of fourth rank tensors [3]. Such inversions may be performed by representing these tensors in terms of a certain “standard” tensorial basis $T^{(1)}, \dots, T^{(6)}$ (Kunin, 1983):

$$P = \sum_{k=1}^6 p_k T^{(k)} ; \quad N = \sum_{k=1}^6 n_k T^{(k)} \quad (62)$$

Finding these tensors reduces to calculation of factors p_k and n_k . Using the representations for tensors of elastic stiffness and compliance, Eshelby's tensor and unit tensor in terms of this basis yields the following relations for coefficients p_i [220]:

$$\begin{aligned} p_1 &= \frac{1}{2G_0} [(1-\kappa)f_0 + f_1], & p_2 &= \frac{1}{2G_0} [(2-\kappa)f_0 + f_1], & p_3 &= p_4 = -\frac{1}{G_0} f_1 \\ p_5 &= \frac{1}{G_0} [1 - f_0 - 4f_1], & p_6 &= \frac{1}{G_0} [(1-\kappa)(1-2f_0) + 2f_1] \end{aligned} \quad (63)$$

with the following notations defined,

$$\kappa = \frac{1}{2(1-\nu_0)}, \quad f_0 = \frac{\gamma^2(1-g)}{2(\gamma^2-1)}, \quad f_1 = \frac{\kappa\gamma^2}{4(\gamma^2-1)^2} [(2\gamma^2+1)g-3] \quad (64)$$

where shape factor g is expressed in terms of aspect ratio γ as follows

$$g(\gamma) = \begin{cases} \frac{1}{\gamma\sqrt{1-\gamma^2}} \arctan \frac{\sqrt{1-\gamma^2}}{\gamma}, & \text{oblate shape } (\gamma < 1) \\ \frac{1}{2\gamma\sqrt{\gamma^2-1}} \ln \frac{\gamma + \sqrt{\gamma^2-1}}{\gamma - \sqrt{\gamma^2-1}}, & \text{prolate shape } (\gamma > 1) \end{cases} \quad (65)$$

3.3 Stiffness contribution tensor of a fibre

In the case of infinite cylinder $\gamma \rightarrow \infty$, $f_0 \rightarrow 1/2$, $f_1 \rightarrow 0$, the following relations for tensor \mathbf{P} are obtained [3]:

$$\mathbf{P} = \frac{1}{4G_0} \left[(1-\kappa)\mathbf{T}^{(1)} + (2-\kappa)\mathbf{T}^{(2)} + 2\mathbf{T}^{(5)} \right] \quad (66)$$

Using Equation (65), the following expressions for coefficients n_i of the representation (66) for the stiffness contribution tensor of a fibre in terms of elastic constants of the matrix G_0 and of the fibre-matrix elastic constants are as follows [3]:

$$\delta\lambda = \lambda^* - \lambda_0, \quad \delta G = G^* - G_0$$

$$n_1 = \frac{\pi a^2}{S} \frac{(\delta\lambda + \delta G)(\lambda_0 + G_0)}{(\lambda_0 + 2G_0) + (\delta\lambda + \delta G)}, \quad n_2 = \frac{\pi a^2}{S} \frac{4\delta G G_0(\lambda_0 + 2G_0)}{2G_0(\lambda_0 + 2G_0) + \delta G(\lambda_0 + 3G_0)},$$

$$n_3 = n_4 = \frac{\delta\lambda(\lambda_0 + 2G_0)}{(\lambda_0 + 2G_0) + (\delta\lambda + \delta G)}, \quad n_5 = \frac{\pi a^2}{S} \frac{8\delta G G_0}{2G_0 + \delta G}$$

$$n_6 = \frac{\pi a^2}{S} \frac{(\delta\lambda + 2\delta G)(\lambda_0 + G_0) + 2G_0(3\delta\lambda + 2\delta G)}{(\lambda_0 + 2G_0) + (\delta\lambda + \delta G)} \quad (67)$$

where a is the radius of the fibre and S is the representative cross-section area. Instead of volumes ratio, areas ratio appear in the expression for the stiffness contribution tensor of a fibre.

3.4 Stiffness contribution tensor of a crack, an approximate representation

In the case of penny-shaped (circular) crack the following was obtained [3], $\gamma \rightarrow 0$,

$f_0 = \pi\gamma/4$, $f_1 = \kappa\pi\gamma/8$ and tensor \mathbf{P} :

$$\mathbf{P} = \frac{1}{G_0} [\mathbf{T}^{(5)} + (1 - \kappa)\mathbf{T}^{(6)}] \quad (68)$$

The stiffness contribution tensor of a crack in terms of elastic constants of the matrix and crack size was given as:

$$\begin{aligned} n_1 &= -\frac{4}{3} \frac{a^3}{V} \frac{\lambda^2(\lambda + 2G)}{G(\lambda + G)}; \quad n_2 = 0; \quad n_3 = n_4 = -\frac{4}{3} \frac{a^3}{V} \frac{\lambda(\lambda + 2G)^2}{G(\lambda + G)} \\ n_5 &= -\frac{16}{3} \frac{a^3}{V} \frac{G(\lambda + 2G)}{3\lambda + 4G}; \quad n_6 = -\frac{4}{3} \frac{a^3}{V} \frac{(\lambda + 2G)^3}{G(\lambda + G)} \end{aligned} \quad (69)$$

with the change in elastic stiffness due to a crack given by,

$$\mathbf{C} - \mathbf{C}_0 = \frac{a^3}{V} [U_1 \mathbf{I} \mathbf{I} + U_2 \text{tr} \mathbf{J} + U_3 (\mathbf{I} \mathbf{n} \mathbf{n} + \mathbf{n} \mathbf{n} \mathbf{I}) + U_4 (\mathbf{J} \cdot \mathbf{n} \mathbf{n} + \mathbf{n} \mathbf{n} \cdot \mathbf{J}) + U_5 \mathbf{n} \mathbf{n} \mathbf{n} \mathbf{n}] \quad (70)$$

where coefficients U_i are expressed in terms of coefficients n_i as follows:

$$\begin{aligned} U_1 &= n_1 - n_2/2 = -\frac{4}{3} \frac{a^3}{V} \frac{\lambda^2(\lambda + 2G)}{G(\lambda + G)}; \quad U_2 = n_2 = 0 \\ U_3 &= 2(n_3 - n_1) + n_2 = -\frac{16}{3} \frac{a^3}{V} \frac{\lambda(\lambda + 2G)}{(\lambda + G)} \\ U_4 &= n_5 = -\frac{16}{3} \frac{a^3}{V} \frac{G(\lambda + 2G)}{3\lambda + 4G} \\ U_5 &= n_6 + n_1 + n_2/2 - 2n_3 - n_5 = -\frac{16}{3} \frac{a^3}{V} \frac{G(\lambda + 2G)(2\lambda + 3G)}{(\lambda + G)(3\lambda + 4G)} \end{aligned} \quad (71)$$

Establishing the cross-property correlations depends on the possibility to express, with sufficient accuracy, the stiffness contribution tensor of an inclusion in terms of a second rank

tensor. Hence for a solid with one crack, the crack's stiffness contribution tensor N is first reduced, with sufficient accuracy, to one in terms of a second rank symmetric tensor nn :

$$N = G_0 \frac{a^3}{V} [D_1 \mathbf{I} \mathbf{I} + D_2 \mathbf{J} + D_3 (nn \mathbf{I} + \mathbf{I} nn) + D_4 (nn \cdot \mathbf{J} + \mathbf{J} \cdot nn)] \quad (72)$$

where D_i are scalar coefficients that have to be determined.

The “isotropic terms” in Equation (72) are expressed in terms of the second rank and fourth rank unit tensors ($I_{ij} = d_{ij}$ and $2J_{ijkl} = d_{ik}d_{jl} + d_{il}d_{jk}$) and do not depend on the inclusion orientation. The representation (72) implies the following restrictions on coefficients n_i [3]:

$$n_6 + n_1 + n_2/2 - 2n_3 - n_5 = 0 \quad (73)$$

With the exception of a sphere representation, Equation 72 is not exact. Sevostianov and Kachanov [220] showed that Equation (73) is satisfied, with good accuracy, for spheroids within several ranges of parameters that, being sufficiently wide, are relevant for realistic polymer matrix composites.

This can be achieved [3] by constructing a fictitious stiffness contribution tensor \hat{N} , with coefficients \hat{n}_i in the tensorial basis that are obtained from n_i by multiplication of n_i by either $(1 + \delta)$ or $(1 - \delta)$, and choose δ in such a way that condition (73) is satisfied exactly for \hat{n}_i :

$$\begin{aligned} \hat{n}_1 &= n_1(1 - \delta \operatorname{sign} n_1) & \hat{n}_3 &= n_3(1 + \delta \operatorname{sign} n_3) \\ \hat{n}_2 &= n_2(1 - \delta \operatorname{sign} n_2) & \hat{n}_5 &= n_5(1 + \delta \operatorname{sign} n_5) \\ & & \hat{n}_6 &= n_6(1 - \delta \operatorname{sign} n_6) \end{aligned} \quad (74)$$

where

$$\delta = \frac{n_6 + n_1 + n_2/2 - 2n_3 - n_5}{|n_6| + |n_1| + |n_2|/2 + 2|n_3| + |n_5|} \quad (75)$$

The error of this approximation, as estimated by the norm $\max_{ijkl, N_{ijkl} \neq 0} |(N_{ijkl} - \hat{N}_{ijkl})/N_{ijkl}|$, is equal to $|\delta|$. The choice of this norm, as the measure of accuracy of representation (72) corresponds to the requirement that strain responses to all stress states of the actual and fictitious inclusions are close if the norm is small.

From the above, the coefficients for D_i were given as follows:

$$\begin{aligned} D_1 &= (\hat{n}_1 - \hat{n}_2/2)/G_0; \quad D_2 = \hat{n}_2/G_0; \\ D_3 &= (2\hat{n}_3 + \hat{n}_2 - 2\hat{n}_1)/G_0; \quad D_4 = (\hat{n}_5 - 2\hat{n}_2)/G_0 \end{aligned} \quad (76)$$

3.5 Effective elastic properties of fibre reinforced composite containing cracks

For a fibre-reinforced solid with microcracks, the following expressions for the effective stiffness tensor in non-interaction approximation was given [3] as:

$$\begin{aligned} \mathbf{C} = \mathbf{C}_0 + & \left(\rho d_1^c + c_f d_1^f \right) \mathbf{I} \mathbf{I} + c_f d_2^f \mathbf{J} + c_f d_3^f (\mathbf{I} \mathbf{n} \mathbf{n} + \mathbf{n} \mathbf{n} \mathbf{I}) \\ & + c_f d_4^f (\mathbf{J} \cdot \mathbf{n} \mathbf{n} + \mathbf{n} \mathbf{n} \cdot \mathbf{J}) + c_f d_5^f \mathbf{n} \mathbf{n} \mathbf{n} \mathbf{n} + d_3^c (\mathbf{I} \mathbf{a} + \mathbf{a} \mathbf{I}) + d_4^c (\mathbf{J} \cdot \mathbf{a} + \mathbf{a} \cdot \mathbf{J}) \end{aligned} \quad (77)$$

where c_f is the volume fraction of the fibres, k_f is the conductivity of the fibres and coefficients d in Equation (77) listed previously.

3.6 Effective conductivity of a fibre reinforced composite containing cracks.

Sevostianov and Verijenko [223] observed that both mechanical and conductive properties can be described in the same way. To determine the resistivity contribution tensor of an inclusion, the thermal conductivity problem that is mathematically equivalent to the electric conductivity problem, was examined. First, a reference volume V of an infinite three-dimensional solid was considered (with the isotropic thermal conductivity k_0) containing a spherical inclusion with the isotropic thermal conductivity k_* (limiting cases $k_* = 0$ and $k_* = \infty$ correspond to a perfect insulator and a superconductor). Assuming a linear conduction law (linear relation between the far-field temperature gradient \mathbf{G} and the heat flux vector \mathbf{U} per volume V), the linear relation for the change due to the inclusion is given by:

$$\Delta \mathbf{G} = -\frac{1}{V} \mathbf{H}^R \cdot \mathbf{U} \quad (78)$$

where the symmetric second rank tensor \mathbf{H}^R can be called the resistivity contribution tensor of an inclusion and superscript R indicates resistivity, in contrast with \mathbf{H} for elasticity. Equation (78) may be interpreted as the change in temperature gradient that is required to maintain the same heat flux after the inclusion has been introduced.

Utilizing a similar approach as used for the elastic problem, tensor \mathbf{H}^R was expressed in terms of Eshelby's tensor for conductivity \mathbf{s}^K ;

$$\mathbf{H}^R = \frac{V^*}{V} k_0 \left(\frac{k_0}{k_* - k_0} \mathbf{I} - \mathbf{s}^K \right)^{-1} \quad (79)$$

In the case of the spherical pore, tensor \mathbf{s}^K was derived by Levin *et al* (2000) as a part of a more general piezoelectric problem:

$$\mathbf{s}^K = k_0 [f_0(\gamma)(\mathbf{I} - \mathbf{nn}) + (1 - 2f_0(\gamma))\mathbf{nn}] \quad (80)$$

where $f_0(\gamma)$ is given by Equation $\kappa = \frac{1}{2(1 - \nu_0)}$, $f_0 = \frac{\gamma^2(1 - g)}{2(\gamma^2 - 1)}$,

$$f_1 = \frac{\kappa\gamma^2}{4(\gamma^2 - 1)^2} [(2\gamma^2 + 1)g - 3] \quad (64).$$

Substituting this result into Equation (79) yields the following expression for \mathbf{H}^R :

$$\mathbf{H}^R = V^* \frac{1}{k_0} \{A_1 \mathbf{I} + A_2 \mathbf{nn}\} \quad (81)$$

where factors A_1 and A_2 are as follows

$$A_1 = \frac{k_0 - k_*}{k_0 + (k_* - k_0)f_0(\gamma)}, \quad A_2 = \frac{(k_0 - k_*)^2(1 + 3f_0(\gamma))}{[k_* - 2(k_* - k_0)f_0(\gamma)][k_0 + (k_* - k_0)f_0(\gamma)]} \quad (82)$$

For a *cylinder*, $\gamma \rightarrow \infty$ and $f_0(\gamma) = 1/2$.

For a *crack* ($\gamma \rightarrow 0$ and $V_*\gamma \rightarrow (4/3)\pi a^3$);

$$\mathbf{H}^R = \frac{8a^3}{3} \frac{1}{k_0} \mathbf{nn} \quad (83)$$

An important observation relevant for many realistic microstructures (and similar to the one concerning the effective elasticity) is that \mathbf{H}^R for a crack can be used, with good accuracy, for strongly oblate pores (up to $\gamma = 0.15$) [42].

The effective conductivity tensor of the fibre reinforced microcracked material is given as

$$k_0 \mathbf{K}^{-1} = \mathbf{I} + \frac{2c_f}{3} \frac{k_0 - k_f}{k_0 + k_f} \left[\mathbf{I} + \frac{k_0 - k_f}{k_f} \mathbf{nn} \right] + \frac{8}{3} \mathbf{a} \quad (84)$$

3.7 Explicit correlation between elastic and conductive properties

For arbitrarily oriented cracks, the crack density tensor was expressed as [3]:

$$\mathbf{a} = \frac{3}{8} \left[k_0 \mathbf{K}^{-1} - \left(1 + \frac{2}{3} c_f \frac{k_0 - k_f}{k_0 + k_f} \right) \mathbf{I} - \frac{2}{3} c_f \frac{(k_0 - k_f)^2}{k_f} \mathbf{nn} \right] \quad (85)$$

This result is of interest, as it appears, since it recovers the information on the crack field (damage) from the conductivity data. An important observation is that tensors \mathbf{a} and \mathbf{K} , as well as tensors \mathbf{a} and \mathbf{C} are, generally, not coaxial in this case. This is due to the overall anisotropy being caused not only by cracks but by fibres as well. Introducing \mathbf{a} into Equation (70) will yield, in a straightforward way, the cross-property correlation in the closed form. This correlation gives the effective stiffness in terms of \mathbf{K} plus terms that involve \mathbf{nn} and \mathbf{nnnn} . Since direction \mathbf{n} is, generally, not one of the principal directions of \mathbf{K} , the effective stiffness tensor possesses no elements of symmetry, i.e. elastic anisotropy of the general type.

For the case of overall orthotropy, the cross-property correlation simplifies substantially, with \mathbf{C} becoming orthotropic and coaxial to \mathbf{K} , if direction \mathbf{n} is one of the principal axes of crack density tensor \mathbf{a} . In this case, the cross-property correlation has the following form:

$$\begin{aligned}
C_{1111} - C_{1111}^0 &= C_f (d_1^f + d_2^f) + q_f \left[d_1^c (2 + k_0/k_f) + d_3^c + d_4^c \right] \\
&\quad + \frac{3}{8} (d_1^c + d_3^c + d_4^c) (k_{11} - k_0)/k_{11} + \frac{3}{8} d_1^c (k_{22} - k_0)/k_{22} + \frac{3}{8} d_1^c (k_{33} - k_0)/k_{33} \\
C_{2222} - C_{2222}^0 &= C_f (d_1^f + d_2^f) + q_f \left[d_1^c (2 + k_0/k_f) + d_3^c + d_4^c \right] \\
&\quad + \frac{3}{8} d_1^c (k_{11} - k_0)/k_{11} + \frac{3}{8} (d_1^c + d_3^c + d_4^c) (k_{22} - k_0)/k_{22} + \frac{3}{8} d_1^c (k_{33} - k_0)/k_{33} \\
C_{3333} - C_{3333}^0 &= C_f (d_1^f + d_2^f + d_3^f + d_4^f + d_5^f) + q_f \left[d_1^c (2 + k_0/k_f) + (d_3^c + d_4^c) k_0/k_f \right] \\
&\quad + \frac{3}{8} d_1^c (k_{11} - k_0)/k_{11} + \frac{3}{8} d_1^c (k_{22} - k_0)/k_{22} + \frac{3}{8} (d_1^c + d_3^c + d_4^c) (k_{33} - k_0)/k_{33} \\
C_{1122} - C_{1122}^0 &= C_f d_1^f + q_f \left[d_1^c (2 + k_0/k_f) + 2d_3^c \right] \\
&\quad + \frac{3}{8} (d_1^c + d_3^c) (k_{11} - k_0)/k_{11} + \frac{3}{8} (d_1^c + d_3^c) (k_{22} - k_0)/k_{22} + \frac{3}{8} d_1^c (k_{33} - k_0)/k_{33} \\
C_{1133} - C_{1133}^0 &= C_f (d_1^f + d_3^f) + q_f \left[d_1^c (2 + k_0/k_f) + d_3^c (1 + k_0/k_f) \right] \\
&\quad + \frac{3}{8} (d_1^c + d_3^c) (k_{11} - k_0)/k_{11} + \frac{3}{8} d_1^c (k_{22} - k_0)/k_{22} + \frac{3}{8} (d_1^c + d_3^c) (k_{33} - k_0)/k_{33} \\
C_{2233} - C_{2233}^0 &= C_f (d_1^f + d_3^f) + q_f \left[d_1^c (2 + k_0/k_f) + d_3^c (1 + k_0/k_f) \right] \\
&\quad + \frac{3}{8} d_1^c (k_{11} - k_0)/k_{11} + \frac{3}{8} (d_1^c + d_3^c) (k_{22} - k_0)/k_{22} + \frac{3}{8} (d_1^c + d_3^c) (k_{33} - k_0)/k_{33} \\
C_{1212} - C_{1212}^0 &= C_f d_2^f + 2q_f d_4^c + \frac{3}{8} d_4^c (k_{11} - k_0)/k_{11} + \frac{3}{8} d_4^c (k_{22} - k_0)/k_{22}
\end{aligned}$$

$$\begin{aligned}
C_{1313} - C_{1313}^0 &= C_f \left(d_2^f + d_4^f \right) + q_f d_4^c \left(1 + k_0/k_f \right) + \frac{3}{8} d_4^c (k_{11} - k_0)/k_{11} + \frac{3}{8} d_4^c (k_{33} - k_0)/k_{33} \\
C_{2323} - C_{2323}^0 &= C_f \left(d_2^f + d_4^f \right) + q_f d_4^c \left(1 + k_0/k_f \right) + \frac{3}{8} d_4^c (k_{22} - k_0)/k_{22} + \frac{3}{8} d_4^c (k_{33} - k_0)/k_{33}
\end{aligned}
\tag{86}$$

Overall orthotropy covers several practically important situations listed below,

- a. Cracks are normal to the fibres.
- b. Normals to cracks lie in the plane normal to the fibres. If these normals are randomly oriented in the mentioned plane, C is transversely isotropic, otherwise, if they have a preferential orientation in this plane, C is orthotropic.
- c. Cracks are randomly oriented.

Experimental test data is now required to determine the parameters and validate the model.

4 EXPERIMENTAL TEST PREPARATION

A study was conducted to determine the most common materials used in industry as well as organisations that would be interested in providing materials for the manufacture of laminates for this study. Laminates for exposure tests manufactured from commonly used and readily available resins would ensure that the test results are generally applicable to most glass-fibre reinforced polymer components / structures found in Southern Africa. The epoxy systems tested were specified by the resin sponsor. To determine the most common polymer composite resin used, in addition to epoxy, resin manufacturers were approached for assistance. Common polymer resins in use, determined by the highest volume sold and number of customers, were found to be vinylester and polyesters. Vinylesters are used in applications requiring resistance to chemical damage and generally have better mechanical properties in comparison to polyesters. In the polyester resin category, for improved resistance to moisture, isophthalic polyester is preferred with the orthophthalic polyester being a so-called “general purpose” resin. Orthophthalic resins are locally the most widely used polyester resins.

4.1 Material selection

Two epoxy resins, two polyester resins and one vinylester resin has been used for fabricating laminates for exposure testing. Although polyester laminates were fabricated and subjected to natural exposure tests, no further details are provided as extensive analysis was not performed on these type of laminates. The epoxies specified are used in applications requiring good mechanical properties and are therefore widely used in aerospace applications. The 8552 laminates, i.e. laminates containing Hexcel 8552 resin as the matrix, were manufactured from prepreg containing an 8-harness satin weave. 8552 is an aircraft certified, toughened epoxy resin recommended for structural applications requiring high strength, stiffness and damage tolerance. Laminates manufactured using the 8552 resin system are referred to as 8552 laminates in this study.

The second epoxy resin system tested was the Araldite LY 5052 system cured using Aradur 5052 catalyst. This resin system is a cold curing resin used for aerospace and industrial composites, tooling and aircraft repairs. The resin may be used for fabrication using wet lay-up, resin transfer moulding, pressure moulding and filament winding [224]. Laminates manufactured using the 5052 resin system are referred to as 5052 laminates in this study.

The vinylester resin used was the Derekane Momentum 411-350 with the NCS Ultracure AC2, cobalt accelerator and catalysed with M50. Applications of the resin include FRP storage tanks, vessels, ducts and service applications in the food and beverage industry. This resin may be

used in hand lay-up, spray-up, filament winding, compression moulding, resin transfer moulding and pultrusion.

The reinforcement used on all laminates was woven glass fibre. Two types of glass weaves have been used with the predominant being 2×2 twill weave E-glass with an areal weight of 290g/m². The alternate glass weave used was the 8-harness satin weave E-glass fibre with an areal weight of 293g/m². This fibre weave was used in the initial laminate manufacturing trials in preparation for the manufacture of laminates for testing. Once the available satin weave glass-fibre had been used, additional satin weave glass fibre could not be sourced locally in quantities less than 50m. Consequently, the fibre weave used for the manufacture of laminates by hand lay-up was changed from an 8-harness satin weave to a 2×2 twill weave. The 8-harness satin weave was therefore only used as reinforcement on the 8552 prepreg laminates.

As part of this investigation to compare the effectiveness of protective measures, laminate deterioration when protected by shade cloth was studied. Shade cloth is fabricated by weaving monofilaments or both monofilaments and monotapes produced from polyethylene, into a continuous cloth. This cloth deflects naturally occurring UV while allowing hot air to ventilate through the net. The shade cloth selected for the exposure test shields objects from 80% of natural UV radiation. The cloth material used, ALNET Cooltone, meets SABS standards for shade cloth material. UV absorbance of the cloth in the 340nm range, as measured at the University of Stellenbosch, Institute of Polymer Science, was reported as 98.2% [225]. This specific shade cloth was therefore selected as it was commonly available and provided 98.2% shelter from detrimental naturally occurring UV.

4.2 Laminate manufacture

The 8552 epoxy laminates were manufactured using nine layers of prepreg and processed in the sequence illustrated in Figure 8 and described below;

1. Apply full vacuum and 1 bar pressure.
2. Heat to 107°C at a rate between 1.8-3°C/min.
3. Hold temperature at 107°C for 30-60min.
4. Raise pressure to 6-7 bar. Vent vacuum when pressure reaches 2.1 bar.
5. Raise temperature to 177°C at a rate between 1.8-3°C/min.
6. Hold temperature at 177°C for 120min ±10min.
7. Cool at a rate between 1.2-3°C/min to 66°C and vent pressure.

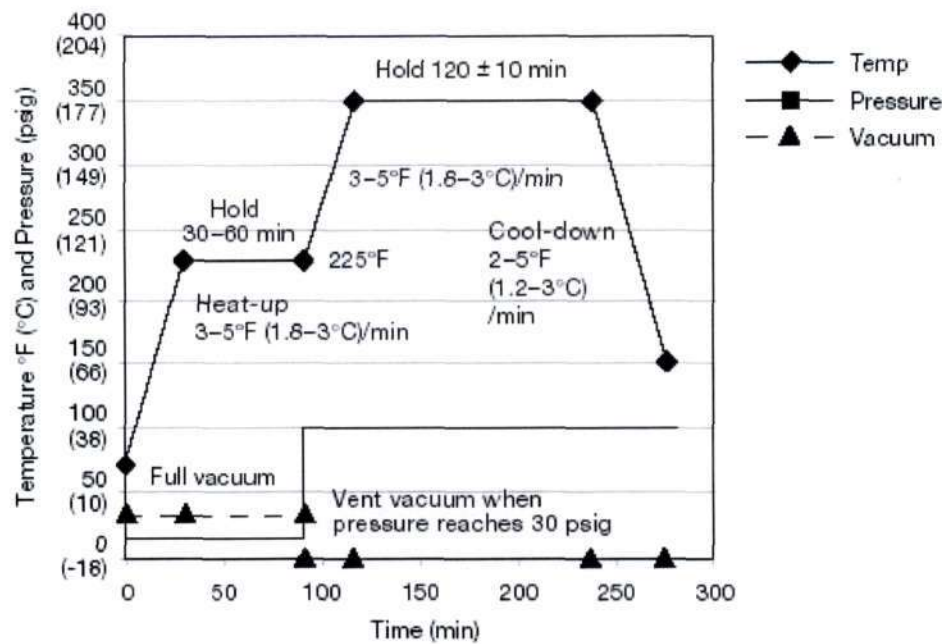


Figure 8 - Graphical illustration of 8552 cure cycle [226]

The fibre-volume fraction of these laminates was calculated to be 51.4% based on results of burnout tests detailed in Appendix F.

The 5052 epoxy laminates were manufactured using ten layers of 2×2 twill weave glass at Denel Aerospace Systems Pty(Ltd) in Pretoria, South Africa. Wet lay-up was performed using a brush to apply the resin, followed by compaction using an aluminium roller after each layer. Compaction by the use of a Mohair roller was preferred, but standard aluminium rollers were found to be adequate. To keep the resin content constant, best practice entailed measuring out the amount of resin required per layer, and ensure that only the resin required per layer is used. However during the lay-up of the first few layers, extra resin was required to adequately wet out the glass.

Lay-up began with a coat of resin being applied to the mould surface. A layer of woven glass was placed upon the resin and properly wetted out from above with resin. The second layer of glass was positioned upon the first and roller compacted. Resin from the layer beneath was thus forced to the top of the lay-up. Resin was added to the top surface to ensure proper wetting before the next layer of glass was positioned. This process of adding a layer of woven glass, roller compacting and wetting out was continued until all ten layers had been positioned. After the last layer, the laminate was compacted by roller to ensure an even distribution of resin. Laminates were left to cure overnight at ambient temperature with a 60°C, 16 hour post-cure

completed the following day. The fibre-volume fraction of these laminates was calculated to be 40.3% based on results of burnout tests detailed in Appendix F.

Manufacture of the vinylester resin laminates by wet lay-up and vacuum bagging proved unsuccessful due to styrene in the hardener boiling at high vacuum pressures (approximately -80kPa) during processing. Styrene was necessary as it was the monomer used in the hardener. Vacuum bagging at eight different vacuum pressures was attempted but insufficient compaction was obtained below 30kPa, the pressure at which the laminates did not contain the white bubbles indicating the boiling of styrene. Manufacture of laminates continued by wet lay-up without vacuum compaction. Various techniques for wetting the lay-up, including tamping with the brush, no "painting" of resin, compacting with a bristled roller and compacting with a smooth roller were attempted. Any attempt to compact with the rollers used resulted in the wetted glass layer lifting of the laminate. Tamping with a brush resulted in additional bubbles being formed in the lay-up, depending upon the state of cure that the resin had reached before application. An attempt was made to flood each layer with resin but that resulted in a resin rich laminate with excess resin that could not all be absorbed by the breather plies.

Vinylester laminates were finally successfully produced at the resin manufacturer's laboratories. Laminates were hand laid on Mylar film and then compression moulded using flat steel plates. Mylar film was used instead of the standard wax based release agents to prevent the cured laminates from bonding to the steel plates during curing. Lay-up began with an initial layer of resin applied to the surface, and then a layer of glass fibre of dimensions 480mm×520mm was placed upon the resin. The glass fibre was wetted out using a ribbed aluminium roller. Additional resin was applied to ensure that fibres were completely wetted. The second layer of glass was positioned upon the first and the procedure repeated until all nine layers of glass had been laid-up, compacted and properly wetted out. A second steel plate covered with Mylar film was placed upon the laminate and mounted in a hydraulic press. Laminate thickness was set to 3mm by spacers on the press and a hydraulic pressure of 500PSI was applied. Gel time was approximately 25min. for the vinylester resin. The laminate was removed from the press only after the exotherm had been completed. Progress of the exotherm was monitored by the state of cure of resin remaining after the lay-up had been completed. Cutting the laminate, using a band-saw, into 150mm×50mm rectangular segments and post-curing was performed a week later. Post cure for the vinylester was performed for 3 hours at 120°C. Laminates were labelled and weighed with the mass being recorded to the nearest milligram before mounting onto exposure panels.

4.3 Exposure locations

Nine different exposure locations were identified as potential test sites at which exposure panels could be installed to ensure that laminates would be exposed to a range of different environments. The description of the environments e.g. high temperature is relative to the range experienced in South Africa. The original nine test locations represent different climates that can be expected based on a meteorology study of South Africa. Based on the variation of environmental degradation factors of UV radiation, moisture and temperature, the nine test sites were reduced to six test sites illustrated in Figure 9.



Figure 9 - Location of test sites in South Africa

A description of the climate at each test site follows;

Irene (Gauteng): This climate is characterised by moderate rain and cool temperatures with frost occurring in winter.

Alkantpan (Northern Cape): The climate experienced is typical of dry, open, grazing areas found in Southern Africa (locally referred to as veld), with rainfall being less than 300mm

per annum. Extreme temperatures, high in summer and low in winter are experienced at this test site.

Durban (KwaZulu-Natal): The region experiences a wet and humid climate. Subtropical conditions prevail at this coastal location.

Komati (Mpumulanga): The surrounding area forms the lowveld region of Mpumulanga. Climate is hot and wet, typical of a tropical savannah region. Skukuza and surrounding areas are characterised by moderate rain, high temperatures, high humidity, and below average sunshine.

Cradock (Eastern Cape): Temperate grass lands are found in this region. This type of climate exists at the foot of mountain ranges. Temperatures increase gradually when travelling along the foot of the mountain range in a Northern direction. A wet and cool climate is predominant.

Bredasdorp (South Western Cape): Moderate temperatures with winter rainfall are common in this region. There is no representative location as the weather varies significantly with position in this region.

The climate at the six test sites contain a range of environmental degradation factors that can be expected in Southern Africa; both acting individually and simultaneously. Variation in climates of test sites enable the relative effect of degradation factors to be determined, e.g. the change of strength due to exposure in a warm, dry climate compared to a warm, wet climate would enable the effect of variation of moisture to be determined. Corresponding changes in damage mechanisms may therefore be attributed to moisture when all other factors are relatively constant.

4.4 Exposure frames

Rectangular specimens of dimensions 150×50mm manufactured for exposure tests were mounted onto exposure frames. Each exposure frame is approximately 1m² in area and holds 108 specimens. The specimens were mounted onto a stainless steel sheet fixed to a steel chassis and masked by a stainless cover containing cut-outs of approximately 130×40mm through which the specimens received exposure. Masked specimen exposure has been employed to reduce edge effects of exposure on the test specimens. The frames were mounted in open spaces away from obstructions that may cast a shadow upon the specimens during the day. British [227] and ASTM [228, 229] standards were used as a guide to set-up and mount the specimens in the natural environment.

The exposure frames were set-up as latitude racks, i.e. the exposed samples were inclined to the horizontal at an angle corresponding to the latitude of the test region. Latitude racks were used to maximise the total solar irradiance to which the samples were exposed. The variance of solar irradiation with angle of exposure is illustrated in Figure 10.

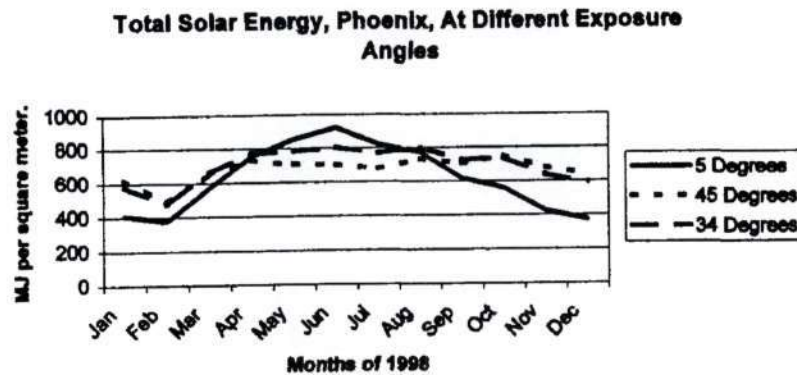


Figure 10 - Variance of solar irradiation with angle of exposure [1]

In South Africa the exposure frames were set at 30° to the horizontal at all test sites to keep the angle of inclination uniform although the latitude of the test sites do vary across the country. Further, all exposure frames face True North as it is in the Northern direction that the incident radiation is maximum for Southern Hemisphere regions. This thus represents the worst case scenario of maximum solar irradiation composite components are exposed to in Southern Africa. Figure 11 overleaf shows exposure frames placed at Durban at the latitude angle. On the epoxy frame, (left exposure frame on the figure) laminates on one-quarter of the exposure frame are protected by shade cloth. The exposure frame on the right contains vinylester and polyester laminates.



Figure 11 - Exposure panels placed at Durban

The sampling period decided upon was approximately 6 months as it was after this exposure duration that changes to the surface of laminates were observed. During the initial stages of specimen exposure, sampling was performed after 10 weeks (2.5 months) and 20 weeks (5 months) of exposure to determine transient changes in mechanical properties, if any. The first set of samples removed after approximately 10 weeks verified no observable degradation had occurred. Subsequent sampling after 5 months of exposure was performed with successive sampling performed as close as possible to a 6 month exposure interval, resource permitting.

5 ENVIRONMENTAL CHARACTERISATION

The environment in South Africa was characterised using data available from the South African Weather Service (SAWS). The data obtained include temperature, humidity, rainfall, wind speed and direction, sunlight hours and global radiation.

5.1 Data

Initially, only historical global radiation data was available to determine the relative severity of exposure at the test locations. MED (Minimal Erythral Dose) units were used as a measure of the relative intensity of UV radiation at the test locations. The measurement quantified UV radiation in terms of the effect it produced. Global radiation, i.e. the cumulative effect of direct and diffuse radiation, was obtained after discussions with SAWS during which it was ascertained that there was equipment in service that measures the current intensity of radiation in the standard units of W/m^2 . Comparison of the global radiation intensity between test sites and at test sites in Northern Hemisphere countries has since become possible. At Florida, a test site at which exposure tests were conducted [9], the radiation intensity is approximately 202W/m^2 [230], similar to that experienced at Komati. Further, this intensity in units of energy could be used to relate damage to the matrix material as it is the energy of the natural radiation that is used to break the bonds of the polymer chains in the matrix. Figure 12 overleaf, illustrates that the range of radiation is a significant percentage of the average with the worst case of deviation being in Cradock (Eastern Cape) where the variation is 42% of the average.

The radiation data has been obtained from historical data spanning more than two decades. Present measurements have not been illustrated as complete data sets over the exposure period could not be obtained. The fragmented data of present measurements have been found to agree well with the historical data and therefore the data shown in Figure 12 although not current, is not inaccurate. Durban appears to have the lowest radiation with Alkantpan the highest. No radiation was available for Bredasdorp but it is assumed that the radiation would be of similar magnitude to Durban based on a UV model developed at the CSIR [231].

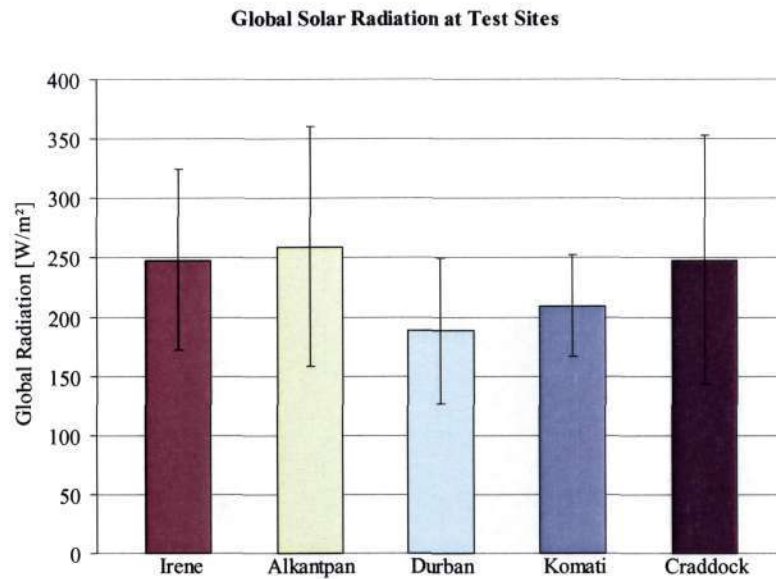


Figure 12 - Radiation data at test sites

Temperatures at all test locations follow a trend, similar in shape to a sine wave, with the maximum temperatures occurring in the middle of summer and the minimum temperatures occurring in the middle of winter. Humidity varies depending on temperature and location. Wind direction depends upon remaining variables including topography of the land.

Temperature, wind speed, humidity and precipitation data were plotted as histograms with the measured climatic variable on the horizontal axis and the frequency on the vertical axis. The frequency where labelled in percent, is obtained by dividing the number of occurrences in each class interval of the histogram by the total number of occurrences. Each class interval is defined by an upper and lower limit which is not always set to equal class intervals. The frequency in percent illustrates the percentage of time on average that values in a specific class interval occur. Frequency in percentage is only plotted for continuous variables, e.g. temperature and humidity. Wind speed and precipitation frequency is plotted as the number occurrences as these are discontinuous variables, i.e. the wind does not always blow nor does it rain every day of the year.

From examining the temperature data, Figure 13, it appears that Komati and Alkantpan experience high temperatures, greater than 30°C, for approximately the same duration in a year. These are therefore test sites with the highest average temperatures. However, on average throughout the year, Komati is warmer than Alkantpan experiencing temperatures in the range 18°C to 28°C more often. It is therefore expected that laminates exposed in this location would be exposed to the warmest climate of all test locations. Alkantpan in addition to experiencing

high temperatures experiences low temperatures in winter resulting in a large range of temperatures experienced throughout the year. This is therefore the coldest climate, among the test sites considered, in winter and similar to that of Craddock experiencing low daily temperatures, less than 10°C, in winter.

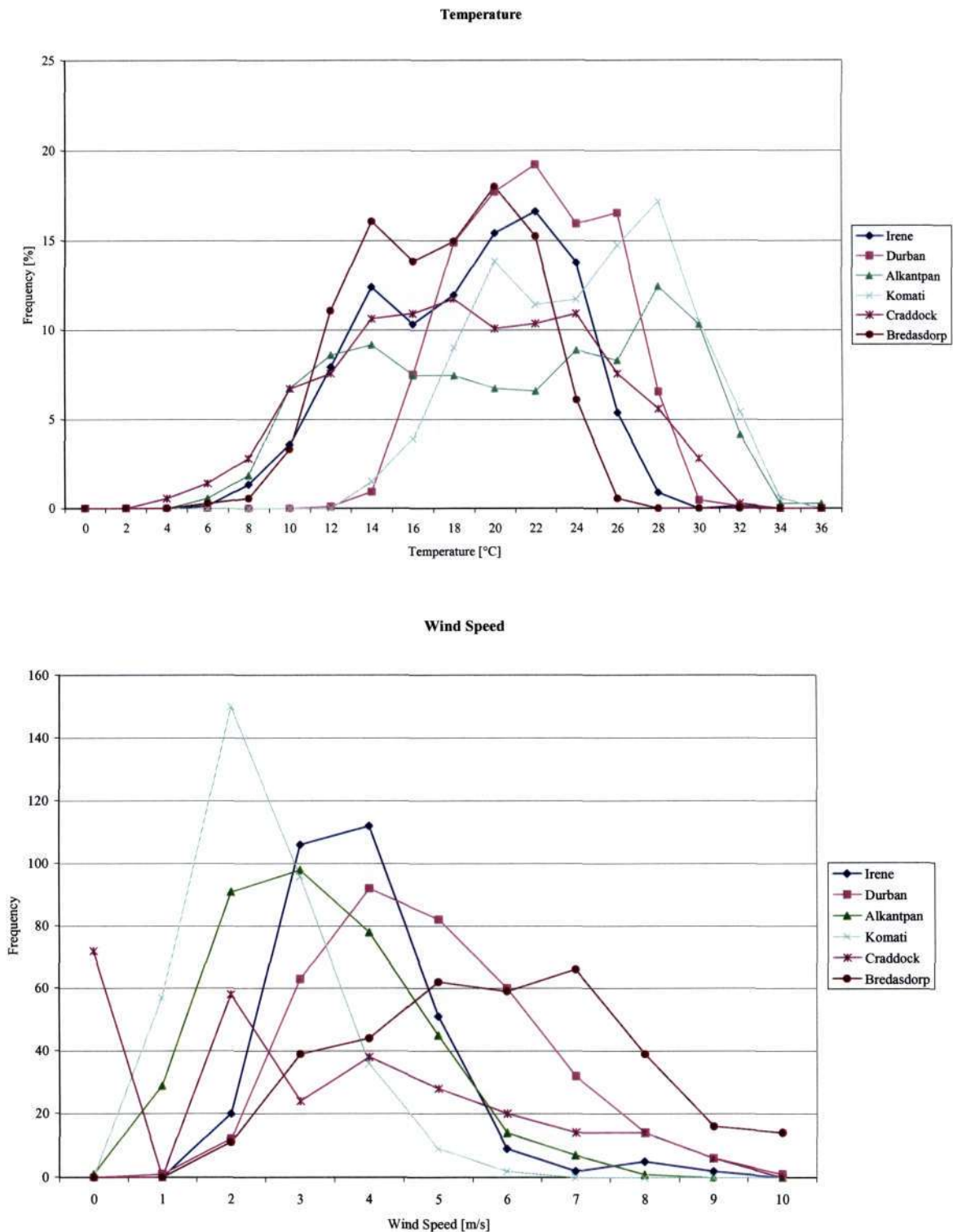


Figure 13 - Temperature and wind speed at test sites

Cradock has a large temperature range as well with temperatures between 4°C to 32°C. Durban appears to be the most uniform climate in terms of temperature fluctuations, when compared to the remaining test sites, with temperatures in Durban being predominantly in the range of 18°C to 26°C.

Wind speed data appear below the temperature data as convective heat transfer from the surface of the laminate is influenced by the wind speed and ambient temperature. Laminates exposed in regions of low wind speed may therefore experience a higher surface temperature than laminates exposed in regions with higher wind speeds, assuming ambient temperature is the same at both regions. All laminates on the panels are positioned facing True North and therefore receive the maximum possible solar incident radiation at a particular region. The test sites with the highest temperatures, Komati and Alkantpan experience different wind speeds. At Komati the predominant wind speed is 2m/s. Alkantpan experiences wind in a larger speed range than Komati with the wind tending to blow more often in Alkantpan than Komati. Cradock with a large range of temperatures experiences wind speeds in the range 2m/s to 8m/s predominantly. Irene experiences the most wind in the 3m/s to 4m/s range with Durban and Alkantpan experiencing wind for approximately the same quantity of time.

Determination of the region that consistently experiences the highest wind speed of all test regions may be obtained comparing the results of integration of the wind speed curve at each test site. The highest numerical value obtained from the integration would imply consistently high wind speed at the particular test site in comparison to the other test sites. Heat transfer from the surface of exposed laminates at this location would therefore be most influenced by wind speed. The results of the integration reveal that Durban experiences the highest wind speed most of the time and Komati the least. Laminates exposed at Komati would therefore experience the least convective heat transfer due to wind.

Humidity and precipitation are shown in Figure 14, as it is these variables that would be responsible for the quantity of moisture available in the atmosphere and among other variables, responsible for the diffusion of water into the laminate. Of all the test sites, Durban is the most humid and Alkantpan the least. High humidity at Durban will be due to the moisture being carried over from the warm sea current along the coast. Durban also experiences the most precipitation and Irene the least. Alkantpan was not found to be as “dry” as previously thought when planning the exposure locations. The region appears to have experienced a wet season as Alkantpan received the second most quantity of precipitation of all test sites. Most precipitation at Alkantpan occurred as light rain (less than 1mm). Due to the low humidity and high temperatures of the region, surface moisture would have been readily lost due to evaporation.

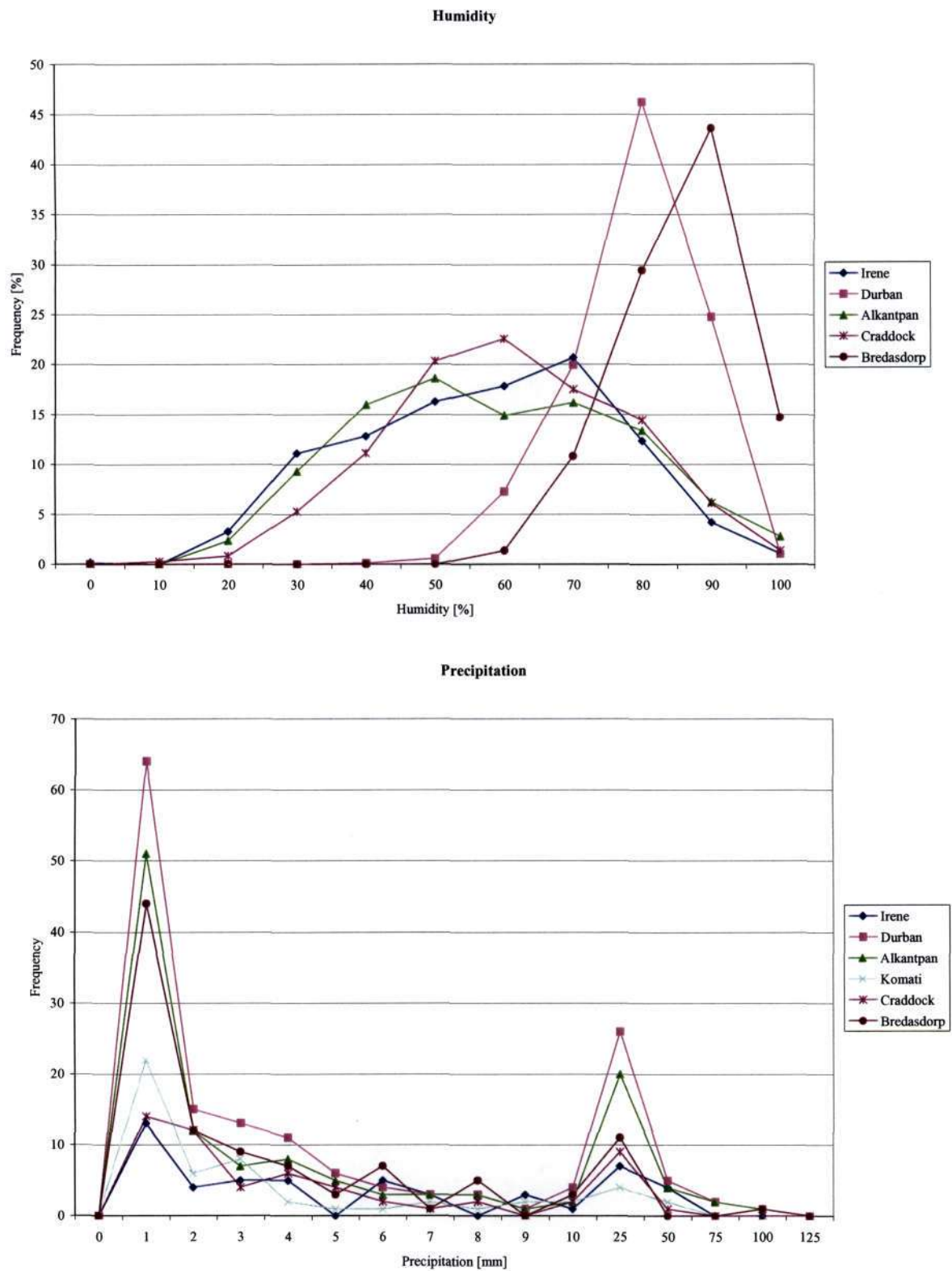


Figure 14 - Moisture measurement in the natural environment

5.2 Discussion

Laminates exposed at Komati may therefore be the warmest for longest as the temperatures are the highest and wind the slowest. Alkantpan laminates will experience large fluctuations in temperature due to the large temperature range and wind blowing frequently when compared to other test locations.

No humidity records for Alkantpan from June 2003 to present were available but the data for Alkantpan may be compared to the data at remaining locations as the humidity is reported as a percentage over the period in which the measurement was recorded. From the data, Durban is the wettest test site due to experiencing the highest humidity and precipitation. Although Alkantpan experienced the second highest frequency of precipitation in the 1mm and 25mm precipitation occurrences, high temperatures in the rainy season combined with low humidity would facilitate evaporation of surface moisture.

The air temperature was recorded as a measure of the ambient temperature of the environment and provided a comparison of the relative laminate temperature between exposure locations. Laminate surface temperature can however vary significantly from the air temperature [1]. Using a portable climatic data capturing device, laminate surface temperature was measured at 40°C when the air temperature was measured as 22°C in Durban. This therefore represents a laminate surface temperature 1.8 times the ambient temperature. Laminate temperature may also be affected by wind speed, wind direction and cloud cover.

Exposure locations have been selected with the best available climate descriptions at the beginning of the exposure tests. However from climatic data captured during the tests, the Alkantpan exposure location was not the “driest” location as expected, with an annual rainfall greater than that experienced at Irene. The reason could be due to climatic variations that span years, with certain regions of the country experiencing continued dry seasons. Alkantpan also does not receive the maximum UV irradiation in South Africa, as initially assumed. According to a UV model of Southern Africa, the regions of maximum UV irradiation are in the vicinity of the Namibian border, however exposure and sampling of laminates at these locations would present logistical problems. Alkantpan therefore still represents a relatively high UV exposure location at which sampling of laminates could be relatively easily performed.

Pollution data at all test sites was not available in the public domain so comparison of the chemical quality of the environment at the test sites could not be performed. Levels of pollution at some test sites are expected to be higher than that found in natural, undisturbed environments

due to industries located within the exposure regions and urbanisation. Pollution occurring in Irene would be due to large industries located in adjacent cities and large volumes of traffic between the cities. Two oil refineries, in addition to factories, situated at Durban contribute to the pollution of the local environment. Little pollution is expected at the small town of Cradock as the region is predominantly used for agriculture and there are no large industries based in the town.

6 SPECIMEN INSPECTION

Specimen inspection was conducted on initially unexposed laminates and then on laminates removed from the exposure panels at specific exposure durations. The inspection, to identify damage, was performed by visual observation, optical microscopy and Scanning Electron Microscopy (SEM). Examination at increasing magnification was performed to determine the type or mode of damage and / or failure. Both macroscopic and microscopic damage could therefore be identified.

Observation of damage position / orientation are described with respect to fibre tows. Longitudinal tows refer to fibre tows that span the length of the rectangular laminates. Transverse tows refer to fibre tows that span the width of the laminate. Examination of the cross-section has been conducted on a plane parallel to the longitudinal weave in most cases.

6.1 Epoxy

6.1.1 Visual examination

Visual examination of the 8552 laminates, Figure 15, after 2.5 months of exposure did not reveal observable damage, but after 9.5 months of exposure, the longitudinal fibre tows were observed with the underlying transverse fibre tow becoming exposed to the environment after 20 months of exposure. With increasing exposure period, the colour of the resin changed from light brown to darker shades of brown on the exposed regions of the laminate.

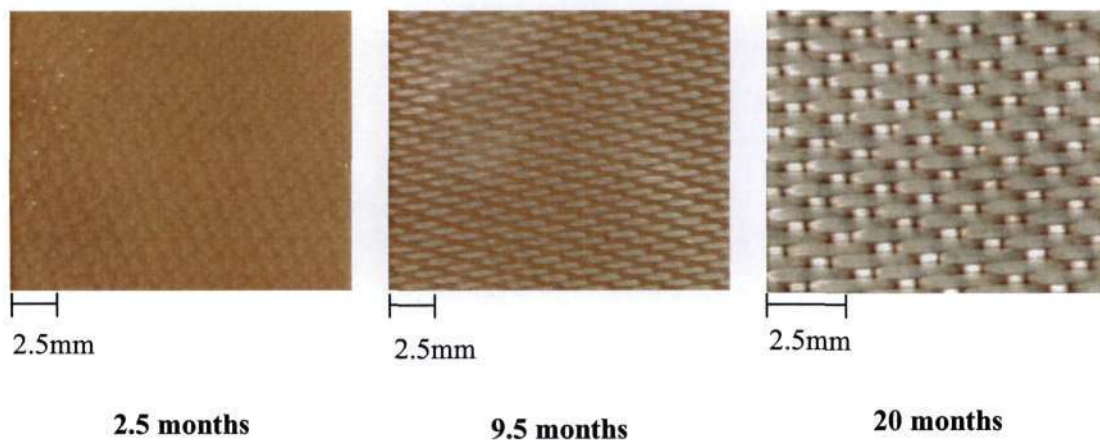


Figure 15 - Surface appearance of 8552 laminates at different exposure periods

A similar trend in-terms of exposure of the appearance first, of the longitudinal tow, and then the transverse tow was observed after examination of 5052 laminates, Figure 16 overleaf. After

2.5 months of exposure, fibre impressions were observed at the surface, i.e. the fibre weave below the surface was visible but the fibres remained covered with resin. After 9.5 months of exposure, fibres on the longitudinal tows were exposed while the transverse tows were protected by resin but visible through the resin. After 20 months of exposure both the longitudinal and transverse tows were exposed. Fibres on the transverse tow are distinguishable depending on the incident angle of the ambient light and reflection of the surface, therefore the transverse tows in Figure 16 do not appear to be of the same colour as the longitudinal tows. The laminates, translucent at the beginning of exposure, changed to darker shades of yellow with increasing exposure duration. After 20 months of exposure the resin was observed to be dark brown in colour as evident in Figure 16.

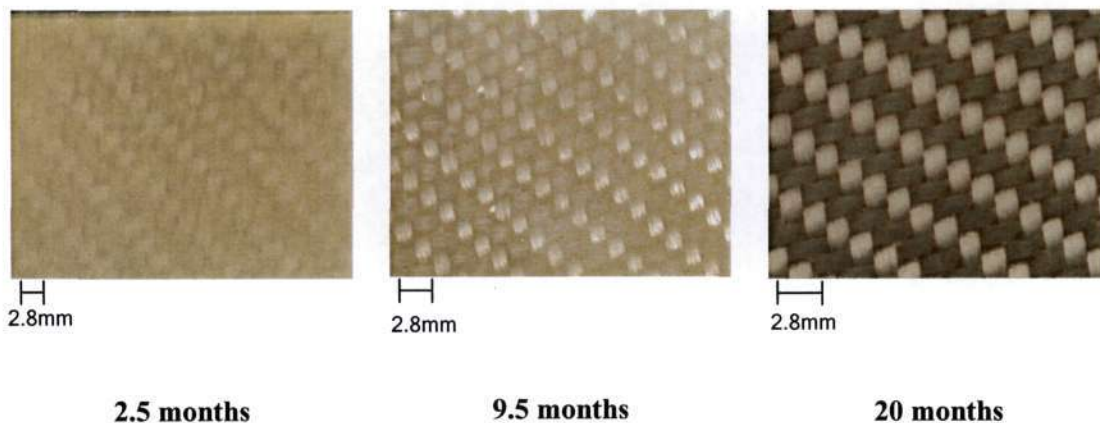


Figure 16 - Surface appearance of 5052 laminates at different exposure periods

The laminates examined and shown in Figure 15 and Figure 16 were exposed at Durban. Observation of fibre tows and changes in colour of the matrix of laminates at the remaining test sites occurred during the same sampling period. Images selected are those that reveal the most change of the laminate surface, therefore not all images captured are presented herein.

On a laminate surface of area $150 \times 50 \text{ mm}$, the central region on the laminate of area $130 \times 40 \text{ mm}$ was exposed to the environment. The remaining area at the edges of the laminate, referred to as the masked area, was covered by the exposure panel cover frame. Examination of the masked area of the laminate did not reveal fibre exposure. The resin in this region appeared intact and not subject to damage or erosion. A colour change of the resin in this region did occur as shown in Figure 17 overleaf. In the case of the 8552 laminates, the colour change was to a darker shade of brown while on the 5052 laminates, the colour change was from being clear to a light shade of yellow. On the exposed regions, the colour change was more drastic, i.e. resin on the exposed regions were observed to be of dark shades when compared to that of the unexposed region.

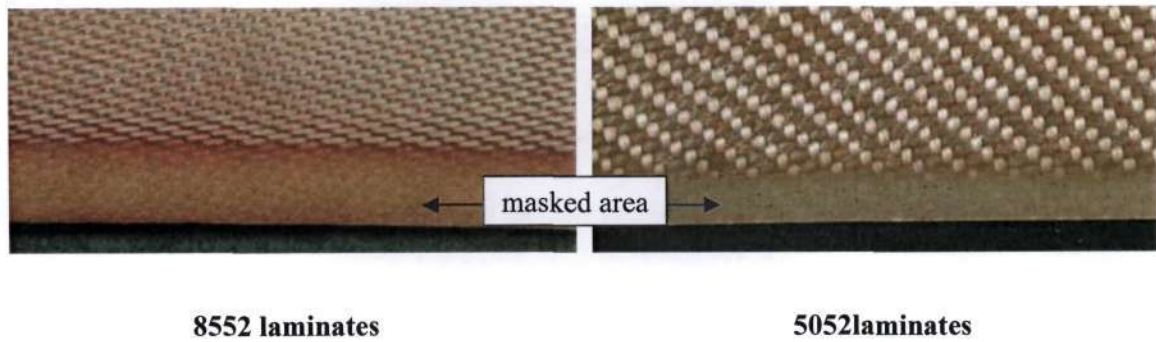


Figure 17 - Comparison of the masked area and exposed area of a laminate

6.1.2 Optical microscopy

Laminates were examined using an optical microscope to identify damage that would be visually undetectable. Cracks on the surface of laminates, Figure 18, referred to as surface crazing was observed after 2.5 months of exposure. Less commonly observed on the surface at this stage of exposure were fibres that had become exposed to the environment due to the loss of resin at the surface.

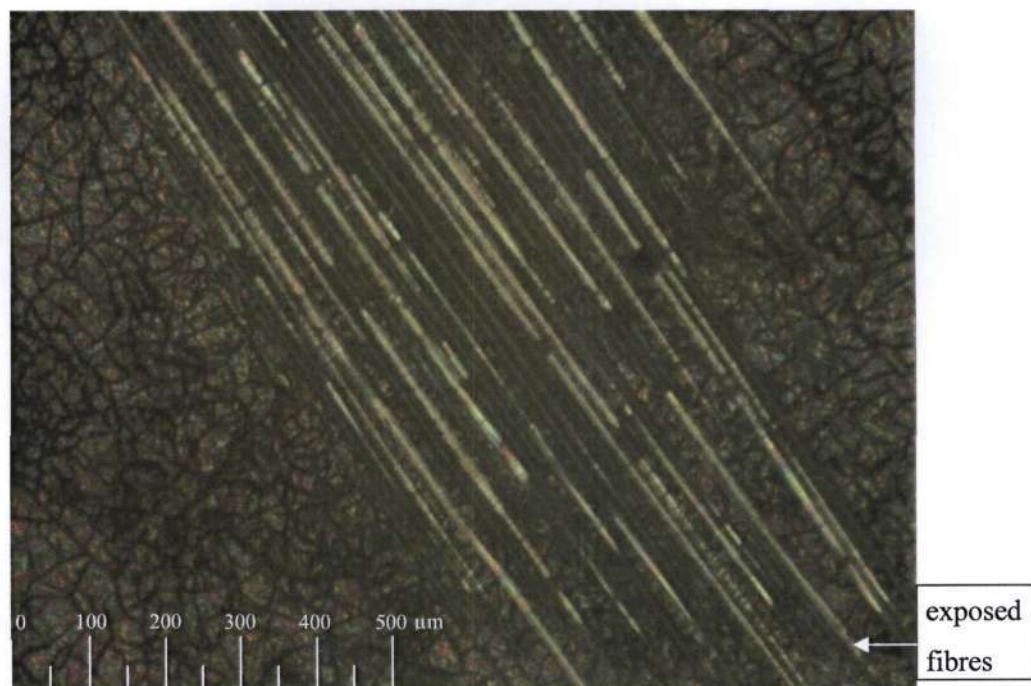


Figure 18 - Crazing on the surface of 8552 epoxy laminates when viewed at 100× magnification after 2.5 months of exposure at Durban

Cracks at the surface were only observed on the unmasked area and not on the masked area. The masked area appeared undamaged, with cracks gradually appearing at the boundary between the masked and unmasked area as appears in Figure 19.

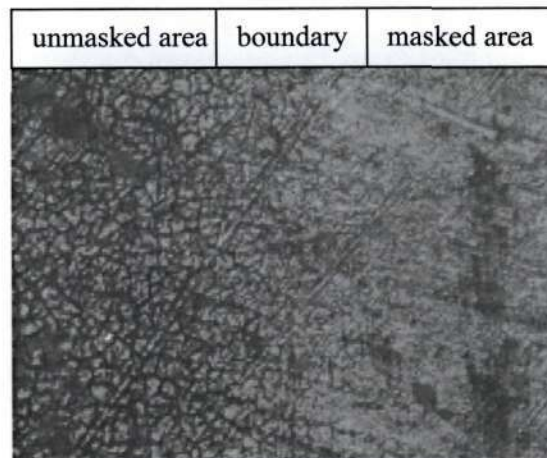


Figure 19 - Boundary between masked and unmasked areas on 8552 epoxy laminates when viewed at 100× magnification after 2.5 months of exposure at Durban

Examination of 8552 laminates after approximately 9.5 months of exposure reveal exposed fibres in the longitudinal weave and fibres in the transverse weave becoming barely visible at this stage of exposure as in Figure 20.

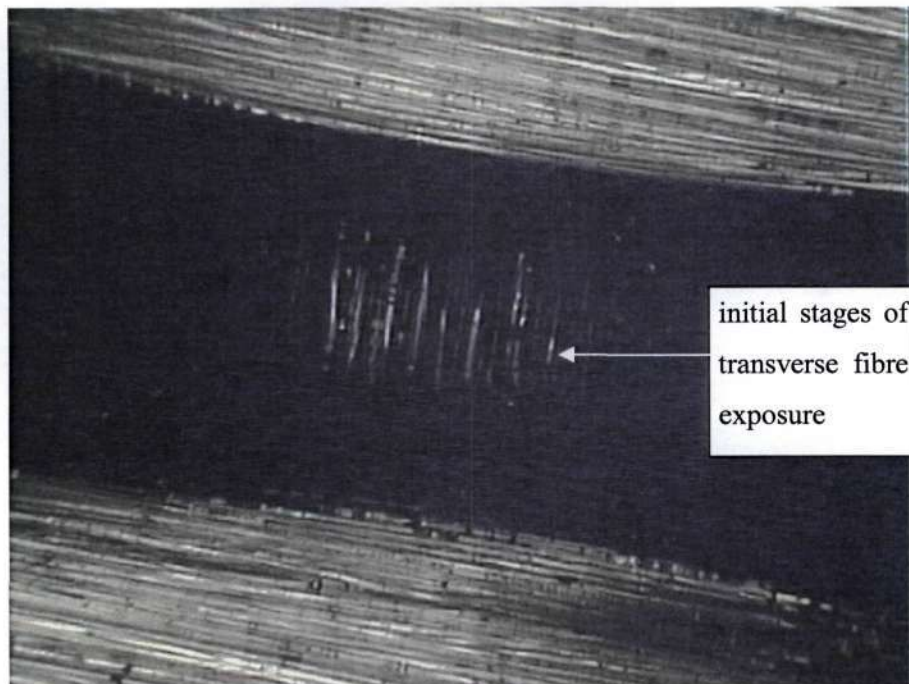


Figure 20 - 8552 epoxy laminate transverse weave exposed when viewed at 100× magnification after approximately 9.5 months of exposure at Durban

Examination of the surface of the 5052 epoxy laminates also reveal cracks and pits / voids on the surface. Cracks at the perimeter of voids have been observed to move radially outwards as observed in Figure 21.

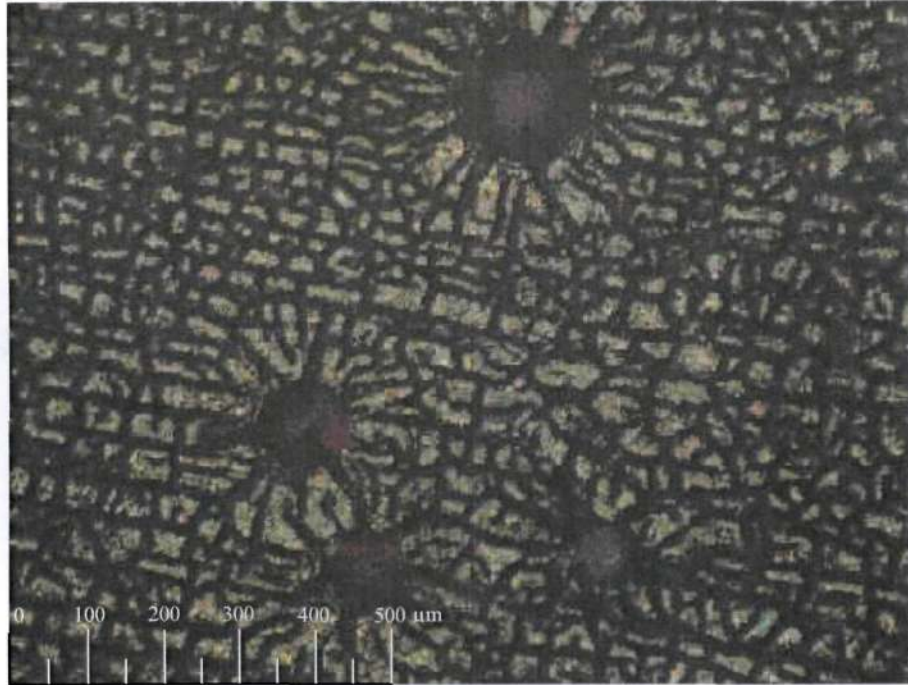


Figure 21 - Surface of a 5052 epoxy laminate when viewed at 100× magnification after 2.5 months of exposure at Durban

6.2 Scanning Electron Microscopy – Epoxy

Specimens had to be carefully prepared for examination using the electron microscope. No published preparation procedure for polymer composites was available in the literature, nor from the manufacturers of the polishing equipment, nor from members of the Scanning Electron Microscopy community. Upon advice from personnel at the electron microscope facility, a method of specimen preparation had to be developed for cutting, mounting and polishing the specimens. The cutting and mounting procedure is described in Appendix A and the polishing procedure developed is described in Appendix B.

6.2.1 8552 epoxy laminates

A layer of resin at the surface was found on all unexposed laminates examined, as visible in Figure 22 overleaf. The surface layer of resin was found to be of minimum thickness on the prepreg, autoclave cured laminates, and the thickest on wet lay-up laminates without compaction.

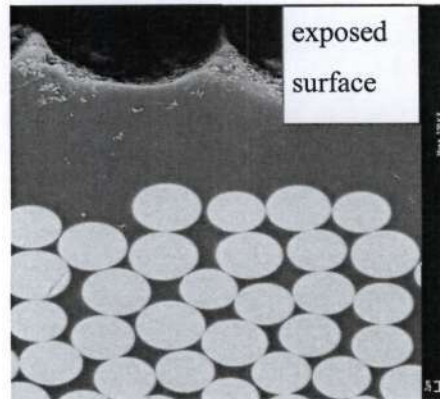


Figure 22 - Unexposed 8552 epoxy laminate

With increasing exposure durations, damage in the form of microcracks with an average depth of $10\mu\text{m}$ was observed on the surface of the laminates as shown in Figure 23. Cracks visible on the fibres are due to the specimen preparation and polishing process.

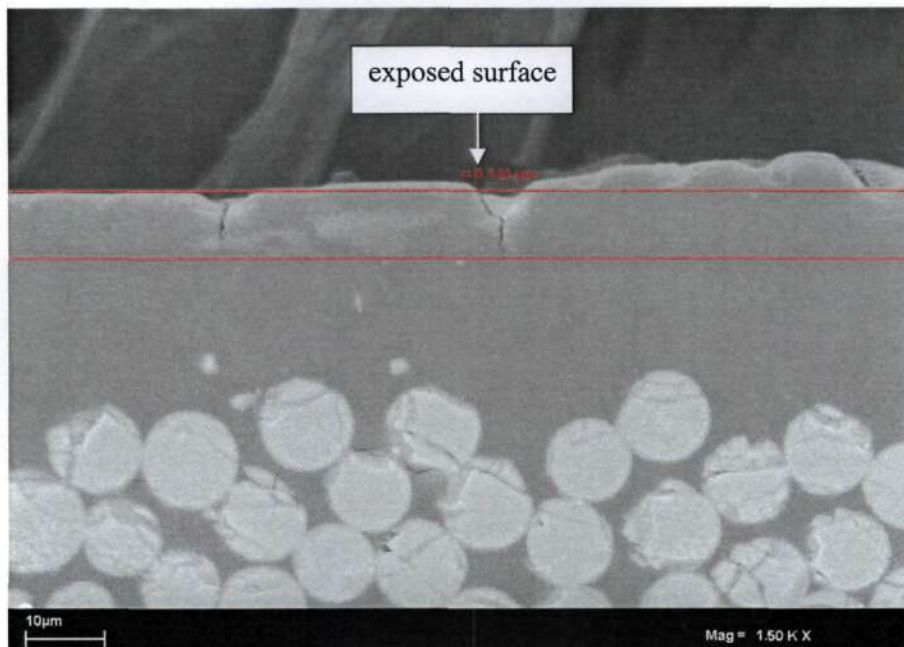


Figure 23 - Cracked layer on surface of 8552 epoxy laminates after 5 months of exposure at Durban

After 9.5 months of exposure, the exposed surface appears to have an uneven surface with peaks and valleys as appears in Figure 24 overleaf.

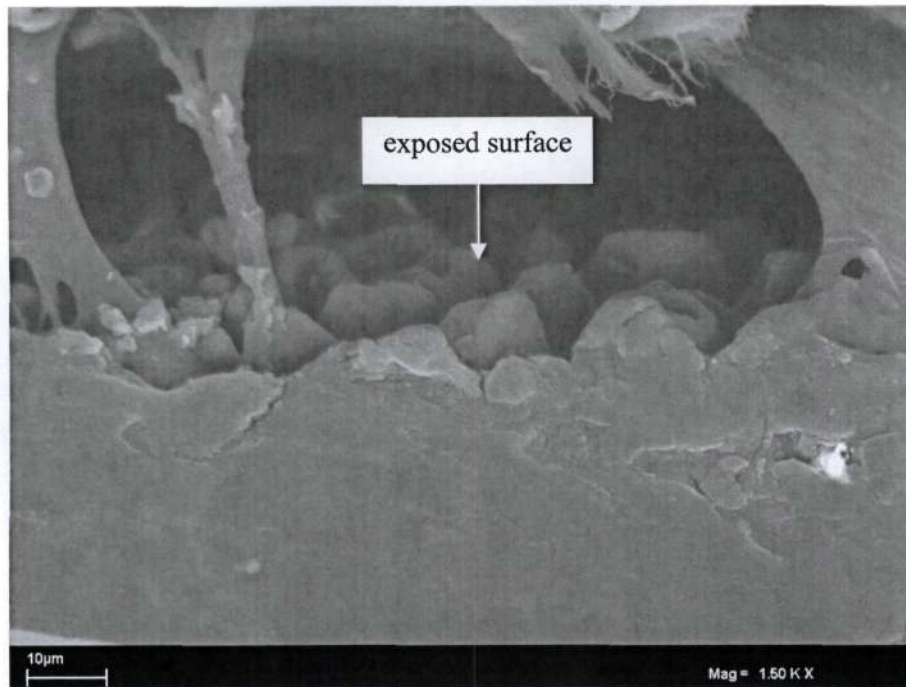


Figure 24 - Uneven surface of 8552 epoxy laminates observed after approximately 9.5 months of exposure at Durban

When the laminates were examined in a cross-section perpendicular to the longitudinal tow, the transverse tows were found to be closest to the surface. Longitudinal tows which appeared below the transverse tows would be protected by a thicker layer of resin above the fibres due to waviness of fibres in a layer of reinforcement. Exposure of fibres on the longitudinal tow, in this case, will therefore imply that almost the entire layer of reinforcement was exposed as most fibres on the longitudinal tows would be below the transverse tows. The fibres in the longitudinal tow were observed to become loose after 14 months of exposure as shown in Figure 25.

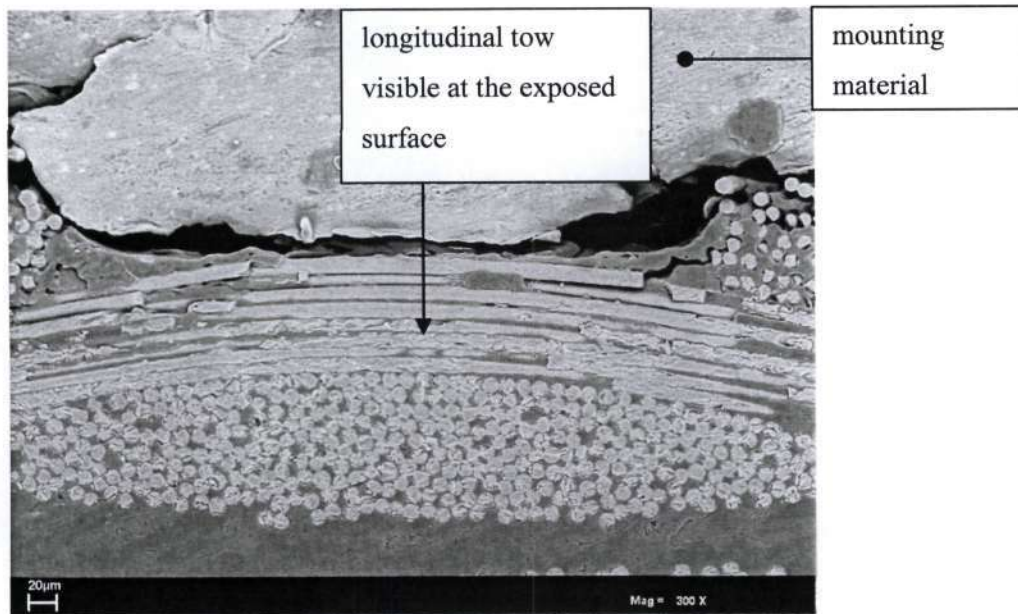


Figure 25 - Loose fibres on the longitudinal tow of 8552 epoxy laminates after 14 months of exposure at Durban

Evident in Figure 25, resin that was present between the transverse tows and above the longitudinal tows, has been eroded at a higher rate than resin reinforced with fibres at the surface, as apparent by the resin still in place on the transverse tows visible on the left and right edge of the figure.

Resin was observed attached to loose fibres at the surface of 8552 laminates as visible in Figure 26. Although the fibres had become loose due to weathering of the resin at the surface, the fibre-resin interface appears not to be disrupted.

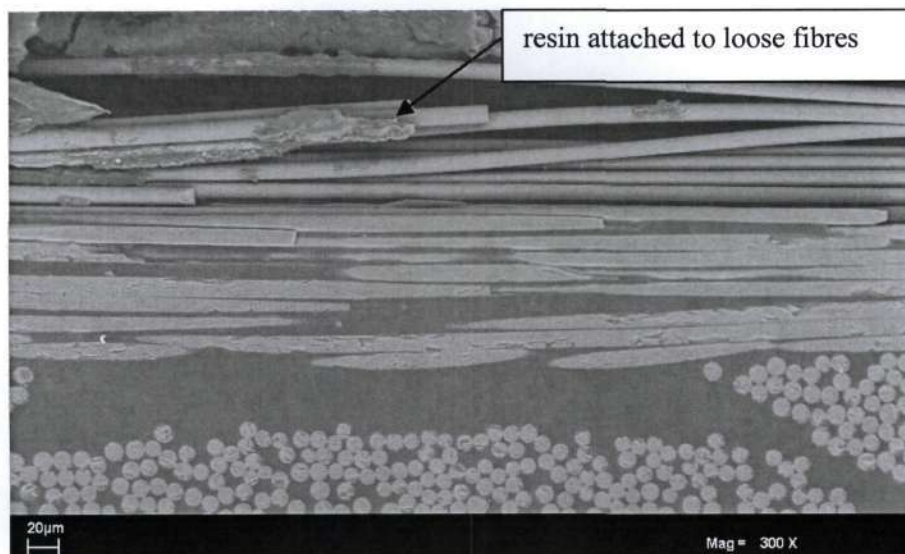


Figure 26 - Resin attached to loose fibres at the surface

6.2.2 5052 epoxy laminates

The surface layer of resin on unexposed 5052 epoxy laminates was found to vary between approximately $40\mu\text{m}$ and $60\mu\text{m}$ (Figure 27).

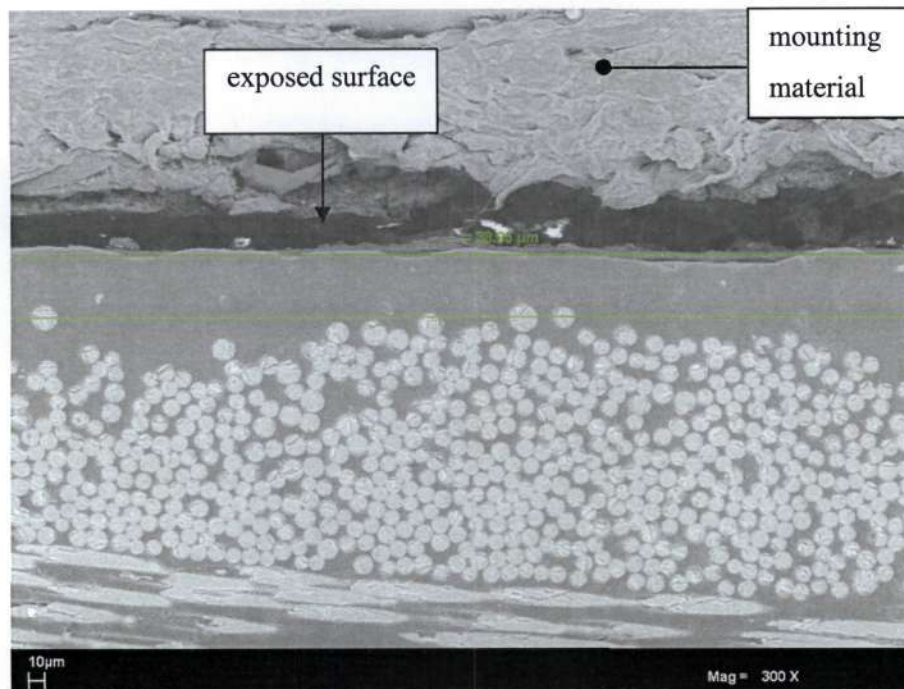


Figure 27 - Depth of surface resin on an unexposed 5052 epoxy laminate measured at approximately $40\mu\text{m}$

The average depth of cracks on the surface of exposed 5052 laminates was approximately $25\mu\text{m}$ in length. However larger surface cracks of approximately $50\mu\text{m}$, as visible in Figure 28, were observed on the surface layer of resin.

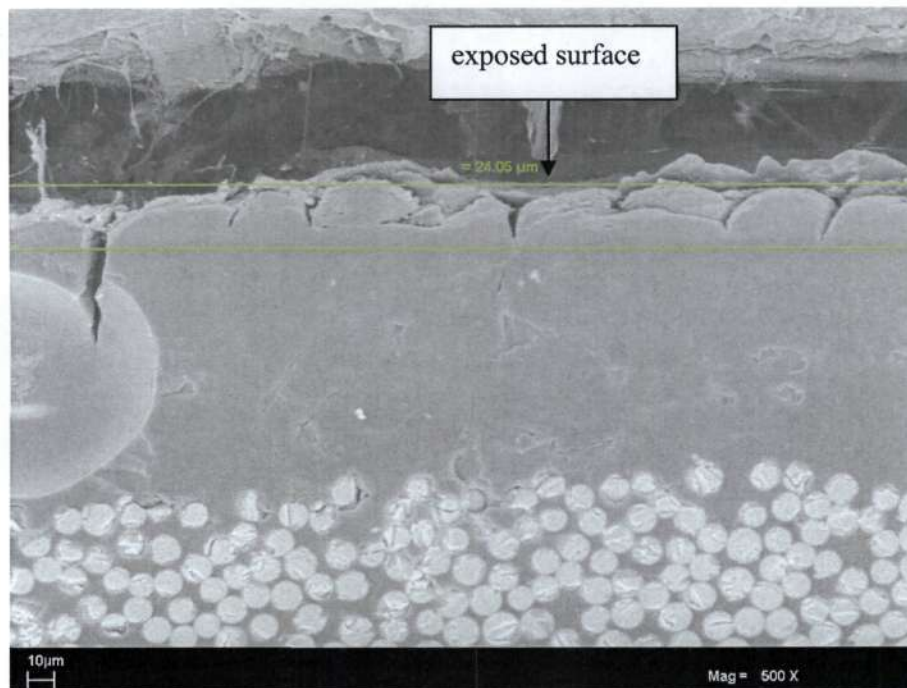


Figure 28 - Cracks on the surface of 5052 epoxy laminates after 9.5 months of exposure at Durban

Although a large layer of resin of approximately the thickness of a layer of reinforcement appears above the fibres in Figure 28, this layer of resin may not be un-reinforced as it appears. Fibres were visible within this layer of resin, Figure 29, through multiple cracks at the surface.

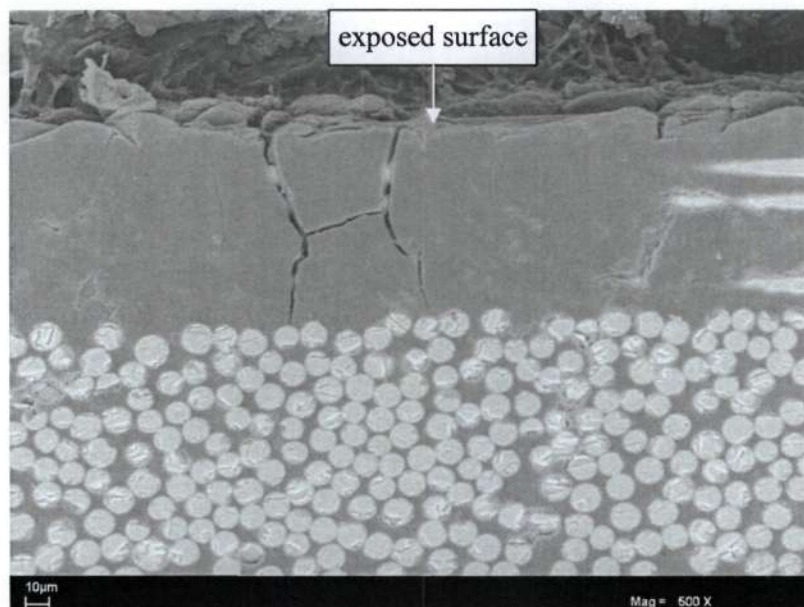


Figure 29 - Fibre visible through cracks on the surface of 5052 epoxy laminates after 9.5 months of exposure at Durban

On the 5052 epoxy laminates examined, the thickest region of resin was found to be at the weave cross-over, i.e. region in which the longitudinal fibres cross from being under transverse

tows to above transverse tows or vice versa. Cracks on the surface of a void in this particular region were observed, Figure 30, after approximately 9.5 months of exposure. These cracks do not originate at the surface of the laminate. Further, cracks originating at the void surface were found to propagate into the adjacent undamaged matrix.

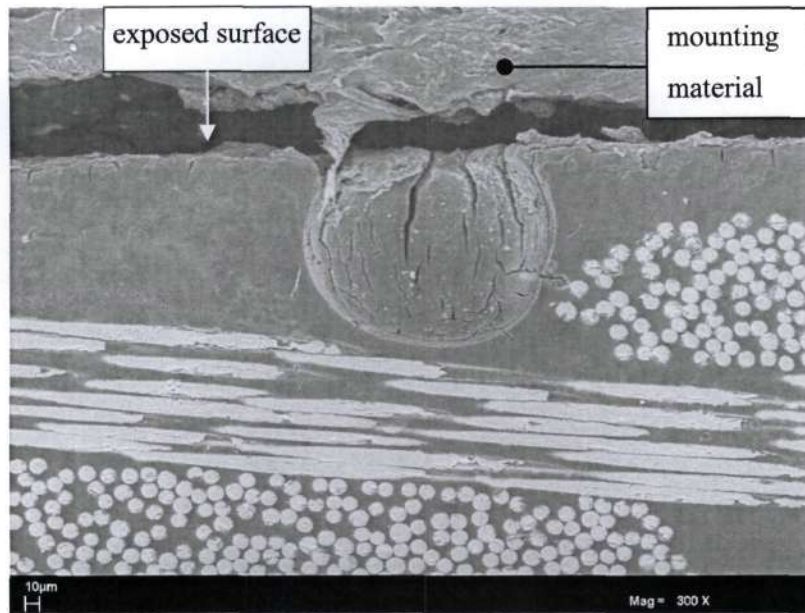


Figure 30 - Cracks on the surface of a void present in a 5052 epoxy laminate when viewed after 9.5 months exposure at Durban

Loose fibre at the surface of the laminate does not appear to have pieces of resin adhering to the surface of the fibre. The surfaces of the loose fibres appear clear of debris, Figure 31. It can therefore be reasonably expected that the fibre-matrix interface was disrupted to a significant extent during weathering.

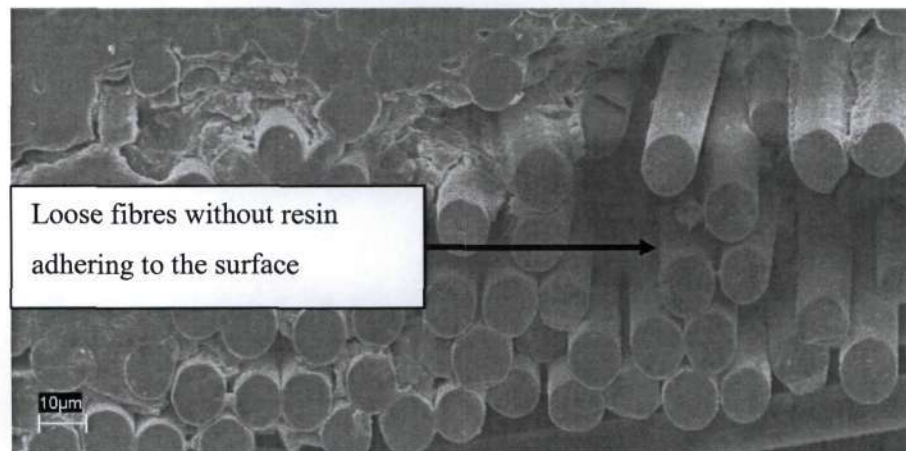
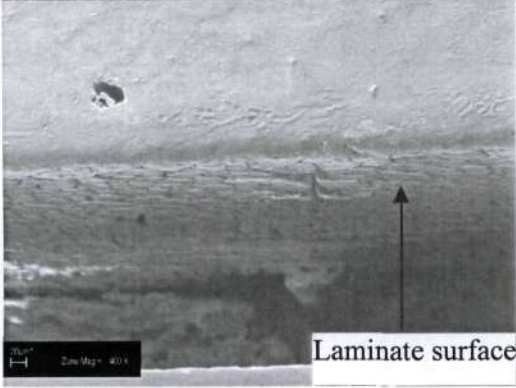
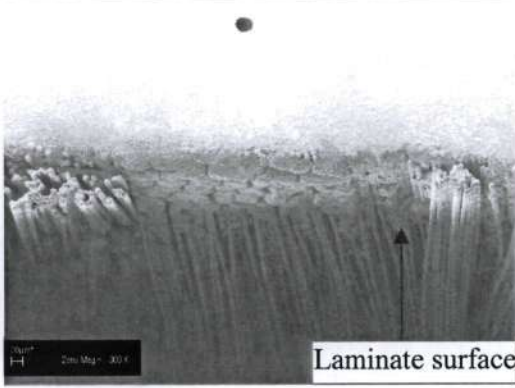
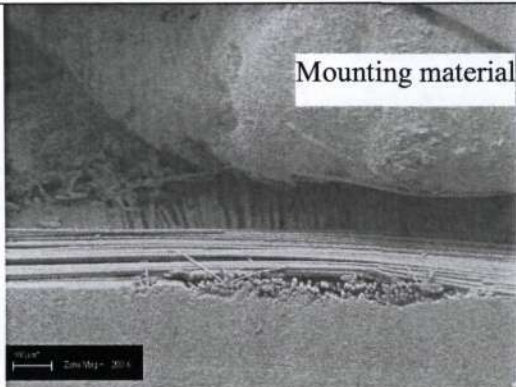
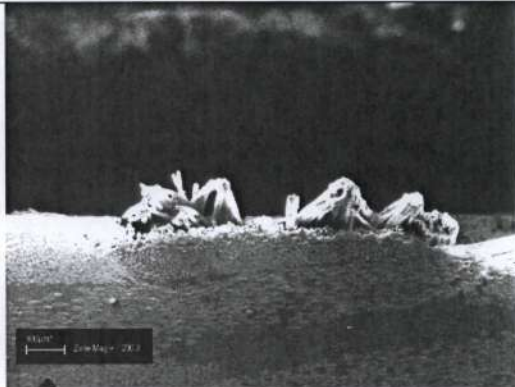
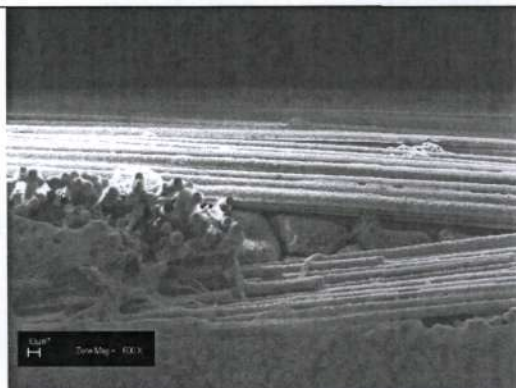
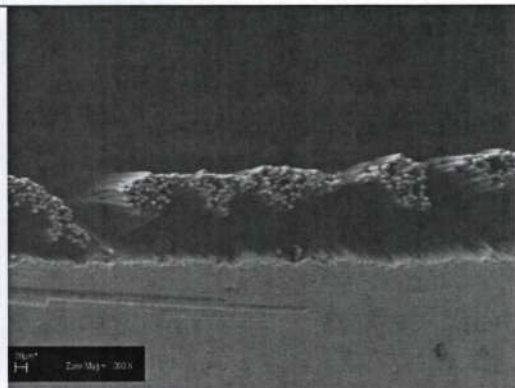


Figure 31 - Resin free fibres at the surface of 5052 epoxy laminates

Damage of laminates at the various test sites appear in Table 4 overleaf.

Table 4 - Variety of damage observed on exposed laminates

 <p>5052 epoxy; 20 months exposure at Alkantpan</p>	 <p>5052 epoxy; 40 months exposure at Alkantpan</p>
Cracked resin surface	Weathered cracked surface resulting in fibre exposure
 <p>5052 epoxy; 40 months exposure at Durban</p>	 <p>5052 epoxy; 26 months exposure at Alkantpan</p>
Longitudinal and transverse tows on topmost weave exposed	Degradation from left to right of image.
 <p>5052 epoxy; 40 months exposure at Bredasdorp</p>	 <p>5052 epoxy; 26 months exposure at Irene</p>
Cracking in resin under fibre tows exposed at the surface	Free tows exposed at the surface

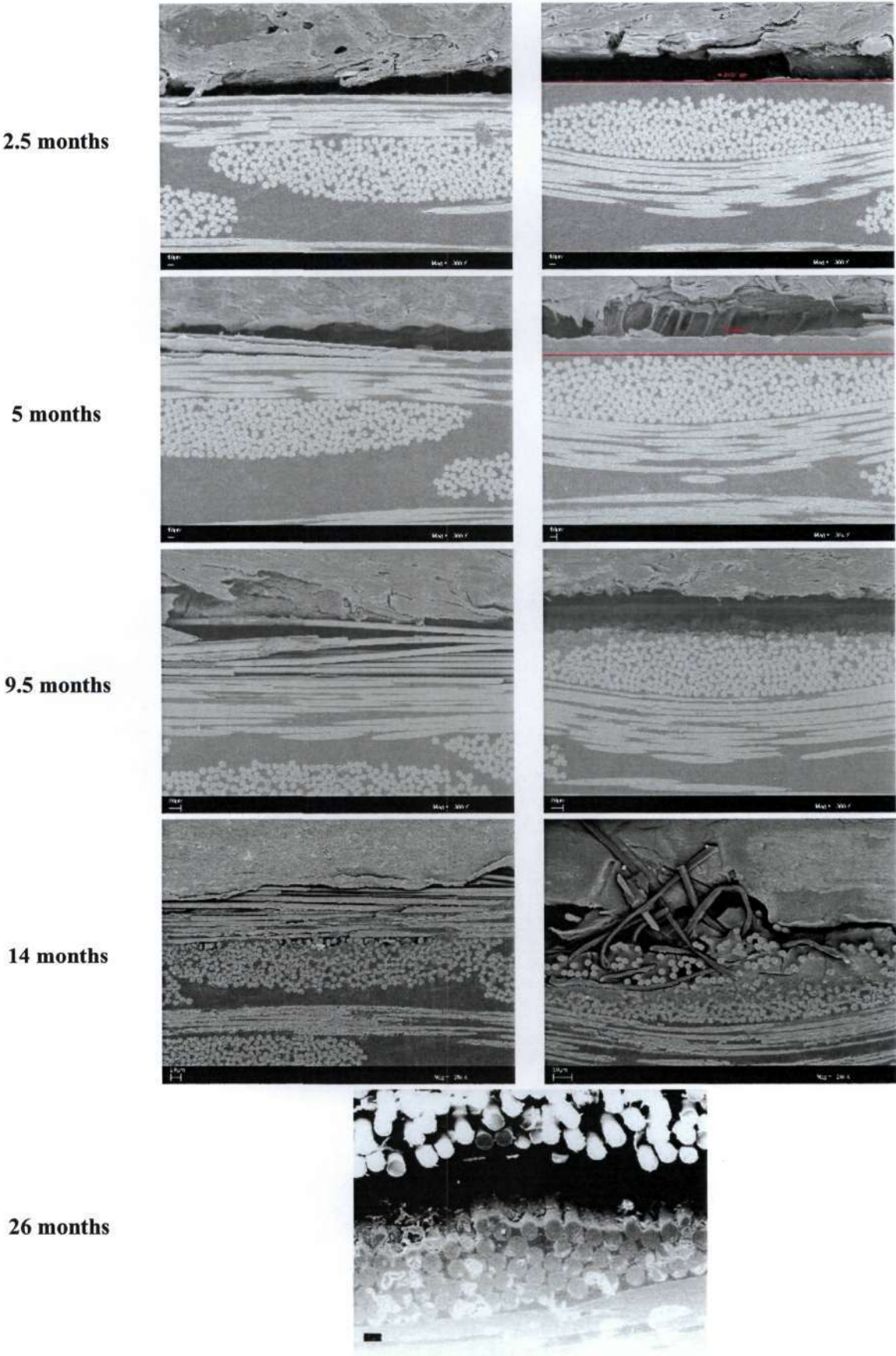
6.3 Epoxy matrix erosion rates

The first attempt to measure the depth of erosion entailed measuring the thickness of the laminate after exposure and subtracting this value from the thickness of the laminate prior to exposure. The difference in thickness would yield the depth of matrix material lost from the exposed surface of the laminate. Initial measurement of laminate thickness using a vernier proved inaccurate once the matrix had eroded to a depth below the fibres, as the measurement using the vernier included the thickness of the fibres. This method was therefore discontinued. The next method of determination of the depth of matrix erosion required that the initial unexposed, un-reinforced thickness of resin at the surface be established and used as a baseline from which the subsequent depth of matrix erosion can be determined. This un-reinforced layer of resin at the surface would depend on the manufacturing method as good compaction would result in a thin layer of un-reinforced resin at the surface. Due to laminates manufactured by wet lay-up having no consistent thickness of a surface layer of resin, an accurate depth of erosion could not be established. Inconsistent compaction which occurred when hand-laying the laminates resulted in an inaccurate measurement of depth of matrix erosion using an unexposed, un-reinforced surface layer as a baseline. This resulted in a falsely large depth of erosion being measured on well compacted laminates. This method of measurement was therefore discontinued. The third method used to calculate the depth of resin eroded, bases the measurement of resin loss on the thickness of a fibre tow. By counting the number of exposed tows and multiplying by the average thickness of a tow, the depth of resin loss in the reinforced section of the laminate may be determined. The depth of the surface layer of resin may be verified / compared to the thickness of the surface layer of resin in the masked area of the laminate which was not eroded. The total depth of resin loss was determined as the sum of the depth of the average surface layer of resin and the depth of resin lost in the reinforced section of the laminate.

The rate of resin loss was calculated by dividing the total depth by the specific exposure period of the laminate. This method of measurement was found to be least influenced by the extent of compaction of the laminates and more accurate than the previous two methods attempted. Depth of resin loss and / or damage across Alkantpan, Irene, Bredasdorp and Durban were found to be similar within the accuracy of the measurement technique. A new, graphical technique to measure the depth of erosion has been developed and described in Appendix C. The accuracy of the graphical technique is limited to 5µm.

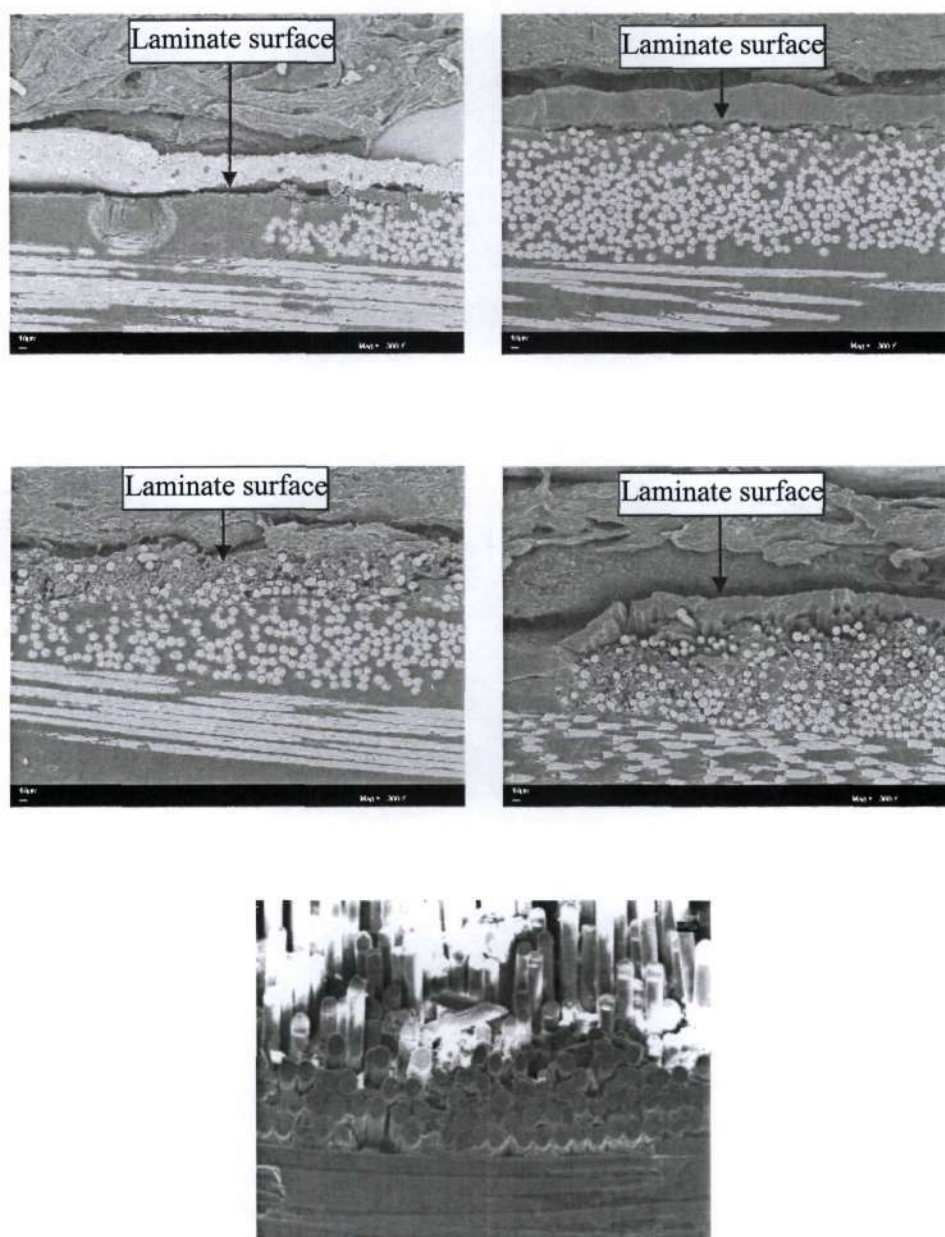
Table 5 shows the extent of fibre exposure of 8552 epoxy laminates exposed at Durban after different exposure periods, with most images captured at a magnification of 300×.

Table 5 - Illustration of fibre exposure on the surface of 8552 epoxy laminates with increasing exposure duration



Measurement of the rate of resin loss was easily determined on the prepreg laminate by examination of the transverse and longitudinal weaves. Both the longitudinal and transverse weaves are therefore shown in Table 5. On the wet lay-up laminates, measurement of the depth of resin loss was readily determined by examining the transverse weave, therefore only the transverse weaves are shown in Table 6. Measurement of resin loss based on measurement of the longitudinal weave on 5052 laminates proved difficult. Table 6 shows the extent of fibre exposure of 5052 epoxy laminates at different exposure periods.

Table 6 - Illustration of extent of fibre exposure, at 300 \times magnification, on the surface of 5052 epoxy laminates exposed at Durban



20 months

Where damage at the interior of the laminate was noticed, in the form of cracks and fibre debonding, the depth of damage was measured and calculated using a similar method to the depth of resin loss study. The depth of resin loss / damage of the different epoxies was recorded after each exposure interval. The depth of resin loss / damage was found to differ between the two epoxies tested, Figure 32, although matrix erosion rates appear similar upon visual examination of the laminates, Figure 15 and Figure 16. The 5052 laminates have lost more material than 8552 laminates due to the higher rate of resin loss from the surface, measured as the gradient of the lines in Figure 32.

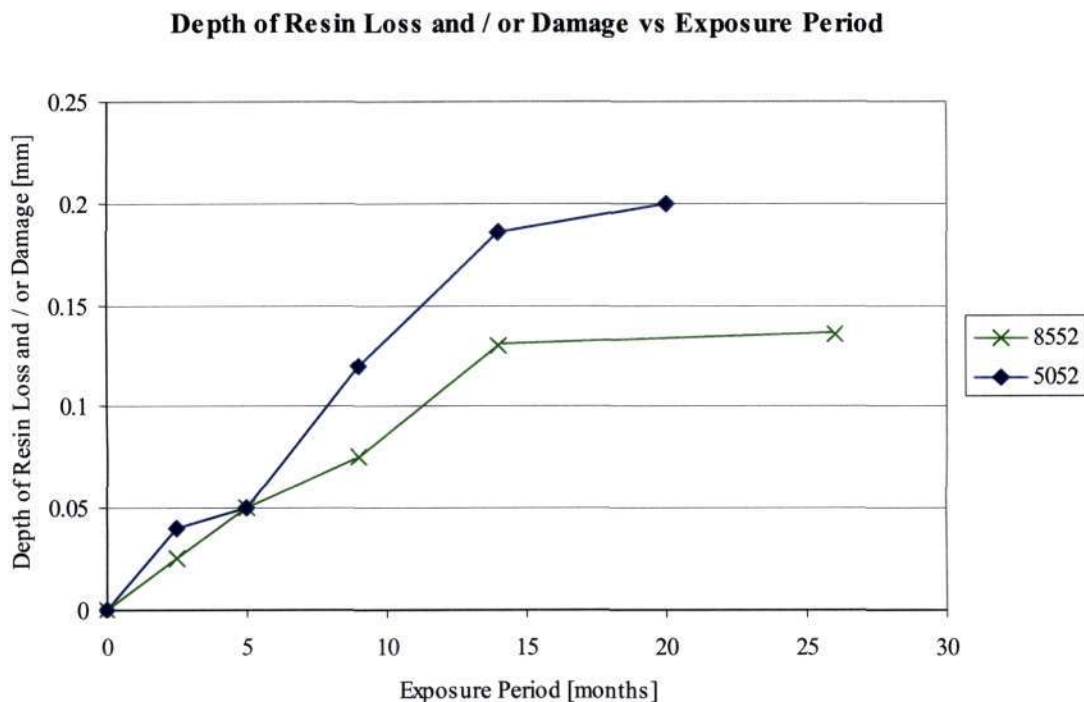


Figure 32 - Comparison of depth of matrix erosion and / or damage of 8552 and 5052 epoxy laminates

The data for thickness measurements after approximately 20 months of exposure of the 8552 laminates and 26 months of exposure for the 5052 laminates are inconsistent along the length of the laminate examined, and therefore do not appear in Figure 32. Further examination of the respective laminates removed at this stage of exposure is required to determine the change in thickness that did occur as evident by fibre tows being visible at the surface.

Three stages of degradation, tabulated in Table 7, were apparent from analysis of the degradation rate data. Degradation rates were calculated using data obtained from resin loss and / or damage measurements illustrated in Figure 32. Successive stages and durations of degradation appear to depend on the specific type of laminates examined.

Table 7 - Degradation rates of epoxy laminates

Stage	8552 laminates [$\mu\text{m}/\text{month}$]	5052 laminates [$\mu\text{m}/\text{month}$]
1	10	10
2	11	16
3	0.7	2

6.4 Vinylester

6.4.1 Optical microscopy

No cracks were observed on the surface of vinylester laminates, but fibre in the tows closest to the surface were visible on the exposed surface, Figure 33, as the exposure duration increased.

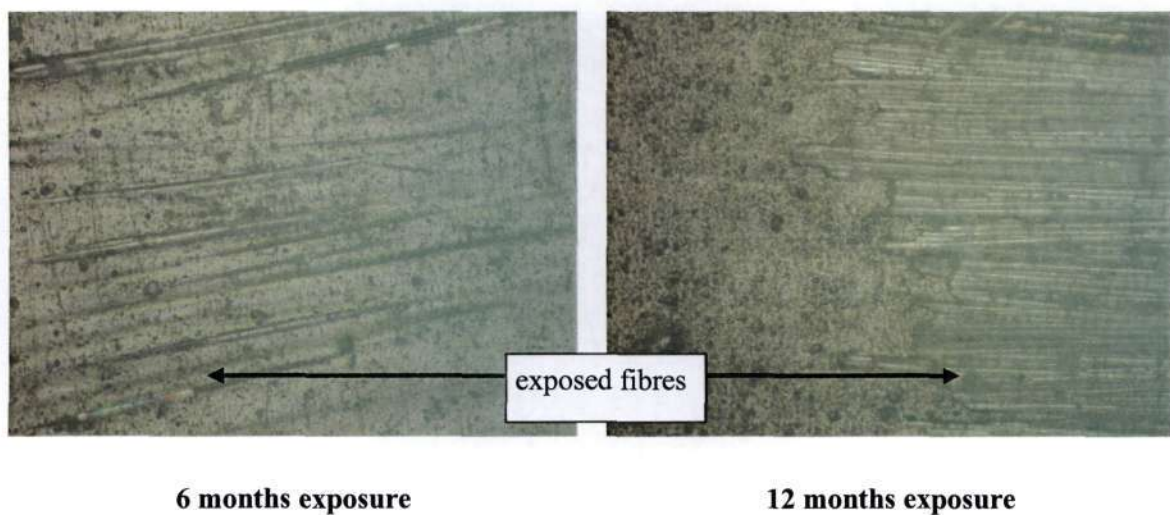


Figure 33 - Surface of vinylester when viewed at 100 \times magnification after exposure at Durban

6.5 Protective measures – Shade Cloth

6.5.1 Visual examination

Significant damage was noticed on unprotected 5052 laminates when compared to shade cloth protected laminates exposed for the same duration as illustrated in Figure 34. On shade cloth protected laminates, fibres remain protected by resin at the surface although fibre pattern was observed on sections of the exposed area. A change in colour of the resin from being originally translucent to slightly yellow was noted. In contrast, fibres on unprotected laminates have

become exposed and a significant change in colour had occurred when compared to laminates protected by shade cloth.

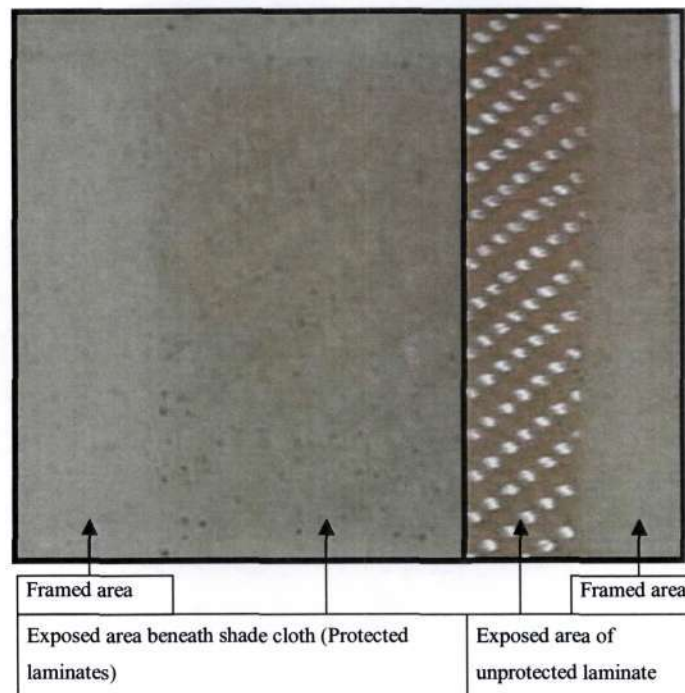


Figure 34 - Comparison of shade cloth protected specimens and unprotected specimens after approximately 9.5 months exposure at Durban

The protected laminates examined were exposed predominantly during Spring, Summer and Autumn, while the unprotected laminates were exposed predominantly during Autumn, Winter and Spring. With the peak natural radiation intensity and longest days occurring in Summer, protected laminates were exposed to the harshest exposure period during a year when compared to laminates that were not protected. The unprotected laminates were exposed during Autumn, Winter and Spring, with natural radiation being the lowest and the days shortest in Winter. The unprotected laminates were therefore not exposed to as harsh a climate as the protected laminates yet appear to incur more damage than the protected laminates.

6.6 Discussion

From examination of all images presented, the glass fibres do not appear to incur damage due to exposure to the natural environment. Damage appears predominantly in the matrix or at the fibre-matrix interface.

Change of laminate mass, to quantify moisture observation, was determined only on laminates exposed after 2.5 months of exposure to the environment. Laminates exposed for longer durations experienced a loss of resin from the surface resulting in fibre exposure; therefore changes in mass would not provide an accurate measure of moisture absorption. No change in mass of 8552 laminates were measured after 10 weeks of exposure at Alkantpan and Irene while laminates exposed at Durban experienced a 0.35% increase in mass. No change in mass of 5052 laminates were measured after 10 weeks of exposure at Alkantpan and Irene while laminates exposed at Durban experienced a 0.1% increase in mass. Laminates exposed at Durban appear to be most affected by moisture occurring in the natural environment. The increase in mass calculated does not take into account resin loss from the surface of the laminate during the 2.5 month exposure period. Mass change measurements were not performed on laminates exposed at Bredasdorp, Komati and Cradock as these laminates were only sampled every six months. Mass changes would therefore be a complex combination of moisture absorption and matrix loss from the surface, with the matrix loss from the surface becoming predominant with increasing exposure duration.

Visually, exposure to the natural environment results in the loss of resin from the surface and the underlying fibres becoming gradually exposed. This was noted on all laminates examined. Fibre exposure of exposed laminates has been noticed during previous durability studies [16, 9]. From observations on Figure 25, page 96, it appears that resin erosion progresses at a higher rate in regions of un-reinforced resin than in regions of reinforced resin. Accompanying the loss of resin from the surface was a change in colour of the matrix. On unprotected 5052 laminates, the change observed was from being initially translucent to yellow to dark brown. On unprotected 8552 laminates, laminates changed to darker shades of brown. The colour change and resin loss from the surface were not as pronounced on laminates protected by shade cloth after approximately 9.5 months of exposure. Shading of the laminates by the use of shade cloth has prevented the rapid loss of resin from the surface and a drastic change in colour of the surface that would have otherwise occurred. As the shade cloth results in shading from natural radiation, it was concluded that the rate of resin loss and colour change are dependent on the intensity of natural UV radiation.

However although the matrix erosion rate decreased from the first stage to the second stage of erosion, the damage rate increases, hence the higher degradation rate of stage two of degradation. Damage in stage two consists primarily of cracks originating at the surface progressing toward the interior. The crack growth to the fibre-matrix interface may be partially responsible for the debonding of the fibres. Matrix erosion is reduced as the loose, exposed fibres provide protection to the cracked matrix from the natural elements.

The presence of the layer of resin at the surface of a laminate protects the fibres below. A thick surface layer of resin may not imply that the fibres below will be protected for a longer duration as this would depend on the weathering resistance of the polymer. The erosion rate of the surface needs to be established before any prediction can be made as to when the fibres closest to the surface become exposed. Resins with a higher resistance to weathering may offer fibre protection for a longer duration. Use of a surface coating, e.g. gelcoat or paint may provide additional protection to the layers of fibre and resin below thereby increasing safe service life of the structure or component.

The dependency of colour change and rate of resin loss on direct exposure is confirmed by examination of the masked areas of the laminate. The masked areas, i.e. the area at the edge of the laminate covered by the frame did not appear to incur any resin loss and only slight discolouration was noted, Figure 19, page 93. Changes in colour of laminates attributed to UV exposure have been measured by Bank *et al* [182]. As fibres become increasingly exposed to the environment, colour changes to the surface of the resin below are not as perceivable due to the resin becoming covered by fibres.

Cracking and fibre exposure was observed on the exposed area of all epoxy laminates. The depth of cracks on the 8552 epoxy laminates appear to be constant and of the order of 10µm. The constant thickness of the cracked layer may be due to two scenarios. The first case being that the loss of resin from the crazed surface resulting in a small cracked layer, facilitates diffusion of moisture and oxygen into the laminate. As diffusion and UV absorption may be limited with depth from the surface, damage in the form of cracks may only manifest at or near the surface. The combination of oxygen, moisture and radiation may act collectively to induce damage at or near the surface. For damage to further progress, material loss from the surface is required to allow for diffusion of oxygen and moisture, and absorption of UV radiation. The second case would be that crack growth, as a consequence of exposure, may progress at a similar rate as depth of resin loss from the surface. The presence of cracks on the surface due to UV radiation has been highlighted by the absence of cracks on masked areas of the laminate and on laminates protected by shade cloth. Therefore the formation of cracks appears to be strongly dependent on exposure to UV irradiation.

Crack development on the surface of the epoxy laminates does not appear to be influenced or occur as a result of moisture only. Laminates protected by shade cloth would have been exposed to the same quantity of moisture due to precipitation and humidity while masked regions would not have been directly exposed to humidity or precipitation. In both cases, with one being

exposed to moisture and the other not, no significant crack development has been observed on the surface.

While cracks on the 8552 epoxy laminates appear to be restricted to approximately $10\mu\text{m}$ from the surface, this does not appear to be the case with the 5052 epoxy laminates. On 5052 laminates, with an average crack depth of $25\mu\text{m}$, larger cracks of approximately $50\mu\text{m}$ in length were observed. These larger cracks may be due to the growth of cracks at the surface. Cracks on the surface of voids present at the surface of the 5052 epoxy laminates appeared to be orientated radially away from the centre of the void. Choi *et al* [18] found that cracks occur in the direction of maximum shear stress, hence the direction of cracks may be related to planes of maximum stress. Underlying fibres were visible through the voids. Upon examination under an optical microscope, fibre tows at the bottom of a hole was noticed. It appears that the fibre roving may have limited the depth of the hole that formed. Holes observed on the surface of wet lay-up laminates may be due to the leaching out of un-reacted constituents which has been previously described by Vauthier *et al* [183]. Leaching of un-reacted polymer is thought to result in holes being formed at the surface. The presence of moisture, due to precipitation, on the surface of the laminate would facilitate this leaching out of un-reacted constituents. The holes therefore present an ideal nucleation site for the growth of defects due to collection of moisture in the holes. Multiple cracks on the surface of holes were noticed as shown in Figure 30, page 99. Crack initiation at the base of the holes in close proximity to fibres may result in cracks propagating along the fibre-matrix interface causing debonding of fibres.

The extent of crack length with respect to the laminate thickness was calculated by dividing the depth of the cracked layer by the thickness of the laminate. For the 8552 laminates this was calculated to be 4.8×10^{-3} and for the 5052 laminates 8.9×10^{-3} . The depth of the damaged layer due to cracking is therefore less than two orders of magnitude smaller than the thickness of the laminate.

Cracks that have propagated to the layer of fibres closest to the surface have disrupted the fibre-matrix interface bond as evident by the cylindrical impressions on the loose pieces of resin at the surface of the laminate; see Table 6 page 103 on the 14 months of exposure image. The surface cracks would have been of sufficient depth to have propagated to the layer of fibres below and then along the fibre-matrix interface resulting in debonding. Although surface cracks appear to be restricted to the surface, the surface layer has been sufficiently worn such that the cracks have reached the first layer of reinforcement. It appears that the majority of surface cracks do not progress to significant depth within the laminate verifying the finding that degradation is predominantly a surface phenomenon. On the laminates examined, debonding

appears to occur on almost the entire transverse tow of fibres. Cracks perpendicular to the fibre axis were observed in Figure 29, page 98. Fibre debonding similar to that noticed by Zhang *et al* [232] has also been observed on epoxy laminates examined. Cracks on the 8552 laminates do not appear to have resulted in fibre debonding as evident by the presence of resin on loose fibres at the surface. A similar observation was noted by Hammami and Al-Ghuilani [233] after having observed spots of resin on degraded laminates subjected to durability testing.

Ageing of laminates at the glass transition temperature appears to have induced cracks only in close proximity to voids. The cracks at the surface of the void may be due to thermal stresses occurring at the small radii of a void resulting in rupture at the void surface due to excessive strain of the matrix. No other damage was observed on thermally aged laminates. Similar cracks were observed on the surface of a void on exposed laminates with no significant damage observed in the surrounding matrix. These types of cracks were only observed on void surfaces at the surface of the laminate. Cracking on the surface of the void on the exposed laminate may therefore be due to thermal cycling experienced by the laminate due to changing ambient temperatures during a 24 hour period.

The depth of resin loss and / or damage was found to be greater on the 5052 laminates when compared to the 8552 laminates at each sampling period. On 8552 laminates, damage was primarily in the form of resin loss from the surface. The 5052 laminates experienced damage due to both fibre exposure and crack propagation toward the centre of the laminate. The combined effect of the two modes of damage may have resulted in a higher depth of degradation and / or damage on the 5052 laminates when compared to the 8552 laminates. As a result of the differing damage rate, the gradient of the curves plotted on the resin loss and / or damage vs. exposure period graph differ. After approximately the first half of the topmost layer of reinforcement has been exposed or damaged, (observed after 14 months of exposure), the rate of damage decreases. This behaviour is thought to be due to the exposed fibres sheltering the fibres and resin beneath from the natural environment thereby limiting the rate of damage progression.

Although care has been taken to quantify the change of depth of the laminate due to material loss, the method of resin loss and / or damage does not take into account any swelling of the laminate due to moisture absorption. Swelling was suspected to occur as it was noticed that although resin was lost from the surface resulting in fibre exposure, the thickness of the laminates remained approximately constant. During the laminate examination and analysis, a successful method of quantifying swelling was not established due to changes in dimensions of the specimen as a result of resin loss.

Both loss of resin at the surface and a change in colour of resin at the surface were noticed on vinylester laminates. No cracks were however noticed on the surface of the laminate. As vinylester is a chemically different resin, being more resistant to corrosive fluids and moisture, a comparison with the epoxy laminates was not undertaken.

The different stages of degradation appear to be dependent on the resin system and method of manufacture of laminates. The 8552 laminates do not exhibit a clear transition from stage one degradation to stage two, although these laminates experience only two stages of degradation. The first stage of degradation is loss of resin from the surface resulting in the exposure of fibres. Due to an increasing number of fibres becoming exposed with time, the loose fibres at the surface provides shelter for the underlying matrix and fibres, hence the degradation rate decreases.

In contrast to the 8552 laminates, the 5052 laminates experience three different stages of degradation characterised by three degradation rates. The first stage of degradation is due to the loss of resin from the surface. This initial resin loss does not result in exposure of fibres and is merely the loss of resin from the surface of the laminates. Once the surface layer of resin had been removed and fibres had become exposed at the surface, surface cracks were observed to propagate to and along the fibre-matrix interface. The close packing of fibres in a layer of reinforcement provides short crack paths between fibres in the resin facilitating damage due to the growth of cracks in the relatively thin layer of degraded material at the surface. The final stage of degradation is affected by the protection of resin and fibre by loose fibres on the surface of the laminate. In comparison to the 8552 resin, the 5052 resin appears more susceptible to cracking due to weathering.

7 COMPRESSION TESTS

Degradation appears to be predominantly a matrix process based on the review of the literature and examination of specimens removed from the exposure panels placed in the natural environment. For the glass-fibre reinforced laminates being tested and examined, there does not appear to be damage induced on the fibres. Therefore, ideally tests that are strongly influenced by matrix dominated properties would therefore be most sensitive to property changes as a result of degradation. Compression tests were therefore initially decided upon to characterise changes in strength as a result of degradation.

As no compression test fixtures were available for use, a set of compression fixtures were designed, manufactured and commissioned. This activity was in-line with the project objective of developing the required equipment for use on the project. Review of different compression fixtures as well as different equipment configurations for compression testing of polymer composites was undertaken. Concept generation, detail design, commissioning, and verification of accuracy of the results are provided in Appendix D.

7.1 Results

During the manufacture of the compression fixtures, specimens were packaged and sent to the Council for Scientific and Industrial Research (CSIR) for compression testing to avoid delays in the project. The test results that follow were obtained from tests conducted at the CSIR. Tabulated results of individual specimens appear in the Appendix E. Unexposed specimens were tested to establish a baseline set of values, (Table 8), against which changes in strength would be compared. A coefficient of variation (v) between 0.05 - 0.06, implies that the average compressive strength of 66.7% of the specimens tested are within 5.5% of the tabulated average.

Table 8 - Ultimate compressive strength of unexposed epoxy laminates

	8552 epoxy laminates	5052 epoxy laminates
Average strength [MPa]	494	385
Standard deviation [MPa]	26	22
Max. [MPa]	515	407
Min. [MPa]	460	358
Range [MPa]	55	49
v	0.053	0.057
Values based on averaging the test results of six specimens per batch		

Test results for exposed specimens were tabulated as a ratio of the average compressive strength measured after a specific exposure duration against the average compression strength of unexposed laminates. The stresses will therefore be symbolically shown as σ/σ_0 . This method has been adopted to easily illustrate changes in compressive strength with respect to the baseline data. Values greater than one represent an increase in strength, values of approximately one represent negligible changes in strength and values less than one represent a decrease in strength.

Sampling and testing of 8552 laminates at ten and twenty weeks were performed to determine initial transient changes in strength, the results of which are presented in Figure 35 overleaf. A 2% reduction in strength occurred on the Irene laminates, but this value is within the standard deviation of 5.3% of the unexposed laminates. The strength reduction is therefore not significant with respect to the variation of the unexposed laminates. Laminates exposed at Alkantpan and Durban have however experienced a reduction in strength after 20 weeks exposure as shown in Figure 35, to the extent that the strength measured differs by more than the standard deviation measured on a batch of the unexposed laminates. Laminates exposed at Alkantpan experienced a negligible increase in strength after 10 weeks of exposure with an upper standard deviation of $1.05 \times \sigma_0$. The subsequent decrease in strength to $0.91 \times \sigma_0$ is the lowest strength of all exposed laminates after 20 weeks exposure. Laminates exposed at Durban appear to have lost strength within the first 10 weeks of exposure followed by partial strength recovery during the next 10 weeks. The trend of increasing compressive strength after exposure has begun, has not been experienced on the 8552 laminates at the remaining locations. The large coefficient of variation of data of 8552 laminates exposed at Durban implies a wide scatter of data points.

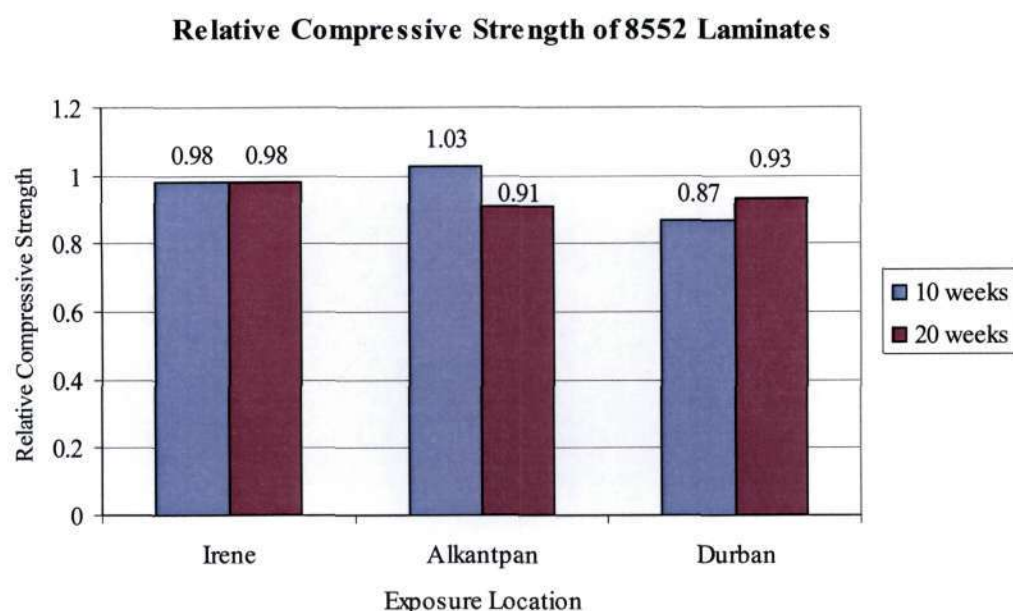


Figure 35 - Change in ultimate compressive strength of 8552 epoxy laminates

After twenty weeks of exposure, laminates exposed at Irene appear to be the least affected by exposure with the average strength decreasing initially by 2% of the unexposed strength. Laminates exposed at Durban appear to be most affected by the exposure with an initial decrease in compressive strength that was most severe when compared to the other locations.

Test results of 5052 laminates exposed at Irene have increased in strength above the standard deviation of unexposed laminates to a value of $1.06 \times \sigma_0$, while the strength of laminates exposed at remaining locations are within the standard deviation of unexposed laminates. Exposure for a further 10 weeks at Irene proved detrimental, with a strength loss of approximately 12% between the 10 week and 20 week exposure. Laminates exposed at Alkantpan although experiencing a negligible increase then decrease in strength, maintained their strength after 20 weeks of exposure to within the standard deviation of the unexposed laminates. Exposure at Durban for 10 weeks did not appear to affect compressive strength with only a cumulative exposure period of 20 weeks resulting in a 6% decrease in strength with a data scatter of 8.9%.

Laminates at Irene and Alkantpan appear to have initially benefited to different extents from 10 weeks of exposure by experiencing an increase in strength above the baseline value, see Figure 36 overleaf. Twenty weeks of exposure at Irene and Durban has proven detrimental to similar extents and although the average strength decreased, the scatter of data from the average was found to be 11% and 8.9% respectively. Exposed 5052 laminates have a large scatter of data

when tested after twenty weeks of exposure. The probable decrease in strength of laminates exposed at Irene and Durban cannot be accurately quantified due to the large scatter of data.

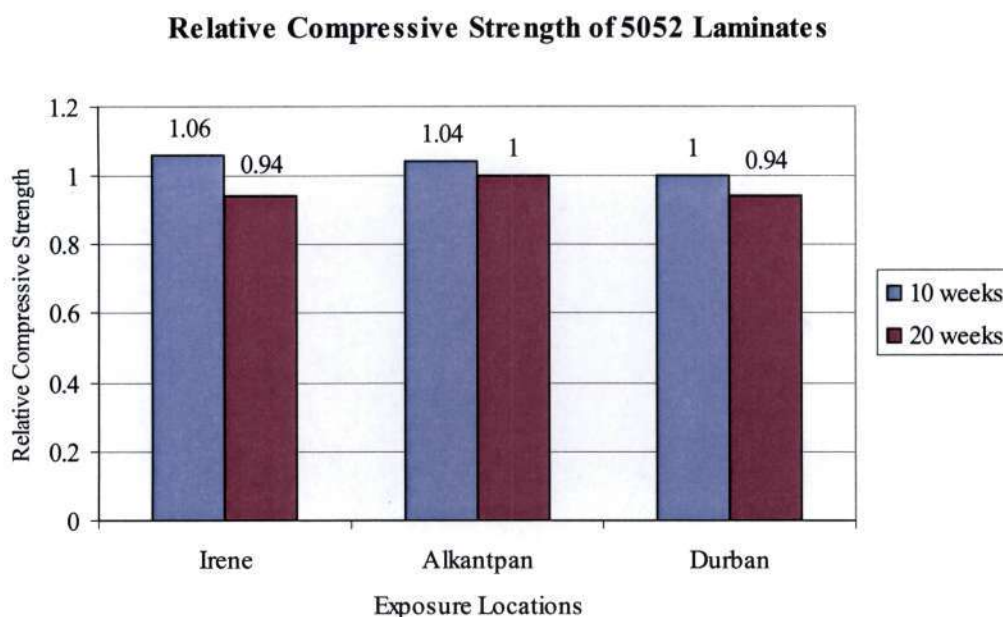


Figure 36 - Change in ultimate compressive strength of 5052 epoxy laminates

7.2 Discussion

It is of interest to note that the unexposed 8552 prepreg laminates have a higher standard deviation and range of strength when compared to the unexposed 5052 wet lay-up laminates. It was expected that the prepreg would have a smaller deviation in properties due to autoclave processing resulting in improved consistency among batches [32]. The wet lay-up system was expected to have a greater standard deviation due to the nature of the processing being highly influenced by the personnel performing the lay-up. The higher standard deviation experienced by the 8552 laminates is thought to be due to the strength of high fibre-volume ratio laminates being more sensitive to fibre microbuckling due to the weave of the reinforcement. The fibre-volume fraction of the 8552 laminates was 51% and that on the 5052 laminates, 40% as determined from burn-out tests documented in Appendix F. Fibre microbuckling is less likely to occur in unidirectional laminates as the fibres are loaded directly in compression whereas in woven composites, the waviness of the fibres as a result of the weaving may facilitate buckling of the fibres.

The weight change, of naturally exposed laminates, due to moisture absorption is difficult to determine as weight loss due to resin loss increases with time. Increasing laminate mass due to moisture absorption with resin loss occurring simultaneously from the surface of the laminate

has been observed by Dubois *et al* [16]. McManus [17] has noted that mass change was a misleading measurement of degradation as it is dependent on a degraded surface and relatively undamaged interior. From examination of precipitation data, it was observed the Alkantpan received an amount of moisture comparable to that of a wet climate. Mass measurements after 2.5 months of exposure however do not show an increase in mass of laminates exposed at Alkantpan, therefore estimates of moisture absorption cannot be based solely on precipitation measurement at the exposure location. Other climatic factors, e.g. temperature and humidity, would influence the quantity of moisture in the atmosphere.

The initial decrease in strength by 2% on the 8552 laminates exposed at Irene, is within the standard deviation of unexposed laminates hence exposure appears to have had a negligible effect on strength during 10 weeks of exposure. This is further apparent by the laminates maintaining the average strength after 20 weeks of exposure. At Alkantpan, the reason for the subsequent rapid reduction in strength of 5052 laminates, 12% in second ten weeks of exposure, may be due to fibres exposed at the surface no longer contributing to the strength as a result of a decreasing support from the worn and damaged resin at the surface. Laminates exposed at Durban have also experienced a similar strength loss of 13%, but this loss of strength occurred during the first 10 weeks of exposure, not the second 10 weeks of exposure as occurred with the Alkantpan laminates. In contrast to the decreasing strength with time, laminates exposed at Durban experienced an increase in strength of 6% between the 10 to 20 weeks sampling interval.

The exposure period of twenty weeks spanned the autumn and winter months in the Southern Hemisphere. Laminates tested at Alkantpan appear to have maintained their strength after 10 weeks with a possible explanation for the rapid loss of strength in the subsequent 10 weeks attributed to the exposure of the first layer of fibres at the surface and the thinner, damaged layer of resin covering the first layer of reinforcement. Care was taken to prepare test specimens from different exposure plates, to obtain a sample representative of the state of exposed laminates. Assuming the resulting fibre exposure of one layer implies that eight of the nine layers would then support the load, the load carrying capacity of the laminate would then be reduced by 11%, which within experimental error is not unrealistic from the measured decrease in strength of 9% experienced by the Alkantpan laminates after 20 weeks of exposure. This may be explained by considering the surface layer of a satin weave laminate, illustrated in Figure 37 overleaf. The transverse tows are visible on the surface of the exposed laminates, hence the top surface layer of resin is no longer present as illustrated in Figure 37.

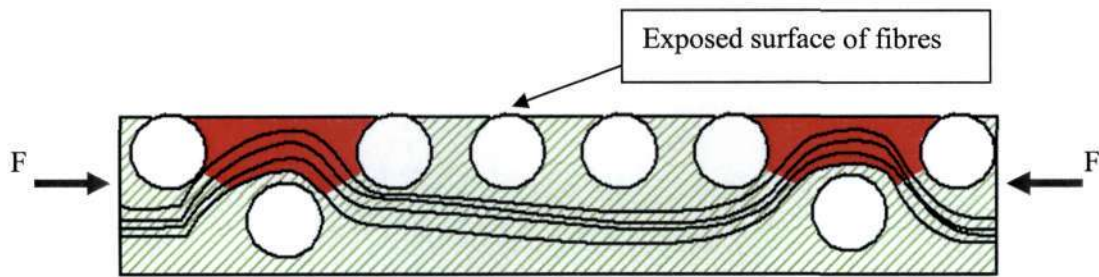


Figure 37 - Damaged region on a single layer of reinforcement at the surface due to buckling of fibres

The laminates at Alkantpan were observed to have the transverse fibres closest to the surface. This would be due to the orientation of the fibres in the cured laminate sheets not being known when the specimens were being cut. The specimens therefore received exposure with the transverse fibres being closest to the environment. When the laminate was loaded in compression, the fibres on the longitudinal weave may have buckled thereby damaging the thin layer of matrix above the fibre, creating a region of weakness in the matrix, illustrated in red in the Figure 37, that would not be able to transfer the load to adjacent transverse fibres across the region of damaged resin. The transverse fibres would provide little support to the applied compressive load and undamaged resin is required to prevent the fibres in the longitudinal tow from buckling as it passes over a transverse tow. The load would in the above case not be carried by the longitudinal fibres, as the region of the damaged matrix would no longer provide sufficient support for the fibres, hence further fibre buckling would occur. Although the fibres in the longitudinal tow are predominantly supported by an undamaged matrix below the transverse tows, fibres in the damaged matrix region would not be able to transfer the applied compressive load to the regions of the longitudinal tow below the transverse tows. Hence the layer of fibres at the surface may not be able to support a compressive load resulting in the load being distributed to the remaining eight layers.

The opposite case where fibres on a longitudinal tow are closest to the surface and are exposed to the environment, apply to laminates exposed at Durban and Irene. These exposed fibres on the longitudinal tow would not carry any load as it would not be surrounded by resin which can provide support for the fibres at the surface in compression. As only a few fibres on the tow in a single layer of reinforcement are exposed, the strength does not appear to be severely compromised with the remaining fibres in the same tow carrying the load. When tested in compression, the longitudinal fibres that pass under a transverse tow, do so in the direction of the centre of the laminate. In this region, the resin is less prone to damage as it is supported by the next level of reinforcement. Hence these laminates, although experiencing similar loss of

resin from the surface are affected differently when loaded in compression due to the lay-up of the material.

The scatter of the strength data of 8552 laminates exposed at Durban after both 10 and 20 weeks exposure is large enough to include the average of the strengths of both the 10 and 20 week exposure period. The strength of laminates exposed at Durban has decreased but the extent to which the strength has decreased cannot be accurately quantified. This decrease in strength may be attributed to the laminates being exposed in a moist environment compared to the relatively dry (less humid) climates of the remaining locations. Between Durban and Irene, laminates exposed at Durban may have experienced the most damage. Laminates at Alkantpan cannot be compared as described during earlier stages of exposure to those at Durban and Irene due to the different weave configuration of the surface layers.

The wet lay-up of the 5052 epoxy laminates appears more susceptible to post-curing effects when exposed. The 5052 laminate exposure appears to be severely influenced by the natural environment at Irene with an initial increase in strength of 6% during the first 10 weeks of exposure followed by a loss in strength of 12% in the subsequent 10 weeks. The initial increase in strength may probably be due to post curing due to the combination of heat and natural radiation. The reason for the resulting decrease may be due to fibre exposure at the surface. Laminates exposed at Alkantpan did not experience as large an increase in strength when compared to laminates exposed at Irene. The increase of 4% experienced is within the standard deviation of unexposed specimens. The first 10 weeks of exposure at Durban appear to have resulted in no change of strength but the subsequent 10 weeks appear to have resulted in a significant strength reduction with once again a large variation in data. Twenty weeks of exposure appear to have resulted in a large scatter of data making it difficult to accurately determine the decrease in strength probably due to exposure of fibres at the surface.

The environment at Irene initially has a negligible effect on the strength of 8552 laminates but results in large strength variations on 5052 laminates. The environment in Alkantpan produces the opposite effect, i.e. negligible strength changes on 5052 laminates but large strength variations on 8552 laminates. Durban appears to have a climate that negatively affects both 8552 and 5052 laminates as both have recorded lower average strengths.

Conclusions regarding strength change may be difficult to establish after twenty weeks exposure as curing of any un-reacted polymer will cause an increase in strength and offset a decrease in strength due to degradation. This post curing effect is more likely in wet lay-up systems even though post curing was performed according to specifications after laminate

manufacture. Due to inadequate post-curing curing in an oven, further post-curing of un-reacted polymer is possible in the natural environment [234].

8 FLEXURE TESTS

The problem experienced with the compression test results could not be promptly resolved. The compression tests performed at the University of KwaZulu-Natal were found to be too sensitive to specimen preparation and not verifiable, repeatable or accurate. Another type of test was therefore required so that the specimens could be promptly tested after sampling.

Literature was reviewed to determine problems experienced by previous researchers in using flexure tests to determine the effect of environmental exposure on polymer composites. A unidirectional flexure test was performed in this regard by Whitney and Husman [235] as the moisture and temperature conditioning applied would result in substantial strength reductions which would cause the failure mode to change from fibre dominated to matrix dominated. The unidirectional flexural strength was considered to be a fibre dominated property. (Matrix failure was found to occur at tests conducted at higher test temperatures.) The formulae used in the calculation of strength did include a shear correction term because epoxy matrix composites generally have large Young's modulus to shear modulus ratio, E/G . With the $E/G = 25$, Whitney and Husman found that the flexural modulus was corrected by 4% due to shear deformation. Of the two epoxy systems tested, the system with a higher postcure had a higher glass transition temperature (T_g) and therefore retained the brittle behaviour at higher moisture concentrations and temperatures. Regarding the comparison between 3-point and 4-point flexure tests, it was proven that the 3-point test results in higher strengths but lower modulus, using Weibull statistical theory. Test results from one of the two epoxy systems tested did however experience a 25% lower strength when tested in 3-point bending. Whitney and Husman offered no explanation for the unexpected test result other than that the data was based only on three specimens.

Flexure tests may be performed with either three point loading or four point loading. Strain on three point tests are easier to determine as it is proportional to the displacement of the cross-head. Four point loading is generally used for high modulus materials. Flexure test methods are applied to composites that are homogenous i.e. fibres orientated at 0° or 90° [236]. For laminated materials the result will be influenced by ply stacking [237,238]. The applicable standard, ASTM D790M, provides requirements for the minimum dimensions of the loading noses. A factor that needs to be selected before hand is the span-to-depth ratio that would be selected on the basis of the ratio of tensile strength to interlaminar shear strength. For strength ratios less than 8, span-to-depth ratios of 16 is recommended with the ratio increasing for higher modulus materials. A test with a span-to-depth ratio of 32 was attempted but the test was terminated as the large deflections before failure was the limiting factor on the apparatus used.

Four-point bending was used as the test section would be in pure bending, i.e. no shear forces would be present in the test region. There is therefore a uniform stress state in the test region due to a constant bending moment. With three point bending, shear forces are present in the test region and the bending moment increases to a maximum at the midspan under the loading nose. The distance travelled by the cross-head can be used as a deflection measurement therefore the modulus may be determined without using a strain gauge. In 4-point bending, there are no concentrated forces at the midspan that would result in contact stresses.

The modulus of elasticity may be determined by measuring the relative strain (on either the compression or tension surface), deflection of the midspan or slope of the end-faces of the laminate. Tensile failure stresses obtained from flexure tests have been analytically proven [239] to be larger than that obtained from tensile tests.

Flexural tests were considered as an alternative test option as it was possible to place the degraded surface in compression during this type of test. The flexural tests were conducted using ASTM D790M [240] as a guideline. Equipment had to be refurbished before use as corrosion had occurred while the equipment was in storage. Corrosion was removed from the rollers and attachments using emery paper and the fixtures were wiped clean. Roller dimension were verified to be larger than those recommended by the ASTM standard. Commissioning of the test fixtures are described in Appendix G.

Using ASTM E122-89, 'Standard practice for choice of sample size to estimate a measure of quality for a lot or process' as a guide, six specimens were tested per batch, when possible, and the results averaged to determine the representative strength of laminates at a specific location. The maximum, minimum, range, standard deviation and coefficient of variation were determined using standard techniques [241]. The type of distribution on strength or modulus across batches were found to be consistent. Further statistical techniques for analysis of a batch based on different distributions did not yield additional insight into the state of the material.

8.1 Results

Images were captured of the failed specimens to assist in understanding the mode/s of failure. Failure of fibres in tension followed by delamination frequently occurred. The delamination resulted in the last few layers of the reinforcement coming loose after the fibres had snapped. Figure 38 overleaf illustrates delamination of the last layer of reinforcement. Also visible is delamination within the laminate on the lower left corner of the image.



Figure 38 - Delamination observed on failed laminates

Examination of the exposed surface of the laminate reveals failure due to cracking of the matrix at the surface. The exposed surface was on the compression side of the specimen when tested and therefore failure would be due to either compression failure of the matrix or the underlying fibres buckling in compression and thereby exerting pressure on the resin at the surface causing pieces of the matrix to break free. When the fractured surface was viewed from above, the resin fracture appeared as white cracks as shown in Figure 39.

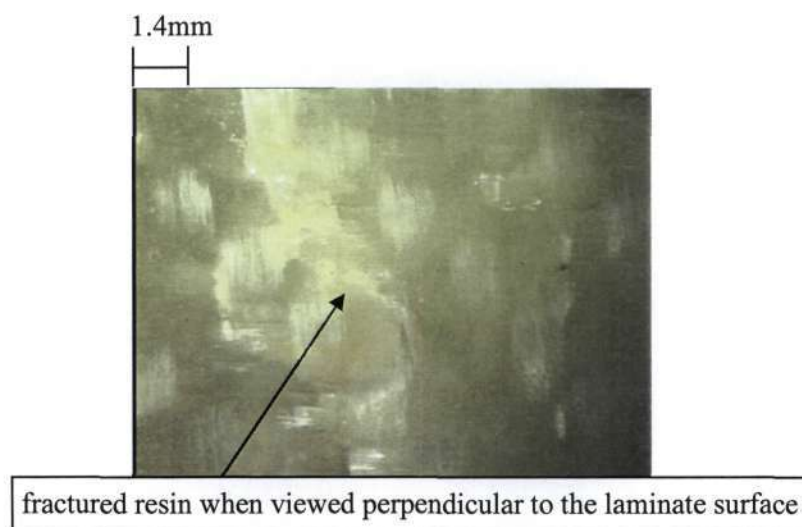


Figure 39 - Fracture of exposed surface in compression

The pieces of resin breaking free of the surface may be observed when the cross-section of the laminate is viewed. The light yellow peaks illustrated in Figure 40 reveal pieces of the matrix breaking loose of the laminate due to buckling of the underlying fibres in compression.

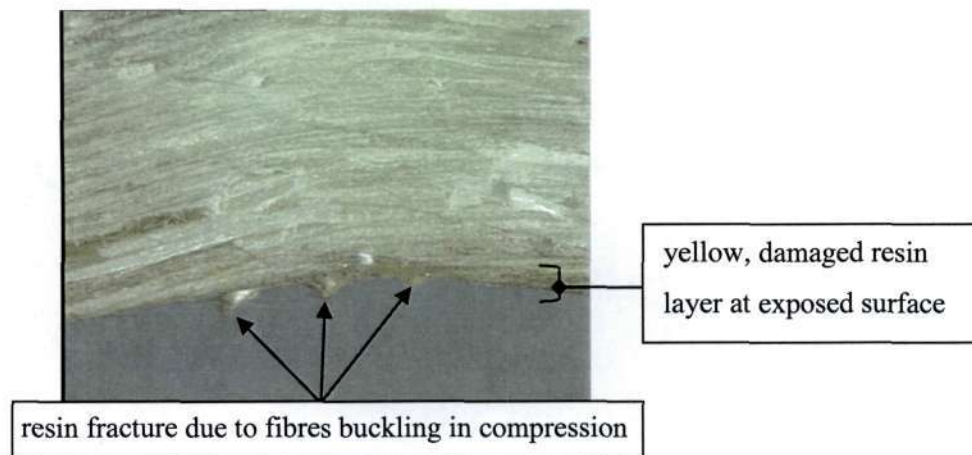


Figure 40 - Resin breaking free from the exposed surface

Further, the degraded resin at the surface which has become yellow in colour from originally being clear in colour, is observed at and below the surface to a depth of approximately one layer of reinforcement.

Strength of exposed specimens was tabulated as a ratio of the average flexural strength measured after a specific exposure duration against the average flexural strength of unexposed laminates. The stresses were therefore symbolically shown as σ/σ_0 . This method has been adopted to easily illustrate changes in flexural strength with respect to the baseline data. Values greater than one represents an increase in strength, values of approximately one represent negligible changes in strength, and values less than one represent a decrease in strength.

The sensitivity of the stress / modulus at a specific load to physical dimensions may be established to determine how the results vary with the measured input. Of specific concern is the effect of thickness on the flexural strength and modulus. This may be determined by evaluating the derivative of the functions in the regions of interest.

The dimensions of the test specimens of rectangular cross-section of width b and depth d may be substituted in the standard formula for flexural strength;

$$\sigma = \frac{My}{I}$$

where :

M is the applied bending moment,

y is the distance from the neutral axis

I is the moment of inertia

(87)

to yield the following relationship;

$$\sigma = \frac{6M}{bd^2}$$

(88)

The derivative of the above equation is

$$\partial\sigma = \frac{-12M}{bd^3} \partial d$$

(89)

The derivative evaluated at range of the function of interest for 5052 laminates is

$$\partial\sigma = -219 \times 10^9 \partial d$$

(90)

Considering the units of stress (MPa) and thickness (mm) taken into account, it can be seen that from Equation 90, the pressure variation in MPa is 219 times the change in thickness in millimetres. So for a 0.2mm decrease in thickness, the stress increases by 44MPa provided the applied load is equal before and after material loss.

A similar procedure applies for modulus, where the formula for modulus is;

$$E = \frac{3}{2} \frac{Ml^2}{bd^3u}$$

(91)

where l is the support span and u the midspan deflection

The derivative of Equation 91 is;

$$\partial E = \frac{-9}{2} \frac{Ml^2}{bd^4u} \partial d$$

(92)

which in the range of the function of interest is

$$\partial E = -23 \times 10^{12} \partial d$$

(93)

With the units of modulus (GPa) and thickness (mm) taken into account, it can be seen that from Equation 93, the pressure variation in MPa is 23 times the change in thickness in millimetres. For a change in thickness of -0.2mm, the increase in modulus is 4.6GPa provided the applied load is equal before and after material loss.

The above calculations may be repeated for 8552 laminates and the results are tabulated below,

Table 9 - Sensitivity of material properties to changes in depth of specimen for equal applied loads

	∂d	$\partial\sigma$		∂E	
8552	-0.1mm	+35MPa	+6.1%	+3.3 MPa	+12.3%
5052	-0.2mm	+44 MPa	+7.4%	+4.6 MPa	+19.6%

The decrease in depth labelled as -0.1mm for 8552 and -0.2mm for 5052 indicates the decrease in laminated thickness that has been observed on the respective laminates after 14 months of exposure. The decrease in laminate thickness can cause a strength change as much as 6.1% of the unexposed, baseline strength for 8552 laminates and 7.4% of the unexposed, baseline strength for 5052 laminates. This would create uncertainty in identifying causes of strength change when examining the strength change with time up to 14 months of exposure. The dependence of modulus on strength change is even more sensitive with a change of 12.3% and 19.6% being calculated for 8552 and 5052 laminates respectively based on unexposed, baseline moduli. Of the two reinforced resin systems, the 5052 appears more sensitive to property variations due to exposure.

To assist with verifying changes in strength due to changes in modulus, the relationship between flexural strength and flexural modulus was required. This relationship, derived in the Appendix H , appears below,

$$\sigma_b = \frac{4du}{l^2} E \quad (94)$$

For the specific geometry and deflection experienced, coefficients of E are tabulated below;

Table 10 - Dependence of flexural strength on flexural modulus

Laminate	Dependence of σ_b on E
8552	$\sigma_b = 0.016E$
5052	$\sigma_b = 0.015E$

The dependence of the flexural stress on flexural modulus, Equation 94, depends on deflection at the midspan. For the laminates considered, the deflection of 8552 laminates was greater than that of the 5052 laminates hence the flexural strength of the 8552 is slightly more sensitive to changes in modulus than the 5052 laminates.

Test results for exposed specimens were tabulated as a ratio of the average flexural strength measured after a specific exposure duration against the average flexural strength of unexposed laminates. The stresses will therefore be symbolically shown as σ/σ_0 . This method has been adopted to easily illustrate changes in flexural strength with respect to the baseline data. Values greater than one represent an increase in strength, values of approximately one represent negligible changes in strength and values less than one represent a decrease in strength.

Actual values recorded as well as the statistical analysis on the recorded values appear in Appendix I. Results from non-standard statistical analyses, eg. T-tests, have not been included as these results provided no further understanding of the data or trends. The variation of relative flexural strength with time for epoxy laminates has been plotted on a set of axes and is illustrated in Figure 41. Laminates exposed at various locations exhibit similar behaviour but the strength fluctuation varies depending on the exposure location. The standard deviation of flexural properties of the 8552 laminates, determined by averaging the standard deviation of all test results, was calculated to be 4% on strength and 5% on modulus.

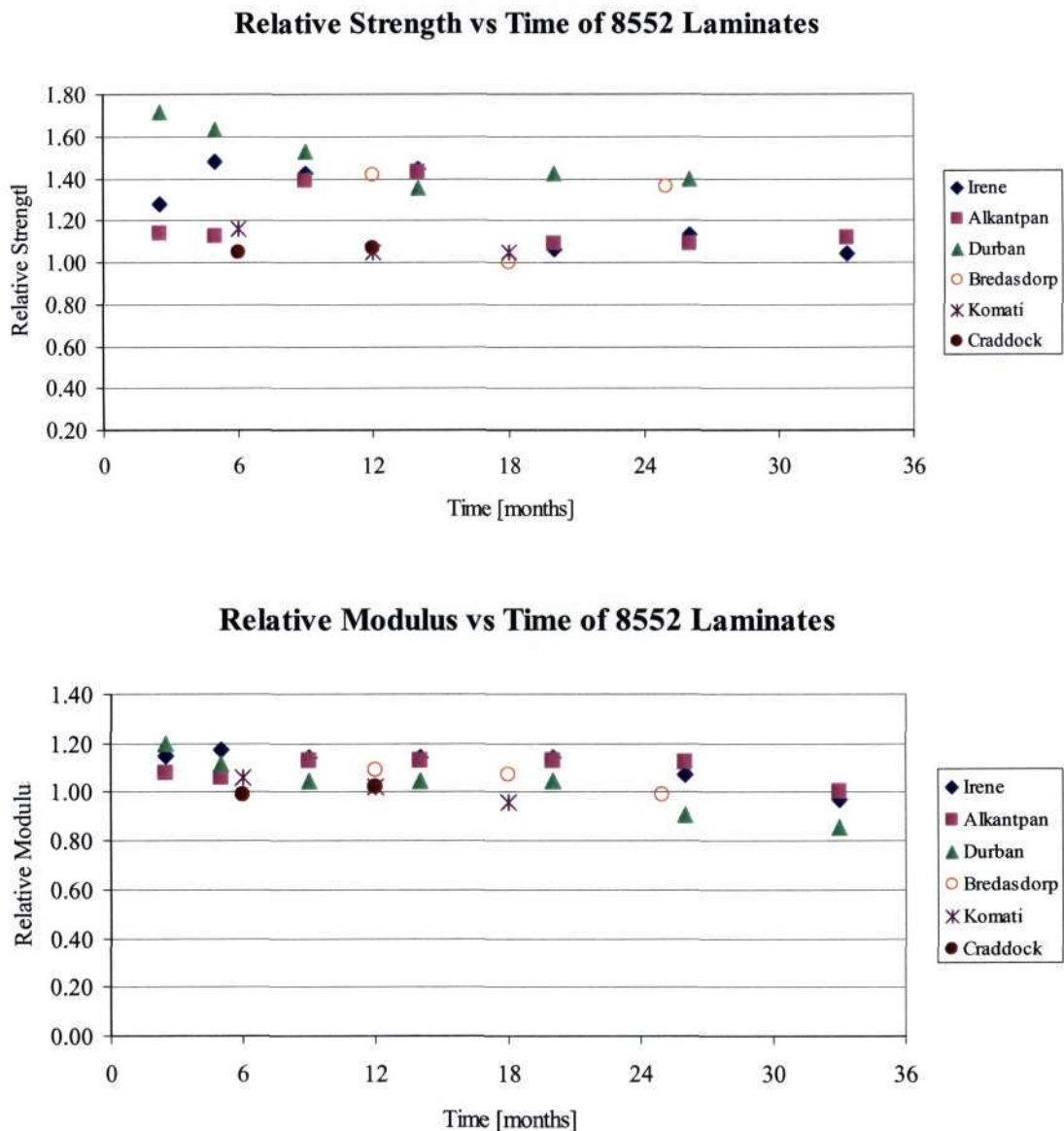


Figure 41 - Change in flexural strength of 8552 laminates with time

Laminates at Irene appear to have experienced an increase in strength of approximately 48% after the first 5 months of exposure with the strength remaining constant during the following 9 months. After 20 months of exposure, a decrease in strength of approximately 40% was measured in comparison to the previous batch sampled, with exposure duration of 14 months. In contrast the modulus of the laminates exposed at Irene experienced an increase in modulus of approximately 14% which remained within the standard deviation of the relative modulus of 1.14 from the beginning of exposure until 26 months of exposure had expired. The modulus then decreased by 14% until 33 months of exposure had expired. No results were reported for laminates tested after 41 months of exposure as the reduced stiffness on the laminates resulted in the edges of the laminates contacting the test fixtures before failure was recorded. These laminates could therefore not be tested until failure although the excessive deflection as a result of the reduced stiffness could be interpreted as a failure in terms of stiffness.

Exposure at Alkantpan resulted in an initial increase in strength of 14% and modulus of 8% during the first five months of exposure. After nine months of exposure, the strength increased by a further 27% to a value of approximately 1.41 and remained at this level for the following six months. The modulus also increased by 7% to a value of 1.13 after nine months of exposure. After 20 months of exposure, the strength decreased by 32% from the previous relative strength value of 1.43 to 1.09. After 33 months of exposure, the strength remained at approximately 1.10 but the modulus decreased by 12% from the previous value of 1.12 to 1.00.

Laminates exposed at Durban did not exhibit the gradual increase then decrease in strength as observed on laminates exposed at Irene and Alkantpan. In contrast the strength of laminates exposed at Durban displayed a rapid increase in strength with a gradual decrease in strength to a constant value. After 2½ months of exposure, a strength increase of 72% was measured on laminates exposed at Durban. This value gradually decreased to a relative strength value of 1.4 after 14 months of exposure. Similarly, the maximum relative modulus of 1.20 was measured after 2½ months of exposure thereafter the modulus decreased by 16% to a value of 1.04 after nine months of exposure. The next step change in modulus occurred after 26 months of exposure to a value of approximately 0.88, i.e. a 20% decrease in modulus. No strength or modulus values were tabulated after 41 months of exposure as the test specimens contacted the test fixture before failure and no ultimate strength data could therefore be obtained. Again, the reduction in stiffness resulting in contact of the specimen with the test fixture may be viewed as laminate failure due to excessive deflection.

The variation of strength of laminates exposed at Bredasdorp revealed no particular trends, with strength values appearing random. The maximum strength on these laminates was measured

after 12 months of exposure at which stage a 42% increase in strength was recorded. The modulus values obtained displayed a decrease in strength after 25 months of exposure with a reduction in modulus of approximately 8% from a value of 1.08 to 0.99.

Laminates exposed at Komati displayed a trend of strength change similar to that observed at Durban, i.e. the maximum relative strength measured of value 1.16 occurred during initial stages of exposure after six months. Thereafter the strength decreased by 11% after 12 months of exposure and remained at this level for the next consecutive six months. Modulus data also displayed a similar trend with a maximum relative modulus of 1.06 being measured after 6 months of exposure, decreasing to a value of 0.96 after 18 months of exposure. Logistical problems prevented timeous sampling of laminates from Komati therefore no data is displayed at any sampling periods. Laminates at Cradock displayed a marginal increase in strength of approximately 6% but no change in modulus during the 12 month exposure period. No further data is available for Cradock as logistical problems prevented timeous sampling of laminates from Cradock.

The 5052 laminates do not exhibit a readily apparent trend as illustrated in Figure 42 overleaf. The standard deviations of both the strength and modulus were determined by averaging the standard deviation of all tests and have been calculated to be 7% for both the flexural strength and modulus. The dotted lines represent significant changes in strength of the 5052 laminates, i.e. the dotted lines represent the range of values which are contained within the standard deviation. On the relative strength vs. time axis, the dotted lines represent the standard deviation about the value of 1.00. On the relative modulus vs. time axis, the dotted lines represent the limits of standard deviation about the value of 0.82 as it was observed that most data values lie with the range of 0.82 ± 0.07 .

The strength variation of 5052 laminates at most locations, fall within the standard deviation of the unexposed specimens. The modulus of most laminates appears to have decreased to an average value of 0.84 with a standard deviation of 7%. Most laminates therefore experienced a 16% decrease in modulus.

The exception of a particular test batch is those laminates exposed at Irene and Durban and tested after 2½ months of exposure. At other tests periods, laminates exposed at these locations fall within the standard deviation on strength of unexposed samples. Data points for the modulus of laminates exposed at Durban appear to coincide with the value of the standard deviation limits marked on Figure 42, but considering the standard deviation of the individual

test batch itself, it has been assumed that for practical purposes the data points are at least on the standard deviation limit.

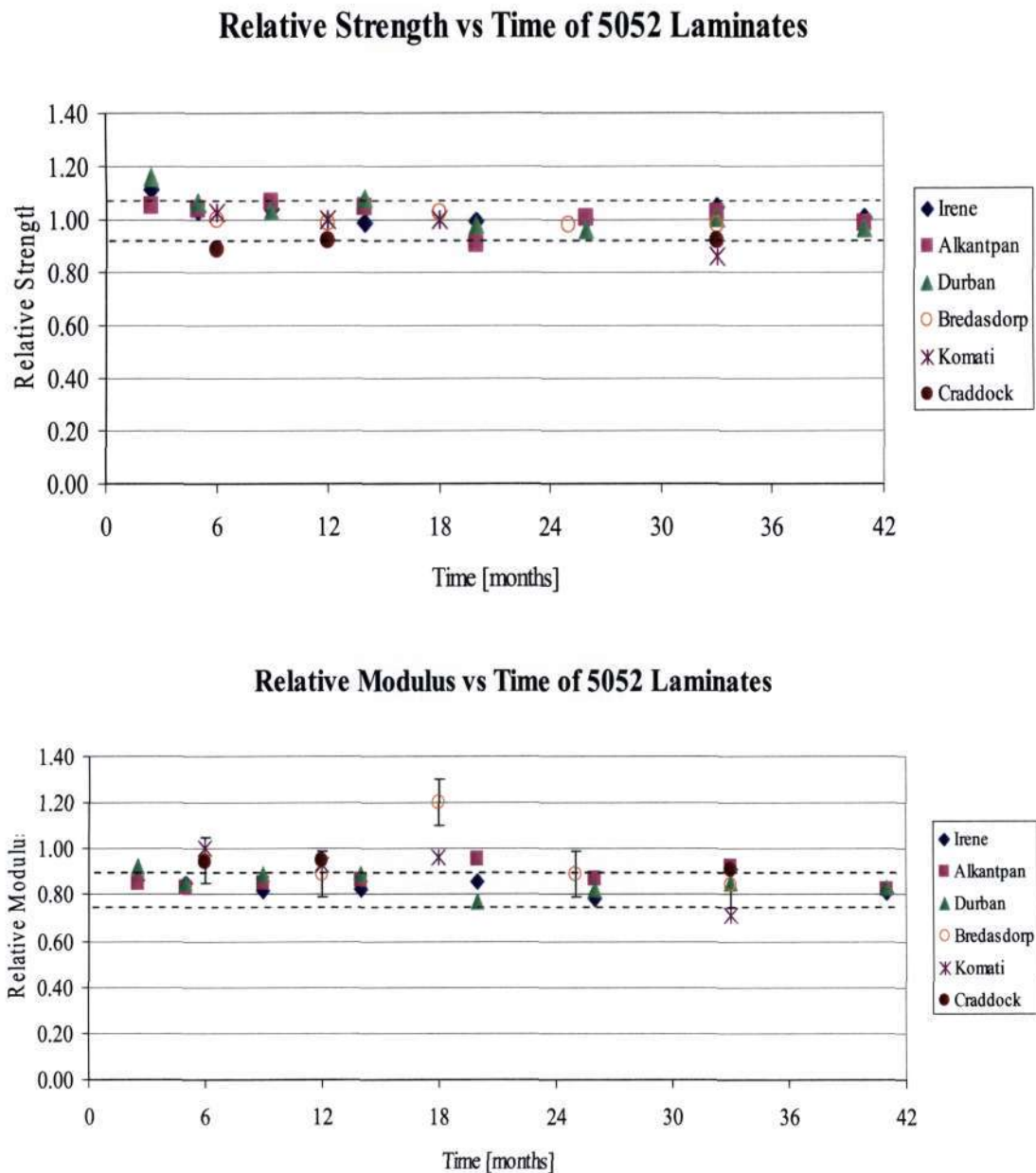


Figure 42 - Change in modulus of 5052 laminates with time

Laminates exposed at Craddock have consistently experienced a strength reduction such that the relative strength values are all below the lower standard deviation. Laminates at this location are therefore of the lowest relative strength in comparison with laminates at the remaining locations. The modulus of the laminates exposed at Craddock is however above the higher

standard deviation of all laminates at all locations. So while the laminates exposed at Cradock are perceived to have lost the most strength, the modulus is least affected by exposure.

The laminates exposed at Komati, though initially experienced negligible strength changes (strength values within the standard deviation), the modulus was found to be above the higher standard deviation. The laminates appear therefore to have experienced no significant changes in strength but a modulus reduction which is lower than laminates exposed at Irene, Alkantpan, Durban and Bredasdorp.

The vinylester laminates were tested and the relative flexural strength data illustrated in Figure 43. The standard deviation on unexposed laminates was approximately 10% of the average and that of the exposed laminates 8% of the average. Vinylester laminates exposed at Alkantpan were preferentially tested as it was observed from strength data that laminates exposed at Alkantpan failed at the lowest flexural load. From test data, laminates exposed at Alkantpan appear to have experienced an increase in strength of 10% while the modulus has decreased by 16% as apparent in Figure 43.

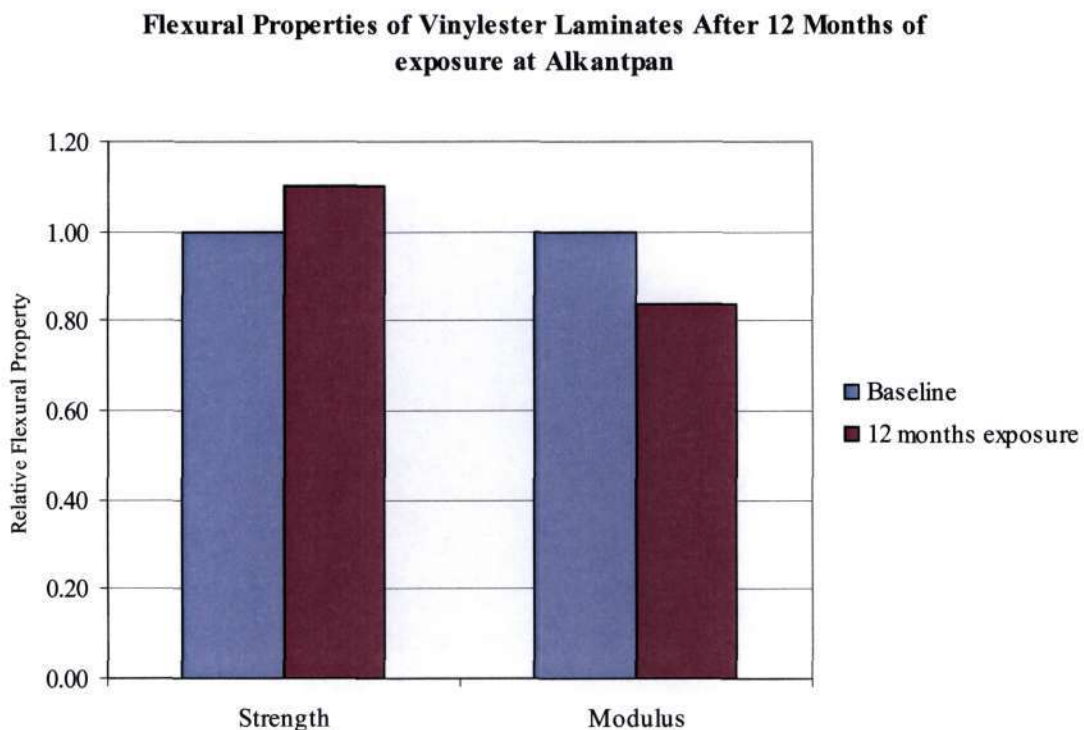


Figure 43 - Flexural properties of vinylester laminates

8.2 Discussion

Startsev *et al* [15] have found that the initial change in properties of glass-fibre reinforced laminates is due to post-curing, established by empirical techniques on exposed laminates, and then damage to the matrix becomes the predominant cause of decrease in mechanical properties. The dynamic shear modulus was one of the parameters that was used to determine the change of mechanical properties due to exposure as these values, from measurement, were found to be consistent across unexposed plates. Startsev *et al* have deduced that the effect of climate changes proceed from the surface only. Dexter [9] also found that the surface was severely damaged due to weathering.

The relationship of fibre-resin ratio on degradation has been studied by Singh *et al* [242] who found that although laminates with a higher fibre-volume ratio had a higher strength when compared to laminates with a low fibre-volume ratio, the degradation in strength was faster in higher fibre-volume ratio laminates. As the 8552 laminates have a higher fibre-volume ratio than 5052 laminates, it was expected that a reduction in strength would be first observed on the 8552 laminates. Examination of the flexural strength results revealed that the 8552 laminates maintained their flexural strength above the baseline strength while statistically the 5052 laminates did not experience a change in strength. As the resin systems, although being epoxy, are different and therefore the data obtained does not agree with the work by Singh [242].

Jones [243] has discussed the problem of flexural strength of multimodulus materials, but on the specimens tested, the test results did not verify the theory. On the glass reinforced epoxy, it seems to be that the laminate is stronger in compression than in tension. From the material datasheet, the flexural modulus is 24% higher than the tensile modulus. If the tensile, compression and flexural modulus were the same, the flexural strength would be a redundant method of measuring Young's modulus. If that is the case, the neutral axis may not lie at the midspan of the beam, thus this complicates the problem. Mujika and Mondragon [244] have determined the relationship between flexural, tensile and compression modulus for carbon fibre composites tested in compression. Such determination requires the measurement of strain on both the tension and compression surface of the laminate loaded in flexure.

The strength and modulus as obtained by flexure tests may not yield straightforward strength and modulus values of multimodulus materials. This may be due to the neutral axis not being located at the centre of the depth of the material. McManus [17] has independently commented that what is measured in traditional flexure tests is the response of some complex structure to some complex loading, not pure material properties. Startsev has used interlayer shear strength

to determine the gradient of properties [14] that occur due to exposure to the environment. This was performed by performing interlayer shear tests at varying depths on 9mm thick samples that had been climatically aged for 10 years.

The degradation of mechanical properties on laminates exposed under sustained loading has not been investigated in this Southern African study. Dexter has observed that there is no significant difference between the strength of stressed and unstressed specimens [9] when loaded to 40% of ultimate baseline strength during exposure. The effect of other forms of environmental damage, e.g. lightning and rain erosion, on strength has not been investigated in this study. Rain erosion is erosion which occurs on polymer components due to high speed travel in rain. Lubin [245] has reported on the relative low resistance of composite materials to rain erosion. Springer *et al* [246] has reported on developments of a mathematical model describing rain erosion on composite materials.

Examining the data, the most noticeable trend of 8552 laminates, is for the strength to increase to a peak, then decrease as appears in the Figure 44. The increase in relative strength above baseline, i.e. greater than a value of one, is most likely due to post-curing of unreacted polymer. This is illustrated by the region 1-2 in Figure 44 being above the relative strength value of one by the quantity α which is a fraction of the strength of the unexposed laminates. The extent of post-curing would depend on ambient temperature, incident irradiation, and polymer system of the matrix, type of hardener used, manufacturing process and parameters of the post-cure. The extent of post-curing, if any, on the 8552 resin system was not determined.

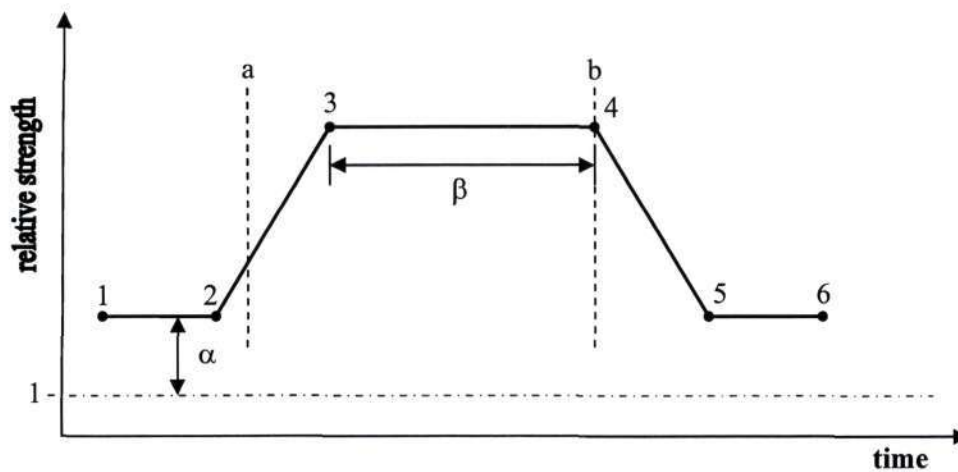


Figure 44 - Characteristics of strength change on 8552 epoxy laminates

A further increase in strength, region 2-3 in Figure 44, may most likely be due to post-curing and loss of material from the surface of the laminate resulting in an increase in flexural strength.

The decrease in thickness decreases the moment of inertia of the laminate which essentially increases the resistance to bending. This is manifested in the test results as an increase in flexural strength although practically this is not so. Hence care needs to be taken when analysing the flexural strength data. However it is expected that post-curing is responsible for a significant contribution to the increase in strength. The increase in modulus observed on the data corroborates this argument. Region 3-4 in Figure 44 is the constant strength region which results after the laminate has reached the maximum absorbed moisture content. At this stage there is no further swelling of the laminate hence the strength remains constant. The duration of this region is depicted by β and is dependent on the seasonal rainfall and humidity at the exposure site. The sooner the seasonal rainfall, the quicker the increase in strength characterised by region 2-3. Hence high moisture environments results in a horizontal shift of the graph in Figure 44 to the left. A region of high humidity will also result in an earlier start to region 2-3. Region 4-5 shows a decrease in strength which is most likely due to significant loss of matrix material from the surface resulting in fibres in the top most layers of the laminate becoming exposed. Region 5-6 is the region of constant strength after the loss of material from the surface. As the rate of resin loss from the surface decreases in comparison to the rate of resin loss in region 4-5, a region of constant stress exist. In conclusion, the extent of post-curing effects the vertical shift of the graph and moisture content of the exposure location affects the horizontal shift of the graph.

From Table 10, a change in modulus of 10% of the baseline modulus (2.6GPa) results in a decrease in strength of 39MPa or 7% of the baseline strength. However this behaviour does not always occur simultaneously as in the case of laminates exposed at Irene and Alkantpan with the modulus change lagging the strength change.

Laminates exposed at Alkantpan and Irene clearly display the behaviour depicted in Figure 44. The increase in relative strength of laminates exposed at Alkantpan can be readily determined from Figure 41 as 13% of the baseline strength. The increase in flexural strength above the baseline value due to post-curing, α , is therefore 13%. Laminates at Irene appear to have started experiencing an increase in strength at an early stage as the initial positive slope, region 2-3, begins after 2½ months of exposure while for laminates exposed at Alkantpan after approximately five months of exposure. The natural environment at Irene had a higher moisture content on average than that at Alkantpan hence the strength changes at Irene occurred sooner thus exhibiting a shift of the curve in Figure 44 to the left until line “a” was above the ordinate. Laminates at Irene therefore reached the maximum absorbed moisture content much sooner than those of Alkantpan. Laminates at both locations displayed a relative strength 44% higher than the baseline strength. After 20 months of exposure, the relative strength began to decrease to 7%

above the baseline strength. The strength was found to remain relatively constant until 33 months of exposure. The increase in modulus of laminates exposed at Alkantpan after 9 months would tend to confirm that post-curing occurred in the laminates and therefore the increase in flexural strength and modulus, by 13%, during the duration. Nine months from the beginning of exposure would set the post-cure period during the summer at Alkantpan. With higher temperatures, post-curing would likely occur. Laminates exposed Irene appear to have completed post-curing after 2½ months of exposure with a 15% increase in strength. The bulk modulus decreases later on during the exposure most likely due to plasticisation of the matrix.

Laminates exposed at Durban and Komati display changes in strength described by Figure 44 to the extent that the curve is shifted to the left until line “b” is at least on the ordinate. This would be expected as both locations experience high humidity and therefore the laminates would reach moisture saturation much sooner than laminates exposed in a dry environment. The shift to the left was so extreme that it is assumed that the laminates post-cured, experienced an apparent increase in flexural strength, and then began to experience a decrease in strength all before 2½ months of exposure had expired. That is to say the laminates would have experienced the strength changes in regions 1-4 during 2½ months of exposure. The post-cure would not have to occur separately but could occur simultaneously with moisture absorption. The change to Figure 44 would be that region 1-2 would not exist but the gradient of line in region 2-3 would increase to reflect apparent rapid increase in strength due to both post-curing and moisture absorption. The strength decay of laminates exposed at both Durban and Komati appear to reach point 5 at least six months before laminates exposed at Irene and Alkantpan, implying that the reduction in strength due to material loss occurred much sooner in these environments. Hence moisture appears to accelerate the reduction in strength. Durban may have experienced the best post-curing due to experiencing higher temperatures on average throughout the year. The modulus decreases as plastisation occurs, to a constant value, then decreases later after 26 months of exposure. Similar modulus changes were observed at Komati, that is, a continued decrease in modulus with increasing time.

The strength of laminates exposed at Bredasdorp at too random to draw any conclusion and does not display any particular trend. Laminates exposed at Cradock appear least affected by the environment. As with strength changes, no trend in modulus can be determined with any confidence at Bredasdorp. The modulus and strength of laminates exposed at Cradock appears unaffected.

From the data examined of laminates exposed at the six test sites, 8552 laminates exposed at Cradock appear to be the least affected with only a 6% increase in strength and no change in

modulus being observed after 12 months of exposure. The weather data characterises the region as being dry and cool for most of the year when compared to the other sites. Visibly at the test site there is little vegetation in the area adjacent to the test site confirming the dry, cool nature of the area. Laminates are therefore not as severely impacted upon by moisture and temperature. The slight increase in strength may be as a result of post-curing that would occur on most laminates exposed outdoors due to naturally occurring UV-radiation.

The initial strength increase of 5052 laminates exposed at Durban and Irene may be as a result of post-curing and moisture absorption resulting in an increase in flexural strength of 11% and 16% respectively. The moisture absorption would result in the decrease in modulus to below the baseline value of one.

The 5052 laminates exposed at Cradock appear to be the most affected by the exposure as these laminates have experienced a 10% reduction in strength. This value falls outside the standard deviation and therefore in all likelihood, the laminates experienced a decrease in strength. The modulus however seems to be unaffected after a year of exposure. Laminates at Komati appear unaffected by the exposure until after 33 months of exposure.

There does not appear to be a direct link between radiation and flexural strength within the natural intensities experienced by the environment. The percentage moisture absorption as the increase in mass due to moisture absorption could not be directly measured due to the negating effect of material loss from the surface resulting in a decrease in mass. Further post curing of resin in the service environment is possible due to incomplete curing reactions after manufacture [234].

9 ACCELERATED ENVIRONMENTAL AGEING

Accelerated environmental testing was conducted with the dual purpose of establishing manifestations of individual degradation factors and determining the extent of degradation caused by these factors. By comparing the data from the accelerated tests to those from the natural exposure tests, the dominant degradation mechanisms may be identified. Similar types of damage observed between natural and accelerated exposure specimens may assist in determining the behaviour of the underlying degradation mechanisms. The accelerated ageing test facility used in this study was built at the University for accelerated ageing of polymeric composites. The specification of the equipment was therefore based on commonly accepted degradation factors in the ranges that are thought to be most detrimental to polymer composites. As the equipment used was not the industry standard, a review of the operational parameters is presented.

9.1 Environmental chamber design

An environmental chamber has been designed and manufactured at the School of Mechanical Engineering, University of KwaZulu-Natal, to accelerate degradation due to moisture, salt spray, ultraviolet radiation (UV) and temperature (25°C - 70°C). Together with the chamber, a specimen mounting rack has been designed to position specimens within the chamber for conditioning. The chamber would allow for the testing of polymeric composites with a view of predicting the long term performance of composites in Southern Africa. Maintenance performed on the environmental chamber is presented in Appendix J.

The chamber was designed to simulate and accelerate the effect of exposure to the natural environment. This required a light source to simulate sunlight, a water spray to simulate rainfall, with an option to change the liquid used in the spray from distilled water to salt water, and a heat source to simulate an elevated temperature environment. The salt water spray was required to simulate the marine environment in which FRP composite components are used. Further, it was required that the design accommodate visual inspections of the specimens without disturbing the accelerated environment. Components used in the manufacture of the chamber to achieve the above were selected based on functional requirements such as ease of maintenance and cost.

The chassis of the chamber was fabricated from angle iron with four castors attached, one at each corner. The castors were required to meet the design requirement that the chamber be able to be easily moved to different locations. The walls of the chamber were fabricated from 3Cr12 sheet metal and enclose a volume of 0.844m³. This material is not the standard stainless steel

but rather stain proof steel. The chamber has visual indicators to indicate a moisture exposure or UV exposure in progress. A toggle switch is located on the front panel that enables the user to toggle between these two modes. Figure 45 is an image of the completed environmental chamber.



Figure 45 - Accelerated environment test chamber

The light source decided upon to simulate the UV component of natural sunlight was UV fluorescent lamps. The lamps selected provide irradiation in the 295nm to 365nm range with a peak emission at 340nm. Emission of the lamps between 295nm and 400nm is 39W/m^2 . Four such lamps were decided upon to deliver the required intensity. The lamps were mounted on the chamber such that the irradiation surface spans the entire width of the chamber. The lamps protrude out the chamber at both the left and right sides where the electrical connections are located. Electrical connections were specifically mounted exterior to the chamber to reduce corrosion of the electrical contacts due to the high moisture environment within the chamber during testing. The interface at which the UV lamps passed through the chamber walls is sealed with the use of glands.

A vapour mist of distilled water, or salt water, is introduced into the chamber by a spray nozzle. The liquid tanks are located adjacent to the chamber below the spray nozzle. A venturi system siphons liquid from the tanks below the spray nozzle by allowing the passage of compressed air through a venturi restriction. Liquid in the tank is thereby drawn into an accelerating flow in the venturi and emerges at the exit of the venturi through a nozzle in the form of a fine spray. The water delivered to the chamber by this system may be controlled by regulating the air pressure at the inlet to the venturi. Air pressure for the chamber is provided by the common workshop

compressed air supply maintained at seven bars. As the flow rate of liquid into the chamber will decrease as the level in the liquid tank decreases, due to the differential pressure resulting from the height of the nozzle above the free surface of the water increasing with decreasing tank level, the level in the tanks need to be maintained constant to maintain a constant humidity in the chamber. Separate reserve tanks are provided for this purpose. These tanks are mounted separately from the chamber and connected by plastic pipe, exiting the tanks at a valve. The piping enters the main chamber spray tank at a regulating valve used to control the flow of liquid, to maintain a constant level in the spray tank. The control valve employed for this purpose is plastic and of the design commonly found in domestic toilet cisterns. This component was found to be a relatively inexpensive way to control the level of fluid in the spray tank.

The controller used is a standard on / off controller with timer employed to regulate temperature at the desired setting and to switch off power to the UV lamps should the input exposure duration expire. The controller therefore also controls and measures duration of UV exposure. For cycles of UV exposure, when the lamps are turned off for a specific period then turned on again, the controller consecutively continues the measure of the exposure duration beginning at the time value the last exposure was stopped. This facilitates recording of exposure durations for specific batches of materials that undergo multiple exposure cycles. A temperature dial is located below the digital time display at which the desired steady state temperature within the chamber may be set to within a range of 25°C - 70°C. The buzzer fitted to the controller beeps indicating that the exposure time has expired and the UV lamps have been turned off.

A mounting rack has been designed and manufactured to secure test specimens within the chamber a set distance parallel to the UV lamps. The mounting rack is fabricated from 316 stainless steel and shown in Figure 46.



Figure 46 - Specimen mounting rack

9.2 Test procedure

The isophthalic polyester laminates protected by gelcoats were exposed in the environmental chamber. Initially laminates were placed in the exposure chamber for UV cycles of eight hours per day, for five days a week. After 800 hours of exposure had expired, laminates were removed, inspected and weighed. These laminates were then replaced and accelerated UV exposure continued until a cumulative duration of 1600 hours of exposure had been performed. Laminates were removed from the chamber for inspection, weighing (to determine change in mass) and mechanical testing. Remaining laminates were left in the chamber and exposure continued until 2500 hours of exposure had passed, after which laminates were removed for the next interval of inspection and testing. Laminates remaining in the environmental chamber, having been subjected to 2500 hours of accelerated UV exposure, were then subjected to alternate cycles of moisture and accelerated UV exposure. This alternate cycling was performed for a duration of 500 hours. Laminates removed after the alternate cycling was complete were therefore exposed in the chamber for a total of 3000 hours with the first 2500 hours being accelerated UV exposure.

A second procedure to accelerate water absorption by the laminates was performed. This entailed immersing laminates in a bath of water for a duration of two months. The laminates were removed after immersion and allowed to dry at room temperature for three weeks before being inspected and tested.

5052 epoxy laminates were also placed in the chamber to facilitate comparison between natural and accelerated exposure. Prior to exposure in the environmental chamber, the specimens were aged at 80°C for 96 hours in a thermofan oven. This was performed in an attempt embrittle and induce cracking in the matrix of the laminate by ageing the laminate at the glass transition temperature.

9.3 Results

9.3.1 Optical changes

A significant colour change was noticed on laminates without UV protection with the colour change from being initially translucent to yellow. The colour change was measured using a spectrophotometer [250] and changes in yellowness determined, Table 11, for gel coated laminates.

Table 11 - Yellowness measurement of gel coated laminates

Gelcoat	Yellowness Index
NUV	57%
MET	14%
ITIN	21%

No visual damage was observed on polyester laminates when viewed under 100× magnification during all stages of exposure.

In an attempt to induce embrittlement, 5052 epoxy laminates were placed in a thermofan oven for a cumulative period of 96 hours with the temperature controlled at 80°C. Exposure at 80°C was performed in 8 hour intervals per day. This procedure was performed to obtain an embrittled matrix by ageing the laminates at the glass transition temperature of the matrix. Visual damage was observed in the region near the voids of the laminate with the damage being in the form of cracks at, or in the vicinity of the voids as appears in Figure 47.



Figure 47 - Cracks visible originating at voids in a 5052 epoxy laminate after ageing for 96 hours at 80°C

9.3.2 Mass change

The percentage mass loss of the glass reinforced polyester specimens [247, 248, 249, 250], shown in Table 12, does not appear to follow a particular trend. The mass data recorded after 2500 hours of exposure are suspected to be incorrect as the data is not consistent by an order of magnitude with the data at remaining test durations and literature. Mass loss data for laminates

exposed to alternate accelerated UV and moisture cycling are tabulated in the last row of Table 12, to facilitate comparison with laminates subjected only to accelerated UV exposure and thereby determine the effect of combined exposure and UV exposure on laminate mass. Laminates protected by gelcoats with no UV stabilizers (NUV laminates) continually appear to lose mass, irrespective of the presence of moisture introduced in the alternate cycling exposure.

Table 12 - Percentage mass loss on GRP laminates with gelcoats

Exposure Duration	NUV	MET	ITIN
800	0.13	0.29	2.18
1600	0.34	0.68	0.43
2500	14.78	21.30	29.50
3000	0.65	0.23	2.01

The mass loss data in Table 12 when plotted in Figure 48, illustrates the relatively large changes in mass of laminates with the ITIN gelcoat when compared to the remaining gel coat laminates. The changes in mass of the ITIN laminates appear to be erratic over the 3000 hour exposure duration. Mass loss of laminates exposed to the alternate accelerated UV and moisture cycles are illustrated on an adjacent set of axis to facilitate visual comparison of the mass loss measured after each type of exposure. Mass loss of the MET laminates increased with increasing accelerated UV exposure duration but decreased by 0.45% after 500 hours of alternate cycling exposure.

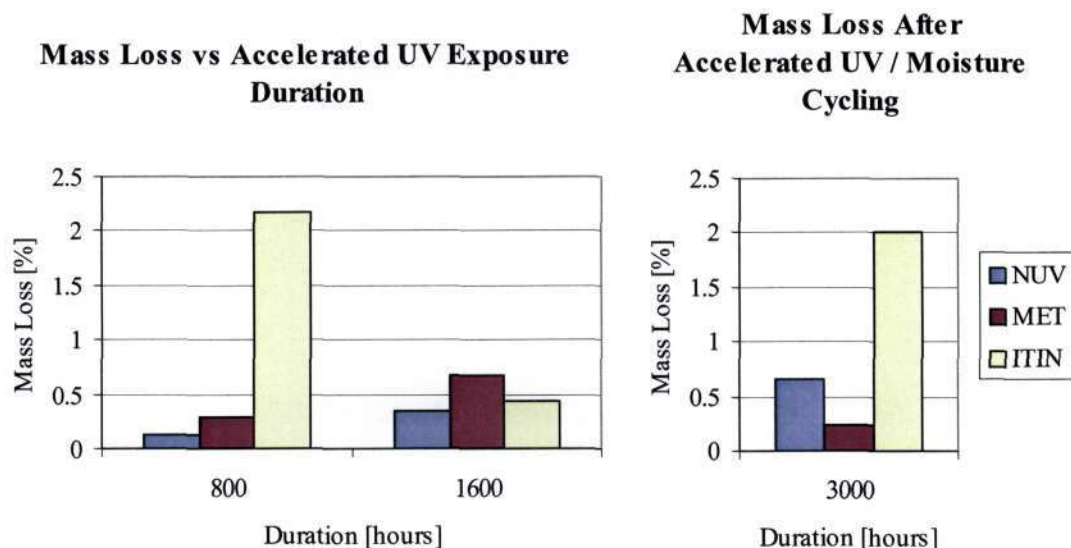


Figure 48 - Mass loss incurred on laminates after accelerated UV exposure and accelerated UV / moisture cycling

The data for the mass loss experienced by specimens after immersion in water [250], illustrated in Figure 49, averages 0.037%. The deviation of the average is 0.004%. Due to the small magnitude of the weight change, 0.037%, the mass loss may be considered negligible. No mass increase, above initial laminate mass, due to moisture absorption was measured.

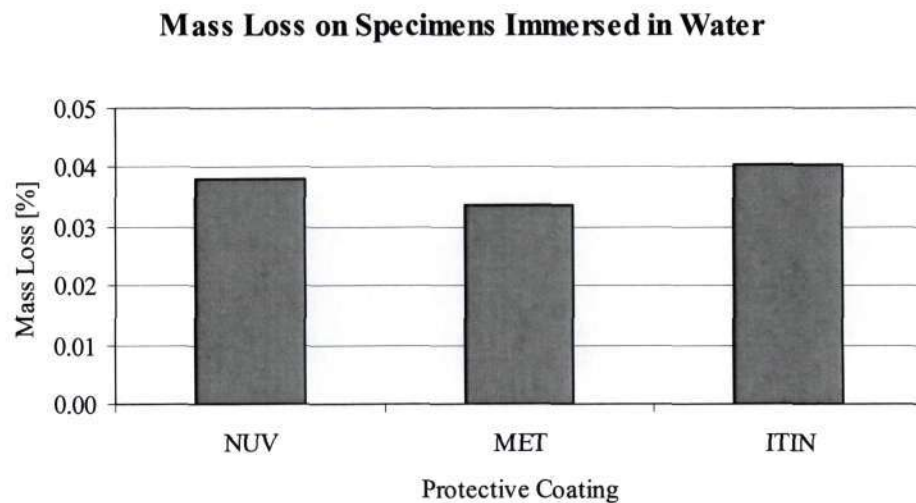


Figure 49 - Mass loss incurred on laminates after water immersion

9.3.3 Strength change

The strength of gel coated laminates were determined by compression tests. Strength of the unexposed laminates were used as baseline values against which subsequent strength measurements, after different stages of exposure, were compared. No mechanical tests were performed after 800 hours of accelerated UV exposure as specimens were removed only for inspection and mass measurement. The strength of NUV laminates appear to be least affected by the accelerated UV exposure, as shown in Figure 50 overleaf, as the strength remains within the standard deviation of the baseline test results throughout the accelerated UV exposure period. The compressive strength of the MET laminates experienced an increase in strength of 19% above the baseline value followed by a decrease in strength of 40%. ITIN laminates similarly experienced an increase in strength of 20% followed by a decrease in strength of 26% of the baseline strength during the accelerated UV exposure period. Laminate strength after alternate exposure has been illustrated on the adjacent axes to facilitate comparison of the effect of alternate exposure and accelerated UV exposure on the strength of laminates. All laminates experienced an increase in strength to above the baseline value after 500 hours of alternate dual cycling exposure had been completed. NUV laminates appear to be have benefited the least with a strength increase of 15% and the ITIN laminates the most with a measured strength increase of 26%.

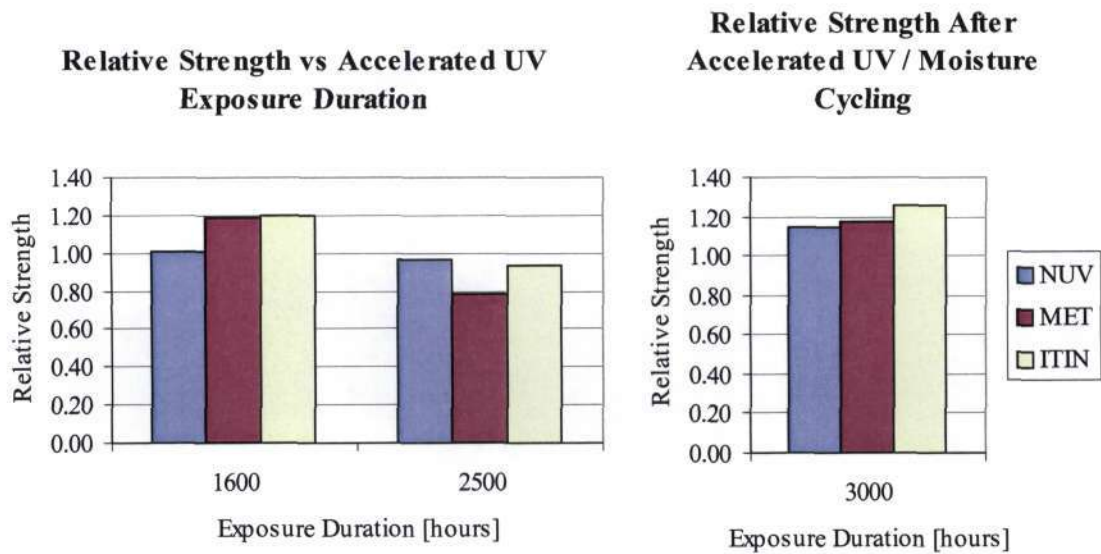


Figure 50 - Relative strength of GRP when subjected to an accelerated UV and moisture environment [250]

The strength of laminates immersed in water, see Figure 51, averages $0.99 \times \sigma / \sigma_0$ with a standard deviation of 6% from the average. The strength of laminates after immersion in water is therefore within the standard deviation of results of unexposed laminates.

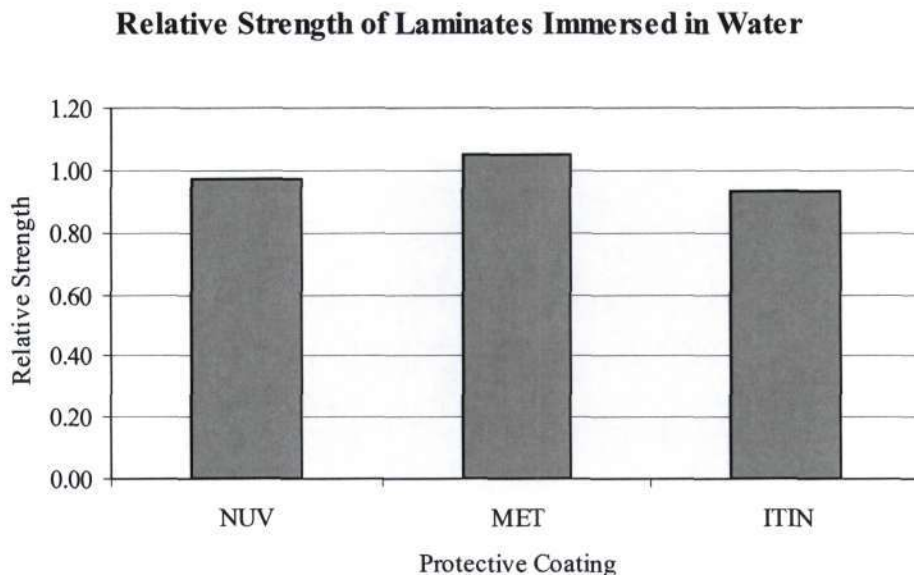


Figure 51 - Relative strength of GRP when measured after immersion in water [250]

Test data of 5052 epoxy laminates subjected to 1617 hours of accelerated UV exposure and 500 hours of alternate accelerated UV and moisture exposure [250] appears in Table 13. Unlike the gel coated laminate strength tests, the 5052 epoxy laminates were tested in 4-point flexure to

facilitate comparison with the natural exposure specimens that have been tested in 4-point flexure. The standard deviation of strength and modulus data was calculated to be 5%. Flexural strength of laminates has remained within the standard deviation of unexposed laminates but the modulus has decreased from the baseline value recorded on unexposed laminates.

Table 13 - Test data of 5052 laminates subjected to accelerated UV and alternate exposure cycles

Parameter measured	Value
Mass loss	15%
Relative Flexural Strength	0.97
Relative Flexural Modulus	0.92

9.4 Discussion

Degradation due to exposure at temperatures above the glass transition temperature, approximately 80°C for most epoxies, was not considered as such temperatures are not commonly encountered in the natural environment. Degradation studies on unreinforced samples of epoxy was not performed as on well compacted composite laminates, large sections of resin are not present as this reduces fibre-volume ratio and hence performance. On composite laminates, resin is present in thin layers. The dynamics of degradation of thin layers of resin differ from the degradation of large layers of resin resulting in thin layers being more prone to damage.

The increase in mass loss with increasing accelerated UV exposure duration may be explained by the emission of volatiles from the laminate. This would be significant on the specimens tested as the specimens were not post-cured and will therefore postcure while in the environmental chamber. The loss of mass after exposure to the alternate UV and moisture cycles was however not expected as it was thought that moisture absorption would increase the mass of the laminates. Strength was observed to decrease with time when subjected to accelerated UV exposure, but then increased when exposed to alternate cycling. Surface stresses caused by exposure to UV may have become relaxed when the laminates were exposed to moisture thus resulting in an overall increase in strength. However significant moisture uptake that would result in an increase in mass to above the unexposed laminate mass was not found on any of the laminates examined.

Laminates immersed in water experienced practically no moisture absorption. The isophthalic laminates are therefore resistant to moisture absorption as expected. Drying of samples after immersion in water may have resulted in diffusion of moisture out of the laminate surface and

into the environment during the three week drying period. Strength did not change significantly with the average strength being 1% lower than that of unexposed laminates. This would also imply that little or no post curing took place in laminates that were immersed in water. Water uptake was more pronounced when laminates were subjected to alternative cycling of accelerated UV and moisture.

The 5052 laminates did not experience a measurable change in strength as the flexural strength was within the standard deviation of unexposed laminates. A decrease in modulus did however occur which would imply that some degradation of mechanical properties has occurred. Matrix failure and fibre buckling were observed on the failed specimens. Ageing at the glass transition temperature may have resulted in embrittlement of the matrix before the laminates were exposed in the environmental chamber. Embrittlement of the matrix may result in a lower modulus. This is in contradiction to the trend that generally strength is more sensitive than modulus.

The yellowness test quantified a change in colour and showed that the gelcoat without UV stabilisers changed colour, of the order of 3 times more, than gelcoats containing stabilisers. However this may not be indicative of damage induced as the strength of laminates not protected by UV stabilisers remained relatively unchanged, i.e. within the standard deviation of unexposed laminates, after 2500 hours of accelerated UV exposure.

Accelerating the effect of pollutants on laminates may be performed by exposing laminates to a higher concentration of pollutants than that found in the environment. Common pollutants found in industrial areas include sulphur dioxide, oxides of nitrogen and carbon, and ozone. White and Turnbull reported that accelerated degradation occurred due to SO_2 , NO_2 or O_3 even in the absence of significant UV intensity [6]. The effect of pollution on additives in the matrix should also be considered. Accelerated degradation due to pollutants has not been performed as part of this study.

10 EMPIRICAL DEGRADATION MODEL

The initial mathematical model has been constructed until a stage requiring experimental test data as verification and input. The model developed was however not used to predict the degradation of mechanical properties of exposed laminates as it was necessary to use a strength criterion which reflects the change in elastic properties. Once this is established, the strength-conductivity dependence may be used. The problem is the accumulated damage itself cannot be used as an indicator of the strength decrease therefore a strength criterion could not be established. As soon as the strength criterion is derived, cross-property connections could be used. However, cross-property connections can instead be utilized as an indicator of the accumulated microcracks. The accumulation of microcracks alone cannot be used as a strength criterion indirectly. An alternative model, (the empirical model), is therefore required to model the degradation in strength.

The empirical model of degradation presented has been proposed to determine the bulk material properties of laminates. During microscopy of wet lay-up laminates without compaction, thick layers of resin, of the order of a thickness of a layer of woven reinforcement, were noticed between the layers of reinforcements. Researchers have made similar observations and calculated the strength of laminates as a composite of layers of woven reinforcement separated by layers of resin as illustrated in Figure 52.

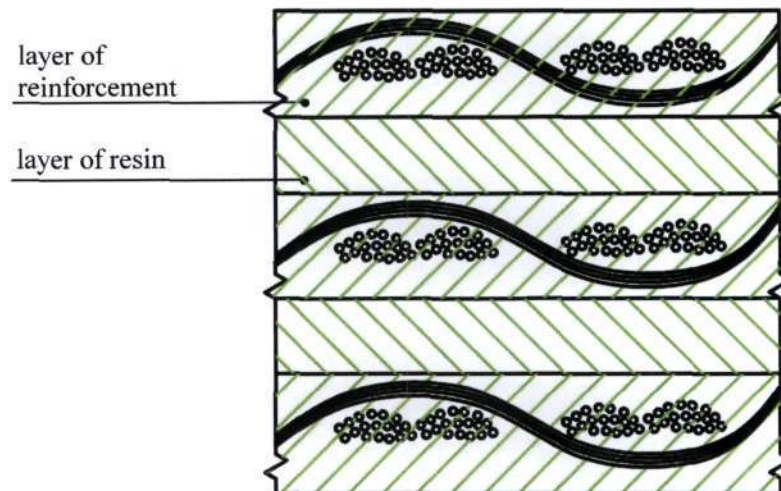


Figure 52 - Alternative model illustrating layers of resin and reinforcement

A single lamina was thus considered as a composite of two layers each containing different properties. The first layer containing the reinforcement is characterised by the properties of a reinforced polymer, while the layer directly below, composed of only resin is characterised by the properties of neat resin. Researchers have found that the strength calculated using the model

described results in improved accuracy of the calculated results when compared to experimental test results.

An alternative degradation model is proposed that considers the degradation as surface phenomena of constant thickness progressing through the laminate. As the cracked damaged layer progresses into the laminate, material is lost from the surface, resulting in a damaged layer of constant thickness. This model is illustrated in Figure 53.

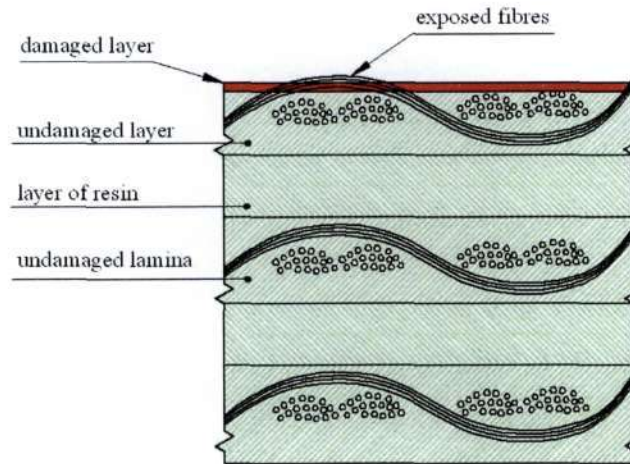


Figure 53 - Alternative degradation model

As damage progresses through the reinforced layer, it is assumed that the fibres in that specific damaged layer do not contribute to the strength of the laminate. Contribution to strength will be only from the remaining undamaged layers. Once the first layer is lost due to weathering, damage will progress to the layer below. Laminate strength may then be calculated based on the strength of remaining undamaged lamina. Compaction during manufacture will result in the reduction in the thickness of resin layers between layers of reinforcement. On laminates with high fibre-volume ratios, the resin layers between layers of reinforcement may be reduced to zero due to effective compaction. This would imply that the fibres are evenly distributed across the depth of the laminate.

Material lost from the surface due to weathering does not contribute to the strength of a damaged laminate, only material present on the laminate contributes to strength. The damaged and undamaged layers co-exist on the laminate with the damaged layer being restricted to the surface of the material as illustrated in Figure 53. The extent of damage in relation to the thickness of the laminate has been established in section 6.3 of this work upon analysis and discussion of observations of damage from Scanning Electron Microscope (SEM) images. The depth of the damaged layer was determined to be less than two orders of magnitude smaller than

the thickness of the laminate. Choi *et al* [18] has considered the problem of surface cracks on the interior of a polymer pipe. As the cracks at the interior of the surface of the pipe were smaller than two orders of magnitude with respect to the wall thickness of the pipe, i.e. plane strain, a 2 dimensional problem of crack growth into the wall of the pipe was considered. The effect of multiple crack paths into the wall of the pipe was modelled based on probability of fracture initiation. The stresses at the degraded layer were determined as a function of a degradation parameter. Using degraded layer thicknesses of 1%, 3% and 5%, in the calculation of stress at the degraded layer, it was observed that the degraded layer thickness used have almost no effect on the stress. It has been concluded that although degradation may result in degradation related stresses, the applied load becomes the dominant factor causing failure.

Following from this work [18], the contribution of the degraded layer to the strength of the laminate has not been considered. The strength of the laminate is therefore only considered to be influenced by the thickness of the undamaged material. The algorithm for the calculation of strength is illustrated in Figure 54 overleaf. The strength calculation is based on the loss of strength due to the reduction in thickness of the undamaged material. Strength values are reduced proportionality to the reduction in thickness of undamaged material.

Increases in strength due to surface phenomena, thought to be due to the relaxation of stresses at the surface that may have occurred during manufacture, are added to the calculated result when a surface layer of resin is present. Upon the loss of the surface layer of resin, the calculated result reflects the strength of the laminate. Increases in flexural strength due to post-curing and probable swelling are accommodated by inclusion of the increase in strength to the calculated result.

The determination of a wet or dry climate, required to decide whether or not to include a moisture factor, was obtained using precipitation and humidity data at the exposure locations. The precipitation and humidity histogram, Figure 14 page 86, was integrated and the result of the two integrations multiplied to obtain a wetness factor. Use of humidity data was required as increasing humidity decreases the loss of moisture from the laminate to the environment. Laminates exposed in a humid climate are therefore less likely to dry out to the extent of laminates exposed in a low humidity climate. A threshold value, below which a climate was classified as dry, was established to be 1×10^6 mm from examination of wetness factors of various test sites. The result of the calculations for the three test sites are presented in Table 14. Units of mm and % were used on precipitation and humidity curves respectively that were integrated. The results of the integrations were multiplied to yield the wetness factors.

Table 14 - Wetness factor calculated for three test sites

Test site	Wetness factor [mm]
Irene	472 590
Alkantpan	812 160
Durban	1 197 120

From the table above, Durban was observed to be the most “wet” of the three locations and above the threshold value of 1×10^6 mm. From strength data analysed, the strength of the laminates exposed in an environment below the threshold value does not appear to be significantly influenced by moisture. The strength of laminates in a dry climate is therefore not modified by a moisture factor.

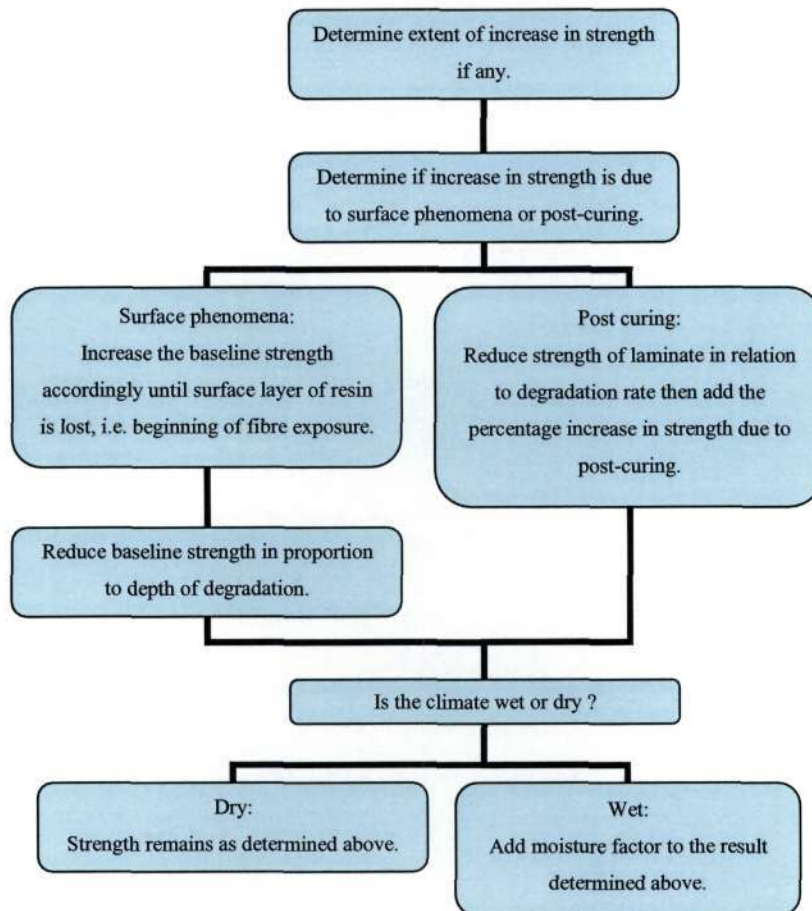


Figure 54 - Algorithm to illustrate calculation of laminate flexural strength

Experimental data are required to select correct parameters for the model described. A determination of rate of resin loss and / or damage, from measurement of damage on exposed laminates, is initially required to predict depth of resin loss and / or damage. Experimental strength data are further required to identify and quantify dominant changes in strength due to

surface phenomena, post-curing and moisture. Quantifying the changes enables the rate of damage of specific degradation modes to be determined and using this information residual strength may be predicted. The specific onset and duration of surface phenomena, moisture effects and post-curing are determined empirically by exposing laminates in the different climates.

10.1 Empirical data

Analysis of empirical data was required to determine parameters characterising surface phenomena, moisture effects and post-curing effects. The empirical data described below has been recalculated from the actual load and displacement data obtained from flexural testing. However the relative strength is calculated using the same specimen geometry for specimens of the same matrix and reinforcement. The calculation of flexural stress therefore is based on the depth of the undamaged specimens. This approach was used to determine the extent of the reduced load carrying capacity of the laminate due to accumulated damage, (physical, chemical and mechanical) in the laminate as ultimately end users of composite components need to know when the load carrying capacity of the structure has been compromised.

Strength of exposed specimens was tabulated as a ratio of the average flexural strength measured after a specific exposure duration against the average flexural strength of unexposed laminates. The stresses were therefore symbolically shown as σ/σ_0 . This method has been adopted to easily illustrate changes in flexural strength with respect to the baseline data. Values greater than one represents an increase in strength, values of approximately one represent negligible changes in strength, and values less than one represent a decrease in strength.

The data presented was only for laminates exposed at Irene, Alkantpan and Durban as either climate or strength data at remaining test sites proved to be similar to those at Irene, Alkantpan and Durban. It was therefore not necessary to include all test sites in evaluating the model.

10.2 Prediction of resin loss / damage

An input to the empirical degradation model is depth of degradation or depth of damage. The depth of damage may be predicted from the observation that damage occurs in stages. The number of degradation stages depends on the resin used and the method of manufacture. An algorithm has been developed to predict the degradation rate of glass-fibre reinforced composites. For a fibre reinforced laminate, constituting of two types of materials, i.e. fibres manufactured of one material and the matrix of another, degradation in properties may be due to either or both materials being damaged and degradation of the interface of the materials. The

algorithm developed does not consider degradation of the fibres as glass-fibres do not appear to incur degradation due to exposure in the natural environment. The algorithm therefore only applies to the case of degradation of the polymer resin and / or the fibre-resin interface. Inputs to the algorithm are degradation rates obtained from experimental testing. The algorithm developed is illustrated in Figure 55 overleaf.

The first step requires knowledge of the primary modes of degradation which may be obtained from examination of laminates exposed in the end-use environment. Once the degradation modes are determined, the calculation proceeds in one of two ways depending on the occurrence of fibre-resin interface damage. Should the fibre-resin interface be intact, degradation will result in the loss of matrix material. This would occur in two stages; hence two degradation rates need to be determined. The first degradation rate is the rate of material loss from the surface. Matrix material will continue to be removed at this rate until a sufficient quantity of fibre has become exposed such that the exposed fibres “protect” the surface layer of the matrix below the fibres. This stage of fibre protection of matrix was found to occur once one-half of the first layer of reinforcement becomes exposed. After this stage degradation, damage will progress at a reduced rate.

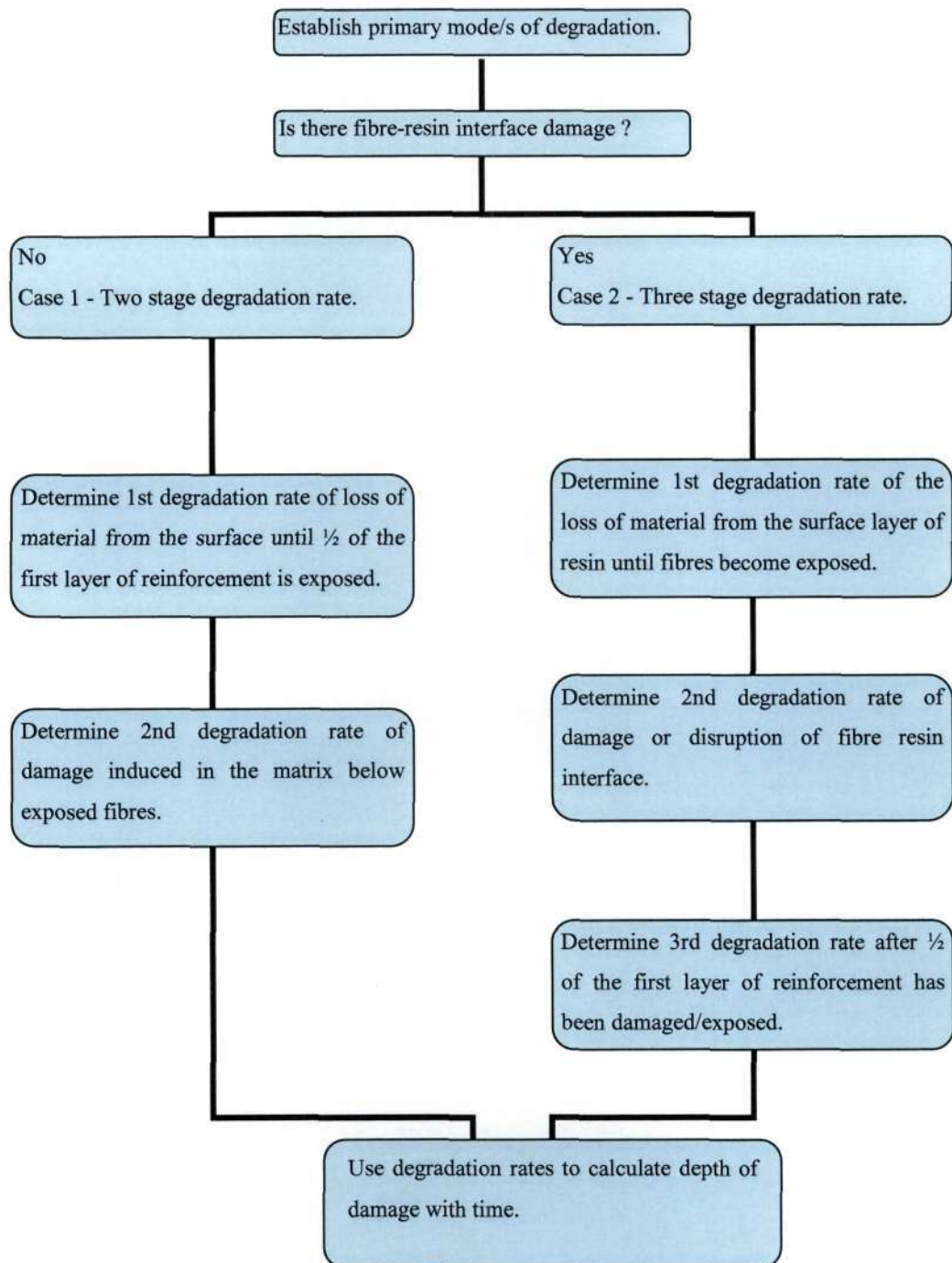


Figure 55 - Flow diagram used to illustrate calculation of depth of resin loss and / or damage

The second case of depth of degradation calculation involves the calculation of three degradation rates corresponding to three states of damage due to damage of both the matrix and fibre-resin interface. The first state of damage, with a corresponding degradation rate, occurs when matrix material is lost from the surface until the fibres in the reinforcement become exposed. The second stage of degradation begins once fibres become exposed. At this stage the damage progression increases as surface cracks rapidly propagate through the upper half of the first layer of reinforcement. If there is a high fibre-volume fraction of a layer of reinforcement,

crack paths through the matrix will be relatively short between fibres. Crack growth resulting in damage of the fibre-resin interface is therefore fairly rapid. The third stage begins when the degradation rate is the slowest when compared to the previous two stages. At this stage, exposed fibres provide “protection” from the environment to the surface of the resin below the fibres, resulting in the slowest degradation rate. Knowing the degradation rates, determined by physical testing, the depth of damage can be predicted. The results of the algorithm implementation, Figure 55, are presented in Table 15.

Table 15 - Prediction of depth of damage of epoxy laminates tested

Time	Case 1	Case 2
	(8552)	(5052)
[months]	[μm]	[μm]
0	0	0
2.5	25	25
5	50	50
9.5	95	122
14	140	194
20	144.2	206
26	148.4	218

The correlation of results of the algorithm with physical observations is evident in Figure 56.

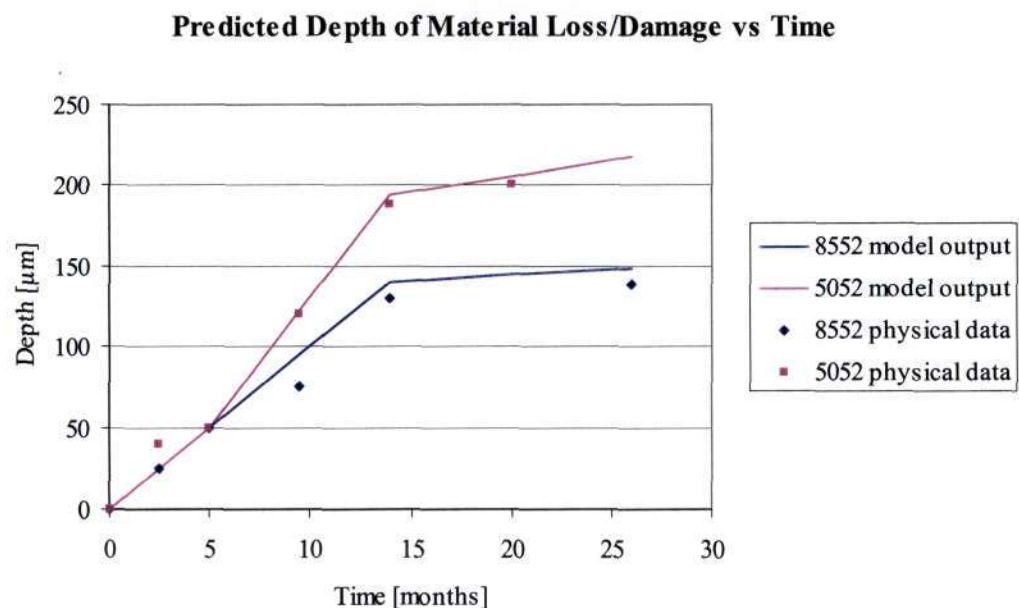


Figure 56 - Predicted material depth loss and / or damage of glass-fibre reinforced epoxy composites

In case 1, two stages degradation was observed on 8552 laminates, degradation is primarily due to loss of matrix material. An observation that has been made is that this case of degradation is independent of compaction of laminates and only dependent on the weathering resistance of the resin. Damage would proceed at a constant speed through the resin rich layer and layers of reinforcements. Protection of the resin from the environment appears to be the only cause of a reduction in material loss and / or damage rate.

Crack resistance of the matrix is accounted for in the determination of degradation rates. A matrix that is more prone to cracking will exhibit a higher damage rate due to faster crack propagation both when protected and unprotected.

The effect of the form of reinforcements is also accounted for by empirical determination of degradation rates. In case 2, found applicable to 5052 laminates, woven fabrics would initially arrest the growth of cracks to a layer of reinforcement. Cracks that progress from the surface through the transverse weave are arrested upon reaching the longitudinal weave of a layer of reinforcement. The arrest of crack growth contributes to the change of degradation rate once half of the first layer of reinforcement is exposed. The effect of fibre orientation therefore influences the rate of damage progression and is hence accounted for. The resistance of different matrices to weathering was noted by observing that the gradient of the depth of material loss and / or damage vs. time curves of 5052 is greater than that for 8552 laminates. The rate of material loss from the surface of both laminates appears to be initially equal but differ once fibres in the first layer of reinforcement become exposed to the environment.

10.3 Strength prediction of epoxy laminates

Knowing the rate of damage progression into the laminate, the strength was predicted based on the loss of contribution to strength of exposed fibres. Exposed fibres are not surrounded by resin hence there is no load transfer between fibres. Further, when laminates were tested in compression, the exposed fibres would not contribute to the stiffness as the loose fibres did buckle in compression due to lack of support. Where the fibres were close to the surface, with a thin layer of degraded material covering the fibres, fracturing of the degraded layer was observed due to buckling of the fibres beneath.

Using load and displacement data from physical bending tests, a “degraded” flexural stress and modulus was calculated using a constant laminate depth (equal to the depth of the unexposed laminate) instead of actual laminate depth measured before testing. Changes in failure loads and

stain therefore translate to flexural stress / modulus which represent the “degradation” of the material. These flexural stresses and moduli are presented in Appendix K.

The predicted laminate strength of 8552 laminates using the algorithm described in Figure 54, page 149, is presented in Appendix L with Figure 57 below illustrating the correlation of the algorithm results with test results (from Appendix K) on laminates exposed at Irene and Alkantpan. Irene and Alkantpan provided a dry climate for exposure of laminates. The increase in strength of approximately 10% of the strength of the laminate after manufacture occurs approximately after the surface layer of resin is lost from the laminate. Loss of a surface layer of resin within 5 months of manufacture may result in relaxation of stresses close to the surface of the laminate resulting in an increase in flexural strength.

The improvement in strength remains only while the first layer of reinforcement remains supported by the matrix. Upon exposure of half the topmost layer of reinforcement, this layer of reinforcement does not contribute to the strength of the laminate. Although approximately half of the fibres remain protected by resin, the fibres that remain protected are exposed to the environment at positions along the length where due to the weave, are above transverse tows and hence closer to the surface. Similarly exposed fibres will at certain positions remain beneath transverse tows and hence remain protected. Therefore all fibres in the upper most layer of reinforcement are exposed to the environment at multiple positions along its length. Exposure of fibres on the upper most layer of reinforcement therefore does not contribute to laminate strength in flexure.

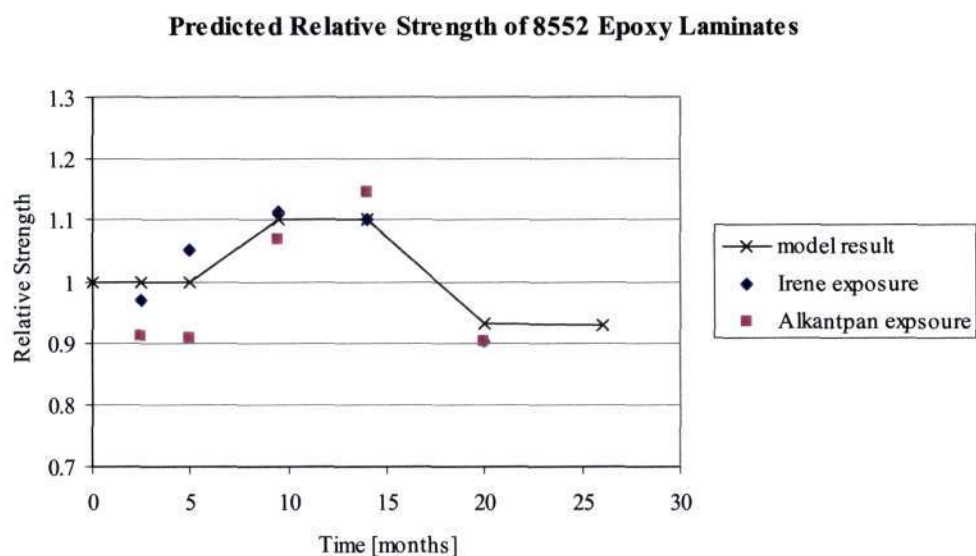


Figure 57 - Prediction of laminate flexural strength based on Case 1 degradation behaviour

The model implements this change in strength in two steps. First, the increase in strength is reduced to zero as the effect of the stress relaxation at the surface only applies once the fibres remain surrounded with the polymer matrix. The unexposed laminate strength at this stage, baseline strength, is further reduced proportionally to reflect the loss of contribution of one layer of reinforcement to the overall strength. On a nine layer laminate, this would imply a strength reduction of $1/9$ or 11% of the baseline strength. The continual decrease in strength, at a slower rate due to the degradation rate decreasing, results in a gradual decrease of strength with time. Experimental data from two test sites follow the trend of the changes in strength as predicted by the model and illustrated in Figure 57.

Prediction of the 5052 laminate flexural strength using the algorithm described in Figure 54, page 149, is presented in Appendix L. Figure 58 illustrates correlation of the algorithm results with test results on exposed laminates at Irene and Alkantpan.

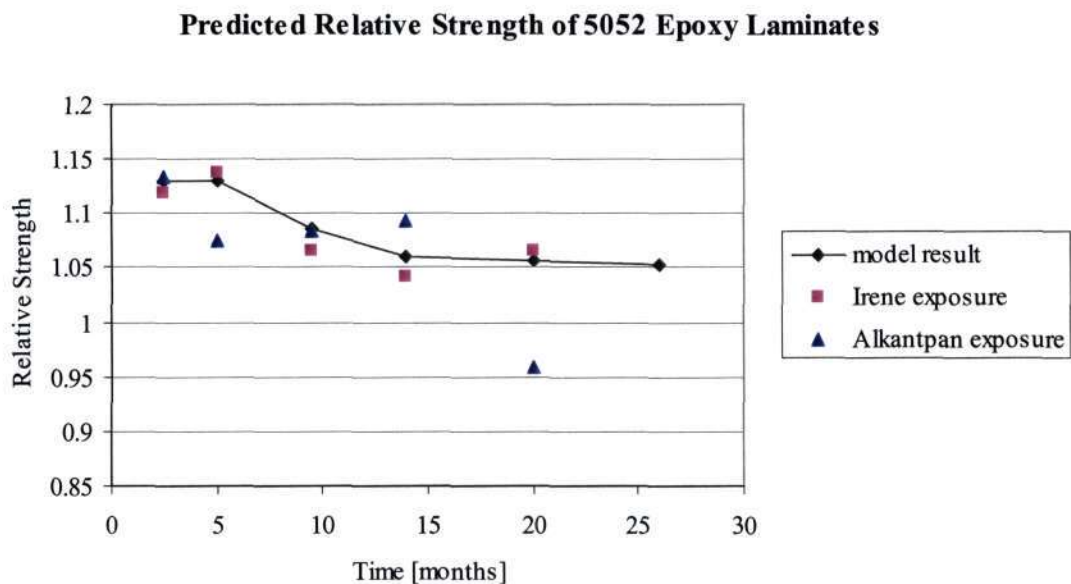


Figure 58 - Prediction of laminate flexural strength based on Case 2 degradation behaviour

The initial increase in strength is thought to be due to post-curing as can be expected of wet lay-up systems. Post-curing of the 5052 laminates resulted in approximately 13% improvement in strength. The model output was calculated by increasing the baseline strength by 13% reflecting an increase in strength. After 5 months of exposure, as fibres at the surface became increasingly exposed, the damage propagation rate increased reflecting the increase in propagation of damage into the laminate. The flexural strength proportionately decreased in relation to the increase in rate of damage. After 14 months of exposure, once the damage propagation rate

decreased, the rate of decrease of flexural strength reduced proportionately. Correlation of experimental test data of laminates exposed at two test sites is illustrated in Figure 58.

The model begins with baseline data determined by tests on unexposed laminates. Change of strength due to matrix loss and / or damage results in the strength decreasing proportionately. Post-curing results in an increase in strength of the laminate, hence the percentage increase in strength due to post-curing is added to the model output which bases degradation calculation on baseline data. Post-curing effects are therefore added to the model output at each calculation period and therefore accounts for the permanent increase in strength due to post-curing as observed during the initial stages of exposure.

The epoxy laminates exposed at Durban did not correlate with the output of the model for dry climates. Examination of the data shows that the 8552 laminates exposed at Durban did experience an increase in strength overall of approximately 15%. The increase in strength may be due to swelling of the laminate causing the cross-section area of laminate to increase thereby resulting in failure of laminates at higher loads. A moisture factor of 0.15, determined empirically, was added to the result of the material loss and / or damage calculation to produce the final result of flexural strength due to exposure. Upon use of the wet climate case in the model to incorporate the increase in strength, a closer correlation was achieved as illustrated in Figure 59.

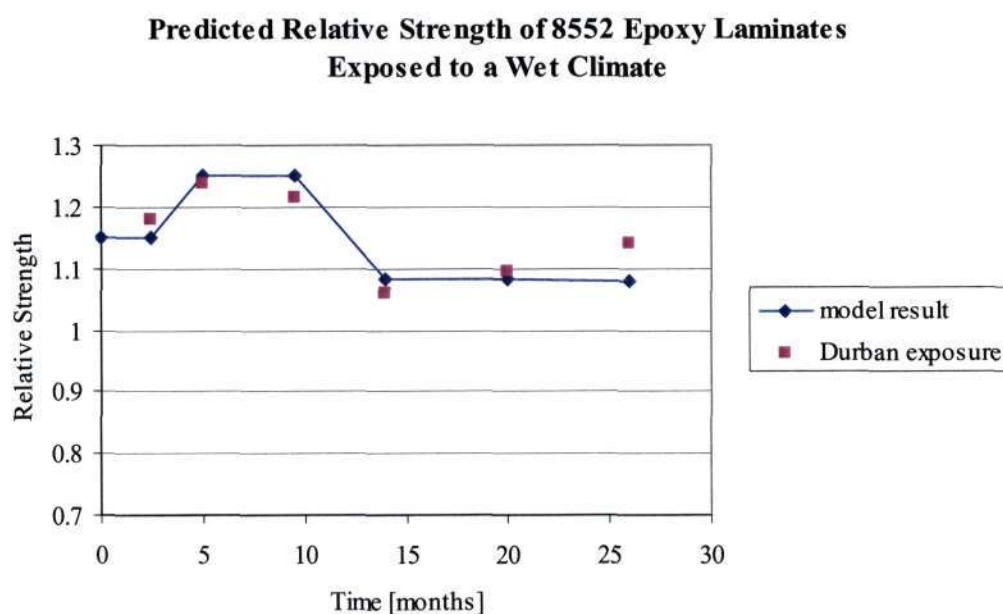


Figure 59 - Predicted strength of 8552 laminates exposed in a wet climate

The strength of the laminate increases then decreases similar to the trend observed in exposure to a dry climate. The same damage mechanisms apply in the wet climate with only addition being incorporation of a moisture factor, throughout the exposure, to account for strength changes due to moisture damage.

The model result for the 5052 laminates exposed at Durban accounts for post-curing and the increase in flexural strength due to moisture effects. A swelling factor of 0.08 was used in the strength calculation. The correlation of model output with experimental data is illustrated in Figure 60.

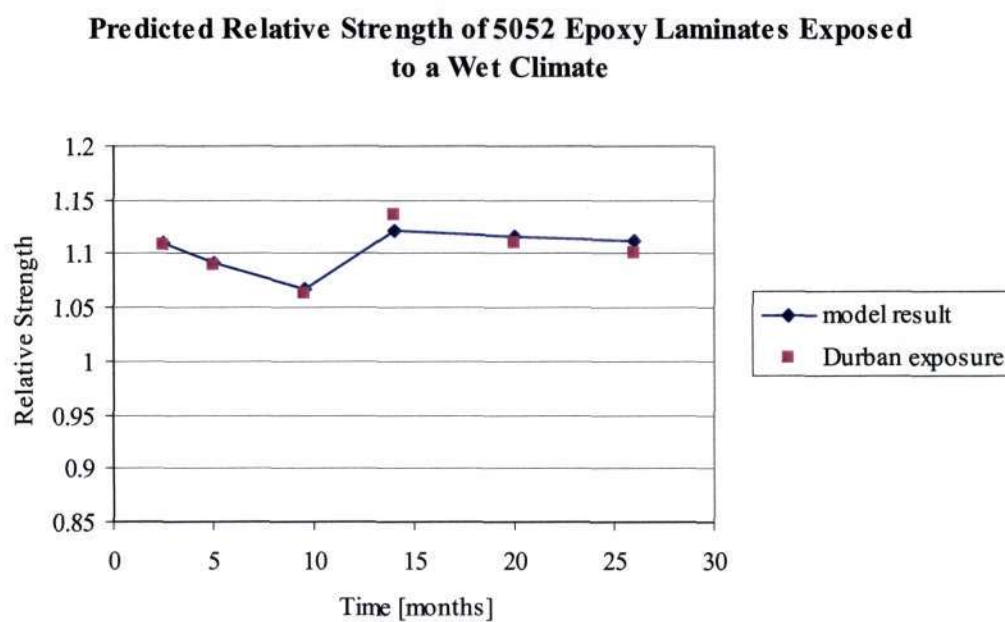


Figure 60 - Predicted strength of 5052 laminates exposed in a wet climate

Figure 60 shows the decreasing strength of the laminate with time with the exception of the strength increase after 14 months of exposure. The moisture factor was applied to damage calculations after 14 months of exposure had expired as it was after this exposure period that the laminates were exposed to a complete rainy season. The increase in strength experienced may be due to swelling of the laminate resulting in the cross-section of specimens increasing in thickness thereby resulting in higher failure loads. The strength of the laminate continued to decrease during the following season.

10.4 Discussion

Degradation models available in the literature based on physical process of moisture diffusion and heat conduction have been found to describe the response of laminates to exposure in

controlled environmental conditions. With regard to moisture diffusion, Springer has reported on various tests describing the effect of moisture on laminates. Both Fickian and non-Fickian diffusion was found to apply. Similarly, data has been obtained from tests that display correlation to the Arrhenius law. The most comprehensive model published [17] using a mechanism based approach coupling all degradation effects remains incomplete.

The results from the alternative degradation model have only been calculated for an exposure duration of 26 months. After this period, the laminate does not conform to original design specifications due to the loss of contribution to strength of an entire layer of reinforcement as well as significant damage to the matrix at the exposed surface. At this exposure duration, depth of damage has progressed until the first layer of reinforcement and the model results have shown good correlation with the experimental test results. Strength was predicted for laminates exposed at Irene, Alkantpan and Durban as either climate or strength data proved to be similar to these three test sites.

A “degraded” flexural stress and modulus was calculated using four point bending stress data and constant laminate depth, equal to the depth of the unexposed laminate, instead of actual laminate depth measured before testing. Changes in failure loads and strain therefore translate to flexural stress / modulus which represent the “degradation” of the material with time. The output of the model therefore represents the change in flexural properties in comparison to an unexposed laminate.

Degradation of epoxy laminates in a dry climate appears to be predominantly affected by loss of resin from the surface and cracks in the matrix resulting in disruption of the fibre-matrix interface. The extent of the cracking is dependent on the grade and type of resin used. Initial increase in strength is thought to be due to either surface effects or post-curing and the subsequent decrease in strength due to the damage incurred in the laminate.

The moisture factors obtained empirically, 0.15 for the 8552 laminates and 0.08 for the 5052 laminates, may imply that the strength of the 8552 laminates are affected by moisture in the environment to a greater extent than the 5052 laminates. The diffusion of moisture into composite laminates has been observed to obey Fickian diffusion in many cases [31]. However moisture diffusion is dependent on the condition of the surface of the laminate. On laminates exposed to the natural environment, material from the surface is continually lost due to weathering, therefore measurement of diffusion coefficients becomes difficult.

The 8552 laminates appear to be affected by moisture after the first few months of exposure, therefore laminates exposed at Durban, a wet climate, experienced the highest initial increase in strength. The increase in strength may be due to the swelling of the laminate, due to moisture absorption, which would result in an increase in the flexural strength measured. 8552 laminates exposed in dry climates did not experience as large an increase in flexural strength. The moisture factor determined for 8552 laminates appeared to be constant throughout the duration of exposure. In contrast, the 5052 laminates appear to be affected by moisture after a complete rainy season had passed. This phenomenon may be observed in Figure 60, page 158, where the strength of these laminates decrease between 2.5 months and 9.5 months of exposure, then increases between 9.5 and 14 months of exposure, the period of the rainy season. As before, the increase in strength due to moisture is thought to be due to the swelling of laminates resulting in an increase in the flexural strength measured. The moisture factor determined after the completion of the rainy season seems to be constant throughout the following season. The change in strength of 8552 laminates due to moisture appears to have occurred during the first few months of exposure while the 5052 laminates appear to have experienced a change in strength due to moisture only after a rainy season had passed.

11 CONCLUSION

Natural weathering of polymer composites is a result of complex chemical and physical mechanisms acting simultaneously. Due to the lack of published data on the degradation of glass-fibre reinforced composites used outdoors in Southern Africa, atmospheric environmental exposure tests have been initiated. Examination and testing of exposed laminates were required to develop and verify a model describing the degradation of mechanical properties. Epoxy, vinylester and polyester laminates have been exposed at six test sites chosen to represent the range of climates in the region that may be most detrimental to polymer composites. Exposed laminates were secured onto latitude racks and therefore experience maximum solar irradiation at a test location. Inspection and testing of the laminates occurs biannually to determine the predominant modes and rate of damage of the exposed laminates. The environmental degradation of laminates while under sustained loading was not examined as previous research [9] has shown that the effect of sustained loading on degradation to be negligible.

The mathematical model developed for modelling the degradation of laminates utilised a functionally graded material approach wherein degradation was due to the development of cracks and matrix embrittlement at the surface, and the propagation of these cracks into the interior of the laminate. The model required a strength criterion from empirical testing as input. However, due to the thin cracked layer being more than two orders of magnitude smaller than the thickness of the laminate, a strength criterion could not be practically established. The perceived process of degradation and damage accumulation had to be revisited, as based on damage observed on exposed laminates; the damaged cracked layer appeared to be of constant thickness progressing through the depth of the laminate. Material removal from the surface of the damaged layer resulted in fibres becoming exposed to the environment.

As epoxy laminates have been exposed for the longest duration, most data recorded is applicable to the epoxy laminates tested. Degradation modes responsible for the reduction in strength were found to be, amongst other environmental and chemical factors, dependent on the materials being tested and method of manufacture. No damage was observed on glass fibres and, the rate and extent of damage, appears to be strongly dependent on the chemistry of the resin, even within the same type of resin groups, e.g. epoxy, vinylester and polyester. The fibre-resin interface adhesion as well, responsible for load transfer between fibres, depends on the chemical coupling between the matrix and fibre. Poor fibre-resin interface adhesion allows for crack propagation along the interface thus accelerating damage incurred on the laminate. The dynamics of the chemical processes of the constituent materials therefore was found to strongly influence degradation of the exposed laminates.

Colour change and loss of material were the most visible changes of a laminate response to exposure to the environment. With the exposed surface viewed at higher magnification, greater than 100 \times , cracks were observed on the surface. It has been observed that both the colour change and cracks are dependent on ultraviolet exposure. However due to the cracked layer being significantly thin, when compared to the thickness of the laminate, the effect of the cracked layer on strength has been found to be negligible [18]. Hence there does not appear to be a dominant, direct effect of naturally occurring ultraviolet exposure on damage induced in the laminate. The loss of the material from the surface could not be quantified by mass, as the competing effect of moisture absorption results in a simultaneous increase in mass. The change in mass is therefore a complex relation between mass of material lost from the surface and mass gained due to moisture absorption.

On the 8552 epoxy laminates, loss of matrix from the surface was predominantly responsible for the change in strength. Two stages of degradation occurred, the initial degradation rate being the highest due to removal of material from the surface followed by a reduced degradation rate due to protection of the damaged surface by exposed fibres on the surface of the laminate. On the 5052 laminates, three stages of degradation occurred. The first stage of degradation was due to the loss of material from the surface. The second stage of degradation, with the highest damage rate, was due to the progression of cracks into a layer of reinforcement. As a consequence of the crack propagation into the layer of reinforcement, fibre debonding resulted. The third stage of degradation, with the slowest rate of damage, was due to protection of the damaged surface by exposed fibres on the surface of the laminate. These rates of degradation were empirically determined.

Flexural tests were chosen to determine the bulk material properties of the exposed laminates as these tests provided the most accurate and repeatable results using available equipment. Test results have shown increases in strength followed by a decrease. The increase in strength of the 8552 laminates is thought to be due to the relaxation of surface stresses due to manufacturing, whereas 5052 laminates experienced an increase in strength due to probable post-curing of unreacted polymer. The decrease in strength of laminates may have been due to loss of the contribution to the overall strength of the upper layer of exposed reinforcement. Swelling of laminates during exposure was not quantified due to variations of the moisture diffusion coefficient which is dependent on the surface of the laminate. From accelerated testing of laminates, changes in strength were found to be independent of the colour change that had occurred on the surface of laminates.

From observations of exposed specimens an empirical model was developed based on the depth of remaining physically undamaged material. Further, the empirical model included climatic effects which result in post-curing and plasticisation of the physically undamaged material below the surface. The depth of damage, which includes resin loss, was empirically determined and this data was used to calculate the strength of the laminate at each time step. The damaged layer included the cracked layer as well as other manifestations of damage including but not limited to disruption of the fibre-matrix interface. Experimental data correlated with the trend of strength reduction with time as predicted using the model. This model, like most polymer composite degradation models, predicts strength changes of specific materials exposed at specific locations.

Additional tasks that are required as a continuation of this work include further refinement of the mounting procedure of specimens required for Scanning Electron Microscopy. As the exposure duration of presently exposed laminates increase with time, data obtained from the examination and testing of vinylester and polyester laminates are required to establish the modes and rate of degradation on these laminates. Presently no data have been accumulated from tests on polyester laminates.

A different approach to the acceleration of degradation of polymer composites has been considered. As 49% of the energy of the sun which is perceived as heat occurs in the infrared segment of the radiation spectrum [251], heating of test specimens using infrared lamps is proposed. This method would more accurately simulate the coupled effect of heat and oxidation acting on the surface of the laminate due to exposure to the sun. The effect of heat and UV may be simulated by the combined use of infrared and UV lamps in an environmental chamber. No such test has been reported in the literature reviewed and therefore this presents a possible new method of accelerating the degradation of polymer composites with a view to increasing understanding of damage initiation and progression.

12 REFERENCES

- 1 Jacques LFE; Accelerated and outdoor/natural exposure testing of coatings; Progress in Polymer Science, vol. 25, issue 9, November 2000; pg 1337-1362.
- 2 White JR and Turnbull A; Weathering of Polymers: Mechanisms of degradation and stabilization, testing strategies and modelling; Journal of Material Science vol. 29 (1994); pg 584-613.
- 3 Environmental Degradation of Composite Materials (Hystou 8), A collaborative research project between KENTRON, and the Centre of Composite Materials and Structures, University of Natal; Final report January 2002; pp 169.
- 4 Williams JG; Opportunities for composites in the offshore oil industry; Proceedings on the use of composite materials in load-bearing marine structures vol. 2; National Research Council, Arlington, Virginia, September 25-26 (1990); pg 41-65.
- 5 Tamarelle PJC and Sparks CP; Proceedings of nineteenth annual offshore technology conference, Houston, TX; May 1987 (Richardson, TX: Offshore Technology Conference); pp 255.
- 6 Juska T; Effect of water immersion on the matrix/matrix adhesion in thermoplastic composites; Journal of Thermoplastic Composite Materials, vol. 6 (1993); pg 256-274.
- 7 Howarth JT; What designers and processors should know about flame retardant additives; Plastic World, March, 1973; as appears in reference 3.
- 8 Morton J, Kellas S, and Bishop SM; Damage characteristics in drilled carbon fiber composites subjected to fatigue loading - environmental effects; Journal of Composite Materials vol. 22, 1988.
- 9 Dexter HB; Long-term Environmental Effects and Flight Service Evaluation of Composite Materials; NASA Technical Memorandum 89067, January 1987; pp 189.
- 10 Komorowski JP; Hygrothermal effects in continuous fibre reinforced composites Part III; National Research Council Canada, (1983).
- 11 Yoosefinejad A and Hogg PJ; Durability of Fibre Reinforced Composite Materials After Twenty Years of Exposure to Weathering; Proceedings of ICCM 11, vol. V; Gold Coast, Queensland, Australia, July 1997; pg 493-498.
- 12 Fukuda H; Five years outdoor exposure of advanced composite materials; Proceedings of the International Colloquium held in Brussels, Belgium, August 1990; pg 428-436.
- 13 Stratsev OV and Krotov AS; Structural heterogeneity and the physical properties of climatic aged polymeric composite materials; http://iem.phys.dcn-asu.ru/labs/LPP/LPP_Site/english/public/collect/bord2.pdf; February 2004.

- 14 Startsev OV, Krotov AS and Startseva LT; Interlayer shear strength of polymer composite materials during long term climatic ageing; *Polymer Degradation and Stability* vol. 63 (1999); pg 183-186.
- 15 Startsev OV, Krotov AS and Golub PD; Effect of climatic and radiation ageing on properties of glass fiber reinforced epoxy laminates; *Polymer Degradation and Stability* vol. 63 (1999); pg 353-358.
- 16 Dubois C, Monney L, Bonnet N and Chambaudet A; Degradation of an epoxy-glass-fibre laminate under photo-oxidation/leaching complementary constraints; *Composites Part A: Applied Science and Manufacturing* vol.30 (1999); pg 361-368.
- 17 McManus HL, Foch BJ and Cunningham RA; Mechanism-based modelling of long-term degradation; *Journal of Composites Technology and Research* vol. 22, no. 3 (2000); pg 146-152.
- 18 Choi B, Zhou Z, Chudnovsky A, Stivala SS, Sehanobish K and Bosnyak CP; Fracture initiation associated with chemical degradation: observation and modelling; *International Journal of Solids and Structures* (2004), article in press.
- 19 So P and Broutman LJ; The effect of surface embrittlement on the mechanical behavior of rubber-modified polymers; *Polymer Engineering and Science* vol. 22 (1982); pg 888.
- 20 So P and Broutman LJ; The fracture behavior of surface embrittled polymers; *Polymer Engineering and Science* vol. 26 (1986); pg 1173.
- 21 Wolkowicz MD and Gaggar SK; Effect of thermal aging on impact strength acrylonitrile-butadiene-styrene (ABS) terpolymer; *Polymer Engineering and Science* vol. 21 (1981); pg 571.
- 22 Schoolenberg GE; A fracture mechanics approach to the effects of UV-degradation on polypropylene; *J. Mater. Sci.* vol. 23 (1988); pg 1580.
- 23 Schoolenberg GE; A study of ultraviolet degradation Embrittlement of polypropylene polymer; Doctoral thesis, University of Delft (1988).
- 24 Schoolenberg GE and Vink P; Ultra-violet degradation of polypropylene: 1. Degradation profile and thickness of the embrittled surface layer, *Polymer* vol. 32, (1991); pg 432.
- 25 Karpukhin ON; *Int. J. Polym. Mater* vol. 13 (1990); pg 17.
- 26 Schoolenberg GE and Meijer HDF; Ultra-violet degradation of polypropylene: 2. Residual strength and failure mode in relation to the degraded surface layer; *Polymer* vol. 32 (1991); pg 438.
- 27 Magnus R; *Kunststoffe German Plastics* 81 (12) (1991) 19; translation of *Kunststoffe* 81 (1991); pg 113.

- 28 O'Donnell B, Qayyum MM, Tong LI and White JR; *Plast. Rubb. Compos.; Procs. Appl.*; as appears in reference 2.
- 29 Qayyum MM and White JR; Effect of stabilizers on failure mechanisms in weathered polypropylene; *Polym. Degrad. Stab.* vol. 41 (1993); pg 163.
- 30 Osawa Z, Wu S and Konoma F; Properties and chemiluminescence of polypropylene stored for a long period; *Polymer Degradation Stability* vol. 22 (1988); pg 97.
- 31 *Environmental Effects on Composite Materials* vol 3; edited by G.S. Springer; Technomic publishing co. inc. (1988).
- 32 *Engineered Materials Handbook*, vol. 1 Composites; ASM International (1987); pg 825.
- 33 Gilchrist A and Mills NJ; Fast fracture of rubber-toughened thermoplastics used for the shells of motorcycle helmets; *Journal of Material Science* vol. 22 (1987); pg 2397.
- 34 Liao K and Tan YM; Influence of moisture-induced stress on in situ fibre strength degradation of unidirectional polymer composite; *Composites Part B*, (2001); pg 365-370.
- 35 Wiederhom SM and Bolz LH; Stress corrosion and static fatigue of glass; *Journal of American Ceramic Society*, vol. 53, no. 10 (1970); pg 543-548.
- 36 Gupta P; Glass fibres for composite materials, in fibre reinforcements for composite materials; Elsevier: Amsterdam (1988); pg 19-71.
- 37 Liao K, Schultheisz CR, Hunston DL and Brinson LC; Long-term durability of reinforced-reinforced polymer-matrix composite materials for infrastructure applications: A review; *Journal of Advanced Materials*, vol. 30, no. 4 (1998); pg 3-40.
- 38 Liao K, Schultheisz CR and Hunston DL; Effects of environmental aging on the properties of pultruded GFRP; *Composites: Part B*, vol. 30 (1999); pg 485-493.
- 39 Douglas Aircraft Company; Carbon epoxy prepreg-impact resistance, DMS 2224 (1989).
- 40 Choi HS, Ha JM, and Ahn KJ; Mechanical behaviour of unidirectional carbon epoxy/epoxy laminate with moisture absorption; *Proceedings of Korean Society for Composite Materials*, Choong Nam National University, Taejon, Korea, May 1995; pg 101-108.
- 41 Choi HS and Ahn KJ; Thermo-micro mechanical behaviour of unidirectional composites under uniform temperature change; *Journal of the Korean Society for Composite Materials*, vol. 8, no. 4, (1995); pg 11-25.
- 42 Bunsell R; Long-term degradation of polymer-matrix composites; *Concise Encyclopedia of Composite Materials*, 2nd edition; Pergamon, New York, 1994.
- 43 Belani JG and Broutman LJ; Moisture induced resistivity changes in graphite-reinforced plastics; *Composites*, October 1978; pg 273-277.

- 44 Choi HS, Ahn KJ, Nam JD and Chun HJ; Hygroscopic aspects of epoxy/carbon fibre composite laminates in aircraft environments; *Composites Part A*, vol. 32 (2001); pg 709-720.
- 45 Apicella A, Nicolais L and Cataldis C; Characterization of the morphological fine structure of commercial thermosetting resins through hygrothermal experiments; *Advances in Polymer Science*, vol. 66 (1985); pg 189-207.
- 46 Apicella A, Nicolais L, Astarita G and Drioli E; Effect of thermal history on water absorption, elastic properties and the glass transition of epoxy resins; *Polymer* vol. 20 (1979); pg 1143-1148.
- 47 Leie AK, Hirve MM, Badiger MV and Mashelkar RA; Predictions of bound water content in poly-isopropylacrylamide gel; *Macro-molecules* vol. 30 (1997); pg 157-159.
- 48 Apicella A and Nicolais L; Effect of water on the properties of epoxy matrix and composite; *Advances in Polymer Science*, vol. 72 (1985); pg 69-77.
- 49 Shen CH and Springer GS; Effects of moisture and temperature on the tensile strength of composites; *Environmental Effects on Composites Materials*, vol. 1, ed. Springer GS, Technomic Publishing Co., Wesport, CT (1981); pg 79.
- 50 Russell AJ and Street KN; Moisture and temperature effects of mixed-mode delamination fracture of unidirectional graphite epoxy; *Delamination and Debonding of Materials*, ed. Johnson WS; ASTM STP 876 (1985); pg 349.
- 51 Grayson MA and Wolf CJ; Diffusion of Water in Carbon Epoxy Composites; Fifth Internal Conference on Composites Materials - ICCM-V, San Diego, USA, 1985; TMS Publication (1985); pg 1463.
- 52 Grayson MA and Wolf CJ; The solubility of water in poly/aryl-ether-ether-ketone (PEEK); *Journal of Polymer Science: Part B Polymer Physics*, vol. 25 (1987); pg 31-41.
- 53 Lucas JP and Odegard BC; *Advances in Thermoplastics Composites*, ed. G. Newaz, ASTM STP 1044 (1989); pg 231.
- 54 Lucas JP; Unpublished research presented at the TMS Meeting, Chicago, IL, October 1992.
- 55 Whitney JM and Browning CM; *Advanced Composite Materials - Environmental Effects*, ed. Vinson JR, ASTM STP 658 (1978); pg 43.
- 56 Wang Q and Springer GS; Moisture absorption and fracture toughness of PEEK polymer and graphite fibre reinforced PEEK; *Journal of Composites Materials*, vol. 23 (1989); pg 434-447.
- 57 Jordan WM and Bradley WL; Mechanisms of fracture in toughened graphite-epoxy laminates; *Toughened Composites*, ed. NS Johnston, ASTM STP 937 (1987); pg 95.

- 58 Bradley WL and Cohen RN; Matrix deformation and fracture in graphite reinforced epoxies; *Delamination and Debonding of Materials*, ed. Johnson WS, ASTM STP 876 (1985); pg 389-404.
- 59 Lucas JP and Zhou J; Moisture absorption effects on delamination fracture mechanisms of carbon fibre polymeric matrix composites; *Proceedings of ICCM-11, Gold Coast, Australia, 14-18 July 1997*, vol. V; pg 633-641.
- 60 Morgan RJ and O'Neal JE; The durability of epoxies; *Polymer - Plastics Technology Engineering*, vol. 10, No. 1 (1978); pg 49-116.
- 61 Morgan RJ, O'Neal JE and Fanter DL; The effects of moisture on the physical and mechanical integrity of epoxies; *Journal of Materials Science*, vol. 15 (1980); pg 751-764.
- 62 Garg AC and Ishai; Hygrothermal influence of delamination behavior of graphite/epoxy laminates; *Engineering Fracture Mechanics*, vol. 22 (1985); pg 423-447.
- 63 Imaz JJ, Rodriguez JL, Rubio A and Mondragon I; Hydrothermal environment influence on water diffusion and mechanical behavior of carbon epoxy/epoxy laminates; *Journal of Materials Science Letters*, vol. 10 (1991); pg 662-665.
- 64 ECRGLAS Technical Status; Owens-Corning Fibreglass Corporation; Toledo, Ohio, 1991.
- 65 Kliger HS and Barker ER; A comparative study of the corrosion resistance of carbon and glass fibres; 39th Annual conference, Reinforced Plastics/composites institute, The Society of the Plastics Industry, Inc. Jan. 16-19, paper 5-E, (1984); pg 1-7.
- 66 Smith CS; *Design of Marine Structures in Composite Materials*; Elsevier, N.Y. (1990); pg 98 -103.
- 67 Bond D, Bader M and Smith P; Finite element modelling of fibre reinforced composite transverse diffusivity; *Proceedings of ICCM-10, Whistler, B.C., Canada, August 1995*, vol. VI, pg 289-296.
- 68 Chiou P and Bradley WL; The effect of seawater exposure on the fatigue edge delamination growth of a carbon/epoxy composite; *Proceedings of ICCM-9, Madrid, Spain, 12-16 July 1993*, vol. V; pg 516-523.
- 69 Kriz RD and Stinchcomb WW; Effect of moisture, residual thermal curing stresses, and mechanical load on the damage development in quasi-isotropic laminates; *Damage in Composite Materials*, ASTM STP 775, KL Reifsnider, Ed.; American Society for Testing and Materials, Philadelphia (1982); pg 63-80.
- 70 Chateauminois A, Chabert B, Soulier JP and Vincent L; Effects of hygrothermal aging on the durability of glass/epoxy composites. Physico-chemical analysis and damage mapping in static fatigue; *Proceedings of ICCM-11, Gold Coast, Australia, 14th-18th July 1997*, vol. V; pg 593-600.

- 71 Hull D; An Introduction to Composite Materials; Cambridge University Press (1981).
- 72 Morgan RJ; Structure-property relationships and the environmental sensitivity of epoxies; *Developments in Reinforced Plastics-1*, ed G Pritchard; Applied Science Publishers, London (1980); pg 211.
- 73 Ishida H, and Koenig JL; Reinforcement mechanism of glass-glass reinforced plastics under wet conditions: A review; *Polymer Engineering and Science*, vol. 18, no. 2 (1978); pg 28.
- 74 Carter HG and Kibler KG; Langmuir-type model for anomalous moisture diffusion in composite resins; *Journal of Composite Materials*, vol. 12 (1978); pg 88.
- 75 Vinson JR; *Advanced Composite Materials - Environmental Effects*; ASTM Special Technical Publication (1978); pg 658.
- 76 Hale JM and Gibson AG; Strength reduction of GRP composites exposed to high temperature marine environments; *Proceedings of ICCM-11*, Gold Coast, Australia, 14th-18th July 1997, vol. V; pg 411-420.
- 77 Bradley WL, Wood CA, Pratt BA and Chatawanich CS; The effect of moisture on the interfacial strength of graphite-epoxy and E-glass-epoxy composites; *Proceedings of ICCM-11*, Gold Coast, Australia, 14-18 July 1997, vol. V; pg 483-492.
- 78 Chen EJH and Croman RB; Micro-debonding investigation of the effects of thermal residual stress on the bond strength of a graphite/polyamide composite; *Composites Science and Technology*, vol. 48 (1993); pg 173-179.
- 79 Drzal LT, Rich MJ and Lloyd PE; Adhesion of graphite fibres to epoxy matrices: I. The role of fibre surface treatment; *Journal of Adhesion*, vol. 16 (1982); pg 1-30.
- 80 Browning CE, Husman GE and Whitney JM; Moisture effects in epoxy matrix composites; *Composite Materials: Testing and Design*, ASTM STP-617 (1977).
- 81 Collings TA and Copley SM; On the accelerated ageing of CFRP; *Composites*, vol. 14, no. 3 (1983); pg 180-8.
- 82 Curtis PT and More BB; The effects of environmental exposure on the fatigue behaviour of CFRP laminates; *Composites*, vol. 14, no. 3 (1983).
- 83 Lee BL and Holl MW; Effects of moisture and thermal cycling on in-plane shear properties of graphite fibre-reinforced cyanate ester resin composites; *Composites-Part A*, vol. 27A (1996); pg 1015-22.
- 84 Verpoest I and Springer GS; Moisture absorption characteristics of aramid-epoxy composites; *Journal of Reinforced Plastic and Composites* vol. 17 (1988).

- 85 Allred RE; The effect of temperature and moisture content on the flexural response of kevlar/epoxy laminates: part I - [0/90] filament orientation; *Journal of Composite Materials* vol. 15 (1981).
- 86 Allred RE; The effect of temperature and moisture content on the flexural response of kevlar/epoxy laminates: part II - [+/-45,0/90] filament orientation; *Journal of Composite Materials*, vol. 15 (1981).
- 87 Sala G; Composite degradation due to fluid absorption; *Composites: Part B*, vol. 31 (2000); pg 357-373.
- 88 Foch BJ and McManus HL; Modelling of environmentally induced damage in polymer matrix composites; *Proceedings of ICCM-11, Gold Coast, Australia, 14-18 July 1997*, vol. V, pg 433-443.
- 89 Bowles KJ; A thermally modified polymer matrix composite material with structural integrity to 371°C; *Proceedings Twentieth SAMPE Technical Conference, Minneapolis, MN, September 1988*.
- 90 Roberts GD and Vannucci RD; Effect of solution concentration and aging conditions on PMR-15 resins; *SAMPE Journal*, Mar/Apr 1986; pg 24-28.
- 91 Ming L; The environmental effects of carbon fiber reinforced polyethersulphone composites; *Proceedings Tenth International Conference on Composite Materials, Whistler, B.C., Canada, August, 1995*; pg 297-303.
- 92 Chang WJ, Chen TC and Weng CI; Transient hygrothermal stresses in an infinitely long annular cylinder; *Journal of Thermal Stresses*, vol. 14 (1991); pg 439-454.
- 93 Cunningham R and McManus H; Coupled diffusion-reaction models for predicting the distribution of degradation in polymer matrix composites; *Presented at the 1996 ASME International Mechanical Engineering Congress and Exposition Atlanta, GA, November 1996*.
- 94 Martin RH, Siochi EJ and Gates TS; Isothermal aging of IM7/8320 and IM7/5260; *Presented at the 7th Technical Conference on Composite Materials; The Pennsylvania State University, University Park, PA, October, 1992*.
- 95 Chester RJ and Baker AA; Environmental durability of F/A-18 Gr/Ep composites; *Proceedings Tenth International Conference on Composite Materials, Whistler, B.C., Canada, August, 1995*, pg 239-246.
- 96 Burcham LJ, Van Landingham MR, Eduljee RF and Gillespie JW; Moisture effects on the material behavior of graphite polyimide composites; *Proceedings Ninth International Conference on Composite Materials, Newark, DE, September, 1994*.

- 97 Beckwith SW and Wallace BD; Effects of aging and environmental conditions on kevlar/epoxy composites; SAMPE Quarterly, vol. 14, no.6, July, 1983.
- 98 Whiteside JB, Delasi RJ and Schulte RL; Distribution of absorbed moisture in graphite/epoxy laminates after real-time environmental cycling; Long Term Behavior of Composites, ASTM STP 813, O'Brien TK, Ed.; American Society for Testing and Materials, Philadelphia (1983); pg 192-205.
- 99 Mandell JF; Origin of moisture effects on crack propagation in composites; Dept. of Materials Science and Engineering Research Report R77-4; Massachusetts Institute of Technology; December 1977.
- 100 Lucas JP and Zhou J; Moisture interaction characteristics and fracture in polymer composites; Proceedings Tenth International Conference on Composite Materials, Whistler, B.C., Canada, August, 1995; pg 247-256.
- 101 Miriyala SK, Tucker WC, Brown R and Rockett TJ; The mechanism of galvanic blistering in carbon fiber composites; Proceedings of ICCM-9, Madrid, Spain, 12-16 July 1993, vol. V; pg 546-553.
- 102 Fontana MG; Corrosion Engineering; McGraw-Hill, Inc., New York, USA (1986); pg 43.
- 103 Tucker WC and Brown R; Blister formation on graphite/polymer composites galvanically coupled with steel in seawater; Journal of Composite Materials vol. 23, April 1989; pg 389-395.
- 104 Miriyala SK, Tucker WC, Rockett TJ and Brown R; Degradation of carbon reinforced polymer composites under galvanic coupling conditions; 33rd ASME/AIAA Structures, Structural Dynamics and Materials Conference, Dallas, Texas; April 1992.
- 105 Tucker WC, Brown R, Rockett TJ and Miriyala SK; Blistering of Graphite/Polymer Composites Galvanically Coupled to Metals in Sea Water; Annual Report, Office of Naval Research, USA, 1992.
- 106 Donnellan TM and Cochran RC; Galvanic degradation of polyamide based composites; Third International Conference on Polymers in a Marine Environment, London, October 1991.
- 107 Sloan FE; The Effects of Long Term Seawater Exposure on Graphite/Epoxy Composite Materials; PhD. Thesis, University of California, San Diego, 1991.
- 108 Castaing Ph, Tsouvalis N and Lemoine L; Proceedings of Nautical Construction with Composite Materials, Actes de Colloques IFREMER N0 75, paper 34, (1992).
- 109 Castaing Ph and Lemoine L; Proceedings of Journees Specialisees AMAC-COMETT, (1993).
- 110 Deuff M; Loisirs Nautiques, 189, 27 (1987).

- 111 Farrar NR and Ashbee KHG; Destruction of epoxy resins and of glass-fibre-reinforced epoxy resins by diffused water; *J. Applied Physics* vol. 11 (1978); pg 1009.
- 112 Crump S; Study of blister formation in gel coated laminates; *Proceedings of 41 Annual Conference S.P.I., session 13-C* (1986).
- 113 Kootsookos A, Mouritz AP and St John NA; Comparison of the seawater durability of carbon and glass-polymer composites; *Proceedings of ICCM-13, Beijing, China, 25-29 June 2001, Paper 1200*.
- 114 Kenny JM and Torre L; High temperature properties and applications of polymers; *American Chemical Society*, vol. 9 (1995); pg 141-154.
- 115 Turi A; *Thermal characterization of polymeric materials*, Second edition, vol. 2; Academic Press.
- 116 Whitney JM and Browning CE; *Experimental Mechanics* vol. 25, no. 3 (1985); pg 294-300.
- 117 Potter RT and Purslow D; The environmental degradation of notched CFRP in compression; *Composites*, vol. 14 no. 3 (1983); pg 206-225.
- 118 Barker AJ and Balasundaram V; Compression testing of carbon fibre-reinforced plastics exposed to humid environments; *Composites* vol. 18, no. 3 (1987); pg 217-226.
- 119 Browning CE, Husman CE and Whitney JM; Moisture effects in epoxy matrix composites; *AFML-TR-77-41*, 1977.
- 120 Obst AW, Van Landingham MR, Eduljee RF, Gillespie JW Jr, Griesheim GE and Tosi KF; The effect of hygrothermal cycling on the microcracking behavior of fabric laminates; *Proceedings of International SAMPE Technical Conference, Covina (CA): SAMPE* vol. 28 (1996); pg 994-1002.
- 121 Smith LV and Weitsman YJ; The immersed fatigue response of polymer composites; *Int Journal of Fracture* vol. 82 (1996); pg 31-42.
- 122 Case SW; *Mechanics of fiber-controlled behavior in polymeric composite materials*; PhD dissertation, Blacksburg (VA), Virginia Polytechnic Institute and State University, 1996.
- 123 Patel SR and Case SW; Durability of a graphite/epoxy woven composite under combined hygrothermal conditions; *International Journal of Fatigue* 22 (2000); pg 809-820.
- 124 Shen CH and GS Springer; Moisture absorption and deabsorption of composite materials; *Journal of Composite Materials* vol. 10, no. 1 (1976); pg 2-20.
- 125 Springer GS; *Environmental effects; Composites Design*, 4th Ed., S Tsai ed., *Think Composites*, Dayton, Ohio, 1988; pg 16-1 to 16-18.
- 126 Tsai SW and Hahn HT; *Introduction to Composite Materials*; Technomic Publishing, Lancaster PA; 1980.

- 127 Weitsman Y; A rapidly convergent scheme to compute moisture profiles in composite materials under fluctuating ambient conditions; *Composite Materials* vol. 15, no. 7 (1981); pg 349-358.
- 128 Upadhyay PC and Prucz J; Parametric damage modelling of composites due to moisture absorption; *Journal of Reinforced Plastics and Composites* vol. 11 (1992); pg 198-210.
- 129 Crank J; *The Mathematics of Diffusion*, 2nd Ed.; Clarendon Press, Oxford, England, 1975.
- 130 Springer GS; *Environmental Effects on Composite Materials*; Technomic Publishing, Lancaster, PA, vol. 1 and 2, 1981.
- 131 Chamis CC; Simplified composite micromechanics equations for hygral, thermal and mechanical properties; *SAMPE Quarterly*, April, 1984; pg 14-23.
- 132 Cai LW and Weitsman Y; Non-Fickian moisture diffusion in polymeric composites; *Journal of Composite Materials* vol. 28, no. 2, (1994); pg 130-154.
- 133 Fick A; *Analytical Physics* vol. 170, 1855; pg 59.
- 134 Shirrell CD; Diffusion of water vapour in graphite/epoxy composites; *Advanced Composite Materials - Environmental Effects*, ASTM STP 658, JR Vinson Ed.; American Society for Testing and Materials, 1978; pg 21-42.
- 135 Woo M and Piggott MR; Water absorption of resins and composites: IV. Water Transport in fibre reinforced plastics; *Journal of Composites Technology & Research* vol. 10, no. 1, Spring 1988; pg 20-24.
- 136 McKague EL Jnr., Reynolds JD and Halkias JE; Moisture diffusion in fibre reinforced plastics; *Journal of Engineering Materials and Technology*, Transactions of the ASME, Jan 1976; pg 92-95.
- 137 Halpin J and Tsai S; Effects of environmental factors on composite materials; AFML-TR 67-423 (1969).
- 138 Augl JM and Berger AE; The effect of moisture on carbon fibre reinforced composites I: diffusion; Naval Surface Weapons Centre, NSWC/WOL TR 76-7, 27 September 1976.
- 139 Kondo K. and Taki T; Moisture diffusivity of unidirectional composites; *Journal of Composite Materials* vol. 16 (1982); pg 82-93.
- 140 Gibiansky LV and Torquato S; Connection between the conductivity and bulk modulus of isotropic composite materials; *Phil. Trans. Roy. Soc.*, 1995, A353; pg 243-278.
- 141 Levin VM; On the coefficients of thermal expansion of heterogeneous material; *Mechanics of Solids* vol. 2 (1967); pg 58-61.
- 142 Milton GW; Bounds on the electromagnetic, elastic and other properties of two-component composites; *Physical Review Letters* vol. 46 (1981); pg 542-545.

- 143 Cherkaev AV and Gibiansky LV; The exact coupled bounds for effective tensors of electrical and magnetic properties of two-component two-dimensional composites; Proceedings of Royal Society Edinburgh, 1992, A122; pg 93-125.
- 144 Markov KZ; Heterogeneous Media: Micromechanics Modelling Methods and Simulations, Ed.: Markov KZ and Preziosi L; Birkhauser (1999); pg 1-162.
- 145 Gibiansky LV and Torquato S; Rigorous link between the conductivity and elastic moduli of fiber reinforced materials; Proceedings of Royal Society, 1996, A452; pg 253-283.
- 146 Gibiansky LV and Torquato S; Bounds on the effective moduli of cracked materials; Journal of Mechanics and Physics of Solids vol. 44, no. 2, 1996; pg 233-242.
- 147 Schapery RA; Stress analysis of viscoelastic composite materials; Journal of Composite Materials 1 (1967); pg 228.
- 148 Schapery RA; On the characterization of nonlinear viscoelastic materials; Polymer Engineering and Science vol. 9 (1969); pg 295.
- 149 Schapery RA; Viscoelastic behavior and analysis of composite materials; Mechanics of Composite Materials, Academic Press, 1974; pg 85.
- 150 Gates TS and Feldman M; Time dependent behavior of a graphite/thermoplastic composite and the effects of stress and physical aging; Technical Memorandum 109047, Hampton, VA: NASA Langley Research Center, 1993.
- 151 Hastie RL and Morris DH; The effects of physical aging on the creep response of a thermoplastic composite; American Society for Testing and Materials (1993); pg 163.
- 152 Gates TS and Feldman M; The effects of physical aging at elevated temperatures on the viscoelastic creep of IM7/K3B; Technical Memorandum 109114, Hampton, VA: NASA Langley Research Center (1994).
- 153 Bradshaw RD and Brinson LC; Physical aging in polymers and polymer composites: an analysis and method for time-aging time superposition; Polymer Engineering and Science vol. 37 (1997); pg 31.
- 154 Bradshaw RD and Brinson LC; Determining physical aging reference curves via continuous test data: theory and experimental results; Polymer Engineering and Science, as appears in reference 3.
- 155 Brinson LC and Gates TS; Effects of physical aging on long term creep of polymers and polymer matrix composites; International Journal of Solids and Structures vol. 32 (1995); pg 827.
- 156 Monaghan MR, Brinson LC and Bradshaw RD; Analysis of variable stress history on polymeric composite materials with physical aging; Composites Engineering vol. 4 (1994); pg 1023.

- 157 Pasricha A, Parvatareddy H and Dillard DA; Physical aging effects on polymeric composites subjected to variable stress history; X International Conference on Experimental Mechanics, as appears in reference 3.
- 158 Pasricha A, Dillard DA and Tuttle ME; Effect of physical aging and variable stress history on the strain response of polymeric composites; Composites Science and Technology vol. 57 (1997); pg 1271.
- 159 Hildebrand FB; Advanced Calculus for Applications; Englewood Cliffs, N.J.: Prentice-Hall, 1976.
- 160 Jones FR, Rock JW and Bailey JE; The environmental stress corrosion cracking of glass fibre-reinforced laminates and single E-glass filaments; Journal of Materials Science vol. 18 (1983); pg 1059-1071.
- 161 Jones FR, Rock JW and Bailey JE; Stress corrosion cracking and its implications for the long term durability of E-glass fibre composites; Composites vol.14, no.3 (1983); pg 262-269.
- 162 Wiederhorn SM; Mechanisms of subcritical crack growth in glass; Fracture Mechanics of Ceramics, RC Bradt Plenum Press. Vol. 4 (1978); pg 549-580.
- 163 Pauchard V, Chateauminois A, Grosjean F and Odru P; Development of a S.C.C. model for the prediction of the durability of flexural GFRP beams in humid environments; Proceedings of ICCM-13, Beijing, China, 25-29 June 2001; Paper 1674.
- 164 Pauchard V, Chateauminois A, Grosjean F and Odru P; Micromechanical analysis of delayed fibre fracture in unidirectional GFRP submitted to fatigue in wet environments; as appears in reference 3.
- 165 Pauchard V, Grosjean F, Campion-Boulharts H and Chateauminois A; Application of a stress corrosion cracking model to the analysis of the durability of glass/epoxy composites in wet environments; as appears in reference 3.
- 166 Weibull W; A statistical distribution function of wide applicability; Journal of Applied Mechanics vol. 18 (1951); pg 293-296.
- 167 McManus HL and Chamis C; Stress and damage in polymer matrix composite materials due to material degradation at high temperatures; NASA TM 4682, January, 1996.
- 168 Gumen VR, Jones FR and Attwood D; Polymer (2001); as appears in reference 3.
- 169 Porter D; Group interaction modelling of polymer properties; Ed. Marcel Dekker Inc., New York, 1995.
- 170 Vakil UM and Martin GC; Yield and fracture behaviour of cross-linked epoxies; Journal of Material Science 28 (1993); pg 4442.
- 171 Bicerano J; Prediction of polymer properties; Marcel Dekker Inc, New York, 1996.

- 172 Seddon M; Private communication; as appears in reference 3.
- 173 Wolff EG; Moisture Induced Dimensional Changes in Composites; Proceedings of ICCM-13, Beijing, China, 25th-29th June 2001; Paper 1141.
- 174 Sih GC, Michopoulos JG and Chou SC; Hygrothermoelasticity; Martinus Nijhoff Publishers (Kluwer) 1986.
- 175 Szekeres A, Engelbrecht J, Heller R, Kiss P and Pramila A; Thermo-Hygro-Mechanical tailoring of fiber reinforced composites; Proceedings of the 1st Conference on Mechanical Engineering; Technical University, Budapest, May 1998.
- 176 Toman J and Cerny R; Coupled thermal and moisture expansion of porous materials; Proceedings of Symposium on Thermophysical Properties, NIST, Boulder, June 1994.
- 177 Neumann S and Marom G; Stress dependence of the coefficient of moisture diffusion in composite materials; Polymer Composites vol. 6, Jan 1985; pg 9-12.
- 178 Aditya PK and Sinha PK; Effects of fibre shapes on moisture diffusion coefficients; Journal of Reinforced Plastics and Composites vol. 12, September 1993; pg 973-986.
- 179 Kondo K and Taki T; Moisture diffusivity of unidirectional composites; Journal of Composite Materials vol. 16 (1982); pg 82-93.
- 180 Ripley BD; Simulating spatial patterns: Dependent samples from a multivariate density; Applied Statistics vol. 28 (1979); pg 109-112.
- 181 Lee H and Neville K; Handbook of Epoxy Resins; McGraw-Hill Book Company (1967); pg 6-49 to 6-50.
- 182 Bank LC, Russell TR and Barkatt A; Accelerated test methods to determine the long term behaviour of FRP composite structures: environmental effects; Journal of Reinforced Plastics and Composites vol. 14; June 1995; pg 559.
- 183 Vauthier E, Chateauminois A and Bailiez T; Hygrothermal aging and durability of unidirectional glass-epoxy composites; Proceedings of ICCM 10 vol. VI; Whistler, B.C., Canada, August 1995; pg 185 to 192.
- 184 Martin JW, Chin JW, Byrd WE, Embree E and Kraft KM; An integrating sphere-based ultraviolet exposure chamber design for the photodegradation of polymeric materials; Polymer Degradation and Stability vol. 63 (1999); pg 297-304.
- 185 Gates TS and Grayson MA; On the use of accelerated aging methods for screening high temperature polymeric composite materials; American Institute of Aeronautics and Astronautics, paper (AIAA 99-1296) vol. 2, pg 925-935.
- 186 Brydson JA; Plastics Materials; Iliffe books (1970); pg 80.

- 187 Dade County Florida; Accelerated exposure of roofing materials using a controlled irradiance water cooled xenon arc apparatus; Metro Dade Center, Building and Zoning Department, Miami (1974), as appears in reference 1.
- 188 Verma M and Crewdson L; A study of the colour change of automotive coatings subjected to accelerated and natural SAE weathering tests for exterior materials durability; Society of Automotive Engineers; 1994 Annual Congress, as appears in reference 1.
- 189 Crewdson LFE; Correlation of outdoor and laboratory accelerated weathering tests at currently used and higher irradiance levels – Part II; Materials life society, First International Symposium on Weathering, May 1992, Tokyo, Japan, as appears in reference 1.
- 190 Dewimille B, Bunsell AR; Accelerated ageing of a glass fibre-reinforced epoxy resin in water; Composites vol. 14 (1983); pg 35-40.
- 191 Grossman DM; Journal of Vinyl Tech. vol. 3 (1981); pg 38.
- 192 Alfrey T, Gurnee EF and Lloyd WG; Diffusion in glassy polymers; Journal of Polymer Science, Part C (1966).
- 193 Shirrell CD; Diffusion of water vapour in graphite/epoxy composites; Proc ASTM Symposium on Environmental Effects on Advanced Composite Materials, Dayton, Ohio, September, 1977.
- 194 Fukuda H; Outdoor exposure of advanced composites; Proceedings of the ICCM-7, Guangzhou, China (1989), pg 429-434.
- 195 Benson Dexter H and Baker DJ; Worldwide flight and ground-based exposure of composite materials; ACEE Composites Structures Technology, NASA Conference Publication 2321 (1984), pg 17-50.
- 196 Kumar BG, Singh RP and Nakamura T; Degradation of carbon fiber-reinforced epoxy composites by ultraviolet radiation and condensation; Journal of Composite Materials, vol. 36, no. 24 (2002); pg 2713 - 2733.
- 197 Tsouvalis N; Internal Technical Report N° GO-MM 9117, IFREMER (1991).
- 198 De Wilde WP and Sol H *et al*; Proceedings of Journees rationales AMAC-GAMAC, Pluralis, Paris (1979).
- 199 Blevins RD; Formula/or natural frequency and mode-shape; Van Nostrand Reinhold Co.; (1979).
- 200 Hussein RM; Composite Panels-Plates-Analysis and design; Technomic Publish. Co. (1986).
- 201 Copley SM; A computer program to model moisture diffusion and its application to accelerated ageing of composites; Royal Aircraft Establishment (RAE), TR-82010, 1982.

- 202 Naeem M; The resistance of glass reinforced thermosetting polymers to thermo-humid conditions; PhD Thesis. Loughborough University of Technology, 1995.
- 203 Boinard E, Pethrick RA and MacFarlane CJ; Study of water permeation into glass fibre reinforced composites by thermal analysis and dielectric spectroscopy; Proceedings of the Sixth International Conference on Composite Engineering ICCE/6, June 1999, Orlando, USA; pg 71-72.
- 204 McCrum G, Read BE and Williams G; Anelastic and Dielectric Effects in Polymeric Solids; New York, Dover Publications, Inc. (1967).
- 205 Hasted JB; Aqueous Dielectrics, London, Chapman and Hall, 1973.
- 206 Kirkwood JG; Journal of Chemical Physics, vol. 7 (1939); pg 911.
- 207 Frohlich H; Theory of Dielectrics; Oxford University Press, London (1949).
- 208 Suzuki T, Oki Y, Numajiri M, Miura T, Kondo K, Shiomi Y and Ito Y; Free-volume characteristics and water absorption of novolac epoxy resins investigated by positron annihilation; Polymer vol. 37 no. 14 (1996); pg 3025.
- 209 Adamson M; Thermal expansion and swelling of cured epoxy resin used in graphite/epoxy composite materials; Journal of Materials Science 15 (1980); pg 1736.
- 210 Deng Q, Zandiehnam F and Jean Y C; Free-volume distributions of an epoxy polymer probed by positron annihilation. Temperature dependence; Macromolecules vol. 25 (1992); pg 1090-1095.
- 211 Jean YC, Sandreczki TC and Ames DP; Positronium annihilation in amine-cured epoxy polymers; Journal of Polymer Science (B) vol. 24 (1986); pg 1247.
- 212 Soles CL, Yee AF; A discussion of the molecular mechanisms of moisture transport in epoxy resins; Journal of Polymer Sci Part B, Polymer Physics, 38 (2000); pg 792-802.
- 213 Zhou J, Lucas JP; Hygrothermal effects of epoxy resin. Part I: The nature of water in epoxy; Polymer 40 (1999); pg 5505-5522.
- 214 Xiao G, Delamar M and Shanahan MER; Journal of Applied Polymer Science vol. 65, no. 3 (1996); pg 449.
- 215 Kyritsis A, Pissis P, Gomez Ribelles JL and Monleon Pradas M; Dielectric relaxation spectroscopy in PHEA hydrogels; Journal of Non-Crystalline Solids 172-174 (1994); pg 1041-1046.
- 216 Maggana C and Pissis P; TSDC studies of the effects of plasticizer and water on the sub-T_g relaxations of an epoxy resin system; Journal of Macromolecular Science, Physics B vol. 36, no. 6 1997; pg 749-772.
- 217 Salin IM, Seferis JC, Loechele CL and Rothschilds R; Time-temperature equivalence in thermogravimetry for BMI composites; SAMPE Q. vol. 24, no. 1, Oct. 1992; pg 54-62.

- 218 Young RJ; Analysis of composites using Raman and fluorescence microscopy - a review; *Journal of Microscopy* vol. 85 (1997); pg 199.
- 219 Young RJ; Monitoring deformation process in high-performance fibres using Raman spectroscopy; *Journal of the Textile Institute* vol. 86 (1995); pg 360.
- 220 Kachanov M, Sevostianov I and Shafiro B; Explicit cross-property correlations for porous materials with anisotropic microstructures; *Journal of Mechanics and Physics of Solids* vol. 49 (2001); pg 1-25.
- 221 Sevostianov I and Kachanov M; Explicit cross-property correlations for anisotropic two-phase composite materials; *J Mech Phys Solids* vol. 50 (2002); pg 253-82.
- 222 Sevostianov I and Kachanov M; Compliance tensor of ellipsoidal inclusions; *Int J Fract* vol. 96 (1999); pg 3-7.
- 223 Sevostianov I and Verijenko V; Microcracks in fibre reinforced composites: evaluation of the stiffness lost via change in conductive properties; as appears in reference 3.
- 224 Product data sheet; available from supplier; May 2002.
- 225 <http://www.ultra-shade.com/uvprotection.shtml>; 28 August 2003.
- 226 Hexcel composite datasheet;
<http://www.hexcelcomposites.com/NR/rdonlyres/euzh7qwagqukkc4t6npc72axpy66lkdymher24s2m4j2fqfbw7t5su2rnf3sixmgebkyjnhglcp2wn5rrvgjthqsqzh/HexPly+8552.pdf>;
13 October 2004.
- 227 BS 2782: Part 5: Method 550A: 1981, ISO 4607-1978; Methods of exposure to natural weathering; pp 10.
- 228 ASTM G7-89, Standard practice for Atmospheric Environmental Exposure Testing of Nonmetallic Materials; 1990 annual book of ASTM standards vol. 14.02; pg 888-893.
- 229 ASTM D1435 – 85, Outdoor weathering of plastics; 1990 annual book of ASTM standards vol. 08.01; pg 434-438.
- 230 Renewable Resource Data Center;
http://rredc.nrel.gov/solar/old_data/nsrdb/bluebook/state.html; 20 July 2004.
- 231 http://www.csir.co.za/environmentek/sared/images/solar_thumb.jpg; 15 July 2004.
- 232 Zhang S, Karbhari VM, Lin-Ye and Mai Y; Evaluation of property retention in E-glass/vinylester composites after exposure to salt solution and natural weathering; *Journal of Reinforced Plastics and Composites*, vol. 19, No. 09/2000.
- 233 Hammami A and Al-Ghuilani N; Durability of glass-vinylester composites exposed to seawater and corrosive fluid; *Proceedings of ICCM 14, San Diego, CA, USA; 14-18 July 2003; CD-ROM*.

- 234 P. Moonsamy; Technical service manager - R&D, NCS Resins; Private communication; November 2002.
- 235 Whitney JM and Husman GE; Use of flexure test for determining environmental behaviour of fibrous composites; *Experimental Mechanics* vol. 18, no. 5 (1978); pg 185-190.
- 236 Lantz RB; Boron epoxy laminate test methods; *Journal of Composite Materials*, vol 3, no. 4, October 1969; pg 642-650.
- 237 Whitney J.M., CE Browning and A. Mair; Analysis of the flexure test for laminated composite materials; *Composite Materials: Testing and Design (third conference)*; ASTM STP 546; American Society for Testing and Materials (1974); pg 30-45.
- 238 Whitney JM; *Structural Analysis of Laminated Anisotropic Plates*; Technomic Publishing Co. Inc., Lancaster, PA (1987).
- 239 Pipes RB; *Delware Composites Design Encyclopedia* vol. 6, Test Methods; Technomic Publishing; pg 19-37.
- 240 ASTM D790M-86, Test methods for flexural properties of unreinforced and reinforced plastics and electrical insulating materials; 1990 annual book of ASTM standards vol. 08.01; pg 284-292.
- 241 WM Harper; *Statistics, Second Edition*; Macdonald and Evans; 1976.
- 242 Singh KS, Singh PN and Rao RMVGK; Hygrothermal effects on chopped fibre/woven fabric reinforced epoxy composites, Part B: degradation studies; *Journal of Reinforced Plastics and Composites*, vol. 10, September 1991; pg 457-462.
- 243 Jones RM, Apparent flexural modulus and strength of multimodulus materials; *Journal of Composite Materials*, vol. 10 (October 1976), pg 342-354.
- 244 Mujika F and Mondragon I; Flexure tests for determining tensile and compressive modulus; poster at CompTest 2004, Composites testing and model identification, 21-23 September 2004, University of Bristol, UK; poster session 3, paper no. 59, CD-ROM.
- 245 Lubin G; *Handbook of Composites*; Van Nostrand Reinhold Co. (1982); pp 523.
- 246 Springer GS *et al*; Analysis of rain erosion of coated and uncoated fibre reinforced composite materials; AFML-TR-74-180; August 1974.
- 247 Cray Valley Report; Dlamini PM; 23 June 2003; pp 3.
- 248 Cray Valley Report; Dlamini PM; 22 September 2003; pp 12.
- 249 Cray Valley Report; Dlamini PM; 29 March 2004; pp 7.
- 250 Cray Valley Report; Dlamini PM; 18 August 2004; pp 7.
- 251 <http://www.azsolarcenter.com/design/pas-1.html>; 18 October 2004.

Appendix A - Specimen Preparation for Examination

Examination of unexposed laminates revealed damage to the laminate caused by the cutting action of the bandsaw. The damage was primarily in the form of cracks on both the fibres and the matrix. Cracks on the fibres were observed to run along the length of the fibres while cracks induced in the matrix did not display any particular orientation. The bandsaw blade was examined and it was suspected that wear of the teeth on the blade used during the cutting may have caused the damage observed. The existing blade was removed and a new undamaged blade inserted. Upon examination of the surface cut using the new blade, damage was still evident. Cutting laminates at different feed rates or reversing the direction of the blade did not result in a significant change in surface damage observed. Reversing the blade direction of motion was thought to gradually remove material, using the rear inclined edge of the blade tooth, from the surface and hence reduce damage. Cutting laminates using the blade in the reverse direction increased the damage induced in the matrix and therefore contrary to the Composites handbook. Damage was observed on laminates machined at different saw speeds. At higher speeds, evidence of burning of the matrix was found on the surface machined.

Specimens cut using a diamond rotary saw fitted to an existing carpentry workbench were examined and no damage was observed on the surface visually and at 100× magnification. All further preparation that required cutting of laminates were performed using the diamond saw blade. The surface that had been cut using the diamond blade was dependent upon the speed at which the laminate was cut. At low laminate feed rate, a visually undamaged surface was produced. At double this feed rate, scores were observed on the cut edge. The quality of the edge cut decreased with increasing operating hours of the saw blade due to wear.

Specimens were carefully prepared by cutting a 20×20mm segment from the exposed laminates using the diamond saw. The surface to be examined, i.e. the cut closest to the centre of the exposed plate, was marked after the specimen was cut. The mould used to mount the specimens for polishing had to be cylindrical as the polishing fixture could only accommodate cylindrical mounted specimens of approximately 1 in. in diameter. The use of a standard 1 in. diameter PVC pipe was decided upon to provide a mould cavity for mounting of specimens. Six 25mm long pieces of pipe were cut from a length of PVC pipe and the ends sanded until they were perpendicular to the axis of the pipe. Smooth pipe ends were required to ensure that the pipe would rest flush onto a metal plate without requiring additional sealing. These pipe segments were then used as a mould for mounting of the specimens. A release agent, RAM wax, was applied onto the interior of the pipe moulds and buffed after approximately 10min. The moulds were placed on a sheet of metal polished with the release agent and specimens to be examined

were placed within the mould. The LR20 epoxy resin system was used as the mounting material. A premixed resin/hardener solution was poured into the mould containing the specimen. Specimens were covered by the resin which also leaked between the mould / sheet metal interface. The leak stopped once a force was applied to the mould by hand. Once the force on the mould was released, resin continued to leak at the interface. In an attempt to stop the leak, tacky tape was used to seal the interface. The tacky tape however would not adhere to the mould surface that had already been wet by resin. On the next attempt, after the release agent was applied to the mould, tacky tape was used to seal the mould plate interface, thereby successfully containing the mounting resin within the mould. The specimens were then polished using the MOTOPOL 2000 polishing machine manufactured by Buehler. The polishing process is described in Appendix B.

Upon examination using the scanning electron microscope, the boundaries of the specimen could not be distinguished from the mounting resin. The mounting resin had bonded to the specimen and as both the mounting resin and specimen matrix are polymers, both polymers appeared as one material on images captured using the electron microscope. The problem was discussed with the electron microscope technician who suggested that a coating with a different atomic number be applied. As the electron microscope does not display colour images due to the image being formed by the reflection of electrons from the surface, a barrier with a different atomic number is required to highlight the interface between the mounting resin and the specimen. The laminates were subsequently dipped in silver paint before casting. Upon examination of the coated specimens an interface was not always distinguishable as it was later realised that the silver paint did not adhere to the specimen surface and in most cases collected at the bottom of the mould without sufficiently coating the specimen.

Masking tape was used to cover the specimen before mounting. Initially this was thought to have been the solution, but careful examination of polished specimens revealed that this process was not repeatable. On average, mounting resin contaminated most specimens, with only a few specimens being effectively sealed. As the masking tape was porous, mounting resin was absorbed by the masking tape and adhered to the specimen.

To overcome the porosity of the masking tape, standard light duty aluminium foil was wrapped around the specimen to seal it from the resin and provide a barrier of different atomic number between the specimen and the mounting resin. This process was successful at first but was not repeatable. Wrapping of the specimen in foil resulted in the foil tearing at the edges while the specimens were positioned in the mould. Liquid resin would fill into the cavity between the foil and the specimen through the tear in the foil. In attempt to reduce the flow of resin between the

foil and laminate, the resin was poured into the mould at the beginning of the exotherm. The increased viscosity at this stage would reduce the flow of resin into crevices between the foil and the laminate. However, the resin rapidly gelled once the exotherm began, and therefore it was not possible to fill more than two moulds before the resin gelled.

To provide a nonporous seal between the foil and the mounting resin, insulation tape was used to cover the foil and seal the area to be examined from the mounting resin. The polished area on the specimen was found to be free from mounting resin but the insulation tape would cover the specimen during polishing thus reducing the effectiveness of the polishing. Further, as the tape was in contact with the abrasive grit, fragments of the insulation tape would come loose from the specimen and become lodged on the polishing pad effectively covering the grit and thereby reducing the effect of the polishing. Excess insulation tape on the specimen was removed with a sharp blade where possible. The specimen was initially secured in the upright position in the mould with wire. The use of wood supports with slots to accommodate the specimens was found to be easier to install into the mould to keep the specimens in the upright position during curing of the mounting resin.

Appendix B - Polishing Procedure Used for Polishing Polymer Matrix Composites

The procedure described below is for the polishing of three specimens. Specimens should be ideally polished in a batch of three or six samples. For polishing on a batch of six specimens, the force listed below must be doubled. Polishing was performed using the MOTOPOL 2000 polishing machine manufactured by Buehler.

1. Plane grind

Disk: MD Piano 120

Force: 60 N

Speed: 300rpm

Rotation: clockwise

Duration: 10min

Disk: MD Piano 220

Force: 75 N

Speed: 300rpm

Rotation: clockwise

Duration: 30min

Note:

- Check that all specimens are plane.
- Reset specimens such that further grinding does not result in contact of the polishing fixture and the polishing pad.

2. Fine Grind

Disk: MD Allegro

Grit size: 9 μ m

Force: 105 N

Speed: 150rpm

Rotation: clockwise

Duration: 15min

Disk: MD PAN

Grit size: 3 μ m

Force: 105 N

Speed: 150rpm

Rotation: clockwise

Duration: 15min

Note: Specimen surface should reflect the image of overhead fluorescent light bulbs.

3. Polish

Disk: MD NAP

Grit size: oxide

Force: 90 N

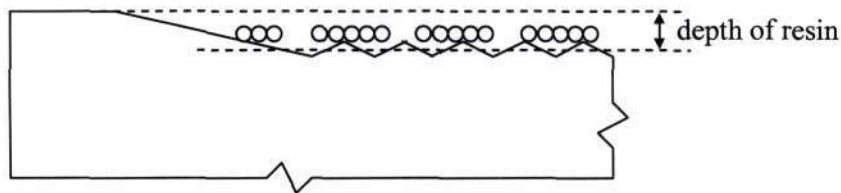
Speed: 150rpm

Rotation: clockwise

Duration: 10min

Appendix C – Graphical Technique for Measurement of Depth of Resin Loss

The determination of depth of resin loss after long exposure period has been determined from using graphical techniques on the pictures obtained from scanning the exposed surface using the scanning electron microscope. The procedure entailed drawing a line on the captured images of the unexposed surface of the laminate, and extending the line to the exposed area. A parallel line is then drawn to the depth of the eroded resin under the exposed fibre. The distance between the lines is then the depth of resin loss and is measured using the scaled surface from the electron microscope images. The accuracy of the method is limited to the pixel size of the digital images. From measurements on the pixels, it has been estimated that the precision is approximately $5\mu\text{m}$.



Appendix D – Compression Fixture Design and Commissioning

D1: Compression tests literature survey

Compressive strength is a difficult parameter to measure as variations in specimen preparation and loading eccentricity influence the results of the test. With most of the tests, Young's modulus and Poisson ratio are determined using strain gauges, and the initial slope of the load deflection curve is used to determine the modulus of the material. Three types of compression tests, referred to as Type I, II and III are covered in the ASTM standards. These different types of compression tests are reviewed below.

Type I

The Celanese fixture incorporates conical grips in matching cylinders as appears in Figure D1, overleaf. The test section of specimens in this type of test is unsupported [D1]. The National Physical Laboratory (NPL) UK, has formulated a Standard Qualification Plan (SQP) aimed at qualifying fibre reinforced polymer composites materials. Measurement of compression strength by the use of the Celanese fixture has been suggested in this SQP [D2]. Another method of compression testing used is the Illinois Institute of Technology Research Institute (IITRI) method where wedge action friction grips, similar to the tension grips in operation, may be employed as shown in Figure D2. The end fittings should be restrained to ensure co-linearity of the centreline. Further, support rollers can be used to support the test region and thereby prevent instability of the test specimen. The Northrop compression test consisting of offset plates incorporating an unsupported region may be utilised as well. This is a simple design in that it is not difficult to set-up and align. The test fixture developed by National Institute of Standards and Technology (NIST) is a compression fixture that may be used in a tensile test machine. This consists of grips that are mounted in fixtures which are guided by rigid bars to move in a co-linear path.

Common problems experienced in compression tests are alignment of the specimens in the fixtures. This would vary depending on which type of fixture is used. Improper mounting may result in buckling failure instead of compression failure. Alignment of the edges are equally important. As most tabs are bonded on the specimen using an adhesive, the method of bonding should ensure that the required degree of alignment between the tabs are obtained.

D1 Pipes RB; Delaware composites design encyclopedia vol. 6, Test methods; Technomic publishing; pg 19-37.

D2 Gower MRL; Towards a standard qualification plan (SQP) for composite materials; presentation at CompTest 2004, Composites testing and model identification, 21-23 September 2004, University of Bristol, UK; session 1; CD-ROM.

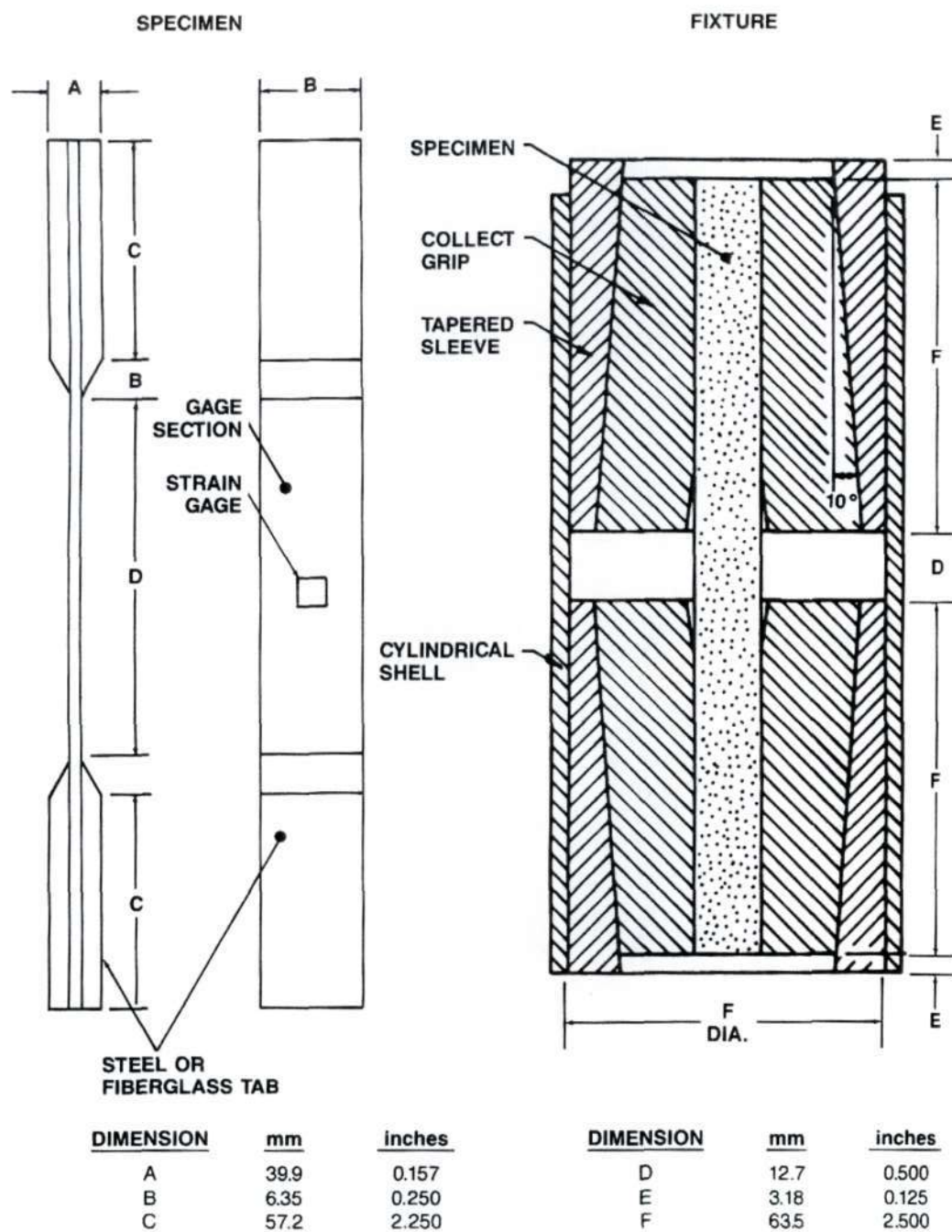


Figure D1 - Celanese test fixture

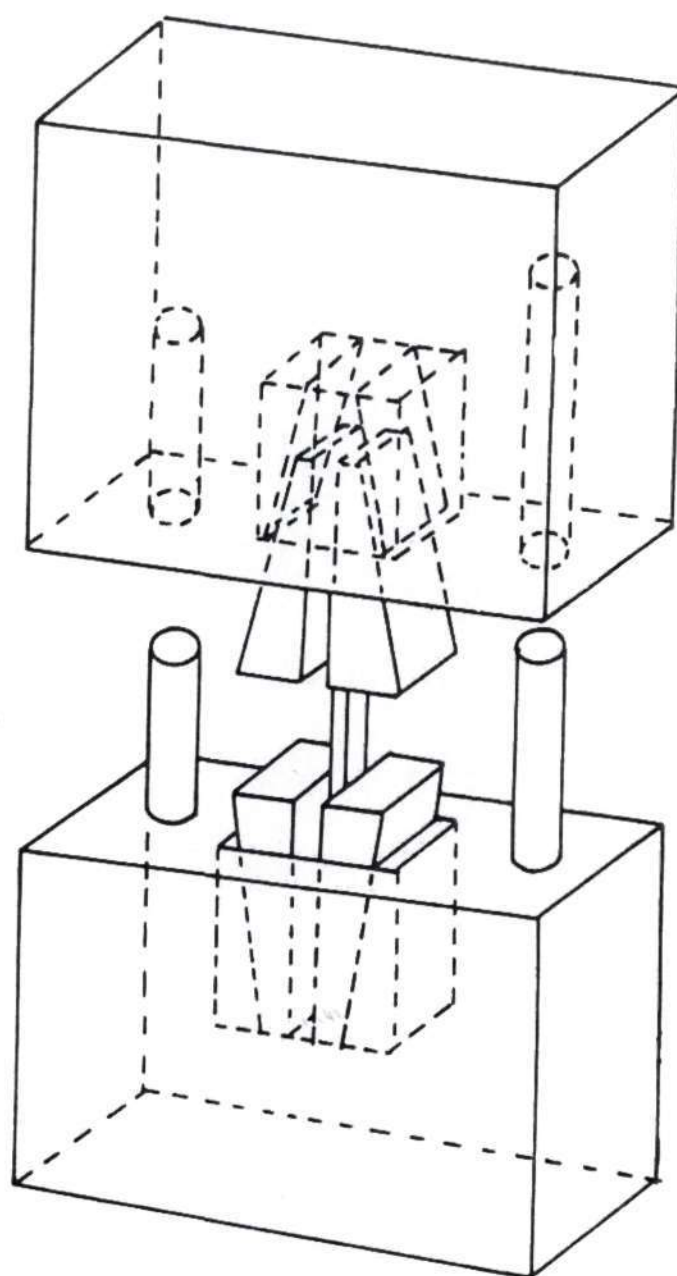


Figure D2 - IITRI fixture [1]

Type II

This type of test method has been developed to enable testing of tension specimens which have longer gauge lengths than standard compression specimens. This would be required to determine the compression strength of specimens that have been loaded by tension in fatigue, or to determine the compression strength after preload in tension. There are two variations of the test method, with all specimens having a relatively long supported test region. The first is the method developed by the Southwest Research Institute (SWRI) which provides support over the full specimen length. The SWRI test fixture is illustrated in Figure D3. In contrast, the second method is that developed by



D3 Lantz RB; Boron epoxy laminate test methods; Journal of composite materials, vol. 3, no. 4, October 1969; pg 642-650.

can be determined using this method but is not generally preferred as it is usually easier and cheaper to produce the standard tensile test specimens.

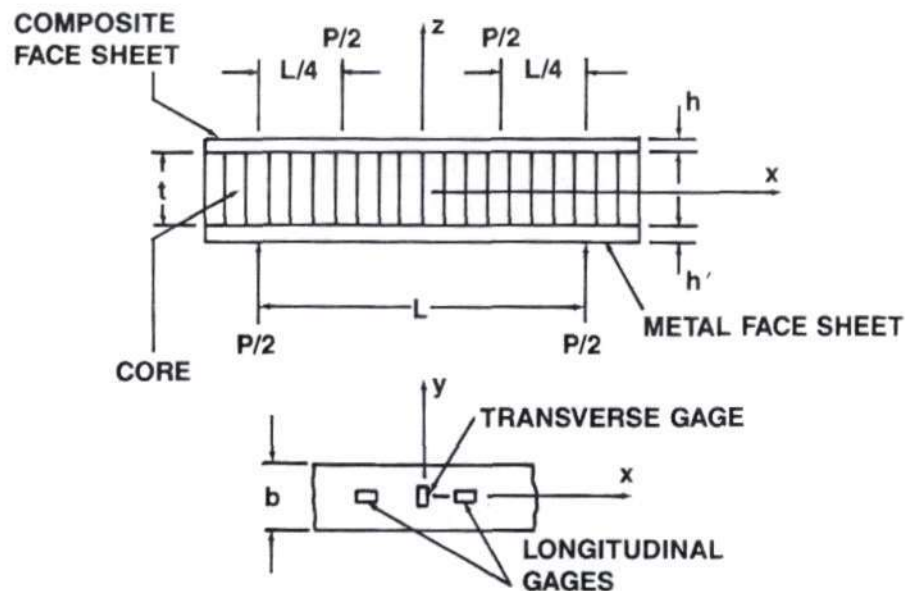


Figure D4 - Type III compression test set-up

The data from type II tests is compatible with the type I tests, however 0° unidirectional compression tests yield lower strengths, and the reason for this has not been established. Using type III tests, Poisson ratio is often higher than data obtained using the standard tensile test coupon. These type of tests yield the highest compression strength. The three types of compression tests addressed in ASTM D3410-75 will generally yield similar compressive strengths for a specific material tested under identical conditions.

D2: Compression fixture design

The aim of the design was to keep the compression fixture as simple as possible and allow for access to the jaws for removal should they become stuck within the holder at the end of a test. A compression fixture was therefore developed based on the configuration illustrated in ASTM D3410 Procedure B and a front open jaw holder. The dimensions of the jaws and the holder were set to be approximately those recommended by the ASTM Standard. Jaw fixtures were designed to be compatible with the present test frame set-up. The jaws and jaw holders were machined in the workshop at the School of Mechanical Engineering. The mountings on the Instron machine were measured and used in the jaw holder design to enable manufactured components to easily fit into the existing equipment. The first design was primarily a block of steel with a cavity machined into the centre, with inclined planes, to accommodate the jaws. The jaw holder was threaded to fit the adapter

attached to the load cell. The base of the jaw holder would be fastened to the travelling cross beam on the machine.

The design was subsequently changed to include guide pins that would align the top and bottom jaw holders. This was done to prevent errors in testing due to misalignment. Until this stage, initial clamping of the specimen was due to a preload. The next design change eliminated this clamping problem by incorporating tightening screws that could move the jaws allowing the jaws to come together thereby clamping the specimen. The screw would have only functioned during the mounting of the specimen in the jaws and not during the loading of the specimen. The design was revised to replace the screw with a thick walled cylinder with threads on the inside. A central shaft connected the threaded cylinder to the jaws. This would serve the function of moving the jaws to clamp on the specimen when the specimen was mounted. The next design revision entailed having the front of the jaws exposed. To enable the jaws to be worked free should they become “stuck” in the jaw holders. The jaw dimensions were set to accommodate standard specimen thicknesses. Grooves were designed into the jaws such that the jaw retaining clips would ensure that the jaws would not rotate in the holder and be constrained to move such that the grip surfaces remained parallel during jaw travel. Dimensions of the jaws were finalised and fabrication drawings were produced of the entire assembly in preparation for manufacturing. Figure D5 is an image of the model produced of the first complete design.

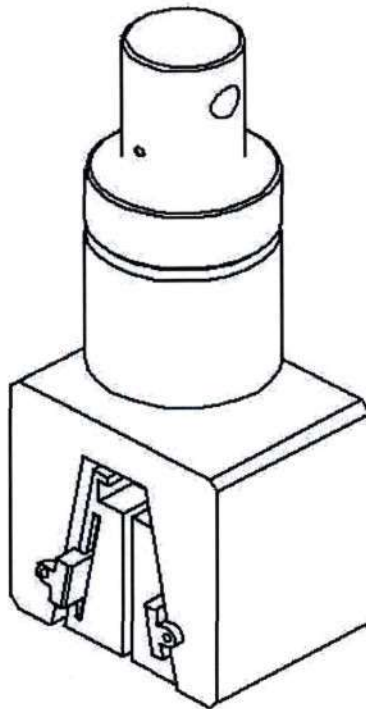


Figure D5 - Initial design of compression fixture

Upon review by a senior member of staff, it was realised that some of the components may already be available as the Mechanical Engineering Department had embarked on building compression jaws in the past but had failed to manufacture all components. Initial components manufactured were found and measured. The design was changed to accommodate the manufactured components. This entailed changing the way the jaw holders were mounted onto the Instron machine and repositioning of the jaw adjustment shaft. The jaw retaining clips were redesigned such that it could be machined from angle iron. Further it was not thought necessary that the jaw retaining clips slot into the jaws to keep the jaws in contact with the jaw holder as this would occur when the jaws are tightened with the specimens in position. The final design of the jaw holder took into account tools available for machining the holder. A set of fabrication drawings were produced including an additional drawing for a second set of jaws to test thinner laminates.

The grade of steel selected for use for the manufacture of existing components was not available. The closest available grade of steel was decided upon in conjunction with the material supplier and staff. Material, DIN number 1.2312, for four sets of jaws was purchased. The fabrication of the jaws were monitored and once complete, the jaws assembled. To reduce the mass of the assembly, two options were available. First, to chamfer the top edges of the jaw holder, or second, to drill holes in regions of large mass. The mass loss of either option proved to be similar. The first option was decided upon as it was aesthetically better than the second option. Strength calculations were performed to determine if the jaw holder could withstand the applied loading. The designed proved to be safe as determined by calculation using the applied load and comparison of the maximum stress calculated to the strength of the material. Finite element analysis, performed with assistance, was used to confirm that the maximum stress experienced by the jaw holder was within the elastic limits of the material. The results from this analysis appear in Figure D6, overleaf. Revised drawings of the holder were completed and submitted to the workshop. The chamfer was machined on the jaw holder and jaw holders painted matt black to prevent corrosion of the steel surfaces.

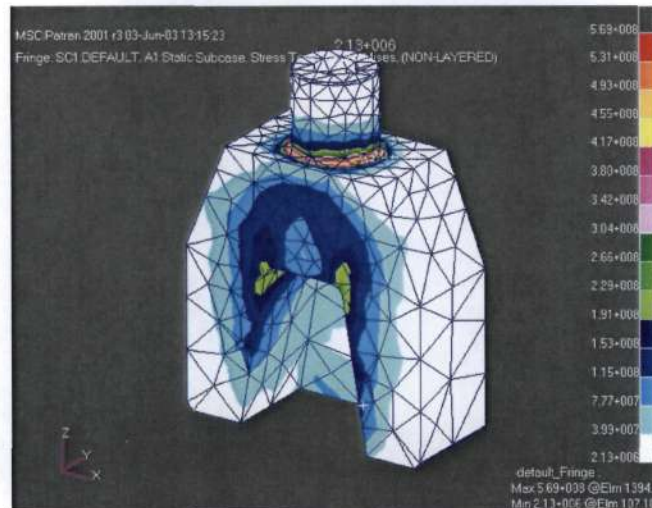


Figure D6 - FEM results on compression jaws

The completed assembly appears in Figure D7 below. The completed jaws were successfully commissioned and tested using 2mm fibre reinforced epoxy specimens. Cap screws on the completed assembly were replaced with hexagonal bolts to facilitate assembly of jaws onto the Instron frame.



Figure D7 - Assembled compression jaws

Tests performed with the jaws on unexposed specimen produced different results when compared to test results from the CSIR. Misalignment of the jaws was suspected as the problem that would lead to failure in buckling rather than pure compression. The jaw holder was dismantled and the dimension of the components verified. At this stage it was realised that the jaws were of different dimensions and not identical within the specified tolerance. This would result in the jaws clamping onto a specimen ends in parallel planes instead of a co-linear vertical plane. Machining of the jaws were considered but

further examination showed that particular pairs of jaws were of similar dimension. At this stage it was realised that the jaws were a matched pair and had to be used as a set. Although the two pairs of jaws were not of the same width, they were similar to the one in the pair. The matched jaw sets was assembled and specimens tested.

The test results at this stage still did not correlate with the test results from CSIR. It was difficult to verify that the centre lines of the jaw holders did line-up. The outer surfaces of the jaws were then used to verify jaw holder alignment. The jaw holders were found to be out of alignment by 0.1mm. Also, the jaw holders were set to a minimum position and an edge clocked to zero to check against movement that would occur in directions other than the vertical direction. Between minimum and maximum jaw position, the jaw holders were found to move in opposite directions in the horizontal plane. The centreline of the jaw holders in these cases would not be collinear which would contribute to misalignment of the jaws. The jaws were however correctly aligned at minimum jaw holder positions.

The jaw holders were dismantled from the Instron test frame to determine the cause of the misalignment. It was found that the central shaft of the jaw holder was of an incorrect dimension thereby allowing free movement of the jaw holder on the shaft that was firmly fixed to the Instron frame when mounted. The quickest solution involving the least machining was to insert commercially available thin walled bushes into the jaw holder. This would remove free movement of the jaw holder while allowing vertical movement. A commercially available bush would have to be turned down to the allowable wall thickness to securely fit onto the shaft. After consultation with the workshop manager, it was decided to machine new shafts as this would require a simple shaft with a keyway to be manufactured. A new shaft was therefore machined. Further, square guide bars were to be fitted to the sides of the jaws. During testing, these would move in slots on the jaw holders and therefore prevent any movement in the horizontal plane. To ensure the accuracy of the guide bars once installed, slots were cut into the existing jaw holders to accommodate the guide bars. The slots were machined such that the installed guide bars would be parallel to the centre of the holders. At this stage it was decided to take the opportunity to improve upon the design of the lower jaw by machining the shaft and base as one component. This would facilitate easy, accurate installation of the lower jaw holder onto the cross beam. Conceptual drawings were produced and the concept approved. Manufacturing drawings were then completed and handed into the workshop for manufacture.

The new fixtures were assembled and minimum free movement of the jaw holder verified. Specimens were tested but there was little improvement in the test results. Lack of frame rigidity was excluded as a possible source of error as the failure load was approximately 5% of the rated frame load of 100kN.

During mounting of the specimens it was noticed that two jaws in a pair would not always travel the same distance when a specimen was mounted. This problem did not occur on the upper jaw holder as gravity ensured that the jaws would always “hang” loose with no specimens in position. When the screw was tightened, the jaw plate would pull both jaws in the pair evenly until the specimen was clamped. On the lower jaw holder, the jaws would fall to a minimum position with the specimen between them. This position would not always be such that the jaws were equidistant from the centre of the jaw holder. Further tightening of the screw would result in the jaws clamping the specimen in an offset position. It is important that the jaws be at the same level when the specimen is secured in position as this would ensure that the specimen is aligned in a common vertical plane. Unequal jaw height would result in one jaw being closer to the centre of the jaw holder than the other in the matching pair. This problem was overcome by holding the jaws at a maximum position while simultaneously turning the screw to bring the jaws closer together thereby clamping the specimens. The jaws were therefore maintained at the same level with respect to each other thus ensuring the specimen was secured at the centre of the jaw holder. However tests on specimens yielded the same poor results as before.

At this stage it was decided to investigate a peculiarity of the load displacement curve in order to identify the problem. It appeared that as the load increased, there was a stage on the curve where the load remained constant then continued to increase as illustrated in Figure D8 overleaf. It was almost as if the specimen was slipping in the jaws. This could not have been the case as the jaws were securely fastened at the start of the test. This behaviour was consistent throughout most tests and occurred at approximately the same load. The contact surface of the jaws with the holder was carefully examined and smear lines were observed. This would imply that the load was not being equally distributed across the jaw / jaw holder interface. Certain high spots were carrying more load than the remaining area of the jaw surface. The extent of the uneven load distribution was not determined. A compliance check of the jaw system was decided upon to verify that the load applied to the jaws was being uniformly measured by the load cell. To perform this check, a rubber block with a linear load displacement curve was placed onto the jaws. The crossbeam was positioned such that the jaws would push against the rubber block. A linear load displacement curve could then be expected as the load cell would measure the force applied to the rubber block. This was however not the case with the characteristic region of constant force being recorded on the increasing load displacement curve. Compression test results on plates manufactured from sheet moulding compound, using end loading, also revealed the constant load condition. This phenomena is therefore independent of the material tested and occurs at approximately the same load. The problem is suspected to be with the drive system of the cross-head on the test frame.

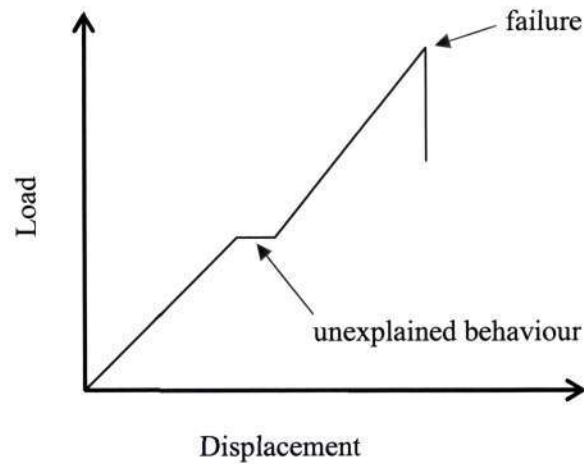


Figure D8 - Typical load displacement graph from compression test

A further observation made was that when the specimens were prepared with aluminium tabs by another member of the research group, specimens failed at higher loads but still not at loads comparable to the results obtained from the CSIR. On these tests, apart from the tabs being different, larger jaws were used to accommodate the thinner tab specimens. The contact area of the larger jaws with the jaw holder also revealed the smear pattern that was observed on the previous set of smaller jaws. A possible explanation for the higher loads recorded by the larger jaws may be that the load transfer occurs more uniformly over the jaw / jaw holder interface.

Appendix E - Compressive Strength Data of Epoxy Laminates

Test machine specifications:

Frame: Instron 5500R

Maximum Load Range: 10 kN (Tension and Compression)

Rated Load (Speed Capacity): 10 kN up to 500mm/min

5 kN between 500 and 1000mm/min

Testing Speed Range: 0.05 to 1000mm/min

For the compression tests performed, the following test parameters were used:

Speed of test: 1.26 mm/min

Preload: none

Mounting: Vertical in compression jaws

Summary of test data appears below.

Exposure duration: 10 weeks

8552 Strength

	No. of specimens	Max.	Min.	Average	Standard deviation	Range	v	s/s ₀
		[MPa]	[MPa]	[MPa]	[MPa]	[MPa]		
Baseline	4	515	460	494	26	55	0.053	1
Irene	6	510	431	486	29	79	0.06	0.98
Alkantpan	6	524	495	508	10	29	0.02	1.03
Durban	6	467	359	431	41	108	0.095	0.87

5052 Strength

	No. of specimens	Max.	Min.	Average	Standard deviation	Range	v	s/s ₀
		[MPa]	[MPa]	[MPa]	[MPa]	[MPa]		
Baseline	6	407	358	385	22	49	0.057	1
Irene	6	420	398	407	9	22	0.022	1.06
Alkantpan	6	432	373	399	20	59	0.05	1.04
Durban	6	404	358	385	16	46	0.042	1

Exposure duration: 20 weeks

8552 Strength

	No. of specimens	Max.	Min.	Average	Standard Deviation	Range	v	s/s ₀
		[MPa]	[MPa]	[MPa]	[MPa]	[MPa]		
Baseline		515	460	494	26	55	0.053	1
Irene	6	543	445	485	41	98	0.085	0.98
Alkantpan	4	530	412	450	54	118	0.12	0.91
Durban	6	506	395	457	36	111	0.079	0.93

5052 Strength

	No. of specimens	Max.	Min.	Average	Standard Deviation	Range	v	s/s ₀
		[MPa]	[MPa]	[MPa]	[MPa]	[MPa]		
Baseline		407	358	385	22	49	0.057	1.00
Irene	6	436	323	362	40	113	0.11	0.94
Alkantpan	6	438	334	385	42	104	0.109	1.00
Durban	6	407	311	361	32	96	0.089	0.94

Appendix F - Fibre-volume Calculation

Burnout tests were performed at Cray Valley laboratories to determine the fibre-volume fraction of epoxy laminates. The 5052 epoxy laminates were labelled as Clear Epoxy and the 8552 epoxy laminates were labelled as Dark Epoxy on the result sheet below titled, Glass Content Analysis.

Glass Content Analysis

Customer: UND

Date: 12 December 2003

Background:

Two samples supplied, laminated with two different epoxy resins and glass fibre. Burn-off at 500°C was carried to measure glass content etc.

	Clear Epoxy 1	Clear Epoxy 2	Dark Epoxy 1*	Dark Epoxy 2*
Initial Mass (g)	8.6963	8.6256	6.7145	6.9534
Final Mass (g)	5.1692	5.1274	4.5284	4.6743
Area (m ²)	0.001776	0.00175	0.001748	0.001766
No. Of layers	10	10	9	9
% Glass	59.44	59.44	67.44	67.22
Resin (g)	3.5271	3.4982	2.1861	2.2791
g/m ² glass	291	293	288	294
Resin: Glass	1 : 1.46	1 : 1.46	1 : 2.07	1 : 2.05

* coded as 327

Tests in duplicate and average as follows:

	Clear Epoxy	Dark Epoxy
Area (m ²)	0.001763	0.001757
% Glass	59.44	67.33
Resin (g)	3.57126	2.2326
g/m ² glass	292	291
Resin: Glass	1 : 1.46	1 : 2.06

Logan Sannasi

Technical Service Chemist - Structural

Nomenclature

w_f: fibre weight fraction

w_m : matrix weight fraction

ρ_f : density of fibre

ρ_m : density of matrix

ρ_c : density of composite

v_f : fibre-volume fraction

Equations used below are available in the literature [F1].

Using the above data the following calculations were performed to determine the fibre-volume fraction of the 5052 epoxy laminates. The % glass on both specimens tested were equal hence the fibre-volume fraction for both 5052 laminates tested are equal.

$$w_f = 0.5944$$

$$w_m = 1 - 0.5944 = 0.4056$$

$$\rho_f = 2540 \frac{\text{kg}}{\text{m}^3}$$

$$\rho_m = 1170 \frac{\text{kg}}{\text{m}^3}$$

$$\frac{1}{\rho_c} = \frac{w_f}{\rho_f} + \frac{w_m}{\rho_m}$$

$$\frac{1}{\rho_c} = \frac{0.5944}{2540} + \frac{0.4056}{1170}$$

$$\rho_c = 1722 \frac{\text{kg}}{\text{m}^3}$$

$$v_f = w_f \frac{\rho_c}{\rho_f} = 0.5944 \frac{1722}{2540} = 40.3\%$$

Using data from the glass content analysis, the following calculations were performed to determine the fibre-volume fraction of the 8552 epoxy laminates.

Specimen 1

$$w_f = 0.6744$$

$$w_m = 1 - 0.6744 = 0.3256$$

$$\rho_f = 2540 \frac{\text{kg}}{\text{m}^3}$$

$$\rho_m = 1300 \frac{\text{kg}}{\text{m}^3}$$

$$\frac{1}{\rho_c} = \frac{w_f}{\rho_f} + \frac{w_m}{\rho_m}$$

$$\frac{1}{\rho_c} = \frac{0.6744}{2540} + \frac{0.3256}{1300}$$

$$\rho_c = 1938 \frac{\text{kg}}{\text{m}^3}$$

$$v_f = w_f \frac{\rho_c}{\rho_f} = 0.6744 \frac{1938}{2540} = 51.5\%$$

Specimen 2

$$w_f = 0.6722$$

$$w_m = 1 - 0.6722 = 0.3278$$

$$\rho_f = 2540 \frac{\text{kg}}{\text{m}^3}$$

$$\rho_m = 1300 \frac{\text{kg}}{\text{m}^3}$$

$$\frac{1}{\rho_c} = \frac{w_f}{\rho_f} + \frac{w_m}{\rho_m}$$

$$\frac{1}{\rho_c} = \frac{0.6722}{2540} + \frac{0.3278}{1300}$$

$$\rho_c = 1935 \frac{\text{kg}}{\text{m}^3}$$

$$v_f = w_f \frac{\rho_c}{\rho_f} = 0.6722 \frac{1935}{2540} = 51.2\%$$

Average fibre-volume fraction for 8552 epoxy laminates;

$$v_f = \frac{1}{2}(51.5 + 51.2) = 51.4\%$$

Appendix G - Test Method Refinement

As roller dimensions were too large to be set at the ASTM recommended distances, the next most practical distance between rollers was used. Different combination of roller orientations and positions were investigated to enable the closest roller distances conforming to the ASTM standard to be used. Based on roller dimensions, specimens of corresponding dimensions were prepared for testing. Upon initial test trials, the 8552 laminates did not fail before the unloaded regions of the specimen came into contact with the edge of the roller supports. These specimen lengths were then reduced such that the specimens did not contact the edge of the roller support. This enabled the specimens to experience larger deflections until ultimate failure occurred. The initial tests were conducted with unexposed specimens to establish a baseline set of results against which a comparison can be made. Should the flexibility of the exposed specimens increase, the edge of the specimens may contact the roller support at locations closer to the rollers as illustrated in Figure G1.

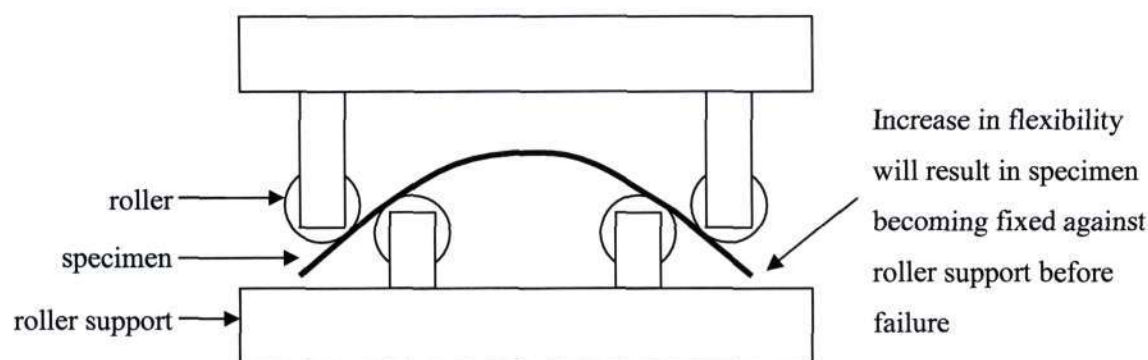


Figure G1 - Illustration of flexure test configuration during test

Specimens of dimension 120×10mm were cut using a circular diamond saw. The 8552 specimens were cut to 90×10mm to ensure failure in the midspan before the ends contact the roller support. Initially specimens were sanded to remove the blade marks but it was later found that the blade marks had no significant impact on the failure modes or results. This was established by comparing specimens that were finished by sanding to those in which there was no further preparation after cutting.

A series of tests were performed to determine the ultimate failure strength of the specimens. The bending strength was calculated and found to be comparable to handbooks. Further tests were performed to determine the flexural modulus. Initially a lever type clock gauge was used to measure the vertical deflection of the specimen at the centre of the midspan. However the deflection of the specimen was larger than the 0.8mm range of the clock gauge. The modulus calculated using the measurement of the

lever type clock gauge within the range of measurement yielded modulus values of approximately 160GPa. This was inconsistent with handbook data for glass-fibre reinforced composites. A steel rule was secured to the rear of the test fixture such that the rule can be used as an abscissa from which the vertical deflection of the midspan of the specimen can be measured. This method proved to be inaccurate due to error of parallax. A camera was mounted adjacent to the test frame to enable pictures of the specimen contour against the steel rule to be captured. Pictures may be taken at specific loads and the corresponding deflection determined reading of the deflection value against the steel rule from the picture. The method would be successful at low deflections but at the large deflections experienced, error of parallax would once again render the measurements inaccurate.

Measurements of the deflection of the free end of the specimens were recorded on subsequent tests. The calculation of the modulus using these measurements yielded modulus values of approximately 15GPa, i.e. within the range of values that can be expected of glass-fibre reinforced composites. This method was however difficult to perform. Further, as the specimen bent into a curve, the free edge travelled closer towards the centre of the specimen in the horizontal plane. At the beginning of the test, the free edge was set to align with the edge of the steel rule but as the test progressed, the free edge would move away from the aligned edge towards the adjacent parallel edge of the ruler. Further movement of the free edge would mean that the free edge vertical deflection cannot be read off the steel rule as the edge had moved too far horizontally, i.e. greater than the width of the ruler.

The next method used to determine the modulus was by measurement of the angular deflection of the free end. Modulus values calculated using the end rotation were within the range of that which can be expected of glass-fibre composites. To measure the free end deflection, the test has to be stopped and a protractor positioned to measure the rotation of the free end. Once the test was re-started, the laminate failed at a lower average load. Stopping the test to measure the rotation of the free end therefore yielded inaccurate ultimate failure strengths. Positioning the protractor to continuously measure rotation proved difficult due the vertical, horizontal and rotational motion of the free end.

An attempt was made to establish midspan deflection and free end rotation based on the travel of the cross-head. Measurement of any one of these parameters would enable the flexural modulus to be calculated from the formula [G1] listed overleaf. Equation G1 has been derived using basic stress relations from strength of materials.

$$E = \frac{6Ml}{bh^3\phi} \quad (G1)$$

$$E = \frac{3}{2} \frac{Ml^2}{bh^3u} \quad (G2)$$

$$s = \frac{Pl}{bh^2} \quad (G3)$$

Where the variables represent the quantities;

E – flexural modulus

M – bending moment

l – distance between loading noses

b – width of specimen

h – depth of specimen

ϕ - rotation at free end

P – applied load

u – midspan deflection

s – flexural strength

Geometric considerations were unsuccessfully applied to relate the cross-beam travel to deflections or rotations using standard beam deflection theory. Reviewing the assumptions of the derivation of the theory, it was realised the assumption of small deflections had been violated as the deflection curve for the case of large deflections is elliptical [G2] and not parabolic as in the case for small deflections.

Stopping the tests to measure deflections was contrary to the guidelines provided in the Delaware Composite Design Encyclopaedia [G3] and this practice was found to result in lower failure strengths. A successful attempt at measuring the modulus was achieved by measuring the deflection at the midspan using a plunger type dial gauge. This was set-up such that deflection of the midspan would move the plunger vertically thus the vertical movement of the plunger could be recorded. The linear modulus vs. load region of the laminate was established by plotting the modulus vs. load curve using multiple deflection measurements recorded. Positioning of the specimen before the commencement of the test was done visually by positioning the cross-head until the specimen visually just contacted the rollers. The plunger of the dial gauge was set to rest on the specimen and the dial adjusted to indicate

G2 Gere JM and Timoshenko SP; Mechanics of Materials, third SI edition; Chapman and Hall (1991); pg 514.

G3 Pipes RB; Delaware composites design encyclopaedia vol. 6, Test methods; Technomic publishing; pg 19-37.

zero displacement. The first deflection measurement recorded was at 100N. Successive deflection measurements were recorded at intervals of 25N for the 8552 specimens until the load reached 200N. The modulus was calculated using the six deflection and load measurements recorded. The modulus for the specimen being tested was then calculated as being the average of the six moduli calculated. For the 5052 specimens tested, deflections were recorded at load intervals of 50N until a load of 300N. Calculation of the modulus for the specimen tested was similar to that used to calculate the modulus of the 8552 material.

Measurements of modulus at loads higher than 200N and 300N for the 8552 and 5052 respectively were influenced by the high probability of damage occurring in the test region resulting in a decrease in modulus. Measurements recorded in the load ranges used, produced acceptable results. Due to the change of deflection being slow, and accuracy of the dial gauge, it was not necessary to stop the test to take measurements. The error in reading the 0.01mm graduated dial gauge due to response time and error of parallax was estimated to be 0.005mm.

Appendix H – Derivation of Dependence of Stress on Modulus

In derivation of the equation that relates flexural strength to modulus, we begin with the following two equations;

$$E = \frac{3}{2} \frac{Ml^2}{bd^3u} \quad \text{and} \quad \sigma = \frac{6M}{bd^2}$$

Re-arranging the terms, we arrive at the following relationship

$$E = \frac{3}{2} \frac{Ml^2}{bd^3u} = \frac{1}{4} \frac{6M}{bd^2} \frac{l^2}{du} = \frac{1}{4} \frac{l^2}{du} \sigma$$

or

$$\sigma = \frac{4du}{l^2} E$$

Appendix I - Flexural Strength Data

Exposure at Irene, Alkantpan and Durban began on March 2002. Exposure at the remaining test sites began on January 2003.

Units of Stress: MPa

Units of Modulus: GPa

Sampling period: June 2002

Test batch info.

Location	Number of specimens	
	8552	5052
Irene	4	5
Alkantpan	4	6
Durban	3	5

8552 Strength							
	max	min	average	SD	range	v	σ/σ_0
Irene	841.71	613.24	725.80	126.82	228.47	0.1747	1.28
Alkantpan	659.07	631.90	645.83	12.66	27.17	0.0196	1.14
Durban	988.72	951.04	972.70	19.46	37.68	0.0200	1.72
8552 Modulus							
	max	min	average	SD	range	v	E/E_0
Irene	33.39	27.81	30.70	2.86	5.58	0.0931	1.15
Alkantpan	29.77	27.44	28.84	1.03	2.33	0.0358	1.08
Durban	32.90	31.17	32.03	0.87	1.74	0.0271	1.20

5052 Strength							
	max	min	average	SD	range	v	σ/σ_0
Irene	702.70	639.23	659.18	27.04	63.47	0.0410	1.11
Alkantpan	694.87	523.63	623.57	59.98	171.24	0.0961	1.05
Durban	784.30	622.57	684.33	65.58	161.73	0.0958	1.16
5052 Modulus							
	max	min	average	SD	range	v	E/E_0
Irene	21.50	18.52	20.23	1.07	2.98	0.0530	0.86
Alkantpan	22.47	17.75	19.99	1.72	4.72	0.0861	0.85
Durban	23.70	20.76	21.62	1.20	2.95	0.0555	0.92

Sampling period: August 2002

Test batch info.

Location	Number of specimens	
	8552	5052
Irene	3	5
Alkantpan	4	4
Durban	3	3

8552 Strength							
	max	min	average	SD	range	v	σ/σ_0
Irene	847.86	822.54	836.36	12.82	25.32	0.0153	1.48
Alkantpan	649.17	623.12	635.87	11.70	26.05	0.0184	1.12
Durban	933.17	917.08	924.01	8.27	16.09	0.0089	1.63
8552 Modulus							
	Max	min	average	SD	range	v	E/E_0
Irene	32.18	30.76	31.38	0.73	1.42	0.0231	1.17
Alkantpan	28.80	27.91	28.36	0.51	0.89	0.0178	1.06
Durban	30.18	29.69	29.87	0.27	0.49	0.0090	1.11

5052 Strength							
	max	min	average	SD	range	v	σ/σ_0
Irene	640.72	563.66	610.10	32.624	77.06	0.0534	1.03
Alkantpan	687.41	572.14	616.62	49.66	115.27	0.0805	1.04
Durban	681.45	575.53	631.58	53.23	105.92	0.0842	1.07
5052 Modulus							
	max	min	average	SD	range	v	E/E_0
Irene	20.18	19.51	19.88	0.25	0.67	0.0126	0.85
Alkantpan	20.83	18.33	19.49	1.31	2.50	0.0676	0.83
Durban	20.38	19.65	19.92	0.40	0.73	0.0200	0.85

Sampling period: January 2003

Test batch info.

Location	Number of specimens	
	8552	5052
Irene	2	2
Alkantpan	3	3
Durban	2	3

8552 Strength							
	max	min	average	SD	range	v	σ/σ_0
Irene	830	782	806.00	33.94	48	0.0421	1.42
Alkantpan	792	781	786.67	5.51	11	0.0070	1.39
Durban	881	847	864.00	24.04	34	0.0278	1.53
8552 Modulus							
	max	min	average	SD	range	v	E/E_0
Irene	31.16	29.89	30.53	0.89	1.27	0.0293	1.14
Alkantpan	31.11	29.79	30.24	0.75	1.32	0.0247	1.13
Durban	28.15	27.85	27.00	0.21	0.30	0.0076	1.04

5052 Strength							
	max	min	average	SD	range	v	σ/σ_0
Irene	655	572	613.5	58.69	83	0.0957	1.04
Alkantpan	651	612	629.33	19.86	39	0.0316	1.06
Durban	644	572	611	36.37	72	0.0595	1.03
5052 Modulus							
	max	min	average	SD	range	v	E/E_0
Irene	20.17	18.15	19.16	1.43	2.02	0.0745	0.82
Alkantpan	20.49	19.68	20.01	0.42	0.81	0.0212	0.85
Durban	21.14	20.29	20.82	0.46	0.85	0.0221	0.89

Sampling period: July 2003

Test batch info.

Location	Number of specimens	
	8552	5052
Alkantpan	5	6
Bredasdorp	6	5
Cradock	6	6
Durban	5	4
Irene	4	5
Komati	6	6

8552 Strength							
	max	min	average	SD	range	v	σ/σ_0
Alkantpan	849.00	774.00	809.60	28.17	75.00	0.03	1.43
Bredasdorp	378.00	333.00	361.50	17.26	45.00	0.05	0.64
Cradock	819.00	447.00	594.50	170.68	372.00	0.29	1.05
Durban	791.00	753.00	767.80	14.60	38.00	0.02	1.36
Irene	839.00	808.00	817.50	14.48	31.00	0.02	1.44
Komati	703.00	628.00	655.33	33.74	75.00	0.05	1.16
8552 Modulus							
	max	min	average	SD	range	v	E/E_0
Alkantpan	31.11	29.79	30.24	0.75	1.32	0.02	1.13
Bredasdorp	9.11	8.43	8.70	0.26	0.68	0.03	0.32
Cradock	28.15	23.71	26.45	1.87	4.44	0.07	0.99
Durban	28.15	27.85	28.00	0.21	0.30	0.01	1.04
Irene	31.16	29.89	30.53	0.89	1.27	0.03	1.14
Komati	29.32	27.49	28.52	0.76	1.83	0.03	1.06

5052 Strength							
	max	min	average	SD	range	v	σ/σ_0
Alkantpan	661.00	565.00	620.00	39.76	96.00	0.06	1.05
Bredasdorp	653.00	544.00	591.00	44.00	109.00	0.07	1.00
Cradock	649.00	404.00	528.00	105.00	245.00	0.20	0.89
Durban	712.00	576.00	638.75	57.65	136.00	0.09	1.08
Irene	602.00	567.00	582.80	14.34	35.00	0.02	0.99
Komati	661.00	545.00	612.00	55.00	116.00	0.09	1.03
5052 Modulus							
	max	min	average	SD	range	v	E/E_0
Alkantpan	20.95	19.40	20.25	0.57	1.55	0.03	0.86
Bredasdorp	27.60	18.60	22.40	3.10	9.00	0.14	0.95
Cradock	28.60	19.10	22.20	3.30	9.50	0.15	0.94
Durban	22.29	19.84	20.89	1.03	2.45	0.05	0.89
Irene	20.84	17.68	19.34	1.48	3.16	0.08	0.99
Komati	25.80	19.80	23.50	2.30	6.00	0.10	1.00

Sampling period: January 2004

Test batch info.

Location	Number of specimens	
	8552	5052
Alkantpan	5	5
Bredasdorp	5	5
Cradock	4	5
Durban	5	5
Irene	5	5
Komati	5	5

8552 Strength							
	max	min	average	SD	range	v	σ/σ_0
Alkantpan	652.00	587.00	619.00	26.54	65.00	0.04	1.09
Bred	940.00	735.00	806.33	246.69	205.00	0.31	1.42
Cradock	799.00	439.00	604.25	175.89	360.00	0.29	1.07
Durban	825.00	781.00	805.60	15.77	44.00	0.02	1.42
Irene	624.00	575.00	602.00	18.06	49.00	0.03	1.06
Komati	639.00	575.00	596.00	25.45	64.00	0.04	1.05

8552 Modulus							
	max	min	average	SD	range	v	E/E_0
Alkantpan	31.11	29.79	30.24	0.75	1.32	0.02	1.13
Bred	32.44	26.47	29.27	2.47	5.97	0.08	1.09
Cradock	29.98	26.11	27.39	1.79	3.87	0.07	1.02
Durban	28.15	27.85	28.00	0.21	0.30	0.01	1.04
Irene	31.16	29.89	30.53	0.89	1.27	0.03	1.14
Komati	30.32	25.53	27.28	2.17	4.79	0.08	1.02

5052 Strength							
	max	min	average	SD	range	v	σ/σ_0
Alkantpan	576.00	482.00	535.40	34.17	94.00	0.06	0.91
Bred	661.00	547.00	583.00	48.00	114.00	0.08	0.99
Cradock	602.00	495.00	545.00	48.00	107.00	0.09	0.92
Durban	642.00	553.00	578.60	36.40	89.00	0.06	0.98
Irene	629.00	540.00	588.80	31.92	89.00	0.05	1.00
Komati	674.00	482.00	592.00	62.00	192.00	0.11	1.00

5052 Modulus							
	max	min	average	SD	range	v	E/E_0
Alkantpan	23.34	21.63	22.51	0.75	1.72	0.03	0.96
Bred	26.00	19.00	21.00	3.00	6.60	0.12	0.89
Cradock	27.90	19.20	22.30	3.30	8.40	0.15	0.95
Durban	19.51	16.90	18.16	1.01	2.61	0.06	0.77
Irene	22.26	18.37	20.14	1.65	3.89	0.08	0.86
Komati	24.80	20.30	21.80	1.70	4.50	0.08	0.93

Sampling period: July 2004

Test batch info.

Location	Number of specimens	
	8552	5052
Alkantpan	5	6
Bredasdorp	6	6
Cradock	No samples	
Durban	5	5
Irene	5	6
Komati	6	6

8552 Strength							
	max	min	average	SD	range	v	σ/σ_0
Alkantpan	1009.00	755.00	878.25	112.60	254.00	0.13	1.55
Bred	581.00	556.00	568.17	8.98	25.00	0.02	1.00
Cradock							
Durban	825.00	781.00	805.60	15.77	44.00	0.02	1.42
Irene	688.00	605.00	642.33	33.54	83.00	0.05	1.13
Komati	627.00	558.00	592.17	25.72	69.00	0.04	1.05
8552 Modulus							
	max	min	average	SD	range	v	E/E_0
Alkantpan	30.85	29.12	30.08	0.81	1.73	0.03	1.12
Bred	31.48	26.84	28.55	1.60	4.64	0.06	1.07
Cradock							
Durban	28.15	27.85	28.00	0.21	0.30	0.01	1.04
Irene	29.65	27.20	28.59	1.00	2.46	0.03	1.07
Komati	28.03	21.28	25.70	2.38	6.76	0.09	0.96

5052 Strength							
	max	min	average	SD	range	v	σ/σ_0
Alkantpan	626.00	539.00	596.00	36.00	87.00	0.06	1.01
Bred	647.00	566.00	608.00	35.00	81.00	0.06	1.03
Cradock							
Durban	631.00	495.00	567.00	50.90	136.00	0.09	0.98
Irene	616.00	533.00	589.00	29.00	83.00	0.05	1.00
Komati	639.00	567.00	591.00	28.00	72.00	0.05	1.00
5052 Modulus							
	max	min	average	SD	range	v	E/E_0
Alkantpan	25.2	18.4	20.4	2.6	6.8	0.129	0.87
Bred	45.6	22.2	28.2	8.9	23.5	0.317	1.20
Cradock							
Durban	19.5	16.9	18.2	1.0	2.6	0.1	0.77
Irene	19.4	16.9	18.4	1.1	2.5	0.059	0.78
Komati	25.6	20.1	22.5	2.1	5.5	0.094	0.96

Sampling period: February 2005

Test batch info.

Location	Number of specimens	
	8552	5052
Alkantpan	5	6
Bredasdorp	6	6
Cradock	No samples	
Durban	5	6
Irene	5	6
Komati	No samples	

8552 Strength							
	max	min	average	SD	range	v	σ/σ_0
Alkantpan	881.00	592.00	693.00	162.96	289.00	0.24	1.22
Bred	803.00	742.00	772.50	43.13	61.00	0.06	1.36
Cradock							
Durban	2174.00	1784.00	1953.50	142.85	390.00	0.07	3.45
Irene	627.00	568.00	590.50	25.57	59.00	0.04	1.04
Komati							
8552 Modulus							
	max	min	average	SD	range	v	E/E_0
Alkantpan	31.50	26.54	28.27	2.80	4.96	0.10	1.05
Bred	29.28	24.50	26.60	2.00	4.78	0.08	0.99
Cradock							
Durban	24.33	21.93	23.16	0.88	2.40	0.04	0.86
Irene	27.43	24.61	26.13	1.17	2.82	0.04	0.97
Komati							

5052 Strength							
	max	min	average	SD	range	v	σ/σ_0
Alkantpan	654.00	560.00	612.00	40.00	94.00	0.07	1.03
Bred	626.00	538.00	577.00	37.00	88.00	0.06	0.98
Cradock							
Durban	659.00	556.00	596.00	36.00	103.00	0.06	1.01
Irene	655.00	601.00	621.00	23.00	54.00	0.04	1.05
Komati							
5052 Modulus							
	max	min	average	SD	range	v	E/E_0
Alkantpan	23.2	20.6	21.6	1.2	2.6	0.054	0.92
Bred	23.0	19.0	21.0	1.0	3.7	0.068	0.89
Cradock							
Durban	21.0	19.0	20.0	1.0	2.4	0.043	0.85
Irene	23.8	19.4	21.3	1.5	4.4	0.069	0.91
Komati							

Sampling period: July 2005

	No. of specimens
Location	5052
Alkantpan	6
Bredasdorp	6
Cradock	4
Durban	6
Irene	6
Komati	6

5052 Strength							
	max	min	average	SD	range	v	σ/σ_0
Alkantpan	608.00	566.00	588.00	15.00	42.00	0.03	0.99
Bred	614.00	560.00	577.00	21.00	54.00	0.04	0.98
Cradock	600.00	502.00	542.00	45.00	98.00	0.08	0.92
Durban	610.00	547.00	571.00	24.00	63.00	0.04	0.97
Irene	737.00	548.00	596.00	72.00	189.00	0.12	1.01
Komati	570.00	467.00	506.00	35.00	103.00	0.07	0.86
5052 Modulus							
	max	min	average	SD	range	v	E/E_0
Alkantpan	20.00	18.60	19.20	0.60	1.40	0.03	0.82
Bred	22.00	18.70	19.80	1.30	3.30	0.07	0.84
Cradock	22.70	20.50	21.30	1.10	2.20	0.05	0.91
Durban	22.90	17.40	19.60	2.00	5.50	0.10	0.83
Irene	22.20	15.80	19.00	3.00	6.30	0.16	0.81
Komati	19.30	14.50	16.80	2.00	4.80	0.12	0.71

Appendix J – Environmental Chamber Maintenance

After extended use on the salt spray cycle, corrosion was noticed on the side walls of the chamber. After the end of the exposure cycle, the chamber was refurbished. As the structural integrity of the chamber remained intact, only the chamber walls required refurbishment. This entailed removing the isolated spots of rust on both the interior and exterior walls of the chamber. The exterior walls of the chamber were then coated with an epoxy paint. Interior walls of the chamber were chemically re-passivated to prevent corrosion.

Although the electrical connections for the UV lamps were situated exterior to the chamber, the electrical contact corroded after three years of service to the extent that the circuit breaker would periodically trip the power supply to the chamber. Corrosion of the contacts is thought to be due to condensation collecting on the UV lamps and then leaking out of the chamber, through the glands and onto the electrical connections at the end. The lamp interface with the chamber walls has been sealed and the electrical contacts at either end of the lamp bank replaced.

A modification has been proposed to facilitate the ease of switching over from salt spray to water spray. Presently this is accomplished by physically removing the inlet siphon pipe to the venturi out of the distilled water tank, placing it into the salt water tank and then bleeding the system. The modification incorporates a valve with inputs from both tanks and the output to the venturi system. Changing of liquids sprayed into the chamber from distilled to salt water would therefore only involve operating the valve to allow the selected fluid to pass through. This system would save the effort of having to reposition piping and bleed the system, thus saving time when a liquid spray change-over is required.

Appendix K – Empirical Model Data

Units of Stress: MPa

Units of Modulus: GPa.

Exposure duration: 2.5 months

8552 Strength							
	max	min	average	SD	range	v	Non-dimensional
Irene	841.71	613.24	725.80	126.82	228.47	0.1747	1.28
Alkantpan	659.07	631.90	645.83	12.66	27.17	0.0196	1.14
Durban	988.72	951.04	972.70	19.46	37.68	0.0200	1.72
8552 Modulus							
Irene	33.39	27.81	30.70	2.86	5.58	0.0931	1.15
Alkantpan	29.77	27.44	28.84	1.03	2.33	0.0357	1.08
Durban	32.90	31.17	32.03	0.87	1.74	0.0271	1.20

5052 Strength							
Irene	702.70	639.23	659.18	27.04	63.47	0.0410	1.11
Alkantpan	694.87	523.63	623.57	59.98	171.24	0.0961	1.05
Durban	784.30	622.57	684.33	65.58	161.73	0.0958	1.16
5052 Modulus							
Irene	21.50	18.52	20.23	1.07	2.98	0.0530	0.86
Alkantpan	22.47	17.75	19.99	1.72	4.72	0.0861	0.85
Durban	23.70	20.76	21.62	1.20	2.95	0.0555	0.92

Exposure duration: 5 months

8552 Strength							
	max	min	average	SD	range	v	Non-dimensional
Irene	847.86	822.54	836.36	12.82	25.32	0.0153	1.48
Alkantpan	649.17	623.12	635.87	11.70	26.05	0.0184	1.12
Durban	933.17	917.08	924.01	8.27	16.09	0.0089	1.63
8552 Modulus							
Irene	32.18	30.76	31.38	0.72	1.42	0.0231	1.17
Alkantpan	28.80	27.91	28.36	0.51	0.90	0.0178	1.06
Durban	30.18	29.69	29.87	0.27	0.49	0.0094	1.11

5052 Strength							
Irene	640.72	563.66	610.10	32.62	77.06	0.0534	1.03
Alkantpan	687.41	572.14	616.62	49.66	115.27	0.0805	1.04
Durban	681.45	575.53	631.58	53.23	105.92	0.0842	1.07
5052 Modulus							
Irene	20.18	19.51	19.88	0.25	0.67	0.0126	0.85
Alkantpan	20.83	18.33	19.49	1.31	2.50	0.0675	0.83
Durban	20.38	19.65	19.92	0.40	0.73	0.0201	0.85

Exposure duration: 9 months

8552 Strength							
	max	min	average	SD	range	v	Non-dimensional
Irene	830	782	806	33.94	48	0.0421	1.42
Alkantpan	792	781	786.67	5.51	11	0.0070	1.39
Durban	881	847	864	24.04	34	0.0278	1.53
8552 Modulus							
Irene	31.16	29.89	30.53	0.89	1.26	0.0293	1.14
Alkantpan	31.11	29.79	30.24	0.75	1.32	0.0247	1.13
Durban	28.15	27.84	27.00	0.21	0.30	0.0076	1.04

5052 Strength							
Irene	655	572	613.5	58.69	83	0.0957	1.04
Alkantpan	651	612	629.33	19.86	39	0.0316	1.06
Durban	644	572	611	36.37	72	0.0595	1.03
5052 Modulus							
Irene	20.17	18.15	19.16	1.43	2.02	0.0746	0.82
Alkantpan	20.49	19.68	20.02	0.42	0.81	0.0212	0.85
Durban	21.14	20.29	20.82	0.46	0.85	0.0221	0.89

Exposure duration: 14 months

8552 Strength							
	max	min	average	SD	range	v	Non-dimensional
Irene	839	808	817.5	14.48	31	0.0177	1.44
Alkantpan	849	774	809.6	28.17	75	0.0348	1.43
Durban	791	753	767.8	14.60	38	0.0190	1.36
8552 Modulus							
Irene	31.16	29.89	30.53	0.89	1.27	0.0293	1.14
Alkantpan	31.11	29.79	30.24	0.74	1.32	0.0247	1.13
Durban	28.15	27.85	27.00	0.21	0.30	0.0076	1.04

5052 Strength							
Irene	602	567	582.8	14.34	35	0.0246	0.99
Alkantpan	661	565	620	39.76	96	0.0641	1.05
Durban	712	576	638.75	57.65	136	0.0903	1.08
5052 Modulus							
Irene	20.84	17.68	19.34	1.48	3.16	0.0766	0.82
Alkantpan	20.95	19.40	20.25	0.57	1.55	0.0282	0.86
Durban	22.29	19.84	20.89	1.03	2.45	0.0493	0.89

Exposure duration: 20months

8552 Strength							
	max	min	average	SD	range	v	Non-dimensional
Irene	624	575	602	18.06	49	0.0300	1.06
Alkantpan	652	587	619	26.54	65	0.0429	1.09
Durban	825	781	805.6	15.77	44	0.0196	1.42
8552 Modulus							
Irene	31.16	29.89	30.53	0.89	1.27	0.0293	1.14
Alkantpan	31.11	29.79	30.24	0.75	1.32	0.0247	1.13
Durban	28.15	27.85	27.00	0.21	0.30	0.0076	1.04

5052 Strength							
Irene	629	540	588.8	31.92	89	0.0542	1.00
Alkantpan	576	482	535.4	34.17	94	0.0638	0.91
Durban	642	553	578.6	36.40	89	0.0629	0.98
5052 Modulus							
Irene	22.26	18.37	20.14	1.65	3.89	0.0817	0.86
Alkantpan	23.34	21.63	22.51	0.75	1.72	0.0332	0.96
Durban	19.51	16.90	18.16	1.01	2.61	0.0554	0.77

Exposure duration: 26 months

8552 Strength							
	max	min	average	SD	range	v	Non-dimensional
Durban	810	750	791	25.12	60	0.0318	1.40
8552 Modulus							
Durban	25.03	23.60	24.35	0.51	1.43	0.0209	0.91

5052 Strength							
Durban	631	495	567	50.90	136	0.0897	0.96
5052 Modulus							
Durban	20.96	18.16	19.34	1.06	2.80	0.0549	0.82

Appendix L - Degradation Modelling Results

Output strength results from algorithm appear below:

Dry environment, Case 1: 8552 model result

Baseline strength: 566.3MPa

Thickness: 2.1mm

Table L1 - Strength prediction using the algorithm (Case 1, dry climate)

Time [months]	Depth of undamaged laminate [mm]	Relative depth	Calculated strength [MPa]	Relative strength	Model output	Irene exposure	Alkantpan exposure
0	2.1	1	566.3	1	1		
2.5	2.08	0.99	559.56	0.99	1	0.97	0.91
5	2.05	0.98	552.82	0.98	1	1.05	0.91
9.5	2.01	0.95	540.68	0.95	1.1	1.11	1.07
14	1.96	0.93	528.55	0.93	1.1	1.10	1.14
20	1.96	0.93	527.41	0.93	0.93	0.90	0.90
26	1.95	0.93	526.28	0.93	0.93		

Dry environment, Case 2: 5052 model result

Baseline strength: 591MPa

Thickness: 2.8mm

Table L2 - Strength prediction using the algorithm (Case 2, dry climate)

Time [months]	Depth of undamaged laminate [mm]	Relative depth	Calculated strength [MPa]	Relative strength	Model result	Irene exposure	Alkantpan exposure
0	2.8	1	591	1			
2.5	2.78	0.99	585.72	0.99	1.13	1.12	1.13
5	2.75	0.98	580.45	0.98	1.11	1.14	1.08
9.5	2.68	0.96	565.25	0.96	1.09	1.07	1.08
14	2.61	0.93	550.05	0.93	1.06	1.04	1.09
20	2.59	0.93	547.52	0.93	1.06	1.07	0.96
26	2.58	0.92	544.99	0.92	1.05		

Wet environment, Case 1: 8552 model result

Baseline strength: 566.3MPa

Thickness: 2.1mm

Moisture factor: 15%

Table L3 - Strength prediction using the algorithm (Case 1, wet climate)

Time [months]	Depth of undamaged laminate [mm]	Relative depth	Calculated strength [MPa]	Relative strength	Model result	Model result including moisture factor	Durban exposure
0	2.1	1	566.3	1	1	1.15	
2.5	2.08	0.99	559.56	0.99	1	1.15	1.18
5	2.05	0.98	552.82	0.98	1.1	1.25	1.24
9.5	2.01	0.95	540.68	0.95	1.1	1.25	1.22
14	1.96	0.93	528.55	0.93	0.93	1.08	1.06
20	1.96	0.93	527.41	0.93	0.93	1.08	1.10
26	1.95	0.93	526.28	0.93	0.93	1.08	1.14

Wet environment, Case 2: 5052 model result

Baseline strength: 591MPa

Thickness: 2.8mm

Moisture factor: 8%

Table L4 - Strength prediction using the algorithm (Case 2, wet climate)

Time [months]	Depth of undamaged laminate [mm]	Relative depth	Calculated strength [MPa]	Relative strength	Model result	Model result including moisture factor	Durban exposure
0	2.8	1	591	1			
2.5	2.78	0.99	585.72	0.99	1.11	1.11	1.11
5	2.75	0.98	580.45	0.98	1.09	1.09	1.09
9.5	2.68	0.96	565.25	0.96	1.07	1.07	1.06
14	2.61	0.93	550.05	0.93	1.04	1.12	1.14
20	2.59	0.93	547.52	0.93	1.04	1.12	1.11
26	2.58	0.92	544.99	0.92	1.03	1.11	1.1